

MECHANOBIOLOGICAL REGULATION OF SEMILUNAR
VALVE DEVELOPMENT

A Dissertation

Presented to the Faculty of the Graduate School
of Cornell University

In Partial Fulfillment of the Requirements for the Degree of
Doctor of Philosophy

by

Duc Hong Pham

August 2020

© 2020 Duc Hong Pham

MECHANOBIOLOGICAL REGULATION OF SEMILUNAR

VALVE DEVELOPMENT

Duc Hong Pham, Ph.D.

Cornell University 2020

Congenital malformations of semilunar valves are common birth defects and often result in aortic valve stenosis and calcification with significant morbidity and mortality. The quest for new therapeutic targets remains a challenge in part because genetics alone does not fully address the etiology of congenital valve defects (CVDs). While altered blood flow in chick can lead to various CVDs that resemble those observed in humans, how hemodynamics drive valve development is still unclear.

Here, we hypothesized that endocardial cells transduce mechanical information into biological programs that regulate semilunar valve morphogenesis. We utilized conditional loss-of-function mouse models and a primary valve endocardial cell 3D culture system to address two hallmarks of valve remodeling: extension and compaction. We revealed that low oscillatory shear stress is transduced by the endocardial cells on the inflow surface of the valve into bone morphogenetic protein (BMP) signaling programs that in turn regulate endocardial proliferation. In contrast, high fluid shear stress inhibits BMP signaling in endocardial cells, thereby restricting growth on the outflow surface. These findings have identified a novel mechanism for

valve extension, in which differential endocardial growth constrains and drives valve growth and elongation in the direction of blood flow.

In regard to mechanisms of valve compaction, we found that endocardial cells on the outflow side of the valve transduce high, unidirectional shear stress into endocardial Notch1 signaling that regulates CXCR4 expression in subendocardial cells. By regulating BMP and WNT signaling, CXCR4 modulates mesenchymal proliferation and induces matrix maturation and tissue compaction. These findings have uncovered a novel mechanobiological valve development program mediated by CXCR4 that has implications in the development of CVDs.

This dissertation work has not only shed light on the interaction between blood flow and valve development programs but also the reactivation of developmental programs in adult valve disease initiation and progression. We provided *prima facie* evidence showing that aortic valve development and disease share side-specific BMP activation and CXCR4 signaling. Therefore, we hope this work will motivate further investigation of valve development mechanisms to inform better therapeutic and engineering strategies, not just for CVDs but also aortic valve disease.

BIOGRAPHICAL SKETCH

Duc H. Pham was born and raised in Ho Chi Minh City, Vietnam. In 2008, he came to the United States to study at Redwood Adventist Academy in Santa Rosa, CA. After graduating from high school, he attended Santa Rosa Junior College (SRJC) and majored in Nursing. Thanks to coursework in anatomy and physiology at SRJC, he was determined to become a Biology instructor someday. In 2013, he transferred to Cornell from SRJC and majored in Biology.

As an Education minor at Cornell, he learned about the American education system and the diverse student bodies on college campuses. He understood personal challenges can hinder one's success beyond college. Since he juggled three jobs while attending SRJC full-time, he did not have enough time to obtain research experience, which was critical to his future goals. Sympathetic towards Duc's plight, Nick Anast, a physiology instructor, hired him as his research assistant, so he could afford quitting one of his jobs. Working with Nick ignited his love for science and helped him earn a research internship at Mayo Clinic and a full-ride scholarship to Cornell.

In 2015, he was heartbroken to learn that Nick had died in a kayaking accident. When Duc heard Nick paid his research stipend out of his pocket, he was lost for words. Touched and inspired by Nick's passion for science and compassion for students, Duc founded the Nick Anast Research Fellowship. The program has provided SRJC students from disadvantaged backgrounds internships at Cornell and allowed Duc to nurture their scientific curiosity through research mentorship.

As a PhD student at Cornell, Duc continued to teach introductory biology, while performing graduate research under the guidance of Professor Jonathan Butcher, Professor Cindy Leifer, Professor Katie Kelly, Professor Marcos Simoes-Costa, and Professor Natasza Kurpios. His dissertation focuses on the mechanobiological regulation of embryonic semilunar valve development. In August 2020, Duc will be an Assistant Professor of Human Anatomy and Physiology at Santa Monica College.

For Lê Thị Tám, my grandmother

ACKNOWLEDGMENTS

This doctoral work was made possible thanks to Professor Jonathan Butcher and funding from the National Institute of Health and National Science Foundation. My tuition, health insurance, and stipend were provided by the Cornell Graduate Teaching Assistantship and the Biological and Biomedical Sciences Program. Dr. Butcher provided research materials, laboratory infrastructure, and mentorship which were instrumental in the success of the project. In addition, Dr. Butcher provided the funding, in conjunction with the Cornell Graduate School, for my conference travel to present the work in this dissertation.

I would like to extend my gratitude to my committee members, Professor Cindy Leifer, Professor Katie Kelly, Professor Marcos Simoes-Costa, and Professor Natasza Kurpios, and my DGS, Professor Dave Lin. They have provided the expertise, empathy, and encouragement that were crucial to the success of my research projects and career development.

I would like to thank my undergraduate mentees, Charles Dai and Belle Lin, who contributed tremendously to the projects. I would like to thank all of my lab mates at the Butcher lab for providing a professional research environment that promotes efficiency while maintaining cordiality. I would like to especially thank David Bassen, who has been a good friend and source of support as well as Terence Gee and Ablajan Mahmut, who gave me great insights and helped improve my morale.

I would also like to thank my cohort friends Pragya Shah, Kaley Wilburn, Shing Hu, and Divya Shiroor for their camaraderie and candor about their graduate school experience. Without them, this journey would have been very lonely.

TABLE OF CONTENTS

BIOGRAPHICAL SKETCH	V
ACKNOWLEDGMENTS	VIII
TABLE OF CONTENTS	X
LIST OF FIGURES	XII
LIST OF TABLES	XIV
LIST OF ABBREVIATIONS.....	XV
CHAPTER 1. INTRODUCTION.....	16
1.1 CLINICAL AND SCIENTIFIC SIGNIFICANCE OF CONGENITAL HEART DEFECTS	17
1.2 OVERVIEW OF OFT VALVE DEVELOPMENT.....	18
1.3 NOTCH REGULATION OF OFT VALVE DEVELOPMENT	23
1.4 BMP REGULATION OF OFT VALVE DEVELOPMENT.....	25
1.5 WNT REGULATION OF OFT VALVE DEVELOPMENT	27
1.6 SHEAR STRESS REGULATION OF VALVE DEVELOPMENT AND DISEASE	30
1.7 REPROGRAMMING OF NOTCH, BMP, & WNT SIGNALING IN AORTIC VALVE DISEASE	37
1.8 REGULATION OF CELL PROLIFERATION IN VALVE DEVELOPMENT AND DISEASE	43
1.9 THESIS OBJECTIVES	50
1.10 REFERENCES.....	54
CHAPTER 2. OSCILLATORY SHEAR STRESS DRIVES ENDOCARDIAL CELL PROLIFERATION BY ACTIVATING BMP SIGNALING DURING VALVE EXTENSION	66
2.1 ABSTRACT.....	67
2.2 INTRODUCTION.....	68
2.3 MATERIALS AND METHODS	71
2.3.1 Animal samples	71
2.3.2 Shear stress bioreactor system	71
2.3.6 Statistics	76
2.4 RESULTS	76
2.4.1 Endocardial accommodation is side-specific.....	76
2.4.2 Endocardial proliferation is associated with BMP signaling on the outflow side.....	79
2.4.3 Low OSS induced, while high LSS inhibited, BMP signaling in valve ECs.....	82
2.4.4 Upregulation of BMP receptors and ligands in response to low OSS.....	85
2.4.5 Enhanced endocardial proliferation in response to low magnitude OSS.....	88
2.4.6 BMP signaling is required for OSS5-induced endocardial proliferation.....	91
2.4.7 Notch signaling is required for modulation of BMP signaling in endocardial cells	94
2.4.8 Wnt/β-catenin mediates differential BMP activation by shear stress.....	96
2.5 DISCUSSION	100
2.6 REFERENCES.....	106
CHAPTER 3. UNIDIRECTIONAL SHEAR STRESS COORDINATES ENDOCARDIAL NOTCH1 AND SUBENDOCARDIAL CXCR4 SIGNALING TO REGULATE FETAL VALVE REMODELING	120

3.1	ABSTRACT.....	121
3.2	INTRODUCTION.....	122
3.3	MATERIALS AND METHODS.....	124
3.3.1	<i>Animal samples</i>	124
3.3.2	<i>Hanging drop culture system, compaction analysis, and micropipette aspiration</i>	125
3.3.3	<i>Shear stress bioreactor system</i>	126
3.3.4	<i>3D endocardial cell culture</i>	127
3.3.5	<i>Immunostaining</i>	128
3.3.6	<i>Gene expression analysis</i>	129
3.3.7	<i>Statistics</i>	130
3.4	RESULTS.....	131
3.4.1	<i>Spatiotemporal expression of CXCR4 and CXCL12 during valve development</i>	131
3.4.2	<i>CXCR4 is required for modulation of mesenchymal cell proliferation</i>	135
3.4.3	<i>CXCR4 is not required for regulation of apoptosis of mesenchymal cells</i>	137
3.4.4	<i>CXCR4 signaling in endocardium-derived mesenchymal cells is sufficient</i>	140
3.4.5	<i>Upregulated BMP signaling in Nfatc1-cre;CXCR4^{fllox/fllox} mutant valves</i>	144
3.4.6	<i>CXCR4 is required for modulation of proliferation via canonical WNT signaling</i>	147
3.4.7	<i>CXCR4 is required for tissue condensation during valve development</i>	148
3.4.8	<i>CXCR4 regulates α-Smooth muscle actin expression via BMP signaling</i>	151
3.4.9	<i>CXCR4 regulates valve compaction via modulating BMP activity</i>	154
3.4.10	<i>CXCR4 is required for matrix maturation during valve development</i>	157
3.4.11	<i>Endocardial Notch1 signaling regulates subendocardial CXCR4 expression</i>	160
3.5	DISCUSSION.....	166
3.6	REFERENCES.....	175
CHAPTER 4. CONCLUSIONS AND FUTURE DIRECTIONS.....		186
4.1	SUMMARY OF FINDINGS AND IMPLICATIONS.....	187
4.2	OSCILLATORY SHEAR STRESS REGULATES CANONICAL WNT SIGNALING VIA β CATENIN.....	188
4.3	OSCILLATORY SHEAR STRESS IS ASSOCIATED WITH NFkB SIGNALING.....	191
4.4	OSCILLATOR SHEAR STRESS IS ASSOCIATED WITH EMT-INDUCING SNAIL1 EXPRESSION.....	193
4.5	MECHANICAL REGULATION OF VALVE COMPACTION IN OFT AND AV VALVES VIA BMP.....	197
4.6	RETINOIC ACID SIGNALING REGULATES AV VALVE REMODELING BY MODULATING BMP.....	201
4.7	REACTIVATION OF CXCR4 SIGNALING DURING VALVE STENOSIS AND CALCIFICATION.....	203
4.8	SHEAR STRESS REGULATION OF THE ENDOCARDIUM IN DEVELOPMENT AND DISEASE.....	205
4.9	REFERENCES.....	210
APPENDIX A. TRIPLE-AMPLIFICATION IMMUNOSTAINING FOR FFPE SECTIONS.....		216
APPENDIX B. IMMUNOSTAINING FOR WHOLEMOUNT TISSUES.....		224
APPENDIX C. PROGENITOR CELL AND TISSUE CULTURE.....		226
APPENDIX D. SHEAR STRESS EXPERIMENT WORKFLOW.....		230
APPENDIX E. QRT-PCR FOR ENDOCARDIAL PATCHES.....		236
APPENDIX F. FIJI IMAGE ANALYSIS CODE DEVELOPMENT.....		239

LIST OF FIGURES

Figure 1.1. Timeline of OFT Valve Development.....	21
Figure 1.2. Regulatory networks of valve formation and remodeling processes.	29
Figure 1.3. Side-specificity of endocardial programs during valve remodeling.	34
Figure 1.4. Side-specificity of Notch/eNOS signaling during valve development and disease.	43
Figure 1.5. Proposed mechanism of cushion excavation and compaction.	53
Figure 2.1. Enhanced endocardial proliferation and growth on the arterial side.	78
Figure 2.2. Enhanced BMP signaling on the arterial side of semilunar valves.....	81
Figure 2.3. Enhanced BMP activation under low oscillatory shear.	84
Figure 2.4. Upregulation of BMP ligands and receptors in response to OSS5.	87
Figure 2.5. Enhanced proliferation under low oscillatory shear.	90
Figure 2.6. Inhibition of BMP signaling downregulates endocardial proliferation under OSS5.	93
Figure 2.7. Enhanced BMP signaling in Notch1-inhibited endocardial cells.	95
Figure 2.8. BMP2 did not increase proliferation under LSS20.	98
Figure 2.9. Shear stress regulates side-specificity of valve endocardial proliferation.	99
Figure 3.1. Spatiotemporal expression of CXCR4 during valve development.....	133
Figure 3.2. Global CXCR4 ablation resulted in hyperplastic and thickened OFT semilunar valves.	134
Figure 3.3. CXCR4 is not required for AVC valve remodeling.....	137
Figure 3.4. Global CXCR4 ablation did not affect mesenchymal cell apoptosis.	138
Figure 3.5. Ablation of CXCR4 in endocardium-derived cells resulted in thickened valve, but preserved coronary arteries.	139
Figure 3.6. Augmented BMP signaling activity in NCKO mutant valves at E17.5.....	142
Figure 3.7. Enhanced canonical WNT signaling via β catenin in NCKO mutant valves at E17.5.	146
Figure 3.8. CXCR4 signaling is required for tissue compaction.	150

Figure 3.9. Aberrant myofibroblastic activation and contractility in NCKO valves.....	153
Figure 3.10. CXCR4 facilitated tissue compaction and myofibroblastic activation via modulating BMP signaling.	156
Figure 3.11. Aberrant matrix maturation in CXCR4 mutant valves.....	159
Figure 3.12. Endocardial Notch1 regulates subendocardial CXCR4 expression.....	164
Figure 3.13. Laminar shear stress induces Notch1 activation in primary chick endocardial cells.	165
Figure 3.14. CXCR4 regulation of outflow out tract valve remodeling.	166
Figure 4.1. Low OSS activates perinuclear localization of β catenin.....	190
Figure 4.2. Active NF κ B signaling is side-specific at E14.5, but not from E17.5 onward.	192
Figure 4.3. Snail1 expression is localized in endocardial cells on the arterial side of OFT valves.	196
Figure 4.4. Mechanical regulation of BMP signaling during valve development.....	201
Figure 4.5. Retinoic acid signaling modulates BMP signaling in AV valves.	203
Figure 4.6. Upregulation of CXCR4 in mice prone to developing calcific aortic valve disease.	205
Figure 4.7. Low OSS activates Notch1 signaling in chick endocardial cells.	209

LIST OF TABLES

TABLE 1.1. KNOWN HUMAN GENE MUTATIONS THAT ARE ASSOCIATED WITH CONGENITAL HEART DEFECTS.....	22
TABLE 1.2. THE EFFECTS OF COMMON SURGICAL INTERVENTIONS ON HEART FUNCTIONS IN CHICK EMBRYOS.....	36
TABLE 1.3. REPORTED HEART MALFORMATIONS AS A RESULT OF COMMON SURGICAL INTERVENTIONS IN CHICK EMBRYOS.....	37

LIST OF ABBREVIATIONS

AVC	Atrioventricular Canal
OFT	Outflow Tract
BMP	Bone morphogenic protein
EMT	Epithelial to Mesenchymal Transition
KO	Knockout
LSS	Laminar shear stress
OSS	Oscillatory shear stress
FSS	Fluid shear stress
P/S	Penicillin/streptomycin
TBS	Tris-buffered saline
qRT-PCR	quantitative real-time polymerase chain reaction
α SMA	α Smooth muscle actin
TGF β	Tissue growth factor β
VEGF	Vascular endothelial growth factor
WNT	Wingless and Int-1
NICD1	Notch1 intracellular domain

CHAPTER 1. INTRODUCTION

*Part of Section 1.6 was written by Belle Lin
*Part of Section 1.8 was written by Charles Dai

1.1 Clinical and Scientific Significance of Congenital Heart Defects

Congenital heart defects (CHDs) are the most common birth defects, affecting about 1% of all live births a year in the U.S (van der Linde, 2011). Bicuspid aortic valve (BAV) is the most prevalent CHDs, affecting about 1-2% of the population and predisposing 30% of those afflicted to more morbidity and mortality than all other CHDs combined (Siu, 2010). In BAV, the aortic valve is composed of two rather than three semilunar cusps of unequal sizes, leading to abnormal cuspal contact and limited valvular mobility. Later in life, the bicuspid valve becomes thickened, diffuse, and calcified, resulting in aortic valve stenosis (AVS), or narrowing of the aortic valve (Siu, 2010). In addition, non-BAV pediatric AVS also exhibits increased deposition of collagen and decreased deposition of elastic fibers, leading to valvular malfunction (Hinton, 2006). Left untreated, AVS causes the heart to work harder to maintain systemic circulation and become weakened over time, leading to heart failure. The most common treatment for severe AVS is aortic valve replacement, an invasive surgery that transplants tissue valves from pig or human deceased donors into patients (Michelena, 2014). However, not only is this procedure associated with high risk of stroke and vascular complications, but the tissue valves also become narrow over the years and need to be replaced (Michelena, 2014). Therefore, new treatments that target the formation of BAV and prevent AVS are desperately needed to alleviate the burden of this congenital defect.

The quest for new therapeutic targets to halt BAV remains a challenge in part because there are no animal models that exhibit a completely penetrant BAV

phenotype (Siu, 2010), but more importantly, because our understanding of valvulogenesis is incomplete. In fact, while early valve formation has been extensively studied, with more than 100 regulatory genes identified (Combs, 2009), little is known about post-formation valve remodeling, especially one that gives rise to the pulmonary and aortic valves. How the amorphous valve primordia get sculpted into their semilunar shape, what starts and sustains subsequent differentiation of the valve mesenchyme, and how the valves become stratified into defined layers remain elusive. Assessment of non-BAV diseased valves revealed disorganized matrix fiber deposition, confirming that valve malformation also involves aberrant post-EMT valve remodeling (Hinton, 2006). Lack of information on the regulation of mid-late valve morphogenesis is a critical gap in our knowledge not only because the etiology of BAV may involve aberrant valve remodeling (Dupuis, 2013; Koenig, 2016) and that reactivated developmental programs could be responsible for adult valve disease (Wirrig, 2014), but a deeper understanding of valve remodeling also informs better valve engineering strategies.

1.2 Overview of OFT Valve Development

During early cardiogenesis, bilaterally symmetric fields of mesoendodermal cells fuse medially to form a linear heart tube with an outer layer of cardiac progenitor cells, a middle layer of acellular hyaluronan-rich matrix (cardiac jelly), and an inner layer of endocardial cells (Butcher, 2007). Although the cardiac jelly is initially present throughout the heart tube, around embryonic day 9.5-10.5 (E9.5-10.5), cellularization and remodeling of the matrix are localized at the atrioventricular (AV) canal, which

eventually forms the AV septum, and the outflow tract (OFT), which gives rise to the aorta and pulmonary artery (Combs, 2009). Cellularization of the cardiac jelly is facilitated by endocardial-mesenchymal transformation (EMT), where endocardial cells lining regions of the AV canal and OFT take up a mesenchymal phenotype and invade the cardiac jelly. Specifically, EMT in the OFT is coordinated by BMP, TGF β , and Notch signaling that induces Snail1/2, thereby downregulating endocardial genes (e.g. VE-cadherin, CD31) and upregulating mesenchymal genes (e.g. α SMA, vimentin) (Timmerman, 2004; Niessen, 2008). These mesenchymal cells proliferate and progressively replace the hyaluronan-rich matrix with proteoglycans and collagen (Schroeder, 2003). These amorphous, compliant, and cellularized masses are now called cushions. In the OFT, these cushions are invaded by a population of cardiac neural crest cells (cNCCs) coming from the aortic arch shortly after E9.5 (Jain, 2011). At around E10.5, EMT happens in the OFT and gives rise to 4 ridges of cushions by E11.5: 2 conotruncal ridges, which comprises of a conus region (at the OFT-right ventricle junction) and a truncus region (distal to the conus region) and 2 intercalated ridges (sandwiched between conotruncal ridges) (Anderson, 2016). By E12.5, the conotruncal cushions fuse and create a septum that separates the OFT into the future aorta and the pulmonary artery and divides the 4 cushion ridges into 2 groups of 3 cushions, which develop into the future 3 cusps of the aortic and pulmonary valves (Combs, 2009).

Although when EMT terminates is still a mystery, after E12.5, the valvular cushions begin sculpting into their semilunar shape through progressive *excavation*, a

poorly understood process driven by “selective growth of the free edges” that produces an epithelial groove between the developing valves and the arterial wall (Hurle, 1980). The later phases of OFT valve remodeling is characterized by the gradual *mesenchymal differentiation* into specialized valve interstitial cells (VICs) (de Vlaming, 2012), which express genes associated with cartilage lineages (e.g. sox9 and aggrecan) and tendon lineages (e.g. scleraxis and tenascin C) (Lincoln, 2006). These VICs organize and stratify the extracellular matrix (ECM) into 3 different layers that are correlated to hemodynamic stimuli: the fibrosa with densely packed collagen circumferentially oriented to provide tensile strength, the spongiosa with glycosaminoglycans and proteoglycan providing a buffer zone for valvular bending and stretching, and the ventricularis composed of elastin and collagen radially oriented to provide elasticity (Garside, 2013). While more than 100 regulatory genes of early cushion formation have been studied, mechanisms of post-EMT valve remodeling remain elusive. More importantly, various genetic abnormalities have been linked to CHDs in humans, which are summarized in Table 1.1.

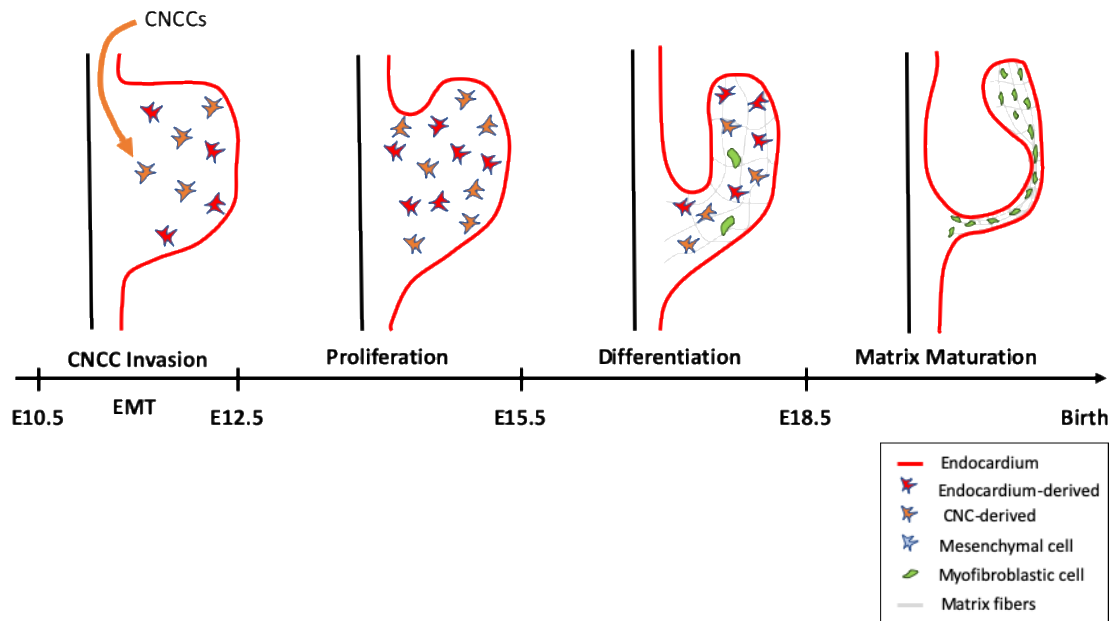


Figure 1.1. Timeline of OFT Valve Development. Valve development starts with cellularization of valve regions by EMT and invasion of cardiac neural crest cells (CNCCs). Subsequently, the valve remodeling processes sculpt the valve primordia into semilunar shape to facilitate unidirectional blood flow from the ventricles into the arteries.

GENE	CHD	References
Notch1	BAV, AS, CoA	Garg, 2005
Notch2;JAG1	BAV, PPH, PS, TOF	Bonachea, 2014
Notch3	BAV	Bonachea, 2014
NOS3	BAV	Dargis, 2016
JAG1	BAV, PAS, TOF	Oda, 1997
NOS1	BAV	Bonachea, 2014
ALK3	VSD, EN	Demal, 2019
ALK2	AVSD	Fahed, 2013
VEGFB, VEGFC	CoA, BAV	Bonachea, 2014
SMAD6	BAV, CoA, AS	Fahed, 2013
AXIN2	BAV	Wooten, 2010
TGFBR2	BAV, ARD	Graham, 2011
WNT4	BAV	Bonachea, 2014

Table 1.1. Known human gene mutations that are associated with congenital heart defects (CHD). BAV= BICUSPID AROTIC VALVE; AS=AORTIC VALVE STENOSIS; CoA=COARTATION OF THE AORTA, PPH=PERIPHERAL PULMONARY HYPOPLASIA; PS=PULMONARY VALVE STENOSIS; TOF=TETROLOGY OF FALLOT; PAS=PULMONARY ARTERY STENOSIS; VSD=VENTRICULAR SEPTAL DEFECTS; EN=EPSTEIN'S ANOMALY; ARD=AORTIC ROOT DILATION

1.3 Notch Regulation of OFT Valve Development

Notch activation involves binding of a transmembrane Notch receptor (e.g. Notch1-4) of a receiving cell to a transmembrane Notch ligand (e.g. Jag1/2 and DLL1/3/4) of a signaling cell (Luxán, 2016). During OFT valvulogenesis, Notch1/2 is highly expressed in cushion endocardium and to a lesser extent in the mesenchyme (Williams, 1995; Timmerman, 2004; Loomes, 2002; Varadkar, 2008), while Notch4 is only detected in endocardial cells (Nosedá, 2004). On the one hand, while Jag2 is expressed only in the myocardium from E11.5-E15.5 (van den Akker, 2007), Jag1 expression gradually increases in the cushion endocardium and restricted to endocardial cells on the arterial (or atrial) side of the OFT and AV cushions by E12.5 (MacGrogan, 2016), suggesting regulation of hemodynamics. On the other hand, DLL4 is highly expressed in the OFT endocardium, substantially decreased by E12.5, and undetectable in the cushion by E14.5 (MacGrogan, 2016). Upon ligation, the Notch receptor changes its conformation, exposing the extracellular cleavage site S2, which is hydrolyzed by disintegrins and metalloproteinases and endocytosed by the signaling cell (Brou, 2000; Wen, 1997). The remaining fragment of the Notch receptor is then cleaved at site S3 by gamma-secretase, which then releases the Notch intracellular domain (NICD) and allows for its nuclear translocation (De Strooper, 1999). In the nucleus, NICD binds to RBPJ, displacing the repressor complex on RBPJ, and recruits co-activators, e.g. MAML (Kurooka, 1998). As a complex, NICD-RBPJ-MAML directly activates expression of Notch target genes, e.g. HEY and HES (Beatus, 2001; Ong, 2006).

In the OFT, Notch signaling represses BMP2 expression in the endocardium as well as the ventricular and atrial myocardium, thereby restricting BMP2 expression to the myocardium of the OFT and AV canal and EMT to those regions (Luna-Zurita, 2010; Rutenberg, 2006; McCright, 2001; Krebs, 2000). Abrogation of Notch1 results in decreased Snail expression and absence of cushion mesenchyme (Krebs, 2003; Xue, 1999), while Notch2/3/4 mutants do not exhibit obvious cushion defects (Varadkar, 2008), suggesting that Notch1 is required and sufficient for cardiac cushion formation. Notch ligand-specific mutants do not show early cushion malformations (Jiang, 1998; Krebs, 2004), suggesting that ligand redundancy may be at play. These data suggest that Notch1 is required for EMT that contributes to the cellularization of the cardiac jelly and formation of the valve primordia.

Even though Notch signaling has been extensively studied in the context of early valvulogenesis, its impact on post-EMT valve remodeling is not well studied. Recently, endocardial Notch1/DLL4 signaling has been shown to be required for EMT during early valve formation, while endocardial Notch1/Jag1 signaling is indispensable for EMT but is required for restraining cushion hypercellularity (Hofmann, 2012; Wang, 2013). Despite having no effects on mesenchymal cell apoptosis, Notch/Jag1 signaling directly upregulates Hbegf, which downregulates BMP signaling and suppresses mesenchymal proliferation (Jackson, 2003; Iwamoto, 2010). Notch1/Jag1 is also required for modulating deposition of proteoglycans and periostin (MacGrogan, 2016), which is required for mesenchymal cell differentiation and matrix maturation (Norris, 2008). Interestingly, ablation of Notch1 in the endocardial cell lineage resulted in

increased mesenchymal cell proliferation. In addition, Notch1 signaling is associated with endocardial TNF α expression, which in turn regulates mesenchymal cell apoptosis (Wang, 2015). In addition to controlling mesenchymal cellularity, Notch1 is also associated with mesenchymal cell differentiation. In fact, Notch1 signaling regulates Twist1 and Msx2, which are early markers of mesenchymal cell differentiation (MacGrogan, 2016). Recently, Notch1/Jag1 signaling has been shown to regulate endocardial secretome proteins, such as TGF β and metalloproteinase inhibitors, responsible for inducing ECM deposition and remodeling (Torregrosa-Carrion, 2019). Taken together, these data suggest that endocardial Notch1 signaling regulates growth and maturation of the underlying mesenchyme. How Notch1 coordinates these remodeling programs remains to be worked out.

1.4 BMP Regulation of OFT Valve Development

Bone morphogenetic proteins (BMPs) 2,4-7 are part of the TGF β superfamily and expressed in the myocardium of the AC canal and OFT during valve formation (Somi, 2004). BMPs bind to two types of receptors: BMP receptor type I, including activin-receptor like kinase (ALK) 2/3/6, and BMP receptor type II, including BMPRII and activin receptor type II (ACTRII) A/B. Ligation of BMP receptors causes phosphorylation of the BMP R-smads: smad1/5/8, which complexes with smad4 and translocates into the nucleus to regulate BMP target genes, such as Id1/2/3 (Garside, 2013). During valvulogenesis, ALK2 is expressed in the endocardium (Zhang, 1996), while ALK3 and BMPRII are ubiquitously expressed in the heart (Sugi, 2004; Luna-Zurita, 2010). BMP2 is expressed in the myocardium of the AV canal and required for

EMT of AV cushion but dispensable for OFT cushion formation (Ma, 2005). In contrast, BMP4 is required for mesenchymal cell proliferation and valve growth, but it is not required for EMT in the OFT (McCulley, 2008). Furthermore, abrogation of ALK2 or 3 leads to downregulation of Snail, attenuation of EMT, and valve defects. Interestingly, endocardial loss of ALK2, but not ALK3, results in a reduction of TGF β -specific smad2/3 phosphorylation, suggesting that BMP signaling induces EMT and/or “primes” the endocardium to be more responsive to TGF β -dependent EMT (Garside, 2013). Taken together, these data show that BMP signaling exhibits ligand compensation, but not receptor redundancy.

While the roles of BMPs in early valvulogenesis are established, their contribution to post-EMT processes is not well understood despite protracted BMP activity in the remodeling valves. Particularly in the chick OFT, during mid-late gestation, BMP4/5/7 are expressed in the myocardium surrounding the valvular cushions, while BMP2/4/6 are restricted to the endocardial cells on the arterial side of the cushion (Somi, 2004). Interestingly, ablation of smad6, an inhibitor of BMP signaling (Hata, 1998; Galvin, 2000), or noggin, a scavenger of BMP ligands, resulted in hypertrophic OFT and AVC valve primordia, suggesting that BMP signaling is responsible for valve growth (Choi, 2007). Recently, BMP signaling has been associated with upstream signaling programs in the endocardial cells that regulate proliferation of mesenchymal cells in a paracrine manner. For example, endocardial cells secrete Heparin-binding epidermal growth factor (HB-EGF) which in turn regulates BMP activation and proliferation in mesenchymal cells (Jackson, 2003). Recently,

endocardial Notch1 signaling regulates HBEGF and modulates BMP6 as well as regulates smad6 expression (MacGrogan, 2016). In addition, canonical WNT signaling in the myocardium regulates BMP2/4 expression, which in turn regulates BMP-dependent mesenchymal cell proliferation in a paracrine manner (Wang, 2018).

Modulation of BMP signaling during valve remodeling is critical for matrix maturation and patterning. During valve remodeling, BMP6 is expressed in OFT valves (Somi, 2004) and is associated with proteoglycan deposition and cartilage-like ECM (Sugi, 2012; MacGrogan, 2016). Mechanistically, BMP4 signaling induces Sox9 and aggrecan (a proteoglycan) expression in the OFT mesenchymal cells during early valve development (Zhao, 2007). Furthermore, fibroblast growth factor-4 (FGF-4) is required for the expression of scleraxis and tenascin and transitioning to tendinous tissue in the OFT valves (Zhao, 2007). The delicate balance between BMP/sox9 and FGF4 signaling programs is critical for the structural maturation of OFT valves (Zhao, 2007, Lincoln, 2006). In fact, upregulation of BMP signaling has been associated with immature ECM with increased deposition of proteoglycan and decreased periostin in the OFT valves (Sierro, 2007; Wilson, 2013; MacGrogan, 2016). Taken together, these findings suggest that BMP signaling is not only important for EMT during early valve development but also cell differentiation and matrix maturation during valve remodeling.

1.5 WNT Regulation of OFT Valve Development

Canonical WNT signaling requires ligation of secreted WNT ligands to frizzled receptors, leading to the translocation of beta-catenin to the nucleus. Nuclear beta-catenin binds to the transcription factor LEF1, inducing production of downstream

target genes, such as LEF1 and Axin2 (Clevers, 2012). Recent research shows that beta-catenin can accumulate in the perinuclear endocytic recycling compartment (ERC) destined for nuclear translocation (Kam, 2009). During early valve development, endocardial WNT signaling promotes EMT in valve primordia (Person, 2005). Recently, signaling during post-EMT valve remodeling has been associated with mesenchymal cell proliferation through cell-autonomous and non-cell autonomous manners. Specifically, canonical WNT signaling reporter transgenic mice revealed that WNT is active in both valvular mesenchyme and the surrounding myocardium (Wang, 2018). Deletion of beta-catenin in the myocardium resulted in decreased BMP4 expression and attenuated BMP activation in the OFT valves, suggesting that canonical WNT signaling drives mesenchymal cell proliferation in a non-cell autonomous manner (Wang, 2018). Furthermore, ablation of beta-catenin in the endocardial cell lineage also led to decreased mesenchymal cell proliferation and valve area, suggesting that WNT signaling also drives proliferation in a cell autonomous manner (Wang, 2018). Interestingly, Wnt9b ligand is expressed in the endocardium during valve remodeling and is required for attenuating mesenchymal growth (Goddard, 2017).

These seemingly contradictory findings are likely due to the intrinsic negative feedback regulation of WNT signaling by its own downstream target Axin2 (Yu, 2005). In fact, ablation of Axin2 resulted in increased proliferation of mesenchymal cells, suggesting that WNT-induced accumulation of Axin2 inhibits further WNT signaling, indicated by a lack of LEF1 nuclear expression (Bosada, 2016). Bosada et al. also implied a role for canonical WNT signaling in regulating matrix patterning during valve

remodeling. Inactivation of WNT signaling led to downregulation of versican, a proteoglycan that is prevalent in the spongiosa and a known target of WNT (Rahmani, 2005), along with expansion of tenascin (Bosada, 2016). It is conceivable that myocardial WNT-induced BMP signaling and mesenchymal cell-autonomous WNT signaling coordinate to modulate matrix stiffening by regulating proteoglycan content.

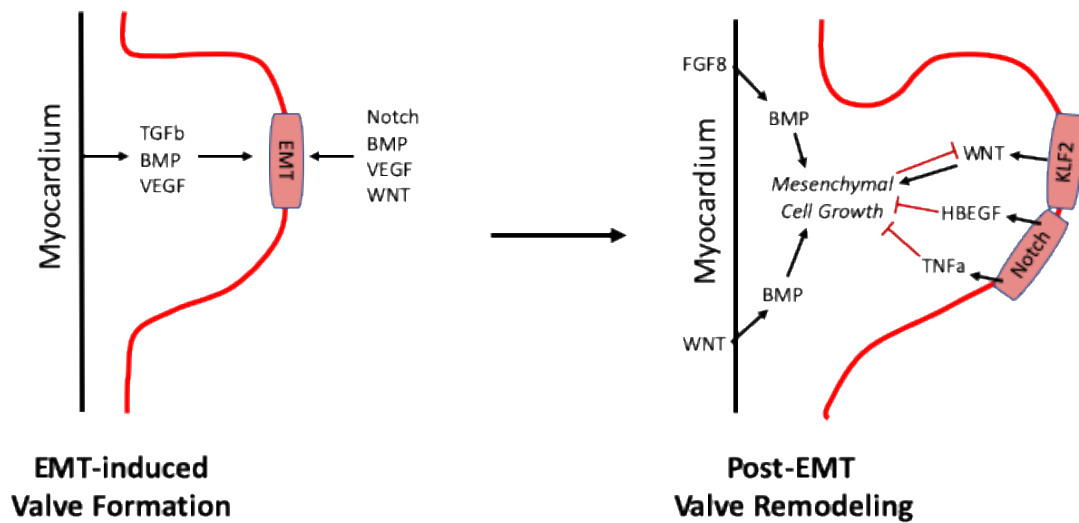


Figure 1.2. Regulatory networks of valve formation and remodeling processes. During early development, myocardial cells secrete factors that induce EMT in the endocardial cells. Even though some of these factors are present during post-EMT valve remodeling, they regulate mesenchymal cell proliferation and valve extension.

1.6 Shear Stress Regulation of Valve Development and Disease

As the heart contracts to force blood into the systemic circulation, heart cells experience various types of mechanical stresses due to the interaction between ventricular walls and blood. In particular, the endocardium experiences shear stress, which is a frictional force exerted by the blood flow that is tangential to the cell surface. Computational fluid dynamics is a computational tool that utilizes some experimental data/knowledge as in input and theoretical models to calculate parameters that cannot be measured directly. For example, CFD has been used to map distribution of shear stress on the endocardium using experimental data acquired through micro-computed tomography (Butcher, 2007), confocal microscopy (Hierck, 2008), and light sheet microscopy (Lee, 2016).

Using CFD, we now know that the inflow surface of valves, i.e. arterial side of the OFT valves and ventricular side of the AV valves, is exposed to high unidirectional laminar shear stress (LSS). However, the outflow surface, i.e. ventricular side of the OFT valves and atrial side of the AV valves, is exposed to oscillatory shear stress (OSS) that is lower in velocity (Kilner, 2000). During valve remodeling, side-specificity of Notch1 (Del Monte, 2007), eNOS (Figure 4A), BMP (MacGrogan, 2016), VEGF (Wang, 2017), and WNT (Goddard, 2017) programs indicates that they are regulated by differential fluid shear stress (FSS) in both the OFT and AV valves (Figure 3). Besides the contributions of FSS to development, altered FSS has also been implicated in valve disease initiation and progression (Sun, 2013). How endocardial cells sense and

transduce different FSS information into developmental or disease signaling programs remains unclear.

A transcriptional profile of human umbilical vein endothelial cells revealed that laminar shear stress (LSS) regulated genes are involved in a number of endothelial cell functions, including proliferation, apoptosis, gene expression, differentiation, inflammation, oxidative metabolism and signaling pathways (Wasserman, 2002; Li, 2005). Endothelial primary cilia are able to respond to low shear stress (2 dyne/cm²) and increase Notch1 in endocardial cells leading to trabeculation in ventricles and heart and vascular development (Goetz, 2014; Samsa, 2015; Lee, 2016). KLF2 and KLF4 in endothelial cells have also been shown to respond to shear stress and influence the Wnt pathway. They, along with Wnt9b, are highly expressed at sites with high shear stress and are critical in valve development. Without KLF2, there is a loss of Wnt9b and other Wnt target genes (Goddard, 2017). While both KLF2 and primary cilia are shear responsive, their distribution has an inverse relationship. Parts that are exposed to high shear stress have high levels of KLF2 and low levels or none primary cilia. Those that are exposed to low shear stress have primary cilia and low levels of KLF2. Following this trend, primary cilia can be found in the arterial side of the OFT cushions (Van der Heiden, 2006). The cilia on the ventricular side are irregular and close to none.

The effect of shear stress is studied in vascular development. It has been found that shear stress induces arterial specification, causing a differentiation between arteries and veins. After E9.5 in mouse embryos, Notch1 was expressed exclusively in arterial endothelium (Jahnsen, 2015). LSS (5 and 10 dyne/cm²) increases arterial

markers such as Notch1, EphrinB2 (downstream of Notch), and CXCR4 and has no effect on venous markers (Sivarapatna, 2015). EphrinB2 increases are dose and time dependent upon LSS (0 up to 20 dyne/cm²) (Masumura, 2009). However, it is worth noting that Notch signaling may not be required in arteriovenous differentiation. Several arteriovenous differentiation genes, including KLF2, Jag1, and COUPTFII were upregulated by LSS (5 dyne/cm²) despite a knockout of Notch1 (Jahnsen, 2015). As well, they found that Notch1 expression is only upregulated in low laminar shear stress (less than 10 dyne/cm²) and oscillatory shear stress (up to 2 ± 3 dyne/cm²). Oscillatory shear stress (OSS) upregulates B-catenin levels and Wnt signaling, which increases target gene angiopoietin-2 in aortic endothelial cells (Li, 2014). Angiopoietin-2 functions in vascular remodeling and integrity. Wnt signaling plays a role not only in adults, but also in embryos. During embryonic development, Wnt/B-catenin and Notch signaling causes endothelial cell differentiation and vascular morphogenesis (Dejana, 2010).

Notch, Wnt, and BMP pathways are critical in adults as well as embryonically and a dysregulation may lead to a number of cardiovascular diseases. In patients suffering from thoracic aortic aneurysm (TAA), endothelial cells were found to have impaired Notch/BMP/Wnt pathways. Aortic endothelial cells from patients were exposed to laminar shear stress with a flow of 12 dyne/cm². After being exposed to shear stress, DLL4 levels remained low. DLL4, a part of the Notch pathway, is important in vascular maturation and angiogenesis (Pedrosa, 2015). Overall, shear stress response was attenuated leading to a decrease in activation of DLL4, SNAIL1, DKK1,

and BMP2, which play key roles in the Notch pathway. Patients with TAA have impaired pathways that are integral in maintaining endothelial integrity and stress resistance (Kostina, 2018).

Notch signaling is important in regulating and preventing diseases. It is involved in valve calcification. In a study conducted using human induced pluripotent stem cell (iPSC) derived endothelial cells, laminar shear stress of 12.5 dyne/cm² causes an increase, via Notch1 dependent pathway, in anti-calcification gene transcription which inhibits BMP, TGF β , and Wnt signaling, compared to those that have a heterozygous nonsense mutation in Notch1 (Theodoris, 2015). LSS also has anti-inflammatory and anti-osteogenic effects. Notch1 also regulates matrix glycoprotein which inhibits soft tissue calcification (White, 2015). Thereby, shear stress protects against valve calcification via the Notch signaling pathway. In addition, Notch signaling is decreased in patients with aortic aneurysm and bicuspid aortic valve (Kostina, 2016). Notch1 is reactivated upon detection of retrograde flow in adult valves (valvular damage, similar to embryonic stages) in order to regenerate cardiac valves in zebrafish (Kefalos, 2019). Interestingly, Notch1 expression is increased in low laminar shear stress (4 dyne/cm²) compared to higher shear stress (10 dyne/cm²) and causes an inflammatory response and plaque formation (Qin, 2016). Low shear stress is found at sites prior to a narrowing of arterial lumen. Overall, at high shear stress with sufficient levels, Notch1 has anti-calcification effects and in low shear stress, it has inflammatory effects.

As well, impaired shear stress (oscillatory shear stress (\pm 5 dyne/cm²)) may lead to atherosclerosis through BMP activation. OSS leads to increased expression of BMP4

in endothelial cells which may lead to cellular proliferation, monocyte adhesion, and inflammation (Sorescu, 2004; Conway, 2010; Dyer, 2014). These are all key steps in early stages of atherosclerosis. In comparison, laminar (“healthy”) shear stress in arteries causes it to be plaque free.

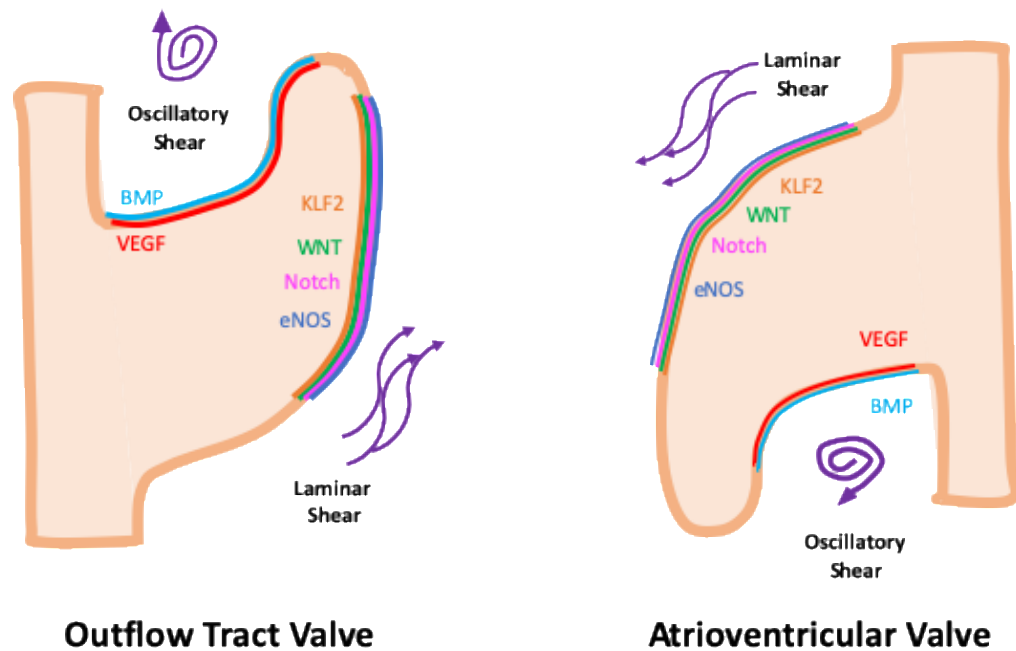


Figure 1.3. Side-specificity of endocardial programs during valve remodeling. The outflow surface of the valve is associated with oscillatory shear stress as well as BMP and VEGF signaling. In contrast, the inflow surface experiences laminar shear stress and is associated with KLF2, WNT, NOTCH, and eNOS signaling.

To study the effects of shear stress on tissue morphogenesis, several *in vivo* interventions in animal models have been used to manipulate blood flow in the developing heart. Notably, by ablating *gata1* and *gata2* genes, which control red blood cell (RBC) production, Vermot et al. has been able to manipulate blood viscosity in

zebra fish and show that shear-sensitive *klf2a* is essential for valvulogenesis. In that study, *gata1*-null zebrafish contained no circulating RBCs, which resulted in a 90% reduction in blood viscosity, while *gata2*-null mutants had 70% lower blood viscosity (Vermot et al., 2009). Besides this method, others have knocked out genes essential for myocardial development and contractility, such as cardiac troponin T (Bartman, 2004) and sodium-calcium exchange protein *Ncx1* gene (Koushik, 2001). Despite the preciseness of genetics-based manipulation methods, ablating genes does affect signaling pathways that can potentially complicate the mechanisms being studied. Alternatively, surgical manipulations in animal models have created a way to study the roles of hemodynamics during heart development without the confounding effects of genetic abnormalities. Due to their 4-chamber heart anatomy and easy access during development, avian embryos have been widely used to study the *in vivo* effects of manipulating blood flow on heart development.

There are many ways to manipulate blood flow through the heart, but most surgical interventions alter hemodynamics by blocking or diminishing blood going in and out of the heart. The most common surgical manipulations include left atrial ligation (LAL) and vitelline vein ligation (VVL), which decreases hemodynamic load and outflow tract banding (OTB), which increases hemodynamic load. Schematics of these surgical interventions are depicted in Figure 1.4 (adapted from Midgett, 2014). The effects of these surgical manipulations on hemodynamics and heart morphogenesis are summarized in Table 1.2 and Table 1.3, respectively.

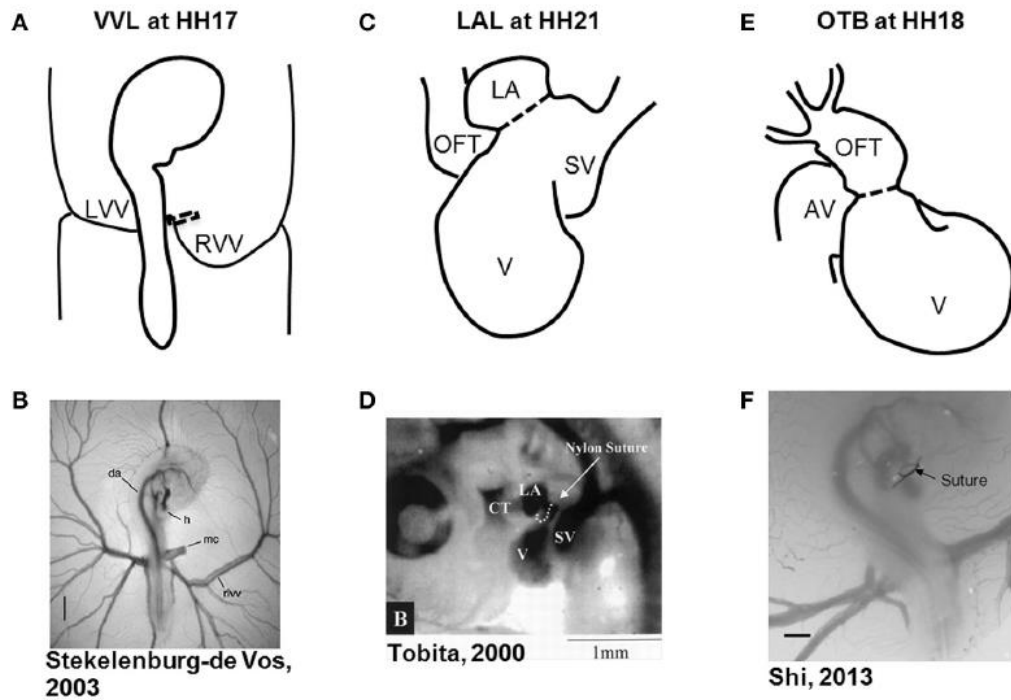


Figure 1.4. Schematics of the common surgical interventions in chick embryos. (Adapted from Midgett, 2014). A and B, Right VVL at HH17. C and D, LAL at HH21. E and F, OTB at HH18. Dotted line represents where the sutures are tied.

Intervention	Preload	Stroke volume	OFT blood velocity
VVL	↑ (Stekelenburg-De Vos, 2007)	↓(acute) (Stekelenburg-De Vos, 2007)	↓(acute) (Rugonyi, 2008)
LAL	↓ (Tobita, 2002)	↓ (Tobita, 2002)	Unknown
OTB	↑ (Shi, 2013)	Unaffected (McQuinn, 2007)	↑ (Rugonyi, 2008)

Table 1.2. The effects of common surgical interventions on heart functions in chick embryos.

Intervention	Heart malformations
VVL	VSD, PAA, AVV, SLV, DORV (Midgett, 2014) VSD, AVV, SLV, DORV (Hogers, 1999)
LAL	LHH, VSD, PAA, AVV, SLV (Midgett, 2014) LHH, VSD (Sedmera, 1999), no AVV (Keller, 2000), SLV (Harh, 1973)
OTB	VSD, PAA, AVV, DORV, TOF (Midgett, 2017) VSD, no AVV, no DORV (Sedmera, 1999)

Table 1.3. Reported heart malformations as a result of common surgical interventions in chick embryos. VSD: ventricular septal defect, PAA: pharyngeal arch artery malformation, AVV: atrioventricular valve malformation, SLV: semilunar valve malformation, DORV: double outlet right ventricle, LHH: left heart hypoplasia.

1.7 Reprogramming of Notch, BMP, & Wnt Signaling in Aortic Valve Disease

Notch1 signaling

Reactivation of developmental pathways has been associated with cancer (Aiello, 2016). Interestingly, many inflammatory pathways responsible for calcific aortic valve disease (CAVD) and myxomatous mitral valve (MMV) are active during valve development (Gretchen 2011), suggesting similar developmental reprogramming in valve diseases. Recently, endocardial Notch1 signaling has been shown to regulate tumor necrosis factor alpha (TNFa) signaling, which in turn regulates mesenchymal cell apoptosis during semilunar valve remodeling (Wang, 2015). Furthermore, TNFa and interleukin-6 have been shown to mediate EMT in embryonic endocardial cells (Nath, 2008; Mahler, 2013) through an NFkB-dependent pathway (Mahler 2013). Mahler et al. also showed that embryonic endocardial cell transformation and invasion requires TGFβ signaling, which is mediated by endocardial Notch1 activation, to drive EMT (Timmerman, 2004). These findings suggest that

Notch1-regulated inflammatory mediators may be co-opted to drive early valve formation, i.e. EMT, and post-EMT valve remodeling processes. Interestingly, we have recently shown that endocardial NFkB signaling mediates endocardial-to-mesenchymal transformation and transmigration during CAVD *in vivo* (Gee, 2020), confirming *in vitro* findings (Hjortnaes, 2015) and supporting the notion that developmental EMT programs driven by inflammatory mediators can become reactivated to drive calcific progression. In contrast, recent endocardial cell lineage analysis showed that EMT is not a feature of myxomatous valve disease, despite *in vitro* experiments that suggested otherwise (Kim, 2019).

On the one hand, Notch1 mutations have been associated with CAVD (Nakaishi, 2016). Specifically, dysfunction of the valvular endocardium is thought to attenuate nitric oxide (NO) secretion by the endocardial cells and mediates valve calcification (Richards, 2013). Endocardial NO has been shown to regulate calcification by valve interstitial cells (VICs) by inhibiting Notch1, signaling in VICs (Bosse, 2013). On the other hand, inhibition of DLL4 attenuates inflammation as well as inhibits osteogenic factors, BMPs, and valve calcification (Fakuda, 2012). Furthermore, since Notch1 mutation cannot explain all clinical cases of CAVD, the role of Notch1 is more complex and might involve differential ligand interactions. Recently, we have shown that disruption to endocardial Notch1 signaling leads to augmentation of endocardial NFkB signaling, endocardial activation, and valve calcification (Gee, in preparation). Interestingly, disease background mice exhibited lower expression of Jag1 compared to the WT control (Figure 1.4B and C). It is conceivable that DLL4 and JAG1 play

differential roles in CAVD that resemble those in valve development. In fact, recent evidence suggests that while DLL4/Notch1 is required to drive EMT during early valve formation, JAG1/Notch1 signaling is required for post-EMT valve remodeling (MacGrogan, 2016). It is possible that Jag1/Notch1 signaling persists into adulthood to maintain endocardial homeostasis, and disruption to the balance of DLL4/JAG1 could lead to endocardial dysfunction, activation, and calcification.

Of note, expression of Jag1 is localized on the ventricularis side in healthy WT mice (Figure 1.4B), suggesting that Notch signaling is regulated by high unidirectional shear stress instead of oscillatory shear stress. The attenuation of Jag1 expression in disease background valve indicates that aberrant Notch1 signaling that results in CAVD could be due to perturbed hemodynamics. In fact, fluid shear stress that deviates from homeostatic patterns has been associated with endocardial dysfunction and inflammation in the valves (Hoehn, 2010). During development, Notch1 seems to be regulated by fluid shear stress as NICD1, indicative of active Notch1 signaling, has been associated with endocardial cells on the ventricular side, but not those on the fibrosa side (Macgrogan, 2016; Wang, 2015). Furthermore, Notch1 signaling has been shown to regulate EMT through activating soluble guanylyl cyclase by NO (Chang, 2011). During valve remodeling, NO production via eNOS continues to be associated with Notch1 signaling in the endocardial cells on the ventricular side (Figure 4A), suggesting that shear-driven Notch1 signaling could relay hemodynamic information to the subendocardial mesenchymal cells via NO in a paracrine fashion. Even though the exact contributions of NO during valve remodeling remain to be elucidated, these

findings suggest that the Shear/Notch1/NO axis regulates valve homeostasis and modulates CAVD progression.

BMP signaling

BMP signaling is critical for early valve formation as it sets up an environment conducive for EMT by coordinating with Notch and TGF β signaling (Garside, 2013). During valve remodeling, BMP regulates mesenchymal cell proliferation and matrix remodeling, and disruption to programs that modulate BMP signaling leads to hyperplastic valves (Jackson, 2003; Sierro, 2007; MacGrogan, 2016). Multiple lines of evidence have shown that BMP signaling becomes quiescent during adulthood and reactivated in CAVD. Specifically, BMP2 and BMP4 have been detected and associated with inflammation in calcific human aortic valves (Mohler, 2001). In diseased valves, psmad1/5/8 nuclear expression has also been detected in VICs and associated with increased cell proliferation, myofibroblastic activation, and disorganized matrix (Wirrig, 2011; Ankeny, 2011). Interestingly, haploinsufficiency of Smad6, a cytoplasmic inhibitor of BMP signaling, has been associated with CAVD. Recently, ablation of the BMPRIa *in vivo* and inhibition of BMP activity using LDN193189 *in vitro* have been shown to inhibit aortic valve calcification (Gomez-Stallons, 2016). These data suggest that BMP signaling is reactivated in CAVD and required for calcification progression.

Interestingly, elevation of BMP signaling, inflammation, and calcified nodules are localized on the fibrosa side of the aortic valve leaflets (Ankeny, 2011), suggesting that perturbed OSS is associated with CAVD initiation. During valve remodeling, we have shown, for the first time, that BMP ligand expression and activation in

endocardial cells are driven by OSS and required for endocardial proliferation (Chapter 3). These data suggest that perturbed hemodynamics could bring out reactivation of BMP programs to induce inflammation and CAVD.

WNT signaling

As with Notch and BMP signaling, canonical WNT signaling (via β -catenin) has been linked to EMT during early valve formation (Person, 2005) and mesenchymal cell proliferation during valve remodeling (Wang 2018). Canonical WNT signaling is associated with human calcified valves (Caira, 2006) and porcine VICs (Gu, 2014) and is thought to mediate VIC activation (Chen, 2011) and osteogenic differentiation (Hartmann, 2006). However, contributions of canonical WNT signaling to CAVD initiation and/or progression remain unclear. Interestingly, more recent evidence suggests that WNT5b and WNT11 ligands are present in the calcified areas, suggesting that non-canonical WNT signaling (via MAP kinase) is also associated with CAVD (Albenese, 2017). Specifically, non-canonical WNT signaling can promote apoptosis, osteogenesis, and matrix deposition in human VICs, which are the hallmarks of CAVD (Albenese, 2017). Interestingly, during development, WNT signaling in the myocardium is associated with BMP ligand expression and BMP activation of mesenchymal cells in the valvular proper (Wang, 2018). Furthermore, since WNT and BMP are tightly correlated with the calcification progression, it is conceivable that WNT could also regulate BMP signaling in CAVD.

As with Notch and BMP signaling, WNT signaling is also linked to mechanical stress in valve development and disease. During valve remodeling, mesenchymal cells

positive for WNT reporter signal concentrate on the fibrosa side (Wang, 2018), while WNT canonical and non-canonical ligands are expressed in endocardial cells on the ventricular side (Goddard, 2017; Wang, 2015). These data suggest that while high unidirectional shear stress could drive WNT ligand expression, it is oscillatory shear that primes the endocardial and mesenchymal cells to respond to WNT. In fact, while WNT5b and 11 ligand expression is strongly correlated with aortic jet velocity, maximum pressure across valve (Pmax), and hypertension (Albenese, 2017), WNT signaling is associated with calcific nodules located in the fibrosa (Caira, 2006). Despite strong correlation with the calcification of VICs in CAVD, the requirement of BMP or WNT for CAVD has not been demonstrated (Menon, 2018). Future studies will need to address whether BMP or WNT can initiate and cause CAVD.

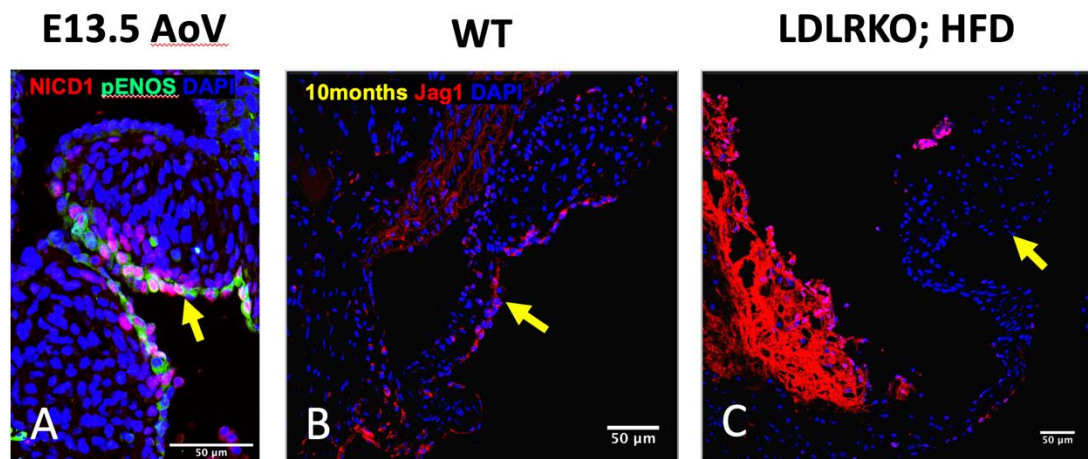


Figure 1.5. Side-specificity of Notch/eNOS signaling during valve development and disease. (A) Immunostaining of Notch1 intracellular domain (NICD1), indicating active Notch1 signaling, and phosphorylated eNOS (pENOS), indicating active nitric oxide production. Yellow arrow indicates endocardial cells constaining with NICD1 and pENOS. (B, C) Immunostaining of Jag1 in calcific aortic valve disease background mice fed with high fat diet (LDLRKO;HFD) and wildtype (WT) controls. Yellow arrow indicates endocardial cells positive for cytoplasmic Jag1.

1.8 Regulation of Cell Proliferation in Valve Development and Disease

Cellular proliferation is thought to contribute to the initiation and progression of CAVD and mitral valve prolapse (MVP) (Loardi, 2011; Kaden, 2005). Therefore, investigating proliferation in valve development can augment our understanding and treatment of valve disease, both congenital and adult.

TGFβ/BMP

TGFβ has been implicated in EMT of the early heart valve (Combs, 2009), but there is evidence that it is also involved in post-EMT proliferation. Wounded VICs exhibit increased TGFβ signaling and proliferation. When treated with a TGFβ - neutralizing antibody, this increase in proliferation is attenuated (Liu, 2008). Inactivated TGFβ signaling by knocking out TGFβR2 in mice decreases proliferation in

inferior AVC mesenchymal cell at E11.5 and E12.5 (Jiao, 2006). TGF β is also involved in apoptosis signaling. TGF β 2 complete knockout mice show a difference in timing and amount of apoptosis in the OFT (Bartram, 2001). Furthermore, ovine endothelial progenitor cells treated with TGF β 1 became proliferative (Sales, 2006).

BMP is a member of the TGF β superfamily and has been shown to be required for EMT in AVCs and required for their development, though surprisingly not required for OFT development (Sugi, 2004). It regulates Twist1 expression through interaction with the BMPR1a receptor in the AV canal (Ma, 2005). Interestingly, Inactivation of BMP4 does not affect EMT in mice endocardial cushions, but causes hypoplasia in OFT cushions at E10.5 and onward, leading to neonatal lethality (McCulley, 2008). Though BMP6 and BMP7 complete knockouts do not express defects in cardiac formation (Garside, 2013), BMP6/7 double knockouts have aberrant proliferation regulation in the OFT cushions, but AVC cushions are unaffected (Kim, 2001). Apoptosis in these knockouts is unaffected. Furthermore, mice that lack the BMP inhibitor Smad6 have increased proliferation in mesenchymal cells (Galvin, 2000).

Twist1/Tbx20

Twist1 is a basic helix-loop-helix transcription factor that is implicated in cell proliferation, migration, and differentiation in embryonic progenitor populations (Shelton, 2008). During valve development, it is expressed in the OFT and AV cushions, and downregulated during remodeling (Chakraborty, 2010). Sustained Twist1 expression promotes proliferation in late embryonic AV valves leaflets, but this effect

diminishes in post-neonatal mice (Chakraborty, 2010). Tbx20 is a T-box transcription factor that is involved in cushion maturation and valve development that has been associated in humans with defects in septation, chamber growth, and valvulogenesis (Shelton, 2007). BMP2 induces both Twist1 and Tbx20 expression (Shelton, 2008), and Twist1 can also bind directly to enhancer elements to promote Tbx20 expression (Lee, 2011). Both Twist1 and Tbx20 are able to promote cushion cell proliferation and migration (Shelton, 2008; Shelton, 2007). One pathway that Tbx20 may do so is through direct regulation of Lef1, a key transcriptional regulator of the Wnt/b-catenin signaling pathway (Cai, 2013). Its importance in heart development is underlined by the fact that mutations in Tbx20 are associated with defects in septation, chamber growth, and valvulogenesis (Shelton, 2008).

Wnt

The conserved Wnt signal pathway controls a wide variety of developmental processes, including proliferation and differentiation. In human adults, increased Wnt expression is associated with CAVD (Alfieri, 2010; Gao, 2015). Wnt signaling is known to be involved in early valve development, but its role in later stages of development has only recently been investigated. At E12.5, Wnt2 is expressed in the cushion mesenchyme and Wnt4 and Wnt9b are expressed in the endothelial cells. At E17.5, Wnt3a and Wnt7b is expressed in the remodeling AV and OFT valves (Alfieri, 2010). In porcine VIC explants, Wnt3a treatment increases proliferation, but this effect is dependent on b-catenin. Apoptosis, on the other hand, is unaffected by the Wnt3a

treatment (Xu, 2013). Wnt9a is expressed in early AV cushion endothelial cells and restricted expression persists throughout later stages (Person, 2005). It mediates b-catenin expression and its overexpression can lead to hyperplasia due to increased proliferation and decreased apoptosis of the cushion cells (Person, 2005). Wnt4 regulates the expression of BMP2 in the early AV canal, and is itself regulated by Notch1. However, knocking out this Notch-Wnt-BMP axis appears to affect EMT and not proliferation in the early developing cushion (Wang, 2013). Overall, Wnt/b-catenin signaling is a promising area of research that has direct impact on the study of heart disease.

Sox9

Sox9 is an SRY-related transcription factor that is related to cartilage formation and male sex determination (Lincoln, 2007). In humans, aberrant Sox9 activity has been linked to vascular calcification (Neven, 2007). In mouse and chick embryos, it is expressed in the endocardial cushions and remodeling leaflets, while loss of Sox9 results in hypoplastic cushions and embryonic lethality between E11.5 and E12.5 (Chakraborty, 2010). Tie2-cre conditional knockouts of Sox9 exhibit hypoplastic cushions related to decreased post-EMT mesenchymal cell proliferation (Lincoln, 2007). This behavior is seen also in the AVCs of E12.5 Zp3-cre and Prm1-cre conditional knockouts (Aiyama, 2004). Indeed, it has been shown that in E12.5 AVCs, Sox9 binds directly to a multitude of genes involved in cell cycle and cell proliferation, including

Trp53 and Fgfr2.31 (Garside, 2015). In cultured avian cushion cells, BMP2 treatment upregulates Sox9 expression (Lincoln, 2006).

HB-EGF

The epidermal growth factor (EGF)-ErbB signaling network includes polypeptide ligands of the EGF family, which includes heparin-binding epidermal growth factor (HB-EGF). HB-EGF binds to three of four of the EGF receptors, EGFR/ErbB1, ErbB2 and ErbB4 (Jackson, 2003; Iwamoto, 2003). Complete HB-EGF knockout mice exhibit aberrant BMP signaling, increased activation of pSmad1/5/8. They also show increased proliferation (but no difference in apoptosis) at E14.5, in both AV and OFT cushions (Jackson, 2003). Thus, HB-EGF secreted from the endocardium inhibits proliferation of mesenchymal cells during remodeling (Iwamoto, 2010). Both ErbB2 knockout and conditional ErbB4 knockout mice develop symptoms resembling human dilated cardiomyopathy (DCM), one of the most fatal cardiac diseases (Iwamoto, 2006).

FGF4

Fibroblast growth factors (FGFs) belong to a heparin-binding protein family that regulate tissue differentiation and patterning and are potent mitogens for endothelial and mesenchymal cells (Sugi, 2003). FGF-4, specifically, is localized in cushion mesenchymal cells in chick stage HH20-25. Receptor FGFR3 expression is confined to the endocardial rim of the AV cushions, while FGFR2 is expressed only in mesenchymal cells. FGFR1 is expressed in both cell populations, as well as in myocardium. When

cushion mesenchymal cells are treated with FGF4, they show significant increases in proliferation (Sugi, 2003). It also demonstrates an antagonistic relationship with BMP2. Treatment of valve precursor cells from perfused cushions with FGF4 or inhibition of BMP signaling promotes scleraxis and tenascin expression in association with dpERK1/2. In contrast, BMP2 treatment or inhibition of FGF signaling induces expression of sox9 and aggrecan (Lincoln, 2006). While FGF4 is involved in mesenchymal proliferation, this evidence also highlights its role in valve cell differentiation.

Notch

Notch is a conserved signaling pathway that regulates cell specification, differentiation, and patterning. Mutations in the Notch pathway is correlated with congenital heart disease and valve calcification (Garg, 2005; MacGrogan, 2011). The Notch signaling pathway is also one that is highly implicated in early valvulogenesis, but its role in post-EMT valve remodeling has again only recently been investigated. Jag1, a Notch1 ligand, can transcriptionally upregulate HB-EGF (Guillermo, 2016), which inhibits mesenchymal cell proliferation (Iwamoto, 2010). Attenuated Notch1 expression in endothelial cells of post-EMT valves results in stenosis of arterial valves, likely caused by increased mesenchymal proliferation in these N1KO mice (Wang 2017). Endothelial-specific Notch1 signaling also promotes expression of Tnf α , which interacts with interstitial cushion cells to induce apoptosis, and N1KO mice also exhibit reduced apoptosis in this cell population (Wang, 2017). Further studies are needed to

determine the downstream targets of Notch in post-EMT remodeling and proliferation.

Nfatc1

Nuclear factor of activated T cells, cytoplasmic 1 (Nfatc1) is a transcription factor that belongs to the NFAT family, and is required for valve formation (Chakraborty, 2010). Mutations of the Nfatc1 gene have been identified in cases of congenital heart defects and tricuspid atresia (Wu, 2013), and expression of the RANKL/Nfatc1 pathway is implicated in calcification of human valves (Combs, 2009). Nfatc1 regulates EMT, and overexpression of Nfatc1 between E10.5 and E12.5 in AV and OFT valve endocardial cells prevents them from undergoing EMT. Loss of Nfatc1 function causes enhanced EMT and decreased proliferation of valve endocardium and mesenchyme in the same time frame, leading to hypoplastic valves at E13.5 (Combs, 2009). Furthermore, loss of calcineurin (Cn) and therefore Cn/Nfatc1 signaling increases apoptosis of the pulmonary valve at E14.5, leading to regression of the cushions and failure to develop valves (Lin, 2012). These studies demonstrate that Nfatc1 is a molecular switch that first induces endocardial cells to undergo EMT, and then post-EMT valve remodeling (Wu, 2013).

VEGF

Vascular endothelial growth factor (VEGF) is an angiogenic factor that is involved in endothelial cell adhesion, cell cycle, and inflammatory cell recruitment during development. VECs treated with VEGF exhibit increased proliferation, which is

induced by VEGFR2 activation of Cn/Nfatc1 and MEK1-ERK1/2 copathways (Comb, 2009). RANKL (receptor activator of nuclear factor κ B ligand) inhibits this increase, and instead promotes expression of an ECM-remodeling enzyme CtsK. In vivo, the VEGF pathway is localized to the proliferating endocardial cells, whereas RANKL is expressed in the valve primordia later in development (Combs, 2009).

ERK1/2 activation and more generally, MAPK signaling is also implicated in the regulation of cushion proliferation. Shp2 is a nonreceptor tyrosine phosphatase that can augment the ERK1/2 pathway. The Q76R-Shp2 mutation causes Noonan syndrome, characterized by dysmorphic features, cardiac abnormalities, and pulmonic stenosis. AV cushion cells with the mutation, which causes increased activity of Shp2, demonstrate increased proliferation. Knocking out the upstream MEK1, this effect disappears (Krenz, 2005). VEGF and RANKL are promising future targets for the study of post-EMT remodeling and valve cell proliferation.

1.9 Thesis Objectives

Even though much of early valve formation involving EMT has been extensively studied, post-EMT valve remodeling remains to be investigated. This is a critical gap in our knowledge because (1) the majority of valve malformations persist into adulthood because the valve primordia do not remodel properly; loss of function studies targeting EMT generally resulted in embryonic lethality and (2) a better understanding of valve remodeling processes inform better therapeutic and engineering strategies for

treating valve diseases; reactivation of developmental pathways has been associated with valve disease initiation and progression.

Heart development relies heavily on the interaction between hemodynamics and cellular programs. This dissertation was thus guided by the central hypothesis that endocardial cells lining the valve transduce mechanical information into biological programs that regulate the four hallmarks of valve remodeling: cell proliferation, cellular differentiation, tissue compaction, and matrix maturation. We addressed this guiding hypothesis by examining the role of chemokine receptor CXCR4 in regulating valve remodeling in chapter 2 and the regulation of endocardial proliferation during valve extension in chapter 3. CXCR4 is a G-protein couple receptor, which binds to its ligand CXCL12 to regulate cell migration during chemotaxis in various contexts (Kiefer, 2011; Teicher, 2010). During development, CXCR4 is important for the migration of endothelial cells (Li, 2013) and cardiac neural crest cells (Escot, 2013) into the heart. Interestingly, global ablation of CXCR4 or CXCL12 has resulted in embryonic lethality, likely due to defects in hematopoiesis, cerebellar development, and cardiac ventricular septal defects (Nagasawa, 1996; Ma, 1998; Zhou, 1998). Interestingly, CXCR4 has been detected in valvular regions during early development, but whether CXCR4 regulates functions of endocardial or mesenchymal cells is unclear. Furthermore, even though CXCR4 is thought to promote cell proliferation, early reports of valve phenotype showed that valves of CXCR4 null mice are thickened and enlarged, suggesting that CXCR4 actually modulates cell proliferation. In chapter 3, we will attempt to add to the discussion of endocardial proliferation by addressing how

differential shear stress environments result in differential endocardial proliferation programs. We will do this by subjecting primary endocardial cells to shear stress of various modes and magnitudes and measuring their molecular responses. We found that BMP is responsive to low oscillatory shear stress, while Notch1 is responsive to high unidirectional shear stress. These programs implicate that since different sides of the valve experience different hemodynamic stimuli, endocardial programs are not uniform across the endocardium. We postulate that these shear-induced differences drive the asymmetrical shaping of the valves during post-EMT remodeling stages.

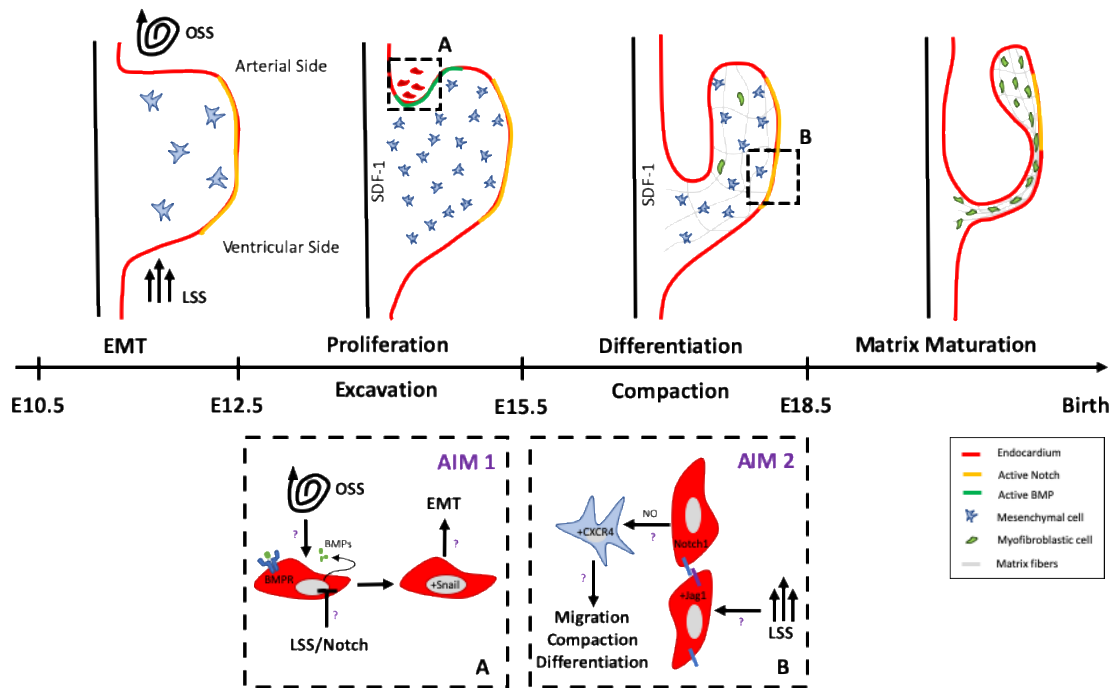


Figure 1.6. Proposed mechanism of cushion excavation and compaction. At E11.5, after cushion formation in the outflow tract, oscillatory shear stress (OSS) induces the production of bone morphogenetic proteins (BMPs) by the endocardium on the arterial side, while laminar shear stress (LSS) drives Notch1 signaling in the endocardium on the ventricular side. OSS-induced BMP activity increases endocardial proliferation on the arterial side. Meanwhile, LSS-driven Notch1 stimulates subendocardial cells to express CXCR4, which in turn drives cellular differentiation, migration, and matrix compaction.

1.10 References

1. Aiello, N. M., & Stanger, B. Z. (2016). Echoes of the embryo: using the developmental biology toolkit to study cancer. *Disease models & mechanisms*, 9(2), 105-114.
2. Albanese, I., Yu, B., Al-Kindi, H., Barratt, B., Ott, L., Al-Refai, M., ... & Rhéaume, E. (2017). Role of noncanonical Wnt signaling pathway in human aortic valve calcification. *Arteriosclerosis, thrombosis, and vascular biology*, 37(3), 543-552.
3. Anderson, R. H., Mori, S., Spicer, D. E., Brown, N. A., & Mohun, T. J. (2016). Development and morphology of the ventricular outflow tracts. *World Journal for Pediatric and Congenital Heart Surgery*, 7(5), 561-577.
4. Ankeny, R. F., Thourani, V. H., Weiss, D., Vega, J. D., Taylor, W. R., Nerem, R. M., & Jo, H. (2011). Preferential activation of SMAD1/5/8 on the fibrosa endothelium in calcified human aortic valves-association with low BMP antagonists and SMAD6. *PloS one*, 6(6).
5. Beatus, P., Lundkvist, J., Öberg, C., Pedersen, K., & Lendahl, U. (2001). The origin of the ankyrin repeat region in Notch intracellular domains is critical for regulation of HES promoter activity. *Mechanisms of development*, 104(1), 3-20.
6. Bonachea, E. M., Zender, G., White, P., Corsmeier, D., Newsom, D., Fitzgerald-Butt, S., ... & McBride, K. L. (2014). Use of a targeted, combinatorial next-generation sequencing approach for the study of bicuspid aortic valve. *BMC medical genomics*, 7(1), 56.
7. Bosada, F. M., Devasthali, V., Jones, K. A., & Stankunas, K. (2016). Wnt/ β -catenin signaling enables developmental transitions during valvulogenesis. *Development*, 143(6), 1041-1054.
8. Bosse, K., Hans, C. P., Zhao, N., Koenig, S. N., Huang, N., Guggilam, A., ... & Lilly, B. (2013). Endothelial nitric oxide signaling regulates Notch1 in aortic valve disease. *Journal of molecular and cellular cardiology*, 60, 27-35.
9. Brou, C., Logeat, F., Gupta, N., Bessia, C., LeBail, O., Doedens, J. R., ... & Israël, A. (2000). A novel proteolytic cleavage involved in Notch signaling: the role of the disintegrin-metalloprotease TACE. *Molecular cell*, 5(2), 207-216.
10. Caira, F. C., Stock, S. R., Gleason, T. G., McGee, E. C., Huang, J., Bonow, R. O., ... & Rajamannan, N. M. (2006). Human degenerative valve disease is associated with up-regulation of low-density lipoprotein receptor-related protein 5 receptor-mediated bone formation. *Journal of the American College of Cardiology*, 47(8), 1707-1712.

11. Chang, A. C., Fu, Y., Garside, V. C., Niessen, K., Chang, L., Fuller, M., ... & Marra, M. (2011). Notch initiates the endothelial-to-mesenchymal transition in the atrioventricular canal through autocrine activation of soluble guanylyl cyclase. *Developmental cell*, 21(2), 288-300.
12. Chen, J. H., & Simmons, C. A. (2011). Cell–matrix interactions in the pathobiology of calcific aortic valve disease: critical roles for matricellular, matricrine, and matrix mechanics cues. *Circulation research*, 108(12), 1510-1524.
13. Choi, M., Stottmann, R. W., Yang, Y. P., Meyers, E. N., & Klingensmith, J. (2007). The bone morphogenetic protein antagonist noggin regulates mammalian cardiac morphogenesis. *Circulation research*, 100(2), 220-228.
14. Clevers, H., & Nusse, R. (2012). Wnt/ β -catenin signaling and disease. *Cell*, 149(6), 1192-1205.
15. Conway, D. E., Williams, M. R., Eskin, S. G., & McIntire, L. V. (2010). Endothelial cell responses to atheroprone flow are driven by two separate flow components: low time-average shear stress and fluid flow reversal. *American journal of physiology. Heart and circulatory physiology*, 298(2), H367–H374.
16. Dargis, N., Lamontagne, M., Gaudreault, N., Sbarra, L., Henry, C., Pibarot, P., ... & Bossé, Y. (2016). Identification of gender-specific genetic variants in patients with bicuspid aortic valve. *The American journal of cardiology*, 117(3), 420-426.
17. De Strooper, B., Annaert, W., Cupers, P., Saftig, P., Craessaerts, K., Mumm, J. S., ... & Goate, A. (1999). A presenilin-1-dependent γ -secretase-like protease mediates release of Notch intracellular domain. *Nature*, 398(6727), 518-522.
18. de Vlaming, A., Sauls, K., Hajdu, Z., Visconti, R. P., Mehesz, A. N., Levine, R. A., ... & Norris, R. A. (2012). Atrioventricular valve development: new perspectives on an old theme. *Differentiation*, 84(1), 103-116.
19. Dejana, E. (2010). The role of wnt signaling in physiological and pathological angiogenesis. *Circulation research*, 107(8), 943-952.
20. Dupuis, L. E., Osinska, H., Weinstein, M. B., Hinton, R. B., & Kern, C. B. (2013). Insufficient versican cleavage and Smad2 phosphorylation results in bicuspid aortic and pulmonary valves. *Journal of molecular and cellular cardiology*, 60, 50-59.
21. Dyer, L. A., Pi, X., & Patterson, C. (2014). The role of BMPs in endothelial cell function and dysfunction. *Trends in Endocrinology & Metabolism*, 25(9), 472-480.

22. Fahed, A. C., Gelb, B. D., Seidman, J. G., & Seidman, C. E. (2013). Genetics of congenital heart disease: the glass half empty. *Circulation research*, 112(4), 707-720.
23. Fahed, A. C., Gelb, B. D., Seidman, J. G., & Seidman, C. E. (2013). Genetics of congenital heart disease: the glass half empty. *Circulation research*, 112(4), 707-720.
24. Fukuda, D., Aikawa, E., Swirski, F. K., Novobrantseva, T. I., Kotelianski, V., Gorgun, C. Z., ... & Aster, J. C. (2012). Notch ligand delta-like 4 blockade attenuates atherosclerosis and metabolic disorders. *Proceedings of the national Academy of Sciences*, 109(27), E1868-E1877.
25. Galvin, K. M., Donovan, M. J., Lynch, C. A., Meyer, R. I., Paul, R. J., Lorenz, J. N., ... & Falb, D. (2000). A role for smad6 in development and homeostasis of the cardiovascular system. *Nature genetics*, 24(2), 171-174.
26. Garside, V. C., Chang, A. C., Karsan, A., & Hoodless, P. A. (2013). Co-ordinating Notch, BMP, and TGF- β signaling during heart valve development. *Cellular and molecular life sciences*, 70(16), 2899-2917.
27. Garside, V. C., Cullum, R., Alder, O., Lu, D. Y., Vander Werff, R., Bilenky, M., ... & Hoodless, P. A. (2015). SOX9 modulates the expression of key transcription factors required for heart valve development. *Development*, 142(24), 4340-4350.
28. Gee, T., Farrar, E., Wang, Y., Wu, B., Hsu, K., Zhou, B., & Butcher, J. (2020). NF κ B (Nuclear Factor κ -Light-Chain Enhancer of Activated B Cells) Activity Regulates Cell-Type-Specific and Context-Specific Susceptibility to Calcification in the Aortic Valve. *Arteriosclerosis, Thrombosis, and Vascular Biology*, ATVBAHA-119.
29. Goddard, L. M., Duchemin, A. L., Ramalingan, H., Wu, B., Chen, M., Bamezai, S., ... & Scherrer-Crosbie, M. (2017). Hemodynamic forces sculpt developing heart valves through a KLF2-WNT9B paracrine signaling axis. *Developmental cell*, 43(3), 274-289.
30. Goetz, J. G., Steed, E., Ferreira, R. R., Roth, S., Ramspacher, C., Boselli, F., ... & Vermot, J. (2014). Endothelial cilia mediate low flow sensing during zebrafish vascular development. *Cell reports*, 6(5), 799-808.
31. Gomez-Stallons, M. V., Wirrig-Schwendeman, E. E., Hassel, K. R., Conway, S. J., & Yutzey, K. E. (2016). Bone morphogenetic protein signaling is required for aortic valve calcification. *Arteriosclerosis, thrombosis, and vascular biology*, 36(7), 1398-1405.

32. Graham, T. (2011). Comparison of clinical presentations and outcomes between patients with TGFBR2 and FBN1 mutations in Marfan syndrome and related disorders. *Yearbook of Cardiology*, 2011, 142-3.
33. Gu, G. J., Chen, T., Zhou, H. M., Sun, K. X., & Li, J. (2014). Role of Wnt/ β -catenin signaling pathway in the mechanism of calcification of aortic valve. *Journal of Huazhong University of Science and Technology [Medical Sciences]*, 34(1), 33-36.
34. Hartmann, C. (2006). A Wnt canon orchestrating osteoblastogenesis. *Trends in cell biology*, 16(3), 151-158.
35. Hata, A., Lagna, G., Massagué, J., & Hemmati-Brivanlou, A. (1998). Smad6 inhibits BMP/Smad1 signaling by specifically competing with the Smad4 tumor suppressor. *Genes & development*, 12(2), 186-197.
36. Hinton Jr, R. B., Lincoln, J., Deutsch, G. H., Osinska, H., Manning, P. B., Benson, D. W., & Yutzey, K. E. (2006). Extracellular matrix remodeling and organization in developing and diseased aortic valves. *Circulation research*, 98(11), 1431-1438.
37. Hjortnaes, J., Shapero, K., Goettsch, C., Hutcheson, J. D., Keegan, J., Kluin, J., ... & Aikawa, E. (2015). Valvular interstitial cells suppress calcification of valvular endothelial cells. *Atherosclerosis*, 242(1), 251-260.
38. Hoehn, D., Sun, L., & Sucusky, P. (2010). Role of pathologic shear stress alterations in aortic valve endothelial activation. *Cardiovascular Engineering and Technology*, 1(2), 165-178.
39. Hofmann, J. J., Briot, A., Enciso, J., Zovein, A. C., Ren, S., Zhang, Z. W., ... & Iruela-Arispe, M. L. (2012). Endothelial deletion of murine Jag1 leads to valve calcification and congenital heart defects associated with Alagille syndrome. *Development*, 139(23), 4449-4460.
40. Hurle, J. M., Colvee, E., & Blanco, A. M. (1980). Development of mouse semilunar valves. *Anatomy and embryology*, 160(1), 83-91.
41. Jackson, L. F., Qiu, T. H., Sunnarborg, S. W., Chang, A., Zhang, C., Patterson, C., & Lee, D. C. (2003). Defective valvulogenesis in HB-EGF and TACE-null mice is associated with aberrant BMP signaling. *The EMBO journal*, 22(11), 2704-2716.
42. Jahnsen, E. D., Trindade, A., Zaun, H. C., Lehoux, S., Duarte, A., & Jones, E. A. (2015). Notch1 is pan-endothelial at the onset of flow and regulated by flow. *PloS one*, 10(4).

43. Jiang, R., Lan, Y., Chapman, H. D., Shawber, C., Norton, C. R., Serreze, D. V., ... & Gridley, T. (1998). Defects in limb, craniofacial, and thymic development in Jagged2 mutant mice. *Genes & development*, 12(7), 1046-1057.
44. Joannes, A., Brayer, S., Besnard, V., Marchal-Sommé, J., Jaillet, M., Mordant, P., ... & Mailleux, A. A. (2016). FGF9 and FGF18 in idiopathic pulmonary fibrosis promote survival and migration and inhibit myofibroblast differentiation of human lung fibroblasts in vitro. *American Journal of Physiology-Lung Cellular and Molecular Physiology*, 310(7), L615-L629.
45. Kam, Y., & Quaranta, V. (2009). Cadherin-bound β -catenin feeds into the Wnt pathway upon adherens junctions dissociation: evidence for an intersection between β -catenin pools. *PloS one*, 4(2).
46. Kefalos, P., Agalou, A., Kawakami, K., & Beis, D. (2019). Reactivation of Notch signaling is required for cardiac valve regeneration. *Scientific reports*, 9(1), 1-8.
47. Kim, A. J., Alfieri, C. M., & Yutzey, K. E. (2019). Endothelial cell lineage analysis does not provide evidence for EMT in adult valve homeostasis and disease. *The Anatomical Record*, 302(1), 125-135.
48. Koenig, S. N., Bosse, K., Majumdar, U., Bonachea, E. M., Radtke, F., & Garg, V. (2016). Endothelial Notch1 is required for proper development of the semilunar valves and cardiac outflow tract. *Journal of the American Heart Association*, 5(4), e003075.
49. Kokubo, H., Tomita-Miyagawa, S., Hamada, Y., & Saga, Y. (2007). Hesr1 and Hesr2 regulate atrioventricular boundary formation in the developing heart through the repression of Tbx2. *Development*, 134(4), 747-755.
50. Kostina, A. S., Uspensky, V. E., Irtyuga, O. B., Ignatieva, E. V., Freylikhman, O., Gavriliuk, N. D., ... & Malashicheva, A. B. (2016). Notch-dependent EMT is attenuated in patients with aortic aneurysm and bicuspid aortic valve. *Biochimica et Biophysica Acta (BBA)-Molecular Basis of Disease*, 1862(4), 733-740.
51. Kostina, A., Bjork, H., Ignatieva, E., Irtyuga, O., Uspensky, V., Semenova, D., ... & Gordeev, M. (2018). Notch, BMP and WNT/ β -catenin network is impaired in endothelial cells of the patients with thoracic aortic aneurysm. *Atherosclerosis Supplements*, 35, e6-e13.
52. Krebs, L. T., Shutter, J. R., Tanigaki, K., Honjo, T., Stark, K. L., & Gridley, T. (2004). Haploinsufficient lethality and formation of arteriovenous malformations in Notch pathway mutants. *Genes & development*, 18(20), 2469-2473.

53. Krebs, L. T., Xue, Y., Norton, C. R., Sundberg, J. P., Beatus, P., Lendahl, U., ... & Gridley, T. (2003). Characterization of Notch3-deficient mice: Normal embryonic development and absence of genetic interactions with a Notch1 mutation. *Genesis*, 37(3), 139-143.
54. Kurooka, H., Kuroda, K., & Honjo, T. (1998). Roles of the ankyrin repeats and C-terminal region of the mouse notch1 intracellular region. *Nucleic acids research*, 26(23), 5448-5455.
55. Lee, J., Fei, P., Packard, R. R. S., Kang, H., Xu, H., Baek, K. I., ... & Chi, N. C. (2016). 4-Dimensional light-sheet microscopy to elucidate shear stress modulation of cardiac trabeculation. *The Journal of clinical investigation*, 126(5), 1679-1690.
56. Li, R., Beebe, T., Jen, N., Yu, F., Takabe, W., Harrison, M., ... & Wang, K. (2014). Shear stress-activated Wnt-Angiopoietin-2 signaling recapitulates vascular repair in zebrafish embryos. *Arteriosclerosis, thrombosis, and vascular biology*, 34(10), 2268-2275.
57. Li, Y. S. J., Haga, J. H., & Chien, S. (2005). Molecular basis of the effects of shear stress on vascular endothelial cells. *Journal of biomechanics*, 38(10), 1949-1971.
58. Lincoln, J., Alfieri, C. M., & Yutzey, K. E. (2006). BMP and FGF regulatory pathways control cell lineage diversification of heart valve precursor cells. *Developmental biology*, 292(2), 290-302.
59. Loomes, K. M., Taichman, D. B., Glover, C. L., Williams, P. T., Markowitz, J. E., Piccoli, D. A., ... & Oakey, R. J. (2002). Characterization of Notch receptor expression in the developing mammalian heart and liver. *American Journal of Medical Genetics Part A*, 112(2), 181-189.
60. Luna-Zurita, L., Prados, B., Grego-Bessa, J., Luxán, G., del Monte, G., Benguría, A., ... & de la Pompa, J. L. (2010). Integration of a Notch-dependent mesenchymal gene program and Bmp2-driven cell invasiveness regulates murine cardiac valve formation. *The Journal of clinical investigation*, 120(10), 3493.
61. Luxán, G., D'Amato, G., MacGrogan, D., & de la Pompa, J. L. (2016). Endocardial notch signaling in cardiac development and disease. *Circulation research*, 118(1), e1-e18.
62. Ma, L., Lu, M. F., Schwartz, R. J., & Martin, J. F. (2005). Bmp2 is essential for cardiac cushion epithelial-mesenchymal transition and myocardial patterning. *Development*, 132(24), 5601-5611.

63. MacGrogan, D., D'Amato, G., Trivisano, S., Martinez-Poveda, B., Luxán, G., del Monte-Nieto, G., ... & Gómez, M. J. (2016). Sequential ligand-dependent notch signaling activation regulates valve primordium formation and morphogenesis. *Circulation research*, *118*(10), 1480-1497.
64. Mahler, G. J., & Butcher, J. T. (2011). Inflammatory regulation of valvular remodeling: the good (?), the bad, and the ugly. *International journal of inflammation*, *2011*.
65. Mahler, G. J., Farrar, E. J., & Butcher, J. T. (2013). Inflammatory cytokines promote mesenchymal transformation in embryonic and adult valve endothelial cells. *Arteriosclerosis, thrombosis, and vascular biology*, *33*(1), 121-130.
66. Masumura, T., Yamamoto, K., Shimizu, N., Obi, S., & Ando, J. (2009). Shear stress increases expression of the arterial endothelial marker ephrinB2 in murine ES cells via the VEGF-Notch signaling pathways. *Arteriosclerosis, thrombosis, and vascular biology*, *29*(12), 2125-2131.
67. McCulley, D. J., Kang, J. O., Martin, J. F., & Black, B. L. (2008). BMP4 is required in the anterior heart field and its derivatives for endocardial cushion remodeling, outflow tract septation, and semilunar valve development. *Developmental Dynamics*, *237*(11), 3200-3209.
68. Menon, V., & Lincoln, J. (2018). The genetic regulation of aortic valve development and calcific disease. *Frontiers in cardiovascular medicine*, *5*, 162.
69. Michelena, H. I., Prakash, S. K., Della Corte, A., Bissell, M. M., Anavekar, N., Mathieu, P., ... & Lancellotti, P. (2014). Bicuspid aortic valve. *Circulation*, *129*(25), 2691-2704.
70. Mohler III, E. R., Gannon, F., Reynolds, C., Zimmerman, R., Keane, M. G., & Kaplan, F. S. (2001). Bone formation and inflammation in cardiac valves. *Circulation*, *103*(11), 1522-1528.
71. Nakanishi, T., Markwald, R. R., Baldwin, H. S., Keller, B. B., Srivastava, D., & Yamagishi, H. (2016). *Etiology and morphogenesis of congenital heart disease: From gene function and cellular interaction to morphology*. Springer Nature.
72. Nath, A. K., Brown, R. M., Michaud, M., Sierra-Honigmann, M. R., Snyder, M., & Madri, J. A. (2008). Leptin affects endocardial cushion formation by modulating EMT and migration via Akt signaling cascades. *The Journal of cell biology*, *181*(2), 367-380.
73. Niessen, K., Fu, Y., Chang, L., Hoodless, P. A., McFadden, D., & Karsan, A. (2008). Slug is a direct Notch target required for initiation of cardiac cushion cellularization. *The Journal of cell biology*, *182*(2), 315-325.

74. Norris, R. A., Moreno-Rodriguez, R. A., Sugi, Y., Hoffman, S., Amos, J., Hart, M. M., ... & Markwald, R. R. (2008). Periostin regulates atrioventricular valve maturation. *Developmental biology*, 316(2), 200-213.
75. Nosedá, M., Chang, L., McLean, G., Grim, J. E., Clurman, B. E., Smith, L. L., & Karsan, A. (2004). Notch activation induces endothelial cell cycle arrest and participates in contact inhibition: role of p21Cip1 repression. *Molecular and cellular biology*, 24(20), 8813-8822.
76. Oda, T., Elkahloun, A. G., Pike, B. L., Okajima, K., Krantz, I. D., Genin, A., ... & Chandrasekharappa, S. C. (1997). Mutations in the human Jagged1 gene are responsible for Alagille syndrome. *Nature genetics*, 16(3), 235-242.
77. Ong, C. T., Cheng, H. T., Chang, L. W., Ohtsuka, T., Kageyama, R., Stormo, G. D., & Kopan, R. (2006). Target selectivity of vertebrate notch proteins collaboration between discrete domains and CSL-binding site architecture determines activation probability. *Journal of Biological Chemistry*, 281(8), 5106-5119.
78. Pedrosa, A. R., Trindade, A., Fernandes, A. C., Carvalho, C., Gigante, J., Tavares, A. T., ... & Duarte, A. (2015). Endothelial Jagged1 antagonizes Dll4 regulation of endothelial branching and promotes vascular maturation downstream of Dll4/Notch1. *Arteriosclerosis, thrombosis, and vascular biology*, 35(5), 1134-1146.
79. Person, A. D., Garriock, R. J., Krieg, P. A., Runyan, R. B., & Klewer, S. E. (2005). Frzb modulates Wnt-9a-mediated β -catenin signaling during avian atrioventricular cardiac cushion development. *Developmental biology*, 278(1), 35-48.
80. Qin, W. D., Zhang, F., Qin, X. J., Wang, J., Meng, X., Wang, H., ... & Zhang, M. X. (2016). Notch1 inhibition reduces low shear stress-induced plaque formation. *The international journal of biochemistry & cell biology*, 72, 63-72.
81. Rahmani, M., Read, J. T., Carthy, J. M., McDonald, P. C., Wong, B. W., Esfandiarei, M., ... & McManus, B. M. (2005). Regulation of the versican promoter by the β -catenin-T-cell factor complex in vascular smooth muscle cells. *Journal of Biological Chemistry*, 280(13), 13019-13028.
82. Richards, J., El-Hamamsy, I., Chen, S., Sarang, Z., Sarathchandra, P., Yacoub, M. H., ... & Butcher, J. T. (2013). Side-specific endothelial-dependent regulation of aortic valve calcification: interplay of hemodynamics and nitric oxide signaling. *The American journal of pathology*, 182(5), 1922-1931.
83. Rutenberg, J. B., Fischer, A., Jia, H., Gessler, M., Zhong, T. P., & Mercola, M. (2006). Developmental patterning of the cardiac atrioventricular canal by

- Notch and Hairy-related transcription factors. *Development*, 133(21), 4381-4390.
84. Samsa, L. A., Givens, C., Tzima, E., Stainier, D. Y., Qian, L., & Liu, J. (2015). Cardiac contraction activates endocardial Notch signaling to modulate chamber maturation in zebrafish. *Development*, 142(23), 4080-4091.
 85. Schroeder, J. A., Jackson, L. F., Lee, D. C., & Camenisch, T. D. (2003). Form and function of developing heart valves: coordination by extracellular matrix and growth factor signaling. *Journal of molecular medicine*, 81(7), 392-403.
 86. Sierro, F., Biben, C., Martínez-Muñoz, L., Mellado, M., Ransohoff, R. M., Li, M., ... & Harvey, R. P. (2007). Disrupted cardiac development but normal hematopoiesis in mice deficient in the second CXCL12/SDF-1 receptor, CXCR7. *Proceedings of the National Academy of Sciences*, 104(37), 14759-14764.
 87. Sivarapatna, A., Ghaedi, M., Le, A. V., Mendez, J. J., Qyang, Y., & Niklason, L. E. (2015). Arterial specification of endothelial cells derived from human induced pluripotent stem cells in a biomimetic flow bioreactor. *Biomaterials*, 53, 621-633.
 88. Somi, S., Buffing, A. A., Moorman, A. F., & Van Den Hoff, M. J. (2004). Dynamic patterns of expression of BMP isoforms 2, 4, 5, 6, and 7 during chicken heart development. *The Anatomical Record Part A: Discoveries in Molecular, Cellular, and Evolutionary Biology: An Official Publication of the American Association of Anatomists*, 279(1), 636-651.
 89. Sorescu, G. P., Song, H., Tressel, S. L., Hwang, J., Dikalov, S., Smith, D. A., ... & Jo, H. (2004). Bone morphogenic protein 4 produced in endothelial cells by oscillatory shear stress induces monocyte adhesion by stimulating reactive oxygen species production from a nox1-based NADPH oxidase. *Circulation research*, 95(8), 773-779.
 90. Theodoris, C. V., Li, M., White, M. P., Liu, L., He, D., Pollard, K. S., ... & Srivastava, D. (2015). Human disease modeling reveals integrated transcriptional and epigenetic mechanisms of NOTCH1 haploinsufficiency. *Cell*, 160(6), 1072-1086.
 91. Tian, Y., Yuan, L., Goss, A. M., Wang, T., Yang, J., Lepore, J. J., ... & Morrisey, E. E. (2010). Characterization and in vivo pharmacological rescue of a Wnt2-Gata6 pathway required for cardiac inflow tract development. *Developmental cell*, 18(2), 275-287.
 92. Timmerman, L. A., Grego-Bessa, J., Raya, A., Bertrán, E., Pérez-Pomares, J. M., Díez, J., ... & de la Pompa, J. L. (2004). Notch promotes epithelial-mesenchymal

- transition during cardiac development and oncogenic transformation. *Genes & development*, 18(1), 99-115.
93. Torregrosa-Carrión, R., Luna-Zurita, L., García-Marqués, F., D'Amato, G., Piñeiro-Sabarís, R., Bonzón-Kulichenko, E., ... & de la Pompa, J. L. (2019). NOTCH activation promotes valve formation by regulating the endocardial secretome. *Molecular & Cellular Proteomics*, 18(9), 1782-1795.
 94. van den Akker, N. M., Molin, D. G., Peters, P. P., Maas, S., Wisse, L. J., van Brempt, R., ... & Gittenberger-de Groot, A. C. (2007). Tetralogy of fallot and alterations in vascular endothelial growth factor-A signaling and notch signaling in mouse embryos solely expressing the VEGF120 isoform. *Circulation research*, 100(6), 842-849.
 95. Van der Heiden, K., Groenendijk, B. C., Hierck, B. P., Hogers, B., Koerten, H. K., Mommaas, A. M., ... & Poelmann, R. E. (2006). Monocilia on chicken embryonic endocardium in low shear stress areas. *Developmental dynamics: an official publication of the American Association of Anatomists*, 235(1), 19-28.
 96. van der Linde, D., Konings, E. E., Slager, M. A., Witsenburg, M., Helbing, W. A., Takkenberg, J. J., & Roos-Hesselink, J. W. (2011). Birth prevalence of congenital heart disease worldwide. *Journal of the American College of Cardiology*, 58(21), 2241-2247.
 97. Varadkar, P., Kraman, M., Despres, D., Ma, G., Lozier, J., & McCright, B. (2008). Notch2 is required for the proliferation of cardiac neural crest-derived smooth muscle cells. *Developmental Dynamics*, 237(4), 1144-1152.
 98. Wang, F., Fisher, S. A., Zhong, J., Wu, Y., & Yang, P. (2015). Superoxide Dismutase 1 In Vivo Ameliorates Maternal Diabetes Mellitus-Induced Apoptosis and Heart Defects Through Restoration of Impaired Wnt Signaling. *Circulation: Cardiovascular Genetics*, 8(5), 665-676.
 99. Wang, J., Sridurongrit, S., Dudas, M., Thomas, P., Nagy, A., Schneider, M. D., ... & Kaartinen, V. (2005). Atrioventricular cushion transformation is mediated by ALK2 in the developing mouse heart. *Developmental biology*, 286(1), 299-310.
 100. Wang, Y., Wu, B., Chamberlain, A. A., Lui, W., Koirala, P., Susztak, K., ... & Zhou, B. (2013). Endocardial to myocardial notch-wnt-bmp axis regulates early heart valve development. *PLoS One*, 8(4), e60244.
 101. Wang, Y., Wu, B., Farrar, E., Lui, W., Lu, P., Zhang, D., ... & Xu, D. (2017). Notch-Tnf signalling is required for development and homeostasis of arterial valves. *European heart journal*, 38(9), 675-686.

102. Wasserman, S. M., Mehraban, F., Komuves, L. G., Yang, R. B., Tomlinson, J. E., Zhang, Y., ... & Topper, J. N. (2002). Gene expression profile of human endothelial cells exposed to sustained fluid shear stress. *Physiological genomics*, *12*(1), 13-23.
103. Watanabe, Y., Kokubo, H., Miyagawa-Tomita, S., Endo, M., Igarashi, K., Ichi Aisaki, K., ... & Saga, Y. (2006). Activation of Notch1 signaling in cardiogenic mesoderm induces abnormal heart morphogenesis in mouse. *Development*, *133*(9), 1625-1634.
104. Wen, C., Metzstein, M. M., & Greenwald, I. (1997). SUP-17, a *Caenorhabditis elegans* ADAM protein related to *Drosophila* KUZBANIAN, and its role in LIN-12/NOTCH signalling. *Development*, *124*(23), 4759-4767.
105. White, M. P., Theodoris, C. V., Liu, L., Collins, W. J., Blue, K. W., Lee, J. H., ... & Srivastava, D. (2015). NOTCH1 regulates matrix gla protein and calcification gene networks in human valve endothelium. *Journal of molecular and cellular cardiology*, *84*, 13-23.
106. Williams, R., Lendahl, U., & Lardelli, M. (1995). Complementary and combinatorial patterns of Notch gene family expression during early mouse development. *Mechanisms of development*, *53*(3), 357-368.
107. Wilson, C. L., Gough, P. J., Chang, C. A., Chan, C. K., Frey, J. M., Liu, Y., ... & Raines, E. W. (2013). Endothelial deletion of ADAM17 in mice results in defective remodeling of the semilunar valves and cardiac dysfunction in adults. *Mechanisms of development*, *130*(4-5), 272-289.
108. Wirrig, E. E., & Yutzey, K. E. (2014). Conserved transcriptional regulatory mechanisms in aortic valve development and disease. *Arteriosclerosis, thrombosis, and vascular biology*, *34*(4), 737-741.
109. Wirrig, E. E., Hinton, R. B., & Yutzey, K. E. (2011). Differential expression of cartilage and bone-related proteins in pediatric and adult diseased aortic valves. *Journal of molecular and cellular cardiology*, *50*(3), 561-569.
110. Wooten, E. C., Iyer, L. K., Montefusco, M. C., Hedgepeth, A. K., Payne, D. D., Kapur, N. K., ... & Huggins, G. S. (2010). Application of gene network analysis techniques identifies AXIN1/PDIA2 and endoglin haplotypes associated with bicuspid aortic valve. *PLoS One*, *5*(1), e8830.
111. Xue, Y., Gao, X., Lindsell, C. E., Norton, C. R., Chang, B., Hicks, C., ... & Gridley, T. (1999). Embryonic lethality and vascular defects in mice lacking the Notch ligand Jagged1. *Human molecular genetics*, *8*(5), 723-730.

112. Yu, H. M. I., Jerchow, B., Sheu, T. J., Liu, B., Costantini, F., Puzas, J. E., ... & Hsu, W. (2005). The role of Axin2 in calvarial morphogenesis and craniosynostosis. *Development*, *132*(8), 1995-2005.
113. Zhang, H., & Bradley, A. (1996). Mice deficient for BMP2 are nonviable and have defects in amnion/chorion and cardiac development. *Development*, *122*(10), 2977-2986.
114. Zhao, B., Etter, L., Hinton Jr, R. B., & Benson, D. W. (2007). BMP and FGF regulatory pathways in semilunar valve precursor cells. *Developmental dynamics: an official publication of the American Association of Anatomists*, *236*(4), 971-980.

CHAPTER 2. OSCILLATORY SHEAR STRESS DRIVES ENDOCARDIAL
CELL PROLIFERATION BY ACTIVATING BMP SIGNALING DURING
VALVE EXTENSION

2.1 Abstract

Rationale: Shear stress and BMP signaling are important for endocardial-mesenchymal transition (EndMT) during early valve formation and MC (MC) proliferation during post-EndMT valve remodeling. However, how BMP signaling regulates endocardial proliferation during valve extension is unknown. Here, we hypothesized that shear stress differentially regulates BMP signaling and endocardial cell (EC) proliferation.

Methods and Results: We monitored BMP activity and EC proliferation in vivo by assessing the spatiotemporal expression of pSMAD15 and PHH3. The ECs on the inflow surface of the valve are associated with oscillatory shear stress (OSS), increased BMP activation, and EC proliferation. In contrast, unidirectional lamina shear stress (LSS) on the inflow side is linked to reduced BMP signaling and EC proliferation. By exposing primary chick embryonic valve ECs to fluid shear stress in a parallel-plate bioreactor system, we showed that low OSS was necessary and sufficient to induce BMP signaling in a ligand-dependent manner. Furthermore, high LSS, through Notch1 signaling, downregulated BMP receptors/ligands and inhibited BMP activation. We further determined that OSS drives BMP signaling by regulating the nuclear translocation of β catenin, which is indicative of canonical WNT signaling. In contrast, LSS inhibits BMP signaling through Notch1-induced downregulation of WNT/ β catenin signaling.

Conclusions: During valve extension, WNT/ β catenin acts a force-driven molecular switch, by which low OSS is transduced into BMP signaling that in turn regulates endocardial proliferation on the outflow side. On the inflow side, high LSS downregulates WNT/ β catenin, thereby inhibiting BMP-induced endocardial growth.

2.2 Introduction

Congenital heart malformations affect about 3 million people) and 40 thousand live births in the United States each year (Roger, 2011; Reller, 2008). Congenital valve malformations (CVMs) account for 20-30% of live births and can lead to functional abnormalities that affect cardiac functions after birth (Hoffman, 2002). The quest for new therapeutic targets remains a challenge in part because genetics alone does not fully address the etiology of CVMs. In fact, only 10-15% of left outflow tract malformations, e.g. aortic valve stenosis, are associated with chromosomal abnormalities (Ferencz, 1989; McBride, 2009). Alternatively, altered blood flow in chick embryos can lead to various CVDs that resemble those observed in human babies (Midgett, 2014), suggesting that hemodynamic aberrations could explain CVMs.

Heart valve primordia are initiated by endocardial-mesenchymal transition (EndMT), by which endocardial cells (ECs) differentiate into MCs, delaminate, and migrate into the space between the endocardium and myocardium (Butcher, 2007). In the outflow tract (OFT), EndMT and the migration of cardiac neural crest (CNC)-derived cells give rise to the mesenchyme of the embryonic semilunar valves (Jain, 2011). After EndMT ceases, atrioventricular (AV) and OFT valve primordia grow in cell number, compact, and extend in the direction of blood flow through generally conserved regulatory networks (Combs, 2009). While the regulation of EndMT during valve formation has been extensively studied, mechanisms of post-EndMT valve remodeling are still elusive. Specifically, even though ECs must grow to facilitate valve expansion

and elongation, little is known about the induction and regulation of valve endocardial growth.

Bone morphogenetic proteins (BMPs) are growth factors expressed in the myocardial regions surrounding the valve primordia (Somi, 2004). BMP signaling is associated with priming ECs for EndMT during early valve formation and regulating MC proliferation during valve remodeling (Garside, 2013). Binding of BMP ligands to two types of receptors: BMP receptor type 1 (e.g. BMPR1A, BMPR1B) and BMP receptor type 2 (BMPR2) canonically induces the phosphorylation and nuclear translocation of smad1/5/8 to regulate cell proliferation. Intriguingly, during valve remodeling, while overactive BMP signaling is associated with MC hyperproliferation (Jackson, 2003; Siirro, 2007), deficient BMP signaling is linked to defective MC differentiation and enlarged valve primordia (Zhang, 2010). These seemingly contradictory studies reflect our lack of understanding about the mechanisms of BMP-dependent regulation of valve remodeling. More importantly, recent studies have only focused on BMP signaling in MCs. Despite the expression and localization of BMP ligands in the valve endocardium post-EndMT (Somi, 2004), how endocardial BMP signaling regulates valve remodeling programs is unclear.

Curiously, expression of these BMP ligands is restricted to the ECs on the outflow side of the developing valves (Somi, 2004), which is associated with low oscillatory shear stress (OSS) (Kilner, 2000). In contrast, ECs on the inflow side of the valve experience high, unidirectional, laminar shear stress (LSS) and exhibit more Notch1 activity (Kilner, 2000; del Monte, 2007). These clues imply that the

endocardium may sense and transduce hemodynamic signals into biological programs that regulate valve remodeling. This simple idea has been difficult to elaborate mechanistically due to two challenges. First, prior studies have not demonstrated a successful approach to isolate and culture a monolayer of age and region-specific embryonic valve ECs. Second, replication of the 3D hemodynamic environments in vitro has proven to be the limiting factor in elucidating developmental mechanisms of fluid shear stress. As a result, virtually no studies have addressed how OSS and LSS differentially regulate the behaviors of ECs during valve remodeling. This is a critical gap in our knowledge because heart valve development is heavily dependent on hemodynamics (Poelmann, 2018). More importantly, a deeper understanding of how the endocardium relays mechanical cues to coordinate valve morphogenesis offers avenues for hemodynamically informed interventions to prevent CVMs or restore valve functions.

Here, we hypothesized that the endocardium transduces shear stress into differential BMP and Notch1 programs that regulate endocardial proliferation. To address this hypothesis, we crossed the boundaries between engineering and developmental biology and implemented a parallel-plate bioreactor system containing 3D constructs of primary valve ECs. We revealed that shear stress induces side-specific endocardial proliferation by regulating BMP and Notch1 programs. We further identified WNT/ β catenin to be a mechanically driven molecular switch that is activated by low OSS to promote BMP-dependent proliferation and deactivated by high LSS-induced Notch1 signaling.

2.3 Materials and Methods

2.3.1 Animal samples

Embryonic hearts were harvested from wildtype mouse embryos at E12.5, E13.5, E16.5, and E18.5 in cold PBS. The outflow tracts were then isolated and fixed in cold paraformaldehyde and processed for wholemount immunostaining. For shear stress experiments, fertilized White Leghorn eggs were incubated at 38C and 80% humidity to Hamburger-Hamilton (HH) stage 33+ (Day 7-8, incubational age). Chick embryos were then harvested in cold EBSS (Sigma). Outflow tracts were then isolated and dissected to expose valve primordia, which were then used to generate 3D collagen constructs with endocardial cells seeded on top.

2.3.2 Shear stress bioreactor system

Each bioreactor consists of a histology microscope slide, biocompatible double-sided tape (W.W. Grainger), 5mm-thick silicone sheet (McMaster-Carr), and a sticky-Slide I Luer (Ibidi). Wells were created in the silicone sheet using a 4-mm disposable biopsy punch (Miltex). The height of the stick-Slide I Luer determined the magnitude of shear stress, which was calculated and validated by Ibidi and used in previously published experiments (Dragt, 2012; Lecarpentier, 2016). The sticky-slide I Luer creates a channel that is 5mm in width and 50mm in length with various heights.

Recent computational fluid dynamics (CFD) analysis indicates that FSS on the outflow side of mouse OFT valves peaks around 21.3 dyne/cm² (Yap, 2013). Furthermore, FSS over the endocardial cells on the ventricular side of OFT valves averages about 20

dyne/cm² (Nandy, 1987; Weston, 1999). Therefore, we subjected the endocardial cells to OSS and LSS at 5 dyne/cm² to simulate low FSS or 20dyne/cm² to simulate high FSS. In our experiments, 0.8-mm high sticky-slides I Luer were used to achieve 5 dyne/cm², while 0.4-mm high slides were used to achieve 20 dyne/cm². The components of the bioreactor were clamped together using binder clips. The female Luers of the channel slide were connected to a male Luer lock with a stop cock and a male Luer lock adapter to prevent leakage during the experiment. The male Luer lock adapters were connected to silicone tubing that had 3.2mm inner diameter (Size 16, Cole-Parmer). For steady shear experiments, flow was generated using Masterflex L/S Brushless variable- speed digital drive; Masterflex L/S 8-channel, 4-roller cartridge pump head; and Masterflex L/S large cartridges (Cole-Parmer). A pulse dampener (Cole-Parmer) was placed between the peristaltic pump and the bioreactors to maintain non-pulsatile laminar flow over the samples.

The media was stored in a polycarbonate bottle with a filling/venting cap (Nalge Nunc International) with 80mL of M199 culture medium, supplemented with insulin-selenium-transferrin, Pen/Strep, and chick serum, as described previously (Gould, 2010). The 0.8-mm and 0.4-mm bioreactors were connected, run in tandem, and exposed to a flow rate of 21.1 mL/min for 24 hours at 37C and 5% CO₂. For the oscillatory shear experiments, flow was generated using a NE-1000 syringe pump (New Era Pump Systems, Inc.). The flow circuit includes the bioreactors connected to a 20-mL syringe (BD Biosciences) that was controlled by a syringe pump. The cells were exposed to a flow rate of 21.1 mL/min and at 1Hz, i.e. the cells were exposed to shear

stress in the forward direction for one-half of the cycle and in the reverse direction for the other half of the cycle.

2.3.3 3D endocardial cell culture

Collagen gels at a concentration of 2 mg/mL collagen were made by mixing 3x Dulbecco's Modified Eagle's Medium (Life Technologies), 10% chick serum (Life Technologies), sterile 18 M Ω water, 0.1 M NaOH, and rat tail collagen I (BD Biosciences). An aliquot of the collagen gel solution was pipetted into the wells in the silicone sheet and allowed to solidify for 1 hour at 37C and 5% CO₂. The dissected outflow tracts were then placed on top of the collagen gel, and excess media was pipetted off to allow for the valve primordia to come in contact with the collagen gel. After 6 hours of incubation at 37°C and 5% CO₂., the valve ECs are repolarized, delaminated, and attached to the surface of the collagen constructs. These ECs were exposed to LSS or OSS at 5 or 20 dyne/cm² for 24 hours.

To inhibit BMP signaling, an Alk2/3 inhibitor (1uM, LDN189193, Sigma) and a BMP ligand scavenger (100ng/mL, Noggin, Sigma) were used, while DAPT was used to inhibit Notch signaling (10uM, Sigma). To inhibit canonical Wnt/ β catenin signaling, XAV939 (Sigma) was diluted in DMSO and used at 1 μ M. The endocardial patches were conditioned with media containing the inhibitor for 1 hour prior to the shear stress experiments. Cells were then exposed to media containing the same concentrations of inhibitors during the shear experiments.

2.3.4 Immunostaining

Samples were fixed with cold 4% paraformaldehyde for 15 minutes, subsequently washed with TBS, permeabilized with 0.3% Triton-X 100 for 20 minutes and washed again in TBS for 2x10 minutes. Samples were then blocked and subsequently incubated with primary antibodies in the blocking solution overnight at 4C. The primary antibodies used were rat mAb against PHH3 (Cell Signaling), mouse mAb MF20 (Thermo Fisher), rabbit mAb against pSMAD15 (Cell Signaling), and mouse mAb against β -catenin (BD Biosciences) and diluted at 1:100. Samples were then washed for 3x10 minutes with TBS and incubated with species-specific Alexa Fluor® 488, 568, or 647 conjugated secondary antibodies in 5% BSA diluted in TBS for 1 hour at room temperature. Samples were then washed again for 3x10 minutes and stained with DAPI. For pSMAD15 staining, samples were incubated with a donkey-anti rabbit secondary antibody conjugated with HRP. Fluorescence signal was amplified using TSA Amplification Kit (Perkin Elmer) and washed in TBS before staining with DAPI. Images were taken using Zeiss LSM880 Confocal/Multiphoton Upright Microscope (u880). Quantification of pSMAD15 and PHH3 was determined based on the percentage of nuclei positive for pSMAD15 and PHH3 using ImageJ.

2.3.5 Gene expression analysis

Total RNA was extracted from endocardial cells on the surface of the 3D collagen gels using Power SYBR™ Green Cells-to-CT™ Kit (Thermo Fisher). The kit was also used to synthesize cDNA was then synthesized from the extracted RNA. Each gel represents a biological replicate, which pools RNA from 2 endocardial patches. qRT-

PCR was performed on samples using reagents from the same kit and MiniOpticon Real-Time PCR Detection System (Biorad, Hercules, CA). Primers are listed in Table 1.

GAPDH	F 5' TATGATGATATCAAGAGGGTAGT 3' R 5' TGTATCCAACTCATTGTCATAC 3'
BMP2	F 5' CCAGCTGTTTTGAGGTGGAT 3' R 5' ATACAACGGATGCCTTTTGC 3'
BMP4	F 5' CCTGGTAACCGAATGCTGAT 3' R 5' CTCCTCCTCTTCTTCGGACT 3'
BMP6	F 5' TCTTCACGTGGACTCTGTGG 3' R 5' TTAAGACCATCCCAGCCAAG 3'
BMPRII	F 5' GCTACCTCGAGGAGACCATTACA 3' R 5' CATTGCGGCTGTTCAAGTCA 3'
BMPRI1A	F 5' TGTCACAGGAGGTATTGTTGAAGAG 3' R 5' AAGATGGATCATTGGCACCAT 3'
BMPRI1B	F 5' GGGAGATAGCCAGGAGATGTGT 3' R 5' GGTCTGATATGGGAGCTGGTA 3'

Table 1. List of chicken primers used in gene expression analysis.

2.3.6 Statistics

Graphs display mean values +/- standard error. Data was analyzed using GraphPad Prism 6.0 for Mac. Results were analyzed by two-way Student t-test or one-way ANOVA with Tukey's multiple comparisons test. Differences between means were significant at $P < 0.05$.

2.4 Results

2.4.1 Endocardial accommodation is side-specific

To assess the endocardial growth during valve development at the tissue level, we measured the perimeter of valve primordia on the outflow and inflow sides (Figure 1D). We found that the outflow perimeter increased from about 12 μ m at E12.5 to 105 μ m at E15.5 and 276 μ m at E18.5 ($P < 0.0001$), suggesting that endocardial length on the outflow side increases during valve remodeling. While we detected a two-fold increase in the endocardial length on the inflow side between E12.5 and E15.5, there was no difference in that between E15.5 and E18.5. Taken together, these data suggest that endocardial proliferation and lengthening that accommodate for valve expansion are prevalent on the outflow side.

EC proliferation is thought to accommodate mesenchymal growth during valve development. In order to elucidate the distribution of endocardial proliferation, we monitor mitotic activity in the endocardium during valve remodeling from E12.5 to E18.5. To do this, we employed whole mount immunostaining for phosphorylated Histone-3 (PHH3), which is indicative of chromosome condensation during mitosis.

Proliferation was determined based on the percentage of PHH3 positive cells (red, Figure 1A-B) over the total number of MCs, which was determined as IB4 (green) positive cells in the valve region. Analysis of endocardial proliferation on the outflow or arterial side (denoted as A, Figure 1B) and the inflow or ventricular side (denoted as V, Figure 1B) in the OFT valves revealed that mitotic activity was higher on the outflow side during E13.5 and E18.5 (Figure 1C).

While there is no significant difference in %PHH3 positive ECs between the arterial (2.19 \pm 0.27%) and ventricular (2.86 \pm 1.05%) at E12.5, we detected a 2% increase in endocardial proliferation on the outflow side and a 2% decrease on the inflow side at E13.5. More importantly, at E13.5 the outflow side showed 4% more mitotic cells compared to the inflow side ($P < 0.0001$). Similarly, the outflow side exhibited 2% and 1% more proliferative cells than the inflow side at E16.5 ($P < 0.01$) and E18.5 ($P < 0.05$), respectively. Furthermore, the percentage of mitotic ECs on the outflow side drops from 4.4% at E13.5 to 2.41% at E16.5 and 1.11% at E18.5, suggesting that proliferation decreases as development proceeds.

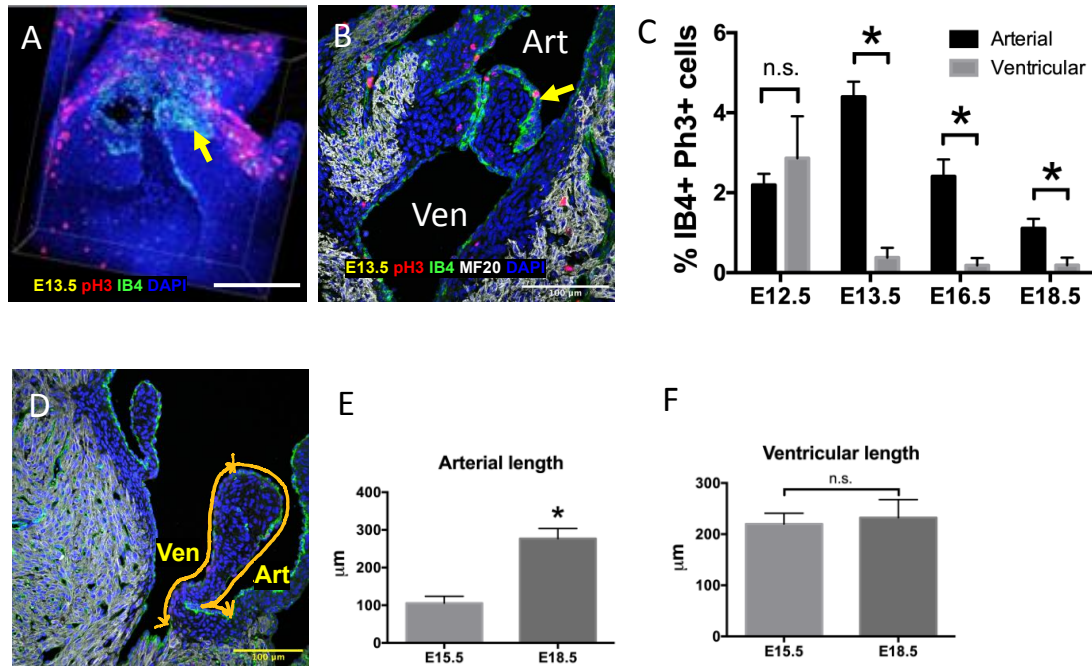


Figure 2.1. Enhanced endocardial proliferation and growth on the arterial side. Representative phospho-histone 3 (PHH3) immunostaining images of E13.5 whole mount reconstruction (A) and 2D section (B) showing more mitotic cells on the arterial side (denoted as Art, Figure 1B) compared to ventricular side (denoted as Ven, Figure 1B). Yellow arrows indicate PHH3 positive cells (red). Myocardial cells were stained with MF20 (white), while endocardial cells were stained with IB4 (green). Nuclei were stained with DAPI. C, Quantification of proliferation based on the percentage of cells double positive for IB4 and PHH3 over the total number of IB3+ cells. Bar graph shows comparisons between arterial and ventricular endocardial cells between E12.5 and E18.5. D, Schematic showed how valve perimeters on the arterial side (Art) and the ventricular side (Ven) were measured. E, Quantification of endocardial length on the arterial side of E12.5, E15.5, and E18.5 embryos. F, Quantification of ventricular length on the arterial side of E12.5, E15.5, and E18.5 embryos. Data are means +/- SEM. N=3-5 embryos per group (C) and N=5-7 embryos per group (E and F). * $p \leq 0.05$ via Student *t* test. Scale bars indicate 100μm.

2.4.2 Endocardial proliferation is associated with BMP signaling on the outflow side

BMP signaling has been shown to be associated with endocardial proliferation during heart and valve development. Furthermore, previous reports have also indicated that expression of BMP2, BMP4, and BMP6 are more prevalent on the arterial side of the OFT valves. Therefore, we assessed BMP activity, by immunostaining for phosphorylated smad1/5 (pSMAD15), in the ECs during valve remodeling. In the aortic valve (AoV) at E14.5, about 32% of ECs on the outflow side were positive for nuclear pSMAD15 (Figure 2C, yellow arrow), compared to about 5% of those on the inflow side ($P<0.05$). Similarly, in the pulmonary valve (PV) at E114.5, about 42% of ECs on the outflow side were positive for nuclear pSMAD15 (Figure 2G, yellow arrow), compared to about 10% of those on the inflow side ($P<0.05$). Furthermore, we detected more pSMAD15-positive ECs on the inflow side of the AV valves (Figure 2Q-T). These findings suggest that BMP signaling, like EC proliferation, is side-specific.

We next determined if BMP signaling is also active during late gestation by examining pSMAD15 levels in both AoV and PV sections at E17.5. Interestingly, about 28% of ECs on the outflow side were positive for nuclear pSMAD15 (Figure 2K, yellow arrow), compared to about 6% of those on the inflow side (Figure 2I) ($P<0.05$). Similarly, in PV at E17.5, about 36% of ECs on the outflow side were positive for nuclear pSMAD15 (Figure 2G, yellow arrow), compared to about 14% of those on the inflow side ($P<0.05$).

Taken together, these data suggest that BMP signaling is more prevalent on the side associated with oscillatory shear stress and endocardial proliferation during valve remodeling. Taken together, these data suggest that BMP signaling is more prevalent on the side associated with oscillatory shear stress and endocardial proliferation during valve remodeling.

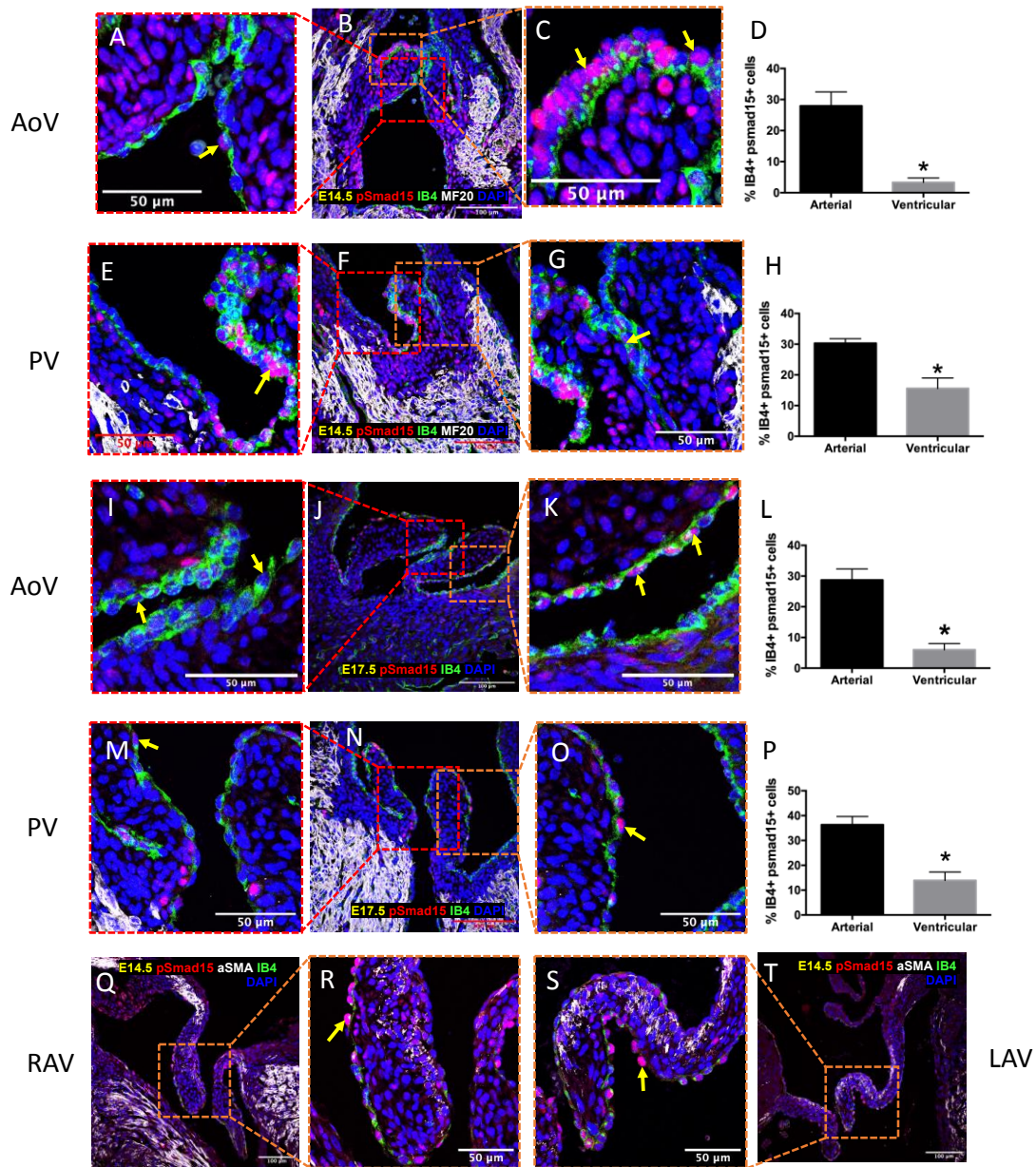


Figure 2.2. Enhanced BMP signaling on the arterial side of semilunar valves. Immunostaining of phosphorylated smad15 (pSMAD15) in AoV (A-C, I-K) and PV (E-G, M-O) at E14.5 and E17.5. Q-T, Immunostaining of pSMAD15 in RAV and LAV at E14.5. Arrows indicate positive pSMAD15 cells (red). Myocardial cells were stained with MF20 or α SMA (white), while endocardial cells were stained with IB4 (green). Nuclei were stained with DAPI. D, H, L, P, Quantification of BMP signaling based on percentage of nuclear pSMAD15 and IB4 double positive cells. Data are means \pm SEM. N=3 embryos per group. * $p \leq 0.05$ via Student *t* test. Scale bars indicate 100 μ m.

2.4.3 Low OSS induced, while high LSS inhibited, BMP signaling in valve ECs

ECs on the outflow side of the valve are subject to oscillatory shear stress (OSS) and those on the inflow side are subject to laminar shear stress (LSS). We determined whether OSS induced BMP signaling in ECs on the outflow side by exposing primary chick embryonic ECs (from ventricular side of the OFT valves) to various shear stress environments of different magnitudes: static (no flow), LSS 20 dynes/cm² (LSS20), LSS at 5 dynes/cm² (LSS5), OSS at 20 dynes/cm² (OSS20), and OSS at 5 dynes/cm² (OSS5). We used β -catenin, which is associated with vascular endothelial cadherin (VE-Cadherin), as a marker of ECs as previously described (Cha, 2016). Assessment of BMP signaling was based on the percentage of ECs positive for nuclear pSMAD15.

To determine whether OSS could induce BMP activation, we compared static and OSS5 or OSS20 which corresponds with the flow environments on the outflow side. ECs exposed to OSS5 exhibited about 23% pSMAD15+ cells, significantly higher than those exposed to no flow (6%) (Figure 3A and B), suggesting that OSS5 is sufficient at inducing primary ECs from the inflow side of the valve, which normally display downregulated BMP signaling in vivo (Figure 2). At OSS20, however, there was a 20% decrease in %pSMAD15+ cells than OSS5 (Figure 3D and E), suggesting that low shear magnitude is required for BMP activation. Furthermore, LSS5 exhibited 7% more %pSMAD15+ cells compared to static (Figure 3B and A), confirming that low shear magnitude is also sufficient to induce BMP activation.

To elucidate whether OSS pattern is required for BMP activation, we compared %pSMAD15+ cells between OSS5 and LSS5. The percentage of pSMAD15+ ECs was 13%

at LSS5, 10% lower than that at OSS5 (Figure 3D and D), indicating that the oscillatory direction of shear was required for BMP activation. These findings suggest that OSS5 is necessary and sufficient for BMP signaling in embryonic valve ECs.

Interestingly, there was no significant difference in %pSMAD15+ positive cells between LSS20 and static (Figure 3C and A), suggesting that high LSS is not sufficient to inhibit BMP activation. However, LSS20 exhibited 6% pSMAD15+ cells lower than LSS5, suggesting that high shear magnitude is required to inhibit BMP activation (Figure 3C and B). Interestingly, there was no significant difference in %pSMAD15 between LSS20 and OSS20, suggesting that unidirectional flow is not required to inhibit BMP signaling. Taken together, these findings indicate that only high shear magnitude, regardless of the flow direction, is required for BMP activation in ECs on the inflow side.

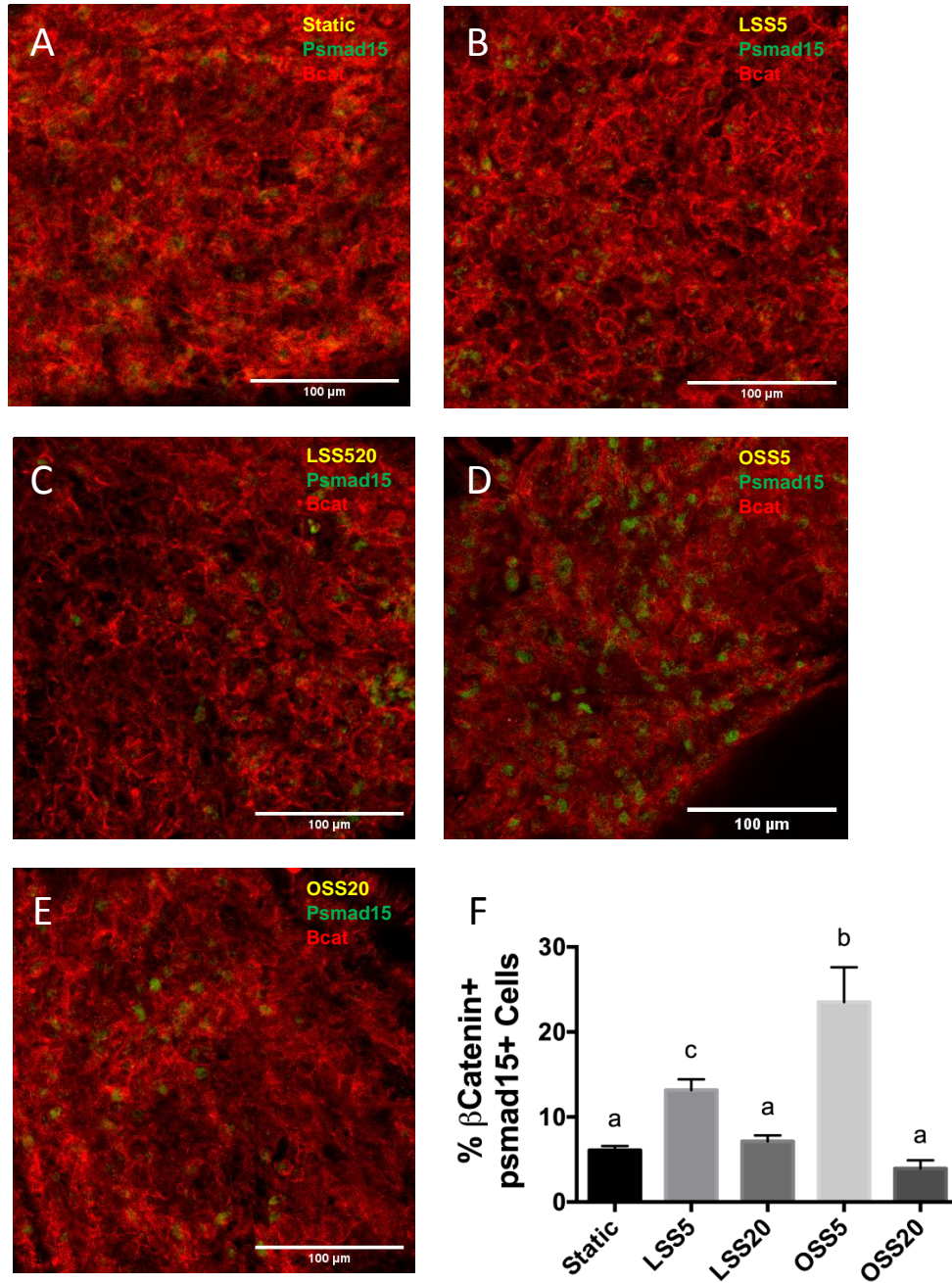


Figure 2.3. Enhanced BMP activation under low oscillatory shear. Immunostaining of phosphorylated smad15 (pSMAD15, green), indicative of active BMP signaling, in static (A), LSS at 5 dynes/cm² (LSS5, B), LSS 20 dynes/cm² (LSS20, C), OSS at 5 dynes/cm² (OSS5, D), and OSS at 20 dynes/cm² (OSS20, E). Endocardial cells were stained with β catenin (red). F, Quantification of BMP activity based on percentage of endocardial cells positive for nuclear pSMAD15. Data are means \pm SEM. N=7-8 endocardial patches per group. Bars that do not share any letters are significantly different ($p < 0.05$ via ANOVA with Tukey multiple comparisons correction). Scale bars indicate 100 μ m.

2.4.4 Upregulation of BMP receptors and ligands in response to low OSS

To determine the underlying mechanism of BMP activation, we examined the expression of the components of the BMP pathway in response to shear. We isolated RNA from primary endocardial patches after 24 hours of exposure to different shear environments and analyzed gene expression normalized to static control via qRT-PCR. In response to OSS5, expression of BMP2, 4, and 6 ligands were significantly higher than those exposed to static, suggesting that low OSS was sufficient to induce expression of BMP ligands that can potentially increase BMP activation in a paracrine manner. Interestingly, while previous research has suggested a role for BMP4 in controlling proliferation in the OFT valves, we detected that BMP2 and 6 are also sensitive to low OSS stimulation (Figure 4A-C). Moreover, cells exposed to OSS5 also exhibited significantly higher expression of BMP ligands compared to those exposed to OSS20, suggesting that low magnitude is required for induction of BMP ligand expression. Similarly, OSS5 resulted in higher BMP ligand expression compared to LSS5, suggesting that the oscillatory flow direction was required for upregulation of BMP ligands.

To determine whether BMP receptor expression is also shear-sensitive, we examined BMP receptor type 1 (BMPR1A and BMPR1B) and BMP receptor type 2 (BMPR2) in response to shear. There was no significant difference in BMPR1A expression between OSS5 and LSS20, suggesting that OSS5 is not responsible for the differential BMP activation between ECs on the inflow and outflow sides (Figure 4D). However, there was a 3-fold decrease in BMPR1A expression in OSS20, compared to

OSS5, which may contribute to downregulation of BMP activation in OSS20. Moreover, BMPR1A expression was significantly lower in LSS5, compared to OSS5, suggesting that the oscillatory direction is required to upregulate BMPR1A expression. Interestingly, examination of the expression of BMPR1B and BMPR2 also revealed upregulation of BMP receptors in ECs exposed to OSS5 (Figure 4E and F), suggesting low OSS upregulation of BMP receptors can contribute to increased BMP activation.

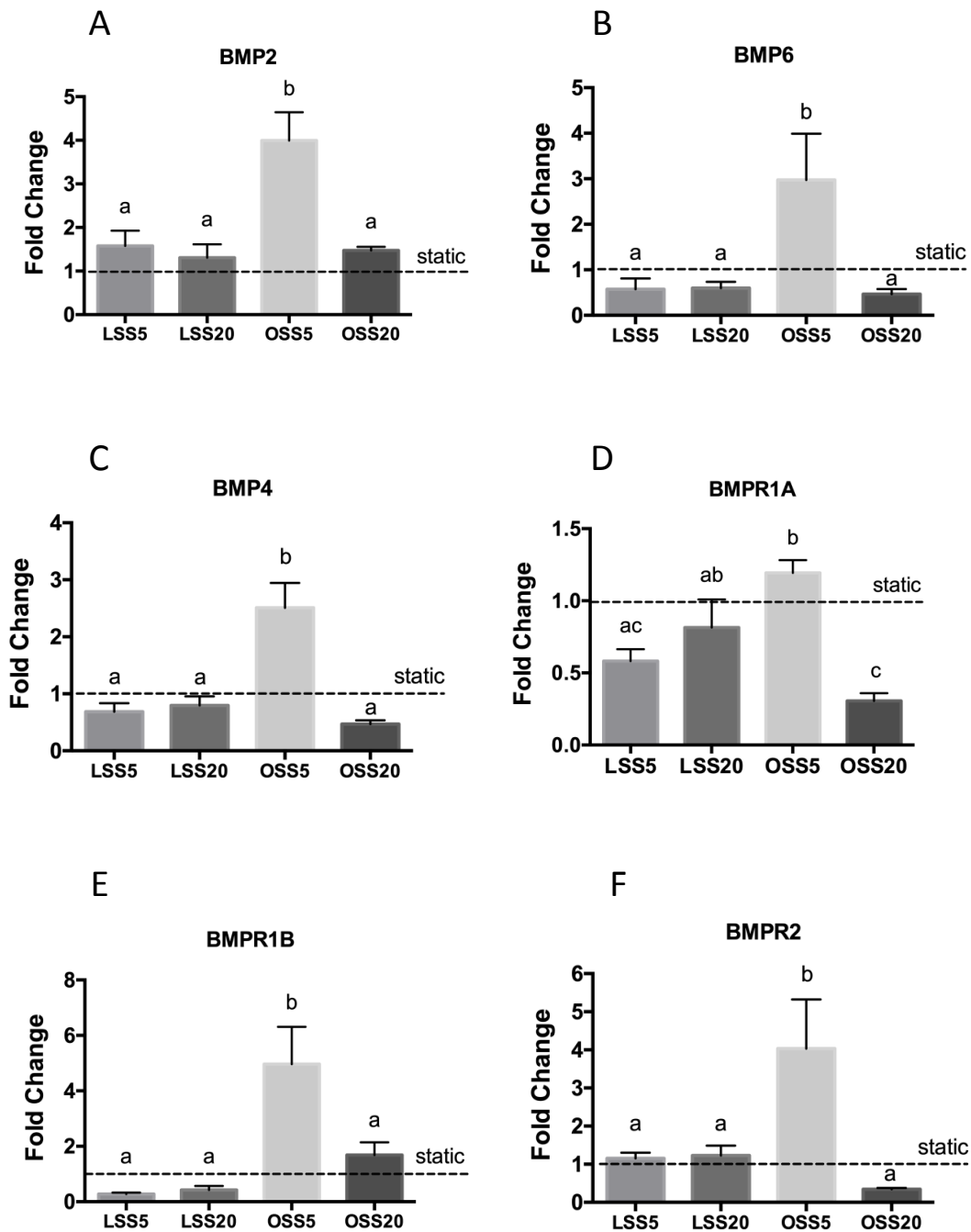


Figure 2.4. Upregulation of BMP ligands and receptors in response to OSS5. Expression of BMP ligands (A-C) and receptors (D-F) in primary embryonic chick valve endocardial cells exposed to LSS5, LSS20, OSS5, and OSS20. Fold change was normalized to static controls. Data are means \pm SEM. N=5 endocardial patches per group. Bars that do not share any letters are significantly different ($p < 0.05$ via ANOVA with Tukey multiple comparisons correction).

2.4.5 Enhanced endocardial proliferation in response to low magnitude OSS

ECs on the outflow side of the OFT valves are associated with higher proliferation (Figure 1) and OSS. We determined whether OSS is a requirement for upregulation of endocardial proliferation by exposing primary chick embryonic ECs to different shear environments and measured mitotic activity via PHH3 immunostaining. Quantification of proliferation was based on the percentage of ECs positive for nuclear PHH3 signal. We detected a 0.8% increase in %PHH3 proliferation in cells exposed to OSS5, compared to those exposed to no flow (Figure 5D and A), suggesting that OSS5 is sufficient to increase proliferation in ECs. To determine whether the requirement of low magnitude, we compared OSS5 and OSS20 (Figure 5D and E). There was a two-fold increase in %PHH3+ cells in cells exposed to OSS5, compared to OSS20, indicating that low shear magnitude is required for increasing endocardial proliferation. To determine if oscillatory flow direction is required for increasing endocardial proliferation, we compared OSS5 and LSS5 (Figure 5D and B). In response to LSS5, there was a 1.3% decrease in %PHH3+ cells, compared to OSS5, suggesting that the oscillatory flow direction is required for increasing endocardial proliferation. These results suggest that OSS5 is necessary and sufficient to induce endocardial proliferation.

We next determined whether high LSS, which is associated with ECs on the inflow side, can inhibit proliferation in ECs. Interestingly, there was no significant difference in proliferation between LSS20 and static control (Figure 5C and A), suggesting that LSS20 is not sufficient to attenuate proliferation. Moreover, there was

virtually no difference in endocardial proliferation between OSS20 and LSS20 (Figure 5E and C), suggesting that proliferation is not dependent on the direction of flow.

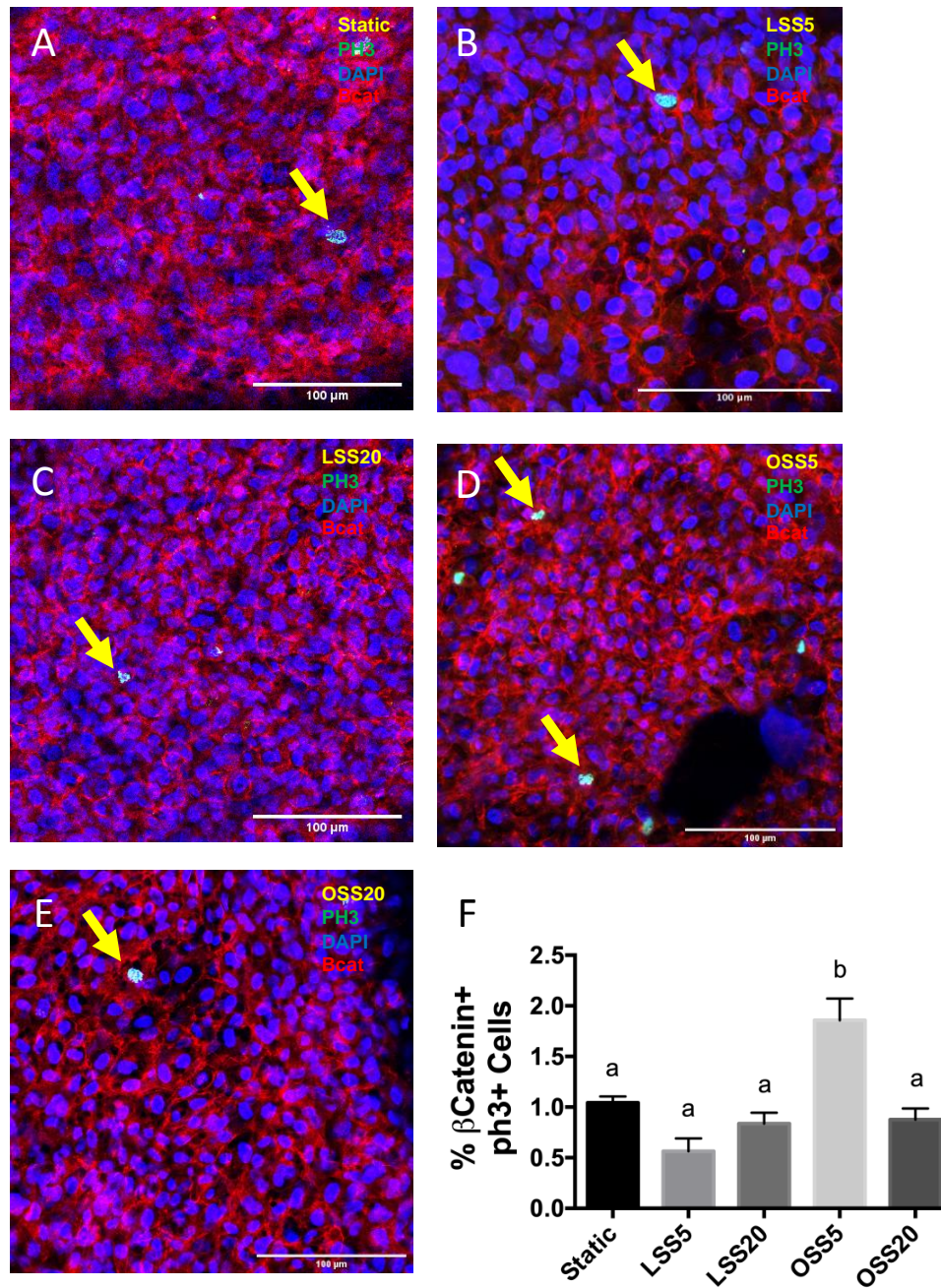


Figure 2.5. Enhanced proliferation under low oscillatory shear. Immunostaining of phosphorylated histone 3 (PHH3), indicative of active mitosis, in static (**A**), LSS at 5 dynes/cm² (LSS5, **B**), LSS 20 dynes/cm² (LSS20, **C**), OSS at 5 dynes/cm² (OSS5, **D**), and OSS at 20 dynes/cm² (OSS20, **E**). Endocardial cells were stained with β catenin (red). **F**, Quantification of PHH3 activity based on percentage of endocardial cells positive for nuclear PHH3. Yellow arrows indicate PHH3+ cells. Data are means +/- SEM. N=7-8 endocardial patches per group. Bars that do not share any letters are significantly different ($p < 0.05$ via ANOVA with Tukey multiple comparisons correction). Scale bars indicate 100 μ m.

2.4.6 BMP signaling is required for OSS5-induced endocardial proliferation

Since BMP signaling and endocardial proliferation are both associated with low magnitude OSS, we determined whether BMP mediates the shear-driven endocardial proliferation. To this end, we pretreated the primary ECs with LDN193189 at 1 μ M, an inhibitor of BMP type I receptors (namely Alk2 and Alk3). We then exposed them to OSS at 5 dynes/cm² in culture media containing LDN193189 and measured BMP activation and proliferation based on the percentage of Pmad15+ and PHH3+ ECs, respectively.

While OSS5 significantly increased %PSMAD15 ECs compared to static (Figure 6A and B), inhibition of BMP signaling by LDN193189 lowered pSMAD15 nuclear translocation by 15%, suggesting that OSS5 activates BMP signaling via Alk2 and Alk3. Since BMP2, 4, 6, and 7 ligands induce BMP signaling via Alk2 and Alk3, these findings corroborated with our expression data showing upregulation of BMP2, 4, and 6 transcripts in response to OSS5 (Figure 2A-C). To expand these findings, we scavenged BMP ligands using Noggin at 100ng/ML and found that noggin decreased %pSMAD15+ cells (Figure 6D). Taken together, these results suggest that OSS5-induced BMP activation is ligand-dependent.

To determine if BMP mediates endocardial proliferation in response to OSS5, we measure proliferation in presence of LDN193189, noggin, and shear. Interestingly, while OSS5 almost doubled endocardial proliferation compared to static controls (Figure 6F and G), inhibition of BMP signaling via LDN193189 in OSS5 returned the

%PHH3+ cells to the static levels (Figure 6H), suggesting that shear-driven endocardial proliferation is mediated by BMP signaling. In addition, in response to BMP inhibition by noggin, endocardial proliferation was also significantly reduced to the static levels (Figure 6I). Taken together, these results suggest that OSS5 induces endocardial proliferation via ligand-dependent BMP activation.

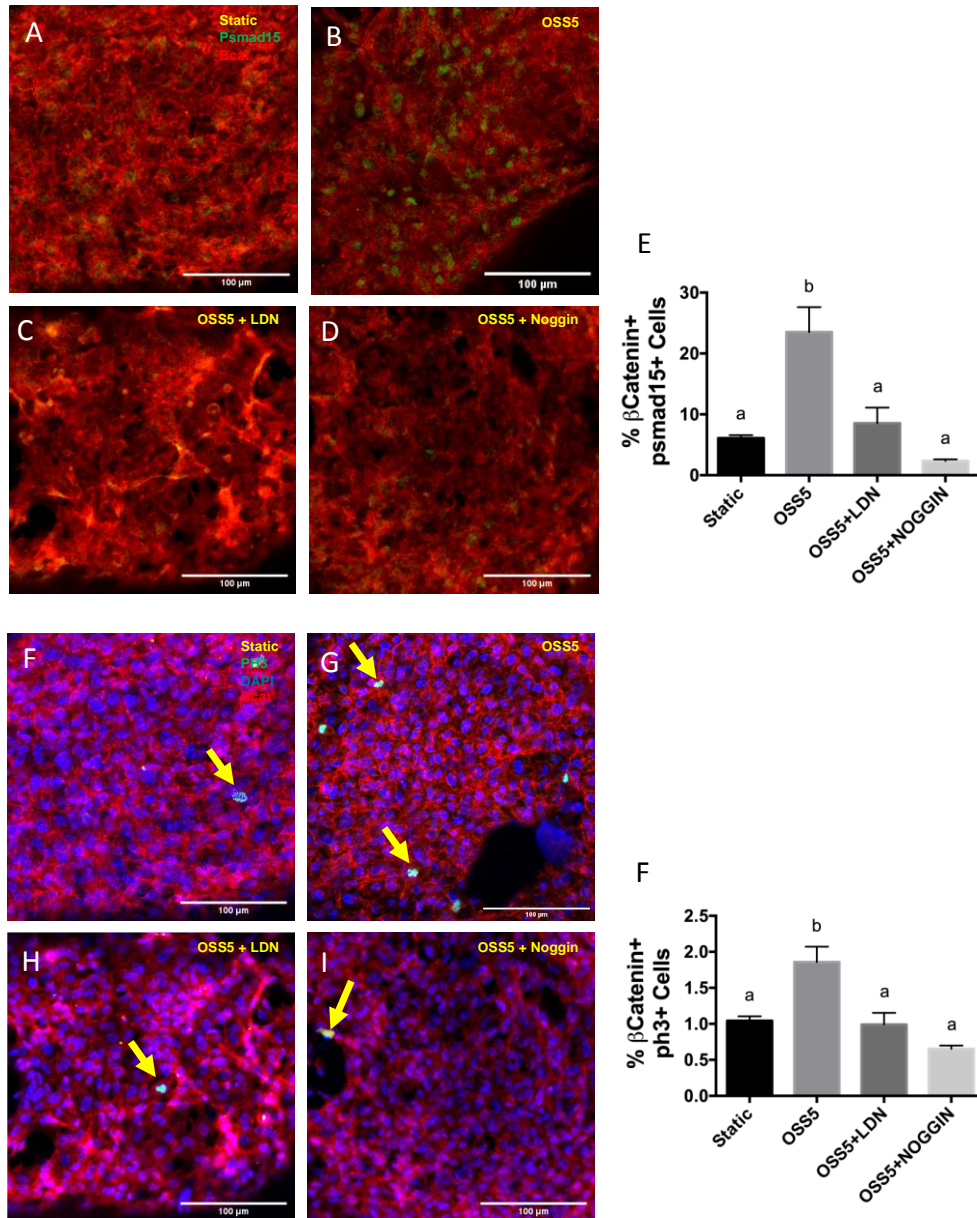


Figure 2.6. Inhibition of BMP signaling downregulates endocardial proliferation under OSS5. **A-D**, Immunostaining of pSMAD15 in static (**A**), OSS5 (**B**), OSS5+LDN193189 (**C**), and OSS5+Noggin (**D**). Endocardial cells were stained with β catenin (red). **E**, Quantification of pSMAD15 activity based on percentage of endocardial cells positive for nuclear pSMAD15. Yellow arrows indicate pSMAD15+ cells. **F-I**, Immunostaining of PHH3 in static (**F**), OSS5 (**G**), OSS5+LDN193189 (**H**), and OSS5+Noggin (**I**). Yellow arrows indicate pSMAD15+ cells. **F**, Quantification of PHH3 activity based on percentage of endocardial cells positive for nuclear PHH3. Data are means \pm SEM. N=7-8 endocardial patches per group. Bars that do not share any letters are significantly different ($p < 0.05$ via ANOVA with Tukey multiple comparisons correction). Scale bars indicate 100 μ m.

2.4.7 Notch signaling is required for modulation of BMP signaling in endocardial cells

Recently, ECs on the inflow side of the OFT valves have been associated with Notch signaling and high LSS. Since high LSS has been associated with inhibition of BMP signaling, we determined whether high LSS mediates the modulation of BMP activity by Notch signaling. To do this, we pretreated the primary ECs with DAPT, an inhibitor of γ -secretase and pan-Notch signaling. We then exposed pretreated ECs to LSS at 20 dynes/cm² in culture media containing DAPT and measured BMP activation and proliferation based on the percentage of PSMAD15+ and PHH3+ ECs, respectively.

While LSS20 significantly increased %PSMAD15 ECs compared to static (Figure 7A and B), inhibition of Notch signaling by DAPT increased pSMAD15 nuclear translocation by 6% (Figure 7C), suggesting that Notch signaling is required for LSS20-driven BMP inhibition. To expand these results, we determine whether Notch inhibition could also induce endocardial proliferation. Interestingly, while there was no significant difference in endocardial proliferation between LSS20 and static controls (Figure 7E and F), inhibition of Notch signaling by DAPT increased %PHH3+ cells by 0.8% (Figure 7G), suggesting that Notch signaling is required for LSS20-driven BMP inhibition.

Taken together, these data suggest that Notch signaling is required for LSS20-induced inhibition of BMP signaling and proliferation in ECs.

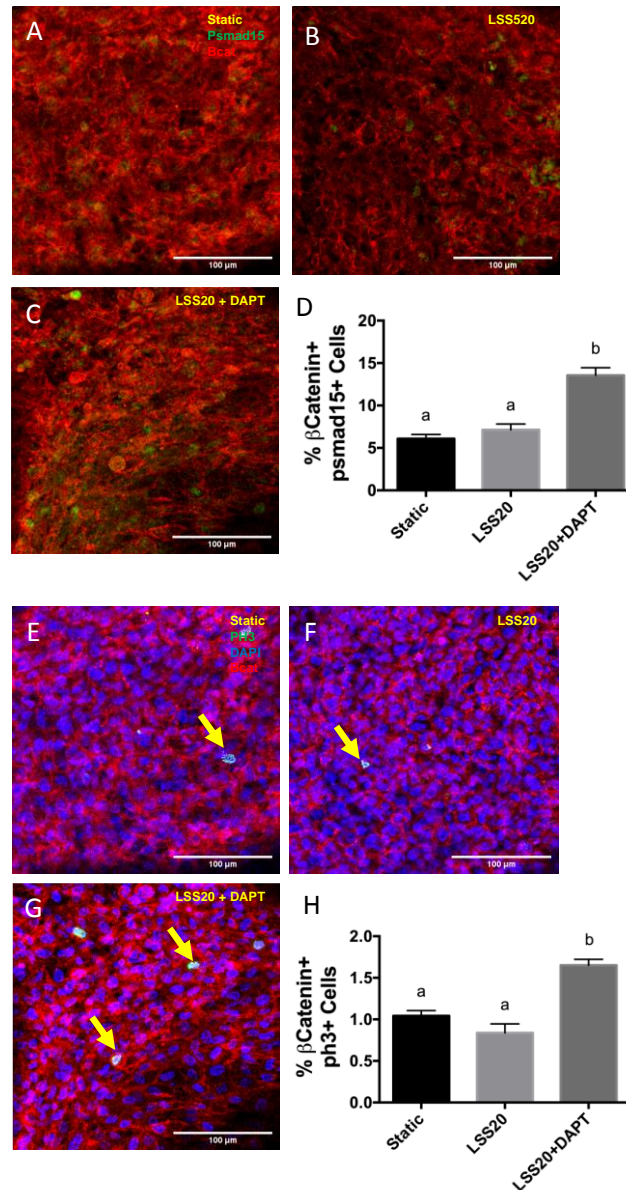


Figure 2.7. Enhanced BMP signaling in Notch1-inhibited endocardial cells. **A-D**, Immunostaining of pSMAD15 in endocardial cells exposed to static (**A**), LSS20 (**B**), and LSS20+DAPT (**C**). Endocardial cells were stained with β catenin (red). **D**, Quantification of pSMAD15 activity based on percentage of endocardial cells positive for nuclear pSMAD15. **E-H**, Immunostaining of PHH3 in endocardial cells exposed to static (**E**), LSS20 (**F**), and LSS20+DAPT (**G**). Yellow arrows indicate PHH3+ cells. **H** Quantification of PHH3 activity based on percentage of endocardial cells positive for nuclear PHH3. Data are means +/- SEM. N=7-8 endocardial patches per group. Bars that do not share any letters are significantly different ($p < 0.05$ via ANOVA with Tukey multiple comparisons correction). Scale bars indicate 100um.

2.4.8 Wnt/ β -catenin mediates differential BMP activation by shear stress

β -catenin is not only an endocardial marker, but its nuclear translocation also induces canonical WNT signaling. Recently, Wnt/ β -catenin has been shown to regulate endocardial proliferation during remodeling of both the OFT and AV valves (Wang, 2017). Here, we found that Wnt/ β -catenin signaling is also sensitive to shear stress (Figure 8E and Figure 5A-D). Specifically, under OSS5, ECs exhibited about twice as much nuclear β -catenin than that under LSS20 ($P < 0.05$, Figure 8E), suggesting that low OSS environment associated with the outflow side of the valve could induce Wnt/ β -catenin signaling. Surprisingly, there was no significant difference in nuclear β -catenin positive cells between OSS5 and static samples, indicating that OSS5 is actually not sufficient to induce Wnt/ β -catenin activation. However, LSS20 and OSS20 significantly reduced the percentage of nuclear β -catenin+ cells by 5% compared to compared to the static control ($P < 0.05$), suggesting that high shear stress, regardless of mode, inhibits Wnt/ β -catenin activation.

Since the OSS5 is associated with both Wnt/ β -catenin and BMP signaling, we determined whether Wnt/ β -catenin mediates shear-induced BMP activation. To this end, we inhibited Wnt/ β -catenin signaling with XAV939 (1 μ M) in ECs exposed to OSS5 and compared BMP activation in these cells to static and vehicle-treated controls. XAV939 maintains membranous β -catenin levels (Figure 8N) and prevent nuclear translocation and propagation of canonical Wnt signaling. Interestingly, XAV939 inhibition under OSS5 significantly reduced pSMAD15+ cells by about 15% ($P < 0.05$, Figure 8M-O), compared to vehicle-treated and static controls, indicating that Wnt/ β -

catenin is required for OSS5 induction of BMP activity. To expand these results, we determined whether Notch signaling mediates LSS20-induced inhibition of Wnt/ β -catenin signaling and downstream BMP activity. To do this, we inhibited Notch signaling using DAPT and measured %nuclear β -catenin positive cells under LSS20 stimulation. Compared to vehicle-treated cells and static controls, DAPT treatment significantly increased the number of ECs positive for nuclear β -catenin by 50% and 10%, respectively ($P < 0.05$, Figure 8A, B, F, and G), indicating that Notch signaling mediates LSS20 attenuation of canonical Wnt signaling and potentially blocks other non-shear related inducer of β catenin nuclear translocation.

To elucidate whether BMP is sufficient to rescue LSS20-induced BMP inactivation, we treated ECs with BMP2 (25ug/mL) under LSS20 stimulation. On the one hand, in response to BMP stimulation, ECs under static conditions exhibited significantly higher %pSMAD15+ and %PHH3+ cells compared to vehicle-treated controls ($P < 0.05$, Figure 8A-D and 8I-L), suggesting that BMP is sufficient to induce BMP activation and proliferation. On the other hand, when ECs exposed to LSS20 were stimulated with BMP2, there was surprisingly no significant increase in %pSMAD15+ or %PHH3+ cells (Figure 8H and P), suggesting that BMP is not sufficient to induce BMP signaling in ECs exposed to LSS20 and that Wnt/ β -catenin signaling is also required. Taken together, these results indicate that shear stress augments or modulates BMP activation by regulating canonical Wnt/ β -catenin signaling.

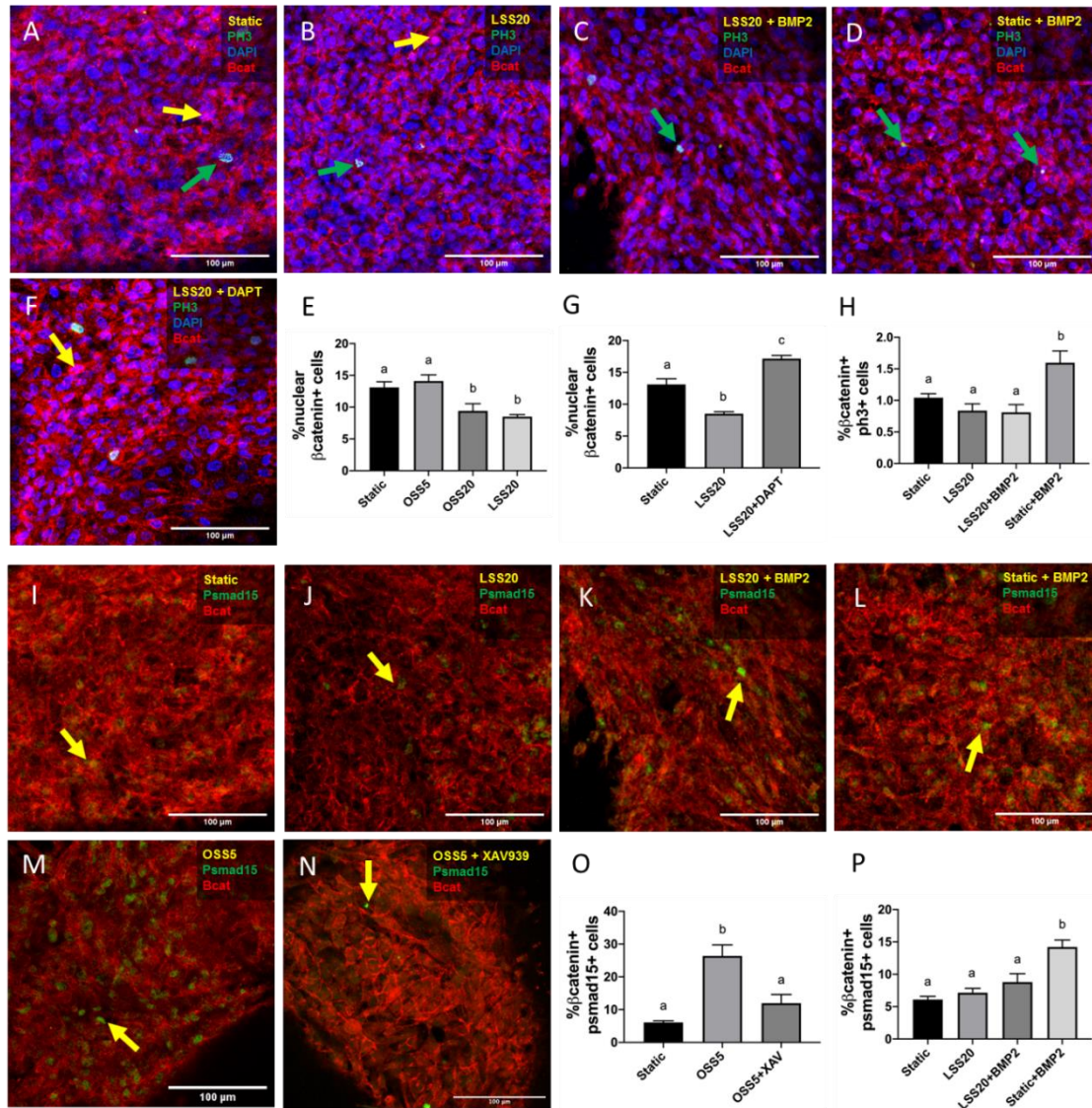


Figure 2.8. Canonical Wnt/ β catenin signaling mediates shear-induced regulation of endocardial proliferation. **A-F**, Immunostaining of PHH3 (green) in ECs exposed to static (**A**), LSS20 (**B**), LSS20+BMP2 (**C**), static+BMP2 (**D**), and LSS20+DAPT (**F**). ECs were stained with β catenin (red). Yellow arrows indicate nuclear β -catenin, while green arrows indicate PHH3+ cells. **E** and **G**, Quantification of canonical Wnt signaling based on percentage of ECs positive for nuclear β -catenin. **H**, Quantification of endocardial proliferation based on percentage of ECs positive for nuclear PHH3. **I-N**, Immunostaining of pSMAD15 in ECs exposed to static (**I**), LSS20 (**J**), LSS20+BMP2 (**K**), static+BMP2 (**L**), OSS5 (**M**), and OSS+XAV939 (**N**). Yellow arrows indicate pSMAD15+ cells. **O** and **P**, Quantification of BMP activation based on percentage of ECs positive for nuclear pSMAD15. Data are means \pm SEM. N=5-7 endocardial patches per group. Bars that do not share any letters are significantly different ($p < 0.05$ via ANOVA with Tukey multiple comparisons correction). Scale bars indicate 100 μ m.

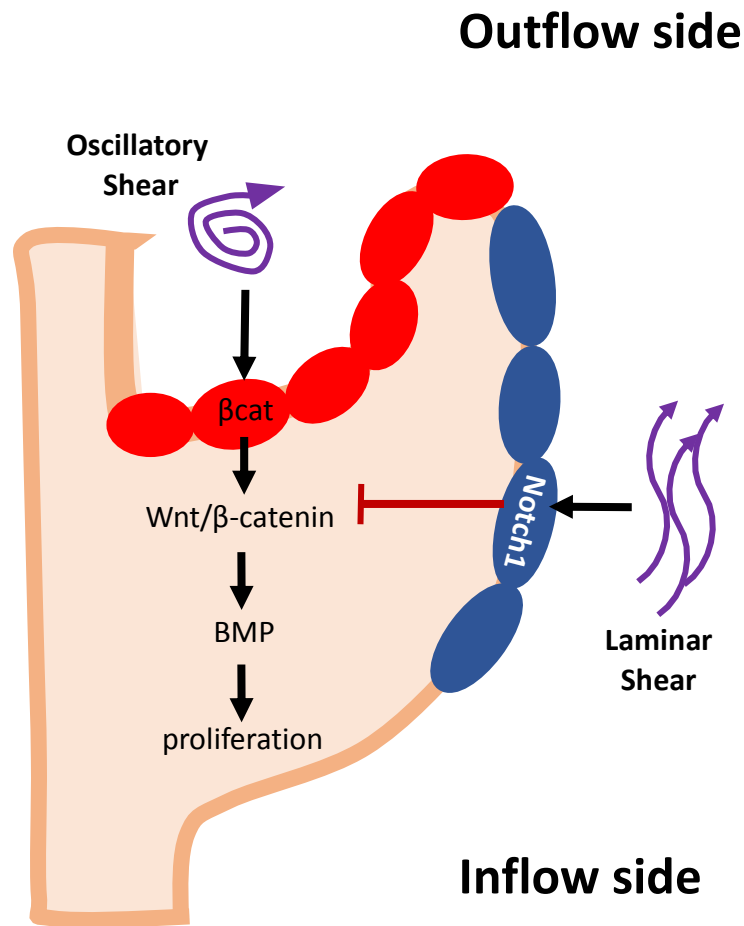


Figure 2.9. Shear stress regulates side-specificity of valve endocardial proliferation. During valve remodeling, expansion of valve primordia requires endocardial cell (EC) proliferation. The endocardium on the outflow side of the developing valve (red) senses and transduces low oscillatory shear stress (OSS) into BMP signaling that drives endocardial proliferation. In contrast, on the inflow side of the valve (blue), ECs under high laminar shear stress (LSS) activate Notch1 signaling, which restricts BMP-driven EC growth. WNT/βcatenin acts a force-driven molecular switch, which is activated by low OSS and deactivated by high LSS to regulate BMP signaling and EC proliferation.

2.5 Discussion

Tremendous scientific efforts have resulted in a plethora of knowledge about early valve formation but not mid-gestation valve remodeling. In fact, genetic abolition of genes critical for EndMT has generally led to insufficient valvular structures and early lethality in mouse models. However, observable CVMs in post-natal humans are, by definition, not embryonically lethal, suggesting that the pathology of CVMs may be due to faulty post-EndMT valve development. Therefore, a lack of understanding about how valves morph and remodel is a critical gap in our knowledge. Here, we investigated how hemodynamic signals, which are essential for heart development but have proven challenging to study, coordinate endocardial proliferation—a hallmark of valve remodeling. To elucidate the hemodynamic regulation of EC behaviors, we exposed primary valve ECs to shear stress of various modes and magnitudes in a 3D environment. Our study has revealed that shear stress regulates BMP-induced EC proliferation by differentially activating the WNT/ β -catenin molecular switch.

Since BMP is well accepted as a growth factor that influences cell proliferation in various contexts (Langenfeld, 2004; Suzuki, 2008; Derynck, 2013), it is almost axiomatic that BMP also drives valvular cell proliferation. However, despite multiple lines of evidence suggesting that overactive BMP signaling leads to hyperproliferation of the embryonic valve MCs (Jackson, 2003; Siervo, 2007; MacGrogan, 2016; Wang, 2018), no studies have delineated the effects of BMP on endocardial growth during valve remodeling. Careful examination of the *in vivo* results of prior studies revealed that ECs, like MCs, exhibited hyperproliferation in response to augmented BMP

signaling, providing us the prima facie evidence that EC proliferation might be regulated by BMP. Consistent with these results, our immunostaining data confirmed that mitotic and BMP-activated ECs are not only colocalized but also restricted to the outflow side of the developing valves, which experiences OSS.

A critical question is how and when shear stress initiates, sustains, and ceases BMP-dependent EC proliferation. We determined that mechanically induced BMP activation and EC proliferation require that the shear stress stimulation is oscillatory and low in magnitude—a mechanical profile associated with the outflow side. Curiously, BMP signaling of LSS5 is significantly higher than of LSS20 and even OSS20, demonstrating that the magnitude of shear stress is a stronger determinant of BMP activation, compared to mode. Furthermore, previous CFD analyses indicated that shear stress around the aortic root is about 10 dynes higher compared to that around the pulmonary root at E17.5 (Yap, 2014). Consistently with these results, we detected less BMP activation in ECs of the PV compared to AoV, further supporting the notion that the magnitude of shear stress and BMP activation are inversely related. It is conceivable that during valve remodeling, the combination of low magnitude and oscillatory mode induces BMP signaling and EC proliferation on the outflow side. In contrast, BMP signaling could be activated to a lesser extent by low LSS, perhaps to facilitate EndMT during early valve formation (Butcher, 2007). As the heart develops and beats more forcefully, ECs experience LSS and OSS of higher magnitudes, which downregulates BMP signaling to terminate BMP-induced endocardial growth.

We further identified WNT/ β catenin to be a force-driven molecular switch, through which shear stress differentially regulates BMP signaling. In our study, β catenin was originally used as a chick endocardial marker as it is a peripheral protein associated with vascular endothelial cadherin5. However, nuclear translocation of β catenin is also indicative of canonical WNT signaling and has recently been found to be sensitive to acute shear in multiple contexts, including endothelial cells (Warboys, 2018). Canonical WNT/ β catenin response to sustained shear stress and contributions to valve formation/malformations remain elusive. Our data demonstrated that in valve ECs, β catenin acts as a BMP molecular switch, which is activated by low OSS and deactivated by high LSS. These results are consistent with in vivo data showing restriction of canonical WNT/ β catenin signaling to the outflow side of the OFT valves using a transgenic reporter mouse line (Wang, 2018). The mechanism of mechanotransduction of β catenin in valve ECs is unclear and warrants further investigation.

Interestingly, our results confirmed that Notch1 downregulates β catenin nuclear translocation, which subsequently inhibits BMP activity and endocardial proliferation. This effect could be attributed to the ability of Notch1 to stabilize and sequester β catenin at the plasma membrane. In fact, ectopic activation of Notch1 resulted in downregulation of nuclear β catenin and canonical WNT signaling (Wang, 2016), possibly by directly associating with β catenin (Kwon 2011; Kim, 2012). While BMP activation and proliferation were upregulated under BMP/static condition, BMP did not rescue the LSS20-induced inhibition of proliferation but did increase BMP

activation. These data demonstrate that LSS20 may inhibit endocardial proliferation through Notch1-induced inhibition of WNT/ β catenin signaling, which is required for BMP activation. On the one hand, it is conceivable that WNT/ β catenin signaling interacts with BMP pathways downstream of BMP ligation. On the other hand, Notch1 signaling could directly interfere with BMP signaling pathway. In fact, Herp2, a target gene of Notch signaling, has been shown to antagonize Id1, a target gene of BMP signaling downstream of pSMAD15 in endothelial cells (Itoh, 2004). In addition, Notch1 upregulates smad6, which in turn modulates BMP signaling upstream of BMP target gene expression in HUVECs (Mouillesseaux, 2016).

In this study, we also presented evidence showing that this shear-driven upregulation of BMP is ligand-dependent. We found that in response to OSS5, ECs upregulated expression of BMP2, 4, and 6 ligands, confirming *in vivo* expression indicating that chick ECs on the outflow side are associated with BMP2, 4, and 6 expression (Somi, 2004). In mice, ablation of BMP4 resulted in nonelongated OFT cushion defects, suggesting that other BMPs could not compensate for the valve defects in these mice (Bai, 2013; McCulley, 2008). In fact, complete ablation of BMP5, 6, and 7 did not result in cushion defects (Kingsley, 1992; Solloway, 1998; Dudley, 1995). Our results demonstrated, consistent with these findings, that BMP4 is the main mediator of low OSS in driving EC proliferation. In contrast, BMP2, 4, 5, and 7 likely coordinate and compensate for each other in the AV valves. Interestingly, BMP2 and 4 double heterozygous mice exhibited AV valve defects, suggesting that AV valve remodeling is dependent on the dosage of BMP2 and 4 (Uchimura, 2009). However,

ablation of both BMP6 and 7 did not result in AV valve malformations. These findings demonstrate a more robust heterogeneity and inter-compensatory nature of BMP ligands in the AV valves, compared to the OFT valves.

Intriguingly, on a tissue morphogenetic level, defective endocardial proliferation programs, e.g. VEGF, BMP, and Nfact1, have been shown to result in nonelongated valve leaflets (Stanukas, 2010; McCulley, 2008; Wu, 2011). While recent studies have only attributed valve growth or overgrowth to aberrant regulation of MC proliferation, our data suggest that endocardial growth and lengthening can be the limiting factor that drives valve extension and shaping. Furthermore, our results strongly suggest a functional coordination between shear stress and BMP signaling in regulating the side-specificity of endocardial proliferation and valve extension. In fact, *in vivo* manipulation of hemodynamics has resulted in abnormal valve formation. For example, vitelline vein ligation, which decreases OFT blood velocity (Rugonyi, 2008) as well as left atrial ligation, which decreases ventricular end-diastolic volume and pressure (Tobita, 2002) have been shown to result in semilunar valve malformation (Hogers, 1999; Broekhuizen, 1999; Harh, 1973).

In conclusion, this study has revealed a novel regulatory program that transduces side-specific hemodynamic information into differential endocardial growth. Mechanistically, low OSS induces WNT/ β catenin signaling and subsequent BMP-dependent endocardial proliferation, while high LSS restricts endocardial growth via Notch1-induced inhibition of β catenin nuclear translocation (Figure 9). These findings establish a novel link between hemodynamic signals and cellular programs

during valve remodeling, providing an avenue for mechanically inspired surgical interventions to restore normal valve morphogenesis or maintain homeostasis.

2.6 References

1. Baeyens, N., Larrivé, B., Ola, R., Hayward-Piatkowskyi, B., Dubrac, A., Huang, B., ... & Tong, H. (2016). Defective fluid shear stress mechanotransduction mediates hereditary hemorrhagic telangiectasia. *Journal of Cell Biology, 214*(7), 807-816.
2. Bai, Y., Wang, J., Morikawa, Y., Bonilla-Claudio, M., Klysik, E., & Martin, J. F. (2013). Bmp signaling represses Vegfa to promote outflow tract cushion development. *Development, 140*(16), 3395-3402.
3. Beppu, H., Malhotra, R., Beppu, Y., Lepore, J. J., Parmacek, M. S., & Bloch, K. D. (2009). BMP type II receptor regulates positioning of outflow tract and remodeling of atrioventricular cushion during cardiogenesis. *Developmental biology, 331*(2), 167-175.
4. Bharadwaj, K. N., Spitz, C., Shekhar, A., Yalcin, H. C., & Butcher, J. T. (2012). Computational fluid dynamics of developing avian outflow tract heart valves. *Annals of biomedical engineering, 40*(10), 2212-2227.
5. Butcher, J. T., & Markwald, R. R. (2007). Valvulogenesis: the moving target. *Philosophical Transactions of the Royal Society B: Biological Sciences, 362*(1484), 1489-1503.
6. Combs, M. D., & Yutzey, K. E. (2009). Heart valve development: regulatory networks in development and disease. *Circulation research, 105*(5), 408-421.

7. Conway, D. E., Williams, M. R., Eskin, S. G., & McIntire, L. V. (2010). Endothelial cell responses to atheroprone flow are driven by two separate flow components: low time-average shear stress and fluid flow reversal. *American journal of physiology. Heart and circulatory physiology*, 298(2), H367–H374. <https://doi.org/10.1152/ajpheart.00565.2009>
8. Dejana, E. (2010). The role of wnt signaling in physiological and pathological angiogenesis. *Circulation research*, 107(8), 943-952.
9. Del Monte, G., Grego-Bessa, J., González-Rajal, A., Bolós, V., & De La Pompa, J. L. (2007). Monitoring Notch1 activity in development: evidence for a feedback regulatory loop. *Developmental dynamics: an official publication of the American Association of Anatomists*, 236(9), 2594-2614.
10. Derynck, R., & Akhurst, R. J. (2013). BMP-9 balances endothelial cell fate. *Proceedings of the National Academy of Sciences*, 110(47), 18746-18747.
11. Derynck, R., & Akhurst, R. J. (2013). BMP-9 balances endothelial cell fate. *Proceedings of the National Academy of Sciences*, 110(47), 18746-18747.
12. Dietrich, A. C., Lombardo, V. A., Veerkamp, J., Priller, F., & Abdelilah-Seyfried, S. (2014). Blood flow and Bmp signaling control endocardial chamber morphogenesis. *Developmental cell*, 30(4), 367-377.
13. Dragt, B. S., van Agtmaal, E. L., de Laat, B., & Voorberg, J. (2012). Effect of laminar shear stress on the distribution of Weibel-Palade bodies in endothelial cells. *Thrombosis research*, 130(5), 741-745.

14. Dudley, A. T., Lyons, K. M., & Robertson, E. J. (1995). A requirement for bone morphogenetic protein-7 during development of the mammalian kidney and eye. *Genes & development*, *9*(22), 2795-2807.
15. Dyer, L. A., Pi, X., & Patterson, C. (2014). The role of BMPs in endothelial cell function and dysfunction. *Trends in Endocrinology & Metabolism*, *25*(9), 472-480.
16. Fang, J. S., Coon, B. G., Gillis, N., Chen, Z., Qiu, J., Chittenden, T. W., ... & Hirschi, K. K. (2017). Shear-induced Notch-Cx37-p27 axis arrests endothelial cell cycle to enable arterial specification. *Nature communications*, *8*(1), 1-14.
17. Ferencz, C., Neill, C. A., Boughman, J. A., Rubin, J. D., Brenner, J. I., & Perry, L. W. (1989). Congenital cardiovascular malformations associated with chromosome abnormalities: an epidemiologic study. *The Journal of pediatrics*, *114*(1), 79-86.
18. Garside, V. C., Chang, A. C., Karsan, A., & Hoodless, P. A. (2013). Co-ordinating Notch, BMP, and TGF- β signaling during heart valve development. *Cellular and molecular life sciences*, *70*(16), 2899-2917.
19. Gaussin, V., Van de Putte, T., Mishina, Y., Hanks, M. C., Zwijsen, A., Huylebroeck, D., ... & Schneider, M. D. (2002). Endocardial cushion and myocardial defects after cardiac myocyte-specific conditional deletion of the bone morphogenetic protein receptor ALK3. *Proceedings of the National Academy of Sciences*, *99*(5), 2878-2883.

20. Goddard, L. M., Duchemin, A. L., Ramalingan, H., Wu, B., Chen, M., Bamezai, S., ... & Scherrer-Crosbie, M. (2017). Hemodynamic forces sculpt developing heart valves through a KLF2-WNT9B paracrine signaling axis. *Developmental cell*, 43(3), 274-289.
21. Goetz, J. G., Steed, E., Ferreira, R. R., Roth, S., Ramspacher, C., Boselli, F., ... & Vermot, J. (2014). Endothelial cilia mediate low flow sensing during zebrafish vascular development. *Cell reports*, 6(5), 799-808.
22. Gould, R. A., & Butcher, J. T. (2010). Isolation of valvular endothelial cells. *JoVE (Journal of Visualized Experiments)*, (46), e2158.
23. Hernández, G. L., Volpert, O. V., Íñiguez, M. A., Lorenzo, E., Martínez-Martínez, S., Grau, R., ... & Redondo, J. M. (2001). Selective inhibition of vascular endothelial growth factor-mediated angiogenesis by cyclosporin A: roles of the nuclear factor of activated T cells and cyclooxygenase 2. *The Journal of experimental medicine*, 193(5), 607-620.
24. Hinton, R. B., & Yutzey, K. E. (2011). Heart valve structure and function in development and disease. *Annual review of physiology*, 73, 29-46.
25. Hurle, J. M. (1979). Scanning and light microscope studies of the development of the chick embryo semilunar heart valves. *Anatomy and embryology*, 157(1), 69-80.
26. Hurle, J. M., Colvee, E., & Blanco, A. M. (1980). Development of mouse semilunar valves. *Anatomy and embryology*, 160(1), 83-91.

27. Itoh, F., Itoh, S., Goumans, M. J., Valdimarsdottir, G., Iso, T., Dotto, G. P., ... & ten Dijke, P. (2004). Synergy and antagonism between Notch and BMP receptor signaling pathways in endothelial cells. *The EMBO journal*, *23*(3), 541-551.
28. Jackson, L. F., Qiu, T. H., Sunnarborg, S. W., Chang, A., Zhang, C., Patterson, C., & Lee, D. C. (2003). Defective valvulogenesis in HB-EGF and TACE-null mice is associated with aberrant BMP signaling. *The EMBO journal*, *22*(11), 2704-2716.
29. Jahnsen, E. D., Trindade, A., Zaun, H. C., Lehoux, S., Duarte, A., & Jones, E. A. (2015). Notch1 is pan-endothelial at the onset of flow and regulated by flow. *PloS one*, *10*(4).
30. Jain, R., Engleka, K. A., Rentschler, S. L., Manderfield, L. J., Li, L., Yuan, L., & Epstein, J. A. (2011). Cardiac neural crest orchestrates remodeling and functional maturation of mouse semilunar valves. *The Journal of clinical investigation*, *121*(1), 422-430.
31. Johnson, E. N., Lee, Y. M., Sander, T. L., Rabkin, E., Schoen, F. J., Kaushal, S., & Bischoff, J. (2003). NFATc1 mediates vascular endothelial growth factor-induced proliferation of human pulmonary valve endothelial cells. *Journal of Biological Chemistry*, *278*(3), 1686-1692.
32. Kefalos, P., Agalou, A., Kawakami, K., & Beis, D. (2019). Reactivation of Notch signaling is required for cardiac valve regeneration. *Scientific reports*, *9*(1), 1-8.

33. Kilner, P. J., Yang, G. Z., Wilkes, A. J., Mohiaddin, R. H., Firmin, D. N., & Yacoub, M. H. (2000). Asymmetric redirection of flow through the heart. *Nature*, *404*(6779), 759-761.
34. Kingsley, D. M., Bland, A. E., Grubber, J. M., Marker, P. C., Russell, L. B., Copeland, N. G., & Jenkins, N. A. (1992). The mouse short ear skeletal morphogenesis locus is associated with defects in a bone morphogenetic member of the TGF β superfamily. *Cell*, *71*(3), 399-410.
35. Kostina, A. S., Uspensky, V. E., Irtyuga, O. B., Ignatieva, E. V., Freylikhman, O., Gavriliuk, N. D., ... & Malashicheva, A. B. (2016). Notch-dependent EMT is attenuated in patients with aortic aneurysm and bicuspid aortic valve. *Biochimica et Biophysica Acta (BBA)-Molecular Basis of Disease*, *1862*(4), 733-740.
36. Kostina, A., Bjork, H., Ignatieva, E., Irtyuga, O., Uspensky, V., Semenova, D., ... & Gordeev, M. (2018). Notch, BMP and WNT/ β -catenin network is impaired in endothelial cells of the patients with thoracic aortic aneurysm. *Atherosclerosis Supplements*, *35*, e6-e13.
37. Langenfeld, E. M., & Langenfeld, J. (2004). Bone Morphogenetic Protein-2 Stimulates Angiogenesis in Developing Tumors11NIH K22 grant CA91919-01A1 and UMDNJ Foundation to J. Langenfeld. *Molecular Cancer Research*, *2*(3), 141-149.
38. Lecarpentier, E., Bhatt, M., Bertin, G. I., Deloison, B., Salomon, L. J., Deloron, P., ... & Tsatsaris, V. (2016). Computational fluid dynamic simulations of

- maternal circulation: wall shear stress in the human placenta and its biological implications. *PloS one*, 11(1).
39. Lee, J., Fei, P., Packard, R. R. S., Kang, H., Xu, H., Baek, K. I., ... & Chi, N. C. (2016). 4-Dimensional light-sheet microscopy to elucidate shear stress modulation of cardiac trabeculation. *The Journal of clinical investigation*, 126(5), 1679-1690.
40. Lee, Y. M., Cope, J. J., Ackermann, G. E., Goishi, K., Armstrong, E. J., Paw, B. H., & Bischoff, J. (2006). Vascular endothelial growth factor receptor signaling is required for cardiac valve formation in zebrafish. *Developmental dynamics: an official publication of the American Association of Anatomists*, 235(1), 29-37.
41. Li, R., Beebe, T., Jen, N., Yu, F., Takabe, W., Harrison, M., ... & Wang, K. (2014). Shear stress-activated Wnt-Angiopoietin-2 signaling recapitulates vascular repair in zebrafish embryos. *Arteriosclerosis, thrombosis, and vascular biology*, 34(10), 2268-2275.
42. Li, Y. S. J., Haga, J. H., & Chien, S. (2005). Molecular basis of the effects of shear stress on vascular endothelial cells. *Journal of biomechanics*, 38(10), 1949-1971.
43. Luna-Zurita, L., Prados, B., Grego-Bessa, J., Luxán, G., Del Monte, G., Benguría, A., ... & De La Pompa, J. L. (2010). Integration of a Notch-dependent mesenchymal gene program and Bmp2-driven cell invasiveness regulates murine cardiac valve formation. *The Journal of clinical investigation*, 120(10), 3493-3507.

44. MacGrogan, D., D'Amato, G., Travisano, S., Martinez-Poveda, B., Luxán, G., del Monte-Nieto, G., ... & Gómez, M. J. (2016). Sequential ligand-dependent notch signaling activation regulates valve primordium formation and morphogenesis. *Circulation research*, *118*(10), 1480-1497.
45. Mahler, G. J., Frendl, C. M., Cao, Q., & Butcher, J. T. (2014). Effects of shear stress pattern and magnitude on mesenchymal transformation and invasion of aortic valve endothelial cells. *Biotechnology and bioengineering*, *111*(11), 2326-2337.
46. Masumura, T., Yamamoto, K., Shimizu, N., Obi, S., & Ando, J. (2009). Shear stress increases expression of the arterial endothelial marker ephrinB2 in murine ES cells via the VEGF-Notch signaling pathways. *Arteriosclerosis, thrombosis, and vascular biology*, *29*(12), 2125-2131.
47. McBride, K. L., Zender, G. A., Fitzgerald-Butt, S. M., Koehler, D., Menesses-Diaz, A., Fernbach, S., ... & Belmont, J. W. (2009). Linkage analysis of left ventricular outflow tract malformations (aortic valve stenosis, coarctation of the aorta, and hypoplastic left heart syndrome). *European journal of human genetics*, *17*(6), 811-819.
48. McCulley, D. J., Kang, J. O., Martin, J. F., & Black, B. L. (2008). BMP4 is required in the anterior heart field and its derivatives for endocardial cushion remodeling, outflow tract septation, and semilunar valve development. *Developmental dynamics: an official publication of the American Association of Anatomists*, *237*(11), 3200-3209.

49. Midgett, M., & Rugonyi, S. (2014). Congenital heart malformations induced by hemodynamic altering surgical interventions. *Frontiers in physiology*, *5*, 287.
50. Mouillesseaux, K. P., Wiley, D. S., Saunders, L. M., Wylie, L. A., Kushner, E. J., Chong, D. C., ... & Samsa, L. A. (2016). Notch regulates BMP responsiveness and lateral branching in vessel networks via SMAD6. *Nature communications*, *7*(1), 1-12.
51. Nandy, S., & Tarbell, J. M. (1987). Flush mounted hot film anemometer measurement of wall shear stress distal to a tri-leaflet valve for Newtonian and non-Newtonian blood analog fluids. *Biorheology*, *24*(5), 483-500.
52. Pedrosa, A. R., Trindade, A., Fernandes, A. C., Carvalho, C., Gigante, J., Tavares, A. T., ... & Duarte, A. (2015). Endothelial Jagged1 antagonizes Dll4 regulation of endothelial branching and promotes vascular maturation downstream of Dll4/Notch1. *Arteriosclerosis, thrombosis, and vascular biology*, *35*(5), 1134-1146.
53. Qin, W. D., Zhang, F., Qin, X. J., Wang, J., Meng, X., Wang, H., ... & Zhang, M. X. (2016). Notch1 inhibition reduces low shear stress-induced plaque formation. *The international journal of biochemistry & cell biology*, *72*, 63-72.
54. Samsa, L. A., Givens, C., Tzima, E., Stainier, D. Y., Qian, L., & Liu, J. (2015). Cardiac contraction activates endocardial Notch signaling to modulate chamber maturation in zebrafish. *Development*, *142*(23), 4080-4091.

55. Shelton, E. L., & Yutzey, K. E. (2008). Twist1 function in endocardial cushion cell proliferation, migration, and differentiation during heart valve development. *Developmental biology*, 317(1), 282-295.
56. Sierro, F., Biben, C., Martínez-Muñoz, L., Mellado, M., Ransohoff, R. M., Li, M., ... & Harvey, R. P. (2007). Disrupted cardiac development but normal hematopoiesis in mice deficient in the second CXCL12/SDF-1 receptor, CXCR7. *Proceedings of the National Academy of Sciences*, 104(37), 14759-14764.
57. Sivarapatna, A., Ghaedi, M., Le, A. V., Mendez, J. J., Qyang, Y., & Niklason, L. E. (2015). Arterial specification of endothelial cells derived from human induced pluripotent stem cells in a biomimetic flow bioreactor. *Biomaterials*, 53, 621-633.
58. Solloway, M. J., Dudley, A. T., Bikoff, E. K., Lyons, K. M., Hogan, B. L., & Robertson, E. J. (1998). Mice lacking Bmp6 function. *Developmental genetics*, 22(4), 321-339.
59. Song, L., Fässler, R., Mishina, Y., Jiao, K., & Baldwin, H. S. (2007). Essential functions of Alk3 during AV cushion morphogenesis in mouse embryonic hearts. *Developmental biology*, 301(1), 276-286.
60. Sorescu, G. P., Song, H., Tressel, S. L., Hwang, J., Dikalov, S., Smith, D. A., ... & Jo, H. (2004). Bone morphogenic protein 4 produced in endothelial cells by oscillatory shear stress induces monocyte adhesion by stimulating reactive

- oxygen species production from a nox1-based NADPH oxidase. *Circulation research*, 95(8), 773-779.
61. Sorescu, G. P., Sykes, M., Weiss, D., Platt, M. O., Saha, A., Hwang, J., ... & Jo, H. (2003). Bone morphogenetic protein 4 produced in endothelial cells by oscillatory shear stress stimulates an inflammatory response. *Journal of Biological Chemistry*, 278(33), 31128-31135.
62. Stankunas, K., Ma, G. K., Kuhnert, F. J., Kuo, C. J., & Chang, C. P. (2010). VEGF signaling has distinct spatiotemporal roles during heart valve development. *Developmental biology*, 347(2), 325-336.
63. Sugi, Y., Yamamura, H., Okagawa, H., & Markwald, R. R. (2004). Bone morphogenetic protein-2 can mediate myocardial regulation of atrioventricular cushion mesenchymal cell formation in mice. *Developmental biology*, 269(2), 505-518.
64. Sun, L., Rajamannan, N. M., & Sucosky, P. (2013). Defining the role of fluid shear stress in the expression of early signaling markers for calcific aortic valve disease. *PloS one*, 8(12).
65. Suzuki, Y., Montagne, K., Nishihara, A., Watabe, T., & Miyazono, K. (2008). BMPs promote proliferation and migration of endothelial cells via stimulation of VEGF-A/VEGFR2 and angiopoietin-1/Tie2 signalling. *Journal of biochemistry*, 143(2), 199-206.
66. Theodoris, C. V., Li, M., White, M. P., Liu, L., He, D., Pollard, K. S., ... & Srivastava, D. (2015). Human disease modeling reveals integrated

transcriptional and epigenetic mechanisms of NOTCH1

haploinsufficiency. *Cell*, 160(6), 1072-1086.

67. Uchimura, T., Komatsu, Y., Tanaka, M., McCann, K. L., & Mishina, Y. (2009). Bmp2 and Bmp4 genetically interact to support multiple aspects of mouse development including functional heart development. *genesis*, 47(6), 374-384.
68. Van der Heiden, K., Groenendijk, B. C., Hierck, B. P., Hogers, B., Koerten, H. K., Mommaas, A. M., ... & Poelmann, R. E. (2006). Monocilia on chicken embryonic endocardium in low shear stress areas. *Developmental dynamics: an official publication of the American Association of Anatomists*, 235(1), 19-28.
69. Wang, Y., Lu, P., Wu, B., Riascos-Bernal, D. F., Sibinga, N. E., Valenta, T., ... & Zhou, B. (2018). Myocardial β -Catenin-BMP2 signaling promotes mesenchymal cell proliferation during endocardial cushion formation. *Journal of molecular and cellular cardiology*, 123, 150-158.
70. Wang, Y., Wu, B., Farrar, E., Lui, W., Lu, P., Zhang, D., ... & Xu, D. (2017). Notch-Tnf signalling is required for development and homeostasis of arterial valves. *European heart journal*, 38(9), 675-686.
71. Wang, Y., Wu, B., Lu, P., Zhang, D., Wu, B., Varshney, S., ... & Sibinga, N. E. (2017). Uncontrolled angiogenic precursor expansion causes coronary artery anomalies in mice lacking Pofut1. *Nature communications*, 8(1), 1-15.

72. Wasserman, S. M., Mehraban, F., Komuves, L. G., Yang, R. B., Tomlinson, J. E., Zhang, Y., ... & Topper, J. N. (2002). Gene expression profile of human endothelial cells exposed to sustained fluid shear stress. *Physiological genomics*, 12(1), 13-23.
73. Weston, M. W., LaBorde, D. V., & Yoganathan, A. P. (1999). Estimation of the shear stress on the surface of an aortic valve leaflet. *Annals of biomedical engineering*, 27(4), 572-579.
74. Weston, M. W., LaBorde, D. V., & Yoganathan, A. P. (1999). Estimation of the shear stress on the surface of an aortic valve leaflet. *Annals of biomedical engineering*, 27(4), 572-579.
75. White, M. P., Theodoris, C. V., Liu, L., Collins, W. J., Blue, K. W., Lee, J. H., ... & Srivastava, D. (2015). NOTCH1 regulates matrix gla protein and calcification gene networks in human valve endothelium. *Journal of molecular and cellular cardiology*, 84, 13-23.
76. Wu, B., Wang, Y., Lui, W., Langworthy, M., Tompkins, K. L., Hatzopoulos, A. K., ... & Zhou, B. (2011). Nfatc1 coordinates valve endocardial cell lineage development required for heart valve formation. *Circulation research*, 109(2), 183-192.
77. Yap, C. H., Liu, X., & Pekkan, K. (2014). Characterization of the vessel geometry, flow mechanics and wall shear stress in the great arteries of wildtype prenatal mouse. *PloS one*, 9(1).

78. Yap, C. H., Saikrishnan, N., Tamilselvan, G., & Yoganathan, A. P. (2012). Experimental measurement of dynamic fluid shear stress on the aortic surface of the aortic valve leaflet. *Biomechanics and modeling in mechanobiology*, *11*(1-2), 171-182.
79. Zhang, H., & Bradley, A. (1996). Mice deficient for BMP2 are nonviable and have defects in amnion/chorion and cardiac development. *Development*, *122*(10), 2977-2986.
80. Zhang, J., Chang, J. Y., Huang, Y., Lin, X., Luo, Y., Schwartz, R. J., ... & Wang, F. (2010). The FGF-BMP signaling axis regulates outflow tract valve primordium formation by promoting cushion neural crest cell differentiation. *Circulation research*, *107*(10), 1209-1219.
81. Zhou, J., Lee, P. L., Lee, C. I., Wei, S. Y., Lim, S. H., Lin, T. E., ... & Chiu, J. J. (2013). BMP receptor-integrin interaction mediates responses of vascular endothelial Smad1/5 and proliferation to disturbed flow. *Journal of Thrombosis and Haemostasis*, *11*(4), 741-755.

CHAPTER 3. UNIDIRECTIONAL SHEAR STRESS COORDINATES

ENDOCARDIAL NOTCH1 AND SUBENDOCARDIAL CXCR4

SIGNALING TO REGULATE FETAL VALVE REMODELING

3.1 Abstract

Rationale: CXCR4 signaling is implicated in epithelial-mesenchymal transition (EMT) and migration of cardiac neural crest cells during early valve formation. Although CXCR4 has been detected in the valve region post-EMT, how CXCR4 signaling regulates valve remodeling processes is unclear. Here, we hypothesized that CXCR4 is required to regulate the hallmarks of valve remodeling: cell proliferation, differentiation, matrix maturation, and tissue compaction.

Methods and Results: We found that CXCR4 and its ligand CXCL12 are expressed in the mesenchymal cells in the subendocardial region during post-EMT valve remodeling stages. Global deletion of CXCR4 resulted in hyperproliferative and thickened outflow tract (OFT) valves. Using endocardial cell lineage specific conditional deletion of CXCR4, we determined that CXCR4 signaling by endocardium-derived mesenchymal cells is sufficient to regulate cell proliferation. In addition, conditional ablation of CXCR4 also revealed that it was required for matrix remodeling and tissue compaction by inhibiting BMP and WNT signaling programs. We also found that endocardial Notch1 signaling regulates subendocardial CXCR4 expression by ablating Notch1 only in the valves endocardial cells. Interestingly, high unidirectional shear stress is responsible for inducing endocardial Notch1 signaling, while oscillatory shear stress inhibits it.

Conclusions: During valve remodeling, endocardial cells transduce hemodynamic information into endocardial Notch1 signaling, which induces subendocardial CXCR4 expression. By regulating BMP and WNT signaling, CXCR4

modulates mesenchymal proliferation and induces matrix maturation and tissue compaction. Taken together, our findings have identified a novel mechanobiological valve development program mediated by CXCR4 that has implications in congenital and adult valve diseases.

3.2 Introduction

Congenital arterial valve defects are common birth defects that account for 20-30% of live births and often lead to degenerative aortic valve stenosis (Hoffman, 2002; Hinton, 2011). Identifying therapeutic targets for arterial valve diseases remains challenging because our understanding of valve development is incomplete. Arterial valve development in the outflow tract (OFT) starts with endocardial-mesenchymal transition (EMT), by which valve endocardial cells delaminate, differentiate into mesenchymal cells, and cellularize the early valve primordia (Butcher, 2007). In addition, cardiac neural crest (CNC)-derived cells also contribute to the valvular mesenchyme (Jain, 2011). After EMT ceases, valve primordia undergo extensive remodeling, including cell proliferation/apoptosis, differentiation, matrix maturation, and tissue compaction (MacGrogan, 2014). Interestingly, regulation of valve development is thought to be generally conserved between the OFT and atrioventricular (AV) valves (Combs, 2009). While EMT during early valve formation is well understood (4-8), mechanisms of post-EMT valve remodeling remain elusive.

Chemokine signaling through CXCR4, a G-protein coupled chemokine receptor, and its only known ligand CXCL12 stimulates mesenchymal cell proliferation,

differentiation, and migration in various contexts (Bhakta, 2006; Yang, 2015; Kawaguchi, 2019). Interestingly, previous research has shown that CXCL12/CXCR4 signaling is associated with ventricular septal defects (Nagasawa, 1996; Ma, 1998; Zhou, 1998). Recently, CXCL12/CXCR4 signaling has been shown to regulate survival and migration of CNC cells into the conotruncal regions of the OFT (Escot, 2013). Furthermore, CXCR4 expression has also been detected in the valve endocardium at E9.5 and associated with EMT during early valve formation (Luna-Zurita, 2010). Surprisingly, even though CXCR4 signaling is thought to stimulate cell proliferation (Kawaguchi, 2019) and cellularize valvular mesenchyme (Luna-Zurita, 2010), CXCR4 ablation resulted in hyperplastic OFT valves (Ivins, 2015). Therefore, even though CXCR4 expression has been detected in the OFT and AV valves during post-EMT stages (Ivins, 2015), its contributions to valve remodeling are unclear.

Here, we determined the regionality, regulation, and requirement of CXCR4 signaling during valve development by deleting CXCR4 specifically in endocardial cell lineage. We found that during valve remodeling stages, CXCR4 expression was restricted to the subendocardial mesenchymal cells on the outflow side of the valve. Despite prevalent contributions of CNC-derived cells in the valve primordia, CXCR4 in the endocardium-derived cells was sufficient to modulate mesenchymal cell proliferation, matrix remodeling, and tissue compaction by inhibiting bone morphogenetic protein (BMP) and Wingless and Int-1 (WNT) signaling. Interestingly, endocardial Notch1 signaling was found to regulate subendocardial CXCR4 expression in a side-specific manner. We further identified high unidirectional laminar shear stress

(LSS) as the upstream regulator of Notch1/CXCR4 program. These findings suggest that during valve remodeling, endocardial cells transduce hemodynamic information into biological programs, which in turn relay developmental cues to and regulate cellular behaviors of the underlying mesenchymal cells.

3.3 Materials and Methods

3.3.1 Animal samples

Mice heterozygous for global deletion of CXCR4 were generously donated by Dr. Takashi Nagasawa and procured from Dr. Natasza Kurpios. To test the requirement of CXCR4 *in vivo*, we bred CXCR4 heterozygous mice to generate global CXCR4 mutant mice. Endocardial cell lineage specific deletion of CXCR4 was generated by crossing CXCR4^{fl/fl} mice (generously donated by Dr. Natasza Kurpios) with Nfatc1-cre (generously donated by Dr. Bin Zhou). Mouse heart sections with endocardial cell specific deletion of Notch1 was generated by Dr. Bin Zhou, as previously described (Wang 2017).

For hanging drop culture and shear stress experiments, fertilized White Leghorn eggs were incubated at 38C and 80% humidity to Hamburger-Hamilton (HH) stage 33+ (Day 7-8, incubational age) or HH36+ (Day 10, incubational age). Chick embryos were then harvested in cold EBSS (Sigma). Outflow tracts were then isolated and dissected to expose the valve primordia, which are then used to generate 3D collagen constructs with endocardial cells seeded on top.

3.3.2 Hanging drop culture system, compaction analysis, and micropipette aspiration

Isolated OFT valve primordia were cultured with M199 culture medium, supplemented with insulin-selenium-transferrin, Pen/Strep, and chick serum, as described previously (Gould, 2010). Valve organoids were placed in 20ul media droplets, allowed to settle at the apex of the droplets, and cultured upside down for 24 hours, as described previously (Chiu, 2010). Cytokines and inhibitors used in hanging drop experiments included: AMD3100 (50uM, Krackeler Scientific, Inc.), Blebbistatin (10uM, VWR/BioVision), LDN193189 (1uM, Sigma), and noggin (100ng/mL, Sigma).

To measure tissue compaction, valve organoids were imaged using an upright brightfield microscope ((Zeiss V20 Stereoscope with Retiga 4000R camera) at 0hour and 24hour in culture. Organoid areas were measured in ImageJ, and compaction was determined by taking the ratio of area at 0hr and that at 24hr.

To determine tissue stiffness, micropipette aspiration technique was implemented, as described previously (Buskohl, 2012). Briefly, at the end of the 24hour culture period, valve organoids were subject to tissue deformation by applying suction with a micropipette tip at various forces (applied pressure). The amount of tissue displaced inside the micropipette (stretch ratio) was proportional to tissue deformation and inversely correlated with tissue stiffness (strain energy density).

3.3.3 Shear stress bioreactor system

Each bioreactor consists of a histology microscope slide, biocompatible double-sided tape (W.W. Grainger), 5mm-thick silicone sheet (McMaster-Carr) , and a sticky-Slide I Luer (Ibidi). Wells were created in the silicone sheet using a 4-mm disposable biopsy punch (Miltex). The height of the stick-Slide I Luer determined the magnitude of shear stress, which was calculated and validated by Ibidi and used in previously published experiments (Dragt, 2012; Lecarpentier, 2016). The sticky-slide I Luer creates a channel that is 5mm in width and 50mm in length with various heights. In our experiments, 0.8-mm high sticky-Slides I Luer were used to achieve 5 dyne/cm², while 0.4-mm high slides were used to achieve 20 dyne/cm². The components of the bioreactor were clamped together using binder clips. The female Luers of the channel slide were connected with a male Luer lock with a stop cock and a male Luer lock adapter to prevent leakage during the experiment. The male Luer lock adapters were connected to silicone tubing that had 3.2mm inner diameter (Size 16, Cole-Parmer).

For steady shear experiments, flow was generated using Masterflex L/S Brushless variable-speed digital drive; Masterflex L/S 8-channel, 4-roller cartridge pump head; and Masterflex L/S large cartridges (Cole-Parmer). A pulse dampener (Cole-Parmer) was placed between the peristaltic pump and the bioreactors to maintain non-pulsatile laminar flow over the samples. The media was stored in a polycarbonate bottle with a filling/venting cap (Nalge Nunc International) with 80mL of M199 culture medium, with insulin-selenium-transferrin, Pen/Strep, and chick serum. The 0.8-mm and 0.4-mm bioreactors were connected, run in tandem, and

exposed to a flow rate of 21.1 mL/min for 24 hours at 37C and 5% CO₂. For the oscillatory shear experiments, flow was generated using a NE-1000 syringe pump (New Era Pump Systems, Inc.). The flow circuit includes the bioreactors connected to a 20-mL syringe (BD Biosciences) that was controlled by a syringe pump. The cells were exposed to a flow rate of 21.1 mL/min and at 1Hz, i.e. the cells were exposed to shear stress in the forward direction for one-half of the cycle and in the reverse direction for the other half of the cycle.

3.3.4 3D endocardial cell culture

Collagen gels at a concentration of 2 mg/mL collagen were made by mixing 3x Dulbecco's Modified Eagle's Medium (Life Technologies), 10% chick serum (Life Technologies), sterile 18 MΩ water, 0.1 M NaOH, and rat tail collagen I (BD Biosciences). An aliquot of the collagen gel solution was pipetted into the wells in the silicone sheet and allowed to solidify for 1 hour at 37C and 5% CO₂. The dissected outflow tracts were then placed on top of the collagen gel, and excess media was pipetted off to allow for the valve primordia to come in contact with the collagen gel. After 6 hours of incubation at 37°C and 5% CO₂., the valve endocardial cells are repolarized, delaminated, and attached to the surface of the collagen constructs. These endocardial cells were then exposed to LSS or OSS at 5 or 20 dyne/cm² for 24 hours.

3.3.5 Immunostaining

For valve organoids and endocardial patches, samples were fixed with cold 4% paraformaldehyde for 15 minutes, subsequently washed with TBS, permeabilized with 0.3% Triton-X 100 for 20 minutes, and washed again in TBS for 2x10 minutes. Samples were then blocked and subsequently incubated with primary antibodies in the blocking solution overnight at 4C. The primary antibodies used were rat mAb against PHH3 (Cell Signaling), rabbit mAb against pSMAD15 (Cell Signaling), mouse mAb against α SMA-cy3 (Sigma), mouse mAb against beta-catenin (BD biosciences), and Notch1 (Abcam) diluted at 1:100. Samples were then washed for 3x10 minutes with TBS and incubated with species-specific Alexa Fluor[®] 488, 568, or 647 conjugated secondary antibodies in 5% BSA diluted in TBS for 1 hour at room temperature. Samples were then washed again for 3x10 minutes and stained with DAPI. For pSMAD15 staining, samples were incubated with a donkey-anti rabbit secondary antibody conjugated with HRP. Fluorescence signal was amplified using TSA Amplification Kit (Perkin Elmer) and washed in TBS before staining with DAPI.

For tissue sections, sections were deparaffinized and rehydrated. Antigen retrieval was done by microwaving slides in citrate buffer at pH6.0 for 15 minutes. After washing with deionized water, sections were then incubated with 1.5% H₂O₂ diluted in methanol to quench endogenous peroxidase. Slides were then washed with TBS and blocked with blocking buffer for 1 hour at RT. Antibodies were then diluted in blocking buffer and applied to sections at 1:100 as followed: rabbit CXCR4 (Abcam), mouse CXCL12 (Millipore), rabbit PHH3 (Cell Signaling), rabbit cleaved caspase3 (Cell

Signaling), mouse MF20 (Thermo Fisher), rabbit pSMAD23 (Cell Signaling), rabbit beta-catenin (Cell Signaling), rabbit LEF1 (Cell Signaling), mouse aSMA-cy3 (Sigma), rabbit Sox9 (Abcam), rabbit COL1A (Abcam), rabbit Notch1 (Cell Signaling), and rabbit NICD1 (Cell Signaling). After primary antibody incubation overnight, sections were washed in TBS and incubated with corresponding secondary antibodies. For pSMAD15, pSMAD23, PHH3, cleaved caspase3, and Notch1, donkey anti-rabbit conjugated with HRP was diluted in 5% BSA/TBS and applied to the sections for 1 hour at room temperature. For CXCR4, CXCL12, LEF1, NICD1, donkey anti-rabbit conjugated with biotin was diluted in 5% BSA/TBS and applied to the sections for 1 hour at room temperature. After washing, signal was then amplified using TSA Amplification Kit (Perkin Elmer) and washed in TBS before staining with IB4 to visualize the endocardium and DAPI to counterstain nuclei.

Images were taken using Zeiss LSM880 Confocal/Multiphoton Upright Microscope (u880) or Zeiss LSM710 Confocal Microscope. For valve organoids, 50-60um deep Z-stacks were taken using the LSM710 scope and used for image analysis. Quantification of pSMAD15, PHH3, notch1 was determined based on the percentage of nuclei positive for each signal using ImageJ. Quantification of aSMA was determined based on the area of positive signal normalized by the total number of cells.

3.3.6 Gene expression analysis

Total RNA was extracted from endocardial cells on the surface of the 3D collagen gels using Power SYBR™ Green Cells-to-CT™ Kit (Thermo Fisher). The kit was also used to synthesize cDNA was then synthesized from the extracted RNA. Each gel

represents a biological replicate, which pools RNA from 2 endocardial patches. qRT-PCR was performed on samples using reagents from the same kit and MiniOpticon Real-Time PCR Detection System (Biorad, Hercules, CA). Primers are listed in Table 1.

GAPDH	F 5' TATGATGATATCAAGAGGGTAGT 3' R 5' TGTATCCAACTCATTGTCATAC 3'
Notch1	F 5' TCTTGCTTGCCTTCATTGGA 3' R 5' GCGCTTCTTCTTGCTCGACT 3'
Hey1	F 5' CGGAGGGAAAGGTTATTTTCG 3' R 5' CAGCAATGGGTGAGATATGTG 3'
Hey2	F 5' CAACCACAACATCTCAGATTATG 3' R 5' CAACTTCAGTCAAGCACTCC 3'
Jag1	F 5' TGCCAGACGGTGCTAAGTG 3' R 5' TCGAGGACCACACCAAACC 3'

Table 2. List of chicken primers used in gene expression analysis.

3.3.7 Statistics

Graphs display mean values +/- standard error. Data was analyzed using GraphPad Prism 6.0 for Mac. Results were analyzed by two-way Student t-test or one-way ANOVA with Tukey's multiple comparisons test. Differences between means were significant at P<0.05.

3.4 Results

3.4.1 Spatiotemporal expression of CXCR4 and CXCL12 during valve development

To examine the involvement of CXCR4 signaling during valve development, we examined the spatiotemporal protein expression of CXCR4 and its ligand CXCL12 using ultra-sensitive immunohistochemistry. Endocardial cells were stained here with endocardium-specific isolectin B4 (IB4, red, Figure 1A-H) to delineate mesenchymal cells (IB4-negative). At E11.5, after EMT cessation, CXCR4 is detected in the subendocardial mesenchymal cells both in the OFT and AVC valve primordia (Figure 1A). At this stage, we observed consistently more CXCR4+ cells in the subendocardial region of the AVC cushions (arrow head) than that of the OFT cushions (arrow). Similarly, at E14.5 CXCR4 expression was only positive in the subendocardial cells (Figure 1B and H), contrary to previous reports, albeit done via in-situ hybridization, suggesting that CXCR4 is present in both the endocardial and mesenchymal cells. Furthermore, CXCR4 expression appeared to be on a gradient that emanated from the subendocardial cells (Figure 1F), suggesting that it may be regulated by the endocardium.

During this remodeling stage of valve development, CXCR4 expression was also side-specific and confined to the ventricular side of the OFT and AVC valve primordia (arrows, Figure 1B and 1H). Moreover, CXCL12, the only known ligand of CXCR4, was prominent in the arterial wall (arrow, Figure 1E) and present in the valve mesenchyme (arrow head), confirming prior observations. During late gestation (E17.5), CXCR4

subendocardial restriction and ventricular side-specificity were still present (Figure 1C and 1G). Interestingly, expression of CXCR4 waned after birth at post-natal day 0 (P0) (Figure 1D).

Overall, these data indicated that the endocardium may transduce hemodynamic, e.g. shear stress, information into biological programs that regulate CXCR4 expression in the subendocardial cells, which may in turn regulate remodeling of the valvular mesenchyme.

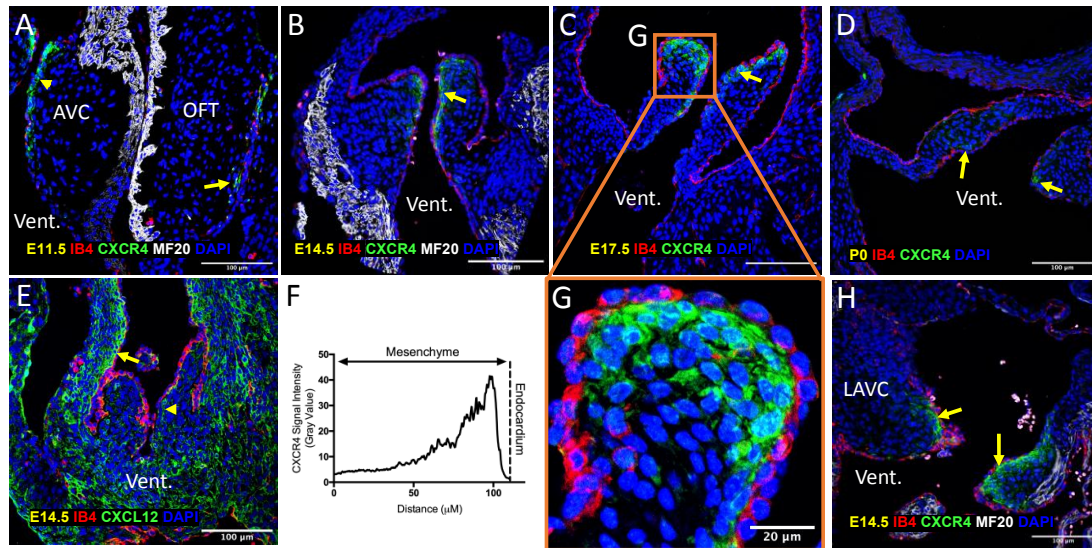


Figure 3.1. Spatiotemporal expression of CXCR4 during valve development. Immunostaining staining of CXCR4 (green, **A – D, G, H**), myocardial cells (MF20, white, **A – D, and H**), endocardial cells (IB4, red, **A – D, E, G, H**), and CXCL12 (green, **C**). Nuclei were stained with DAPI. In **A – H**, the ventricle, atrioventricular canal, and outflow tract are denoted as, vent., AVC, and OFT, respectively. **A**, E11.5 sagittal heart showing CXCR4 staining (green) in the subendocardial cells in the AVC (arrow head) and OFT (arrow). **B – D** show, respectively, E14.5, E17.5, and P0 OFT valves indicating CXCR4 expression is also restricted to the ventricular side (arrows). **G**, Magnified view of the E17.5 OFT valve leaflet in **C**. **E**, OFT valve at E14.5 showing CXCL12 is expressed in the arterial wall and valve mesenchyme. **F**, Histogram of CXCR4 signal intensity based on gray value showing distribution of CXCR4 expression from the endocardium the mesenchyme. **H**, E14.5 section indicating CXCR4 expression in the subendocardial cells on the ventricular side (arrows) of the left atrioventricular cushions (LAVC). Scale bars indicate 100 μm.

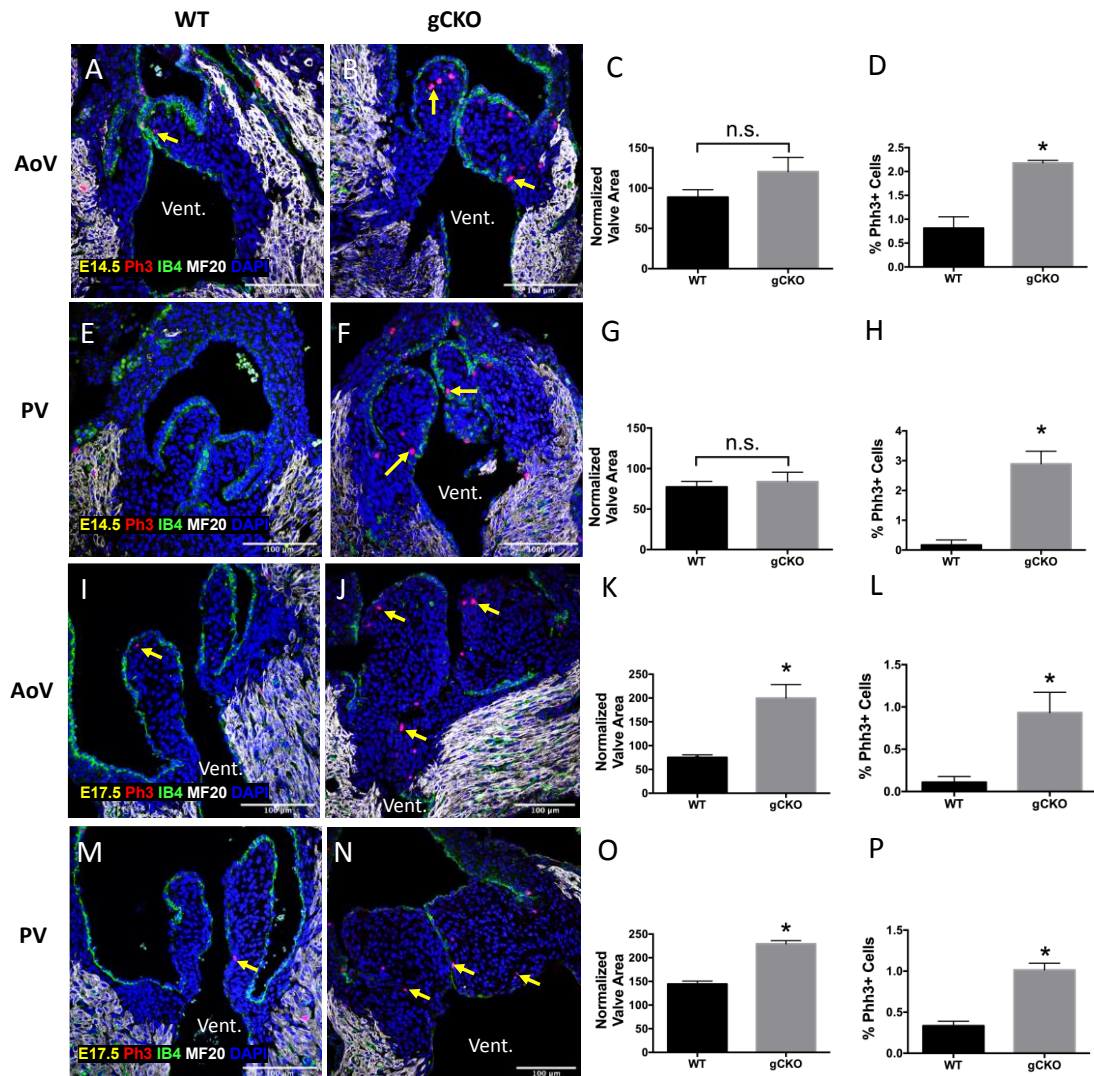


Figure 3.2. Global CXCR4 ablation resulted in hyperplastic and thickened OFT semilunar valves. **A, B, E, F, I, J, M, and N**, Immunostaining of phospho-histone 3 (PHH3) showing that global CXCR4 ablation (gCKO) resulted in higher mesenchymal proliferation in both aortic valve (AoV) and pulmonary valve (PV), compared to control wildtype (WT) at E14.5 and E17.5. Yellow arrows indicate PHH3 positive cells (red). Myocardial cells were stained with MF20 (white), while endocardial cells were stained with IB4 (green). Nuclei were stained with DAPI. Ventricle is denoted as “vent.” Quantification of proliferation via percentage of PHH3 positive mesenchymal cells in WT and gCKO AoV sections at E14.5 (**D**) and E17.5 (**L**) as well as PV sections at E14.5 (**H**) and E17.5 (**P**). Total mesenchymal cells were determined as IB4 negative cells in the valve region encased by MF20+ cells. Quantification of normalized valve area indicated increased thickness in gCKO AoV and PV valves at E17.5 (**K** and **O**, respectively), but not at E14.5 (**C** and **G**). Data are means +/- SEM. N=3-4 embryos per group. * $p \leq 0.05$ via Student *t* test. Scale bars indicate 100um.

3.4.2 CXCR4 is required for modulation of mesenchymal cell proliferation

To determine the role of CXCR4 signaling during valve remodeling, we initially ablated CXCR4 globally by breeding CXCR4 heterozygous (+/-) mice with each other. We collected control WT and global CXCR4 knockout (cGKO) at E14.5 and E17.5 and monitored mesenchymal cell growth via immunostaining for phosphorylated Histone-3 (PHH3), which is indicative of chromosome condensation during mitosis. Proliferation was determined based on the percentage of PHH3 positive cells (red, Figure 2A-P) over total number of mesenchymal cells, which was determined as IB4 (green, Figure 2A-P) negative cells in the valvular region. At E14.5, the percentage of PHH3 positive cells in the aortic valve (AoV) averaged about 0.81% (Figure 2D), compared to 0.17% (Figure 1H) in the pulmonary valve (PV). At E17.5, the percentage of PHH3 positive cells in AoV decreased to 0.11% (Figure 2L), compared to 0.33% (Figure 2P) in the PV. At E14.5, the percentage of PHH3 positive cells was about 2.17% in mutant AoVs, significantly higher than that in WT controls ($P=0.0084$). Similarly, the percentage of PHH3 positive cells was increased to 2.89% in PV at E14.5, about 17 times higher compared to WT controls ($P=0.0136$).

Interestingly, we did not observe any significant difference with regard to valve area at E14.5, despite the increase in mitotic activity (Figure 2C and 2G). However, at E17.5, mutant AoVs and PVs exhibited significantly more thickened valves (Figure 2K and 2O) compared to those in the WT controls ($P=0.0203$ and $P=0.0008$, respectively). Furthermore, the percentage of PHH3 positive cells was significantly higher in mutant AoV (Figure 2I, J, L) and PV (Figure 2M, N, P), compared to that in WT controls. Mitotic

cells in the mutant valves were also scattered across the valve mesenchyme and not restricted to CXCR4 positive cells, suggesting that CXCR4 regulation of proliferation is not cell autonomous. In addition, we did not observe any significant difference in valve area of the left atrioventricular (LAV) and right atrioventricular (RAV) valves between gCKO and WT controls (Figure 3).

Together, these data suggest that global ablation results in significant increase in mesenchymal cell proliferation at E14.5 and E17.5 in both semilunar valves. However, this hyperplasia does not result in significantly thickened valve leaflets until E17.5.

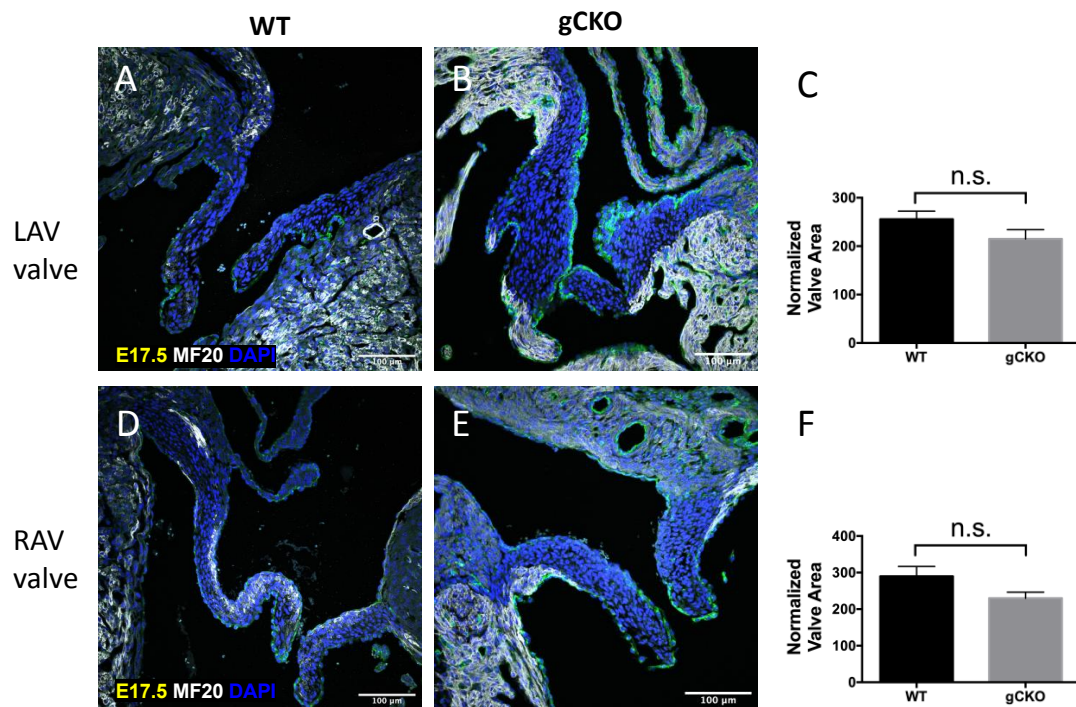


Figure 3.3. CXCR4 is not required for AVC valve remodeling. Measurement of valve area showed no significance difference E17.5 WT vs. gCKO in LAVC (**A-C**) and RAVC (**D-F**). Myocardial cells were stained with MF20 (white), while endocardial cells were stained with IB4 (green). Nuclei were stained with DAPI. **C** and **F**, Quantification of valve area of WT and gCKO RAVC (C) and LAVC (F). Data are means +/- SEM. N=3-4 embryos per group. n.s. = not significant via Student *t* test. Scale bars indicate 100um.

3.4.3 CXCR4 is not required for regulation of apoptosis of mesenchymal cells

Since it has been suggested that hypertrophic valve leaflets can be attributed to decreased mesenchymal cell apoptosis, we determined whether CXCR4 regulated cell apoptosis. To this end, we measured apoptotic activity via immunostaining of active caspase-3 (a-casp3) and quantified percentage of mesenchymal cells positive for a-casp3 at E14.5 and E17.5. We detected low levels of apoptosis in the valve leaflets (Figure 4A-D) and no significant difference between the gCKO and WT control valves (Figure 4E). These data suggest that attenuated apoptosis does not significantly contribute to the hyperplastic phenotype in CXCR4 mutant valves.

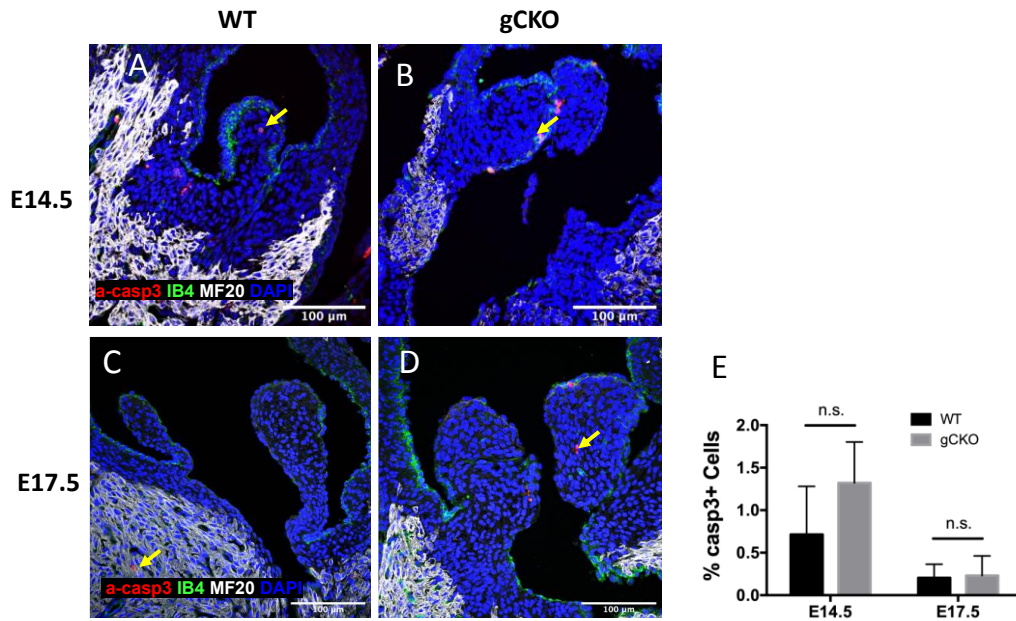


Figure 3.4. Global CXCR4 ablation did not affect mesenchymal cell apoptosis. **A-D**, Immunostaining of active caspase 3 (a-casp3) showing no significant difference between WT and gCKO valve sections at E14.5 and E17.5. Yellow arrows indicate a-casp3 positive cells (red). Myocardial cells were stained with MF20 (white), while endocardial cells were stained with IB4 (green). Nuclei were stained with DAPI. **E**, Quantification of proliferation via percentage of casp3 positive mesenchymal cells in WT and gCKO valves at E14.5 and E17.5. Data are means +/- SEM. N=3-4 embryos per group. n.s. = not significant via Student *t* test. Scale bars indicate 100um.

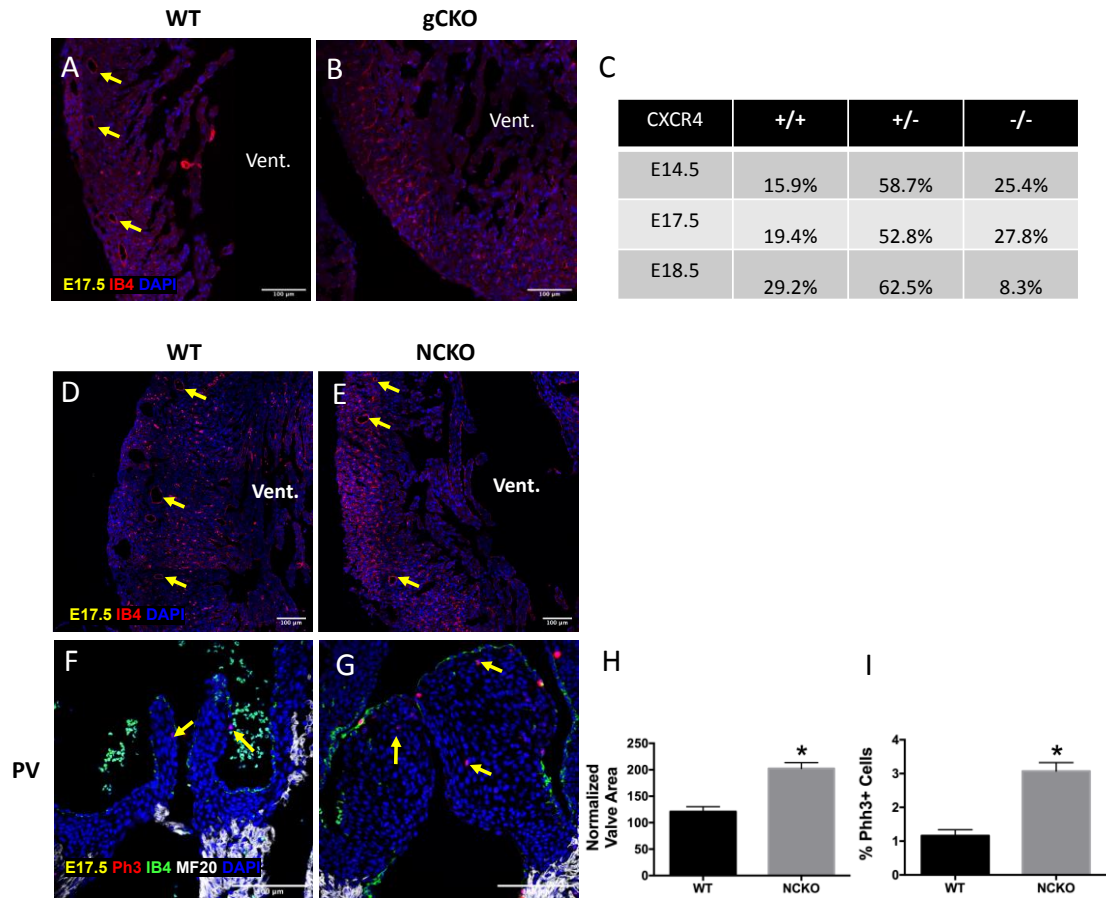


Figure 3.5. Ablation of CXCR4 in endocardium-derived cells resulted in thickened valve, but preserved coronary arteries. Immunostaining for endothelium-specific IB4 (red) showed presence of coronary arteries in WT controls (arrows, **A**) and absence of coronary arteries in gCKO ventricle (**B**) at E17.5. Nuclei were stained with DAPI. Ventricle is denoted as “vent.” **C**, Table showing the percentage of CXCR4 WT (+/+), heterozygous (+/-), and null (-/-) embryos collected. Immunostaining for IB4 (red) showed presence of coronary arteries (arrows) in both *Nfatc1-cre;CXCR4^{flox/flox}* (NCKO) in (**D**) and WT controls (**E**) at E17.5. **H**, Quantification of valve area showed increased overall thickness in NCKO compared to controls at E17.5. **I**, Quantification of PHH3 positive mesenchymal cells in WT and NCKO valves at E17.5. Data are means +/- SEM. N=6 embryos per group. * $p \leq 0.05$ via Student *t* test. Scale bars indicate 100um

3.4.4 CXCR4 signaling in endocardium-derived mesenchymal cells is sufficient

Semilunar valve mesenchyme is thought to be populated by both endocardium-derived mesenchymal cells and cardiac neural crest cells. To determine which subpopulation of mesenchymal cells is responsible for regulation of proliferation via CXCR4 signaling, we ablated CXCR4 in the endocardium-derived mesenchymal cells. To this end, we bred CXCR4 floxed mice into the endocardial and mesenchymal cell-specific Cre driver line *Nfatc1-Cre*. Previous fate mapping experiments using *Nfatc1-Cre* with *Rosa26-LacZ* reporter mice have shown that *Nfatc1* is present in both the valve endocardium and the endocardium-derived mesenchymal cells. Examination of the ventricle of the gCKO hearts showed an absence of coronary arteries (arrows, Figure 5A, B) compared to WT controls. Furthermore, while E14.5 and E17.5 gCKO embryos were born at around 25% following the Mendelian ratio, E18.5 gCKO embryos only made up 8.3% of the embryos (Figure 5C). These results confirmed prior findings that attributed late-gestation lethality of CXCR4 null mice to absent coronary arteries and insufficient ventricular perfusion. Interestingly, *Nfatc1-cre;CXCR4^{flox/flox}* (NCKO) embryos possessed coronary arteries (Figure E), suggesting that genotype is specific to the valves.

More importantly, immunostaining for PHH3 revealed the percentage of PHH3 positive mesenchymal cells (arrows, Figure 5F and 5G) in the NCKO semilunar valve is about 3%, three times higher than that in the WT controls ($P=0.0002$) (Figure 5I). Furthermore, measurements of valve areas showed that NCKO exhibited thickened valve compared to WT controls ($P=0.0002$) (Figure 5H). Similar to gGKO valves, mitotic

cells in the NCKO valves were not restricted to CXCR4 positive cells (Figure 5G), indicating that CXCR4 regulation of mesenchymal cell proliferation is paracrine.

These results suggest that CXCR4 signaling via endocardium-derived cells is sufficient at regulating mesenchymal proliferation. While cardiac neural crest cells contribute significantly to semilunar valves, CXCR4 signaling via cardiac neural crest cells does not contribute significantly to the regulation of mesenchymal cell proliferation.

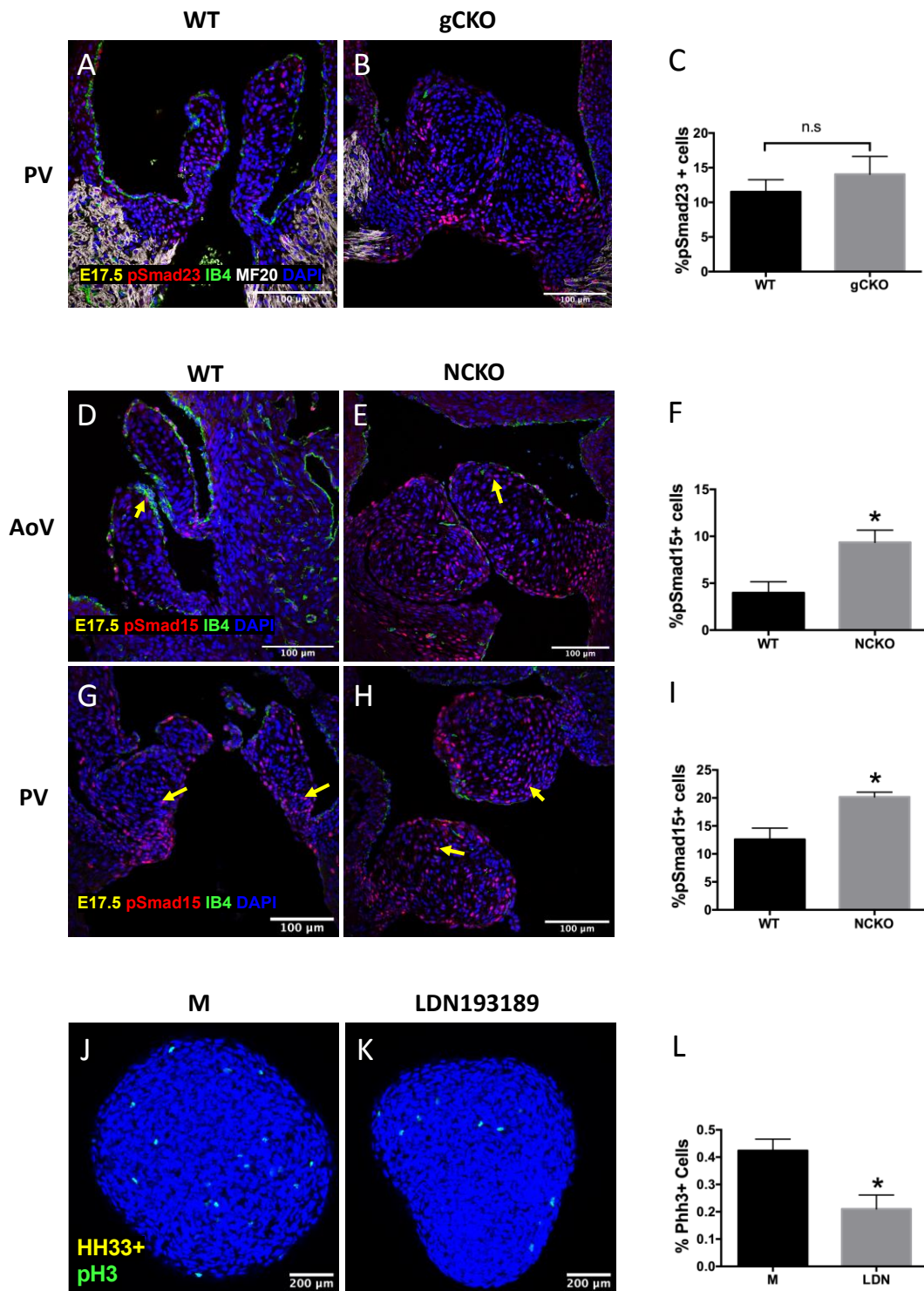


Figure 3.6. Augmented BMP signaling activity in NCKO mutant valves at E17.5. **A** and **B**, immunostaining of phosphorylated smad23 (pSMAD23) in PV at E17.5, showing no significant difference between gCKO and WT controls (**C**). Myocardial cells were

stained with MF20 (white), while endocardial cells were stained with IB4 (green). Nuclei were stained with DAPI. Immunostaining of phosphorylated smad15 (pSMAD15) in AoV (**D** and **E**) and PV (**G** and **H**) at E17.5, showing upregulated BMP activity in NCKO compared to WT (**F** and **I**). Arrows indicate positive pSMAD15 cells (red). **J – L**, immunostaining of chick valve primordia Hamburger-Hamilton stage 33+ (HH33+) for PHH3 (green) showed increased percentage of mitotic cells (**J** and **K**) increased in response to treatment with LDN193189 at 1uM (**L**). All quantification was done via percentage of nuclear pSMAD23, pSMAD15, and PHH3 positive mesenchymal cells over total mesenchymal nuclei. Data are means +/- SEM. N=6 embryos or chick valve primordia per group. * $p \leq 0.05$ via Student *t* test. Scale bars indicate 100um (**A – H**) and 200um (**J – L**).

3.4.5 Upregulated BMP signaling in *Nfatc1-cre;CXCR4^{flox/flox}* mutant valves

Previous research has implicated contributions of transforming growth factor beta (TGF β) and bone morphogenetic protein (BMP), a TGF β superfamily member, to regulating valve growth and remodeling. In particular, mice that lacked *Smad6*, an inhibitor of BMP signaling, or *noggin*, a BMP ligand scavenger, exhibited hypertrophic valve phenotype because of increased BMP signaling. To determine whether CXCR4 signaling controls mesenchymal cell proliferation through TGF β or BMP signaling, we examined levels of nuclear phosphorylated *smad2/3* (pSMAD23), which is indicative of active TGF β signaling or nuclear phosphorylated *smad1/5* (pSMAD15), which is indicative of active BMP signaling in CXCR4 null and WT control valves.

Intriguingly, heart valves of WT and gCKO embryos showed no significant difference in percentage of mesenchymal cells positive for nuclear pSMAD23, suggesting that TGF β is not perturbed in response to CXCR4 ablation (Figure 6A-C). However, examination of WT and NCKO semilunar valves revealed significant higher percentage of nuclear translocated pSMAD15 in the NCKO valves. Specifically, percentage of nuclei positive for pSMAD15 in WT AoV was about 5% (Figure 6D), while NCKO AoV exhibited about a 5% increase (Figure 6E) in nuclear translocation of pSMAD15 ($P=0.0241$) (Figure 6F). Similarly, percentage of nuclei positive for pSMAD15 in WT PV was about 10% (Figure 6G), while NCKO AoV exhibited about a 10% increase (Figure 6H) in nuclear translocation of pSMAD15 ($P=0.0241$) (Figure 6I). Surprisingly, there was a higher percentage of nuclear pSMAD15 positive mesenchymal cells in the PV compared to AoV both in WT and NCKO valves. Furthermore, pSMAD15 positive cells

were distributed throughout the valve mesenchyme, corroborating PHH3 results and suggesting CXCR4 signaling is not cell autonomous. These results indicate that CXCR4 signaling is required for modulation of BMP activity *in vivo*.

To expand these findings, we determined whether BMP signaling is required for regulation of mesenchymal cell proliferation. To this end, we isolated chick valve primordia at Hamburger-Hamilton stage 33+, which corresponds to E14.5 in mice, and cultured them in hanging drops over 24 hours. We inhibited phosphorylation of smad1/5/8 and therefore BMP signaling in these organoids via LDN193189, an inhibitor of BMP type I receptors (Alk2 and Alk3). After immunostaining the organoids for PHH3, we acquired Z-stacks of 60 μm deep into the organoids. Proliferation was assessed based on percentage of PHH3 positive cells in those Z stacks. In response to LDN193189, valve organoids exhibited 0.2% of PHH3 positive mesenchymal cells, compared to untreated condition at 0.4% ($P=0.0091$) (Figure 6J-L), suggesting that BMP signaling is required for mesenchymal cell proliferation during valve development.

Taken together, these results indicate that CXCR4 signaling downregulates BMP activity and therefore mesenchymal cell proliferation. Perturbation of CXCR4 signaling increases BMP activity and mesenchymal cell proliferation in a non-cell autonomous fashion.

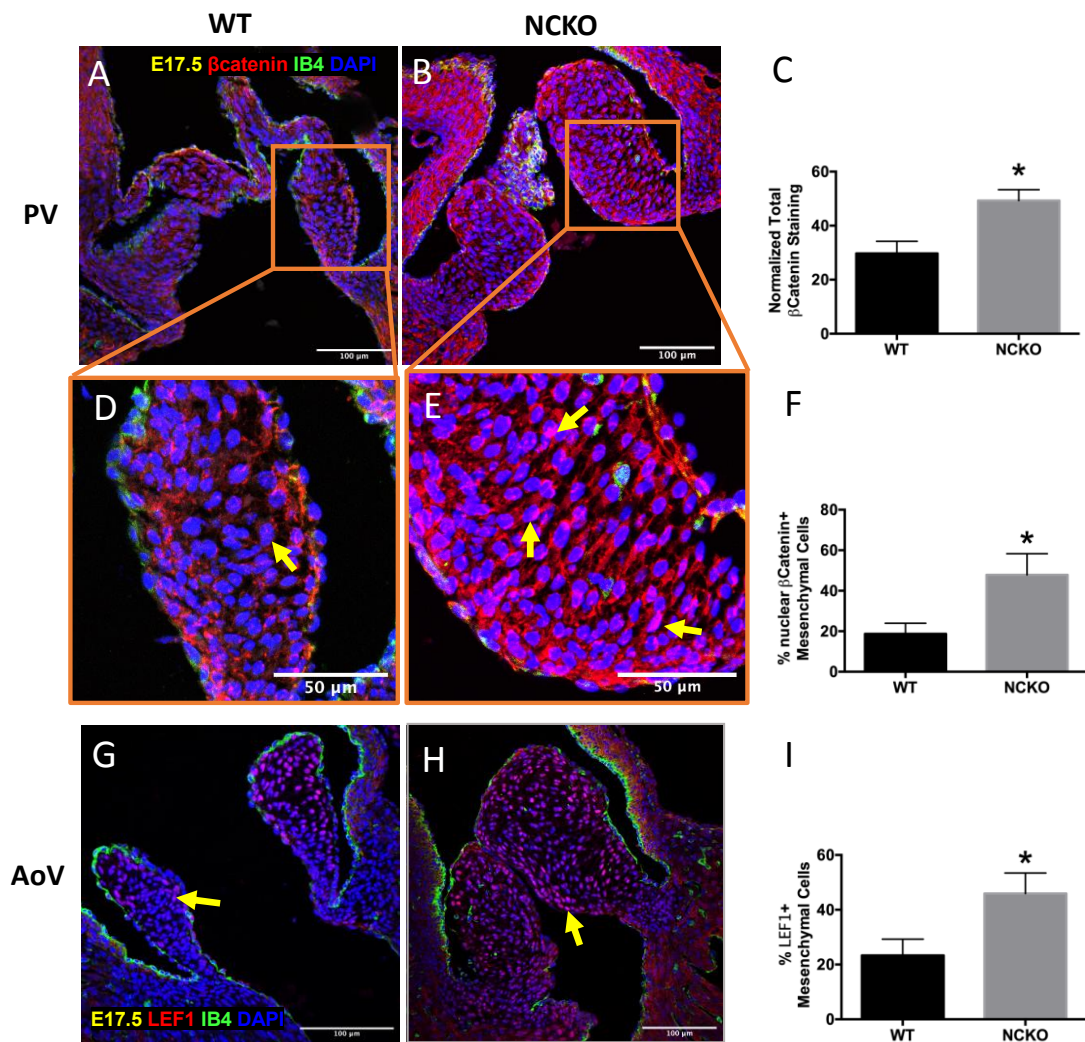


Figure 3.7. Enhanced canonical WNT signaling via β catenin in NCKO mutant valves at E17.5. **A – B**, Immunostaining for β catenin (red) indicating that NCKO embryos showed higher total β catenin levels in PV at E17.5. **C**, Quantification of total β catenin was determined by measuring total stained area of β catenin and normalizing by dividing measured area by total number of mesenchymal cells. **D and E**, Magnified views of the PV sections stained with β catenin in **A** and **B**, respectively. Yellow arrows indicate nuclear translocation of β catenin (**E**). Endocardial cells were stained with IB4, while nuclei were counterstained with DAPI. **F**, Quantification of nuclear translocation of β catenin based on percentage of mesenchymal cells with nuclear β catenin signal (magenta) over total number of DAPI+ mesenchymal cells (blue). **G – H**, Immunostaining for LEF1 (red) showing that NCKO exhibited higher nuclear localization of LEF1 (yellow arrows) in AoV at E17.5. **I**, Quantification of percentage of mesenchymal cells positive for nuclear LEF1. Data are means \pm SEM. N=5 embryos per group. * $p \leq 0.05$ via Student *t* test. Scale bars indicate 100 μ m.

3.4.6 CXCR4 is required for modulation of proliferation via canonical WNT signaling

Recent data suggested that canonical WNT through β catenin also regulates mesenchymal cell proliferation by increasing BMP signaling. To determine whether CXCR4 is required for modulation of canonical WNT signaling, we compared total β catenin and nuclear β catenin levels between NCKO and WT embryos at E17.5. We normalized β catenin staining by measuring total area of β catenin staining and normalizing by total number of mesenchymal cells. Interestingly, whole-valve ablation of CXCR4 resulted in significantly more total β catenin compared to WT controls at E17.5 ($P=0.0123$) (Figure 8A – C). We then assessed nuclear translocation of β catenin, which indicates active canonical WNT signaling. To do this, we quantified the percentage of nuclei with nuclear colocalization of β catenin. We detected about a twofold increase in the percentage of cells positive for nuclear β catenin localization in the NCKO valve compared to WT controls ($P=0.0478$) (Figure 8F), suggesting that canonical WNT signaling is upregulated in mutant valves.

To expand these results, we examined the levels of lymphoid enhancer binding factor 1 (LEF1), a canonical WNT target in NCKO and WT controls at E17.5. We quantified LEF1 expression based on the percentage of mesenchymal cells positive for nuclear LEF1 over total number of mesenchymal cells. We found that in response to conditional CXCR4 ablation, there was a 20% increase in LEF1 nuclear expression ($P=0.0478$), confirming that canonical WNT signaling was upregulated (Figure 8G – I). Furthermore, LEF1 expression was scattered and not restricted to subendocardial cells

expressing CXCR4, suggesting that the increase in CXCR4 also regulates WNT signaling in a non-cell autonomous manner. Taken together, these data suggest that CXCR4 is required for modulation canonical WNT signaling, which is important for proliferation of mesenchymal cell proliferation.

3.4.7 CXCR4 is required for tissue condensation during valve development

Mesenchymal condensation occurs when valve mesenchymal cells compacts extracellular matrix and become densely distributed (*). Valvular remodeling that creates thin and mature leaflets has been linked to mesenchymal condensation. Here, we determined whether the thickened valve phenotype in NCKO valves was due to defective mesenchymal condensation. To this end, we examined mesenchymal cell density of NCKO and WT valves at E17.5 by measuring the total number of nuclei within the valve regions of AoV (Figure 9A and B) and PV (Figure 9D and E). Analysis of cell density in these valves revealed that mesenchymal cell density in WT valves averaged about 14,185 cells per mm² in AoV and 14,376 cells per mm² in PV (Figure 9C and F). Interestingly, conditional ablation of CXCR4 resulted in significant decrease in mesenchymal cell density to 11,327 cells per mm² in AoV (P=0.0048) and 10,701 cells per mm² in PV (P=0.0005). Although previous reports observed defective mesenchymal condensation in the subendocardial regions of the valves, we detected a decrease in mesenchymal cell density throughout the valve primordia (Figure 9A, B, D, and E). These results suggest that CXCR4 regulates mesenchymal condensation in a non-cell autonomous manner.

To expand these findings, we examined mesenchymal cell condensation on a tissue level to ascertain whether CXCR4 regulates tissue compaction in valve organoids. To do this, we isolated OFT valve primordia from chick embryos at HH33+ (about E14.5 in mice) and HH36+ (about E17.5 in mice) and cultured them in hanging drops for 24 hours (Figure 9G – P). We evaluated tissue compaction by calculating the ratio of organoid area at 24hr (A) and 0hr (Ao). In response to CXCR4 inhibition by AMD3100, we detected an 18% decrease in HH33+ organoids ($P=0.0172$) and 11% decrease in HH36+ organoids ($P=0.0282$), compared to untreated controls.

Taken together, these results indicate that CXCR4 inhibition resulted in impaired mesenchymal cell condensation of the surrounding matrix, which led to defective tissue compaction and hypertrophic valves.

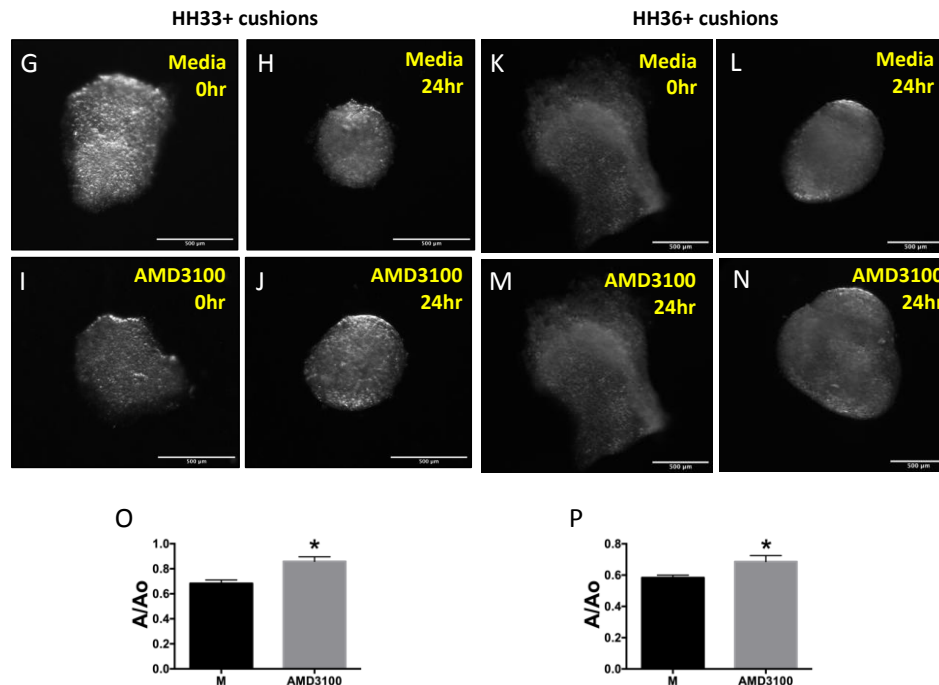
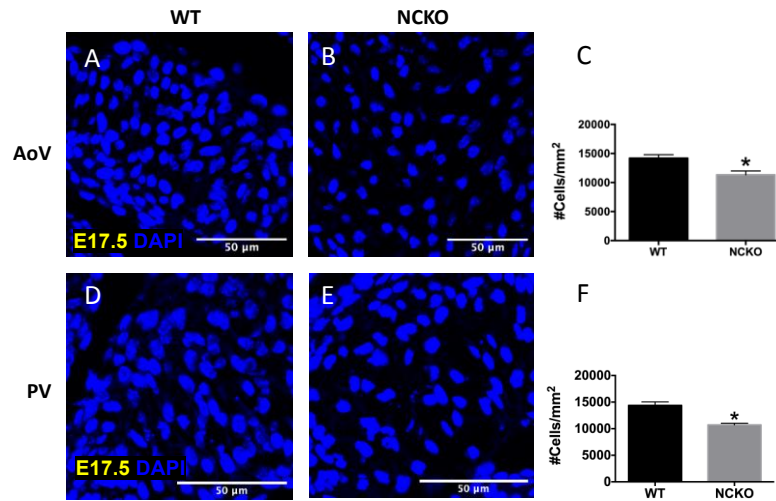


Figure 3.8. CXCR4 signaling is required for tissue compaction. **A – F**, Density of mesenchymal cells of WT and NCKO in AoV (A and B) and PV (D and E) valves E17.5. Nuclei were stained with DAPI (blue). **C and F**, Quantification of cell density in AoV (**C**) and PV (**F**). Cell density was quantified by dividing the total number of cells by the total valve area. **G and H**, Compaction of chick OFT valve primordia at HH33+ after 24 hours of culture in untreated media. **I and J**, Decreased compaction of chick OFT valve primordia at HH33+ after 24 hours of culture in media treated with AMD3100, a CXCR4 inhibitor. **K and L**, Compaction of chick OFT valve primordia at HH36+ after 24 hours of culture in hanging . **M and N**, Decreased compaction of chick OFT valve primordia at HH36+ after 24 hours of culture in media treated with AMD3100. **O and P**,

Quantification of compaction based on the ratio of valve organoid area at 24hr and to 0hr. Data are means +/- SEM. N=6 embryos per group (A – F) and 7 valve organoids per group (G – P). *p ≤ 0.05 via Student *t* test. Scale bars indicate 50um (A – F) and 500um (G – P).

3.4.8 CXCR4 regulates α -Smooth muscle actin expression via BMP signaling

Matrix condensation and tissue compaction during valve development has been associated with myofibroblastic differentiation and activation. A hallmark of this differentiation is the upregulation of α -smooth muscle actin (α SMA), which facilitates myofibroblastic contractility, extracellular matrix condensation, and tissue compaction. Therefore, we determined whether conditional CXCR4 ablation perturbed α SMA expression in the valves. Interestingly, immunostaining results revealed that in response to ablation of CXCR4 in the valve mesenchymal cells, average α SMA expression was about 6 times lower in both the AoV (P=0.0398) and PV (P=0.0107), compared to WT controls. We determined α SMA expression by measuring total area with positive α SMA expression and normalizing by the total number of mesenchymal cells. These results suggest that CXCR4 is required for myofibroblastic activation and contraction apparatus.

To determine whether CXCR4 signaling does this autonomously, we performed colocalization analysis of CXCR4 and α SMA expression at E17.5. We observed that CXCR4 and α SMA were both colocalized in the subendocardial regions of the WT valve (Figure 10G – I). To confirm this observation, we measured the signal intensity of CXCR4 and α SMA (gray value) and plotting the distribution of immunostaining signal

(based on 8-bit, 0-255 units) relative to the endocardium (Figure 10J). The subendocardial region exhibited the highest signal intensity for CXCR4 (green) and α SMA (red). About 20 μ m past the endocardium, signal intensity for both CXCR4 and α SMA decreased significantly. In contrast, signaling intensity for α SMA remained below 50 units throughout the distance. These results indicate that CXCR4 may help differentiate subendocardial mesenchymal cells into myofibroblasts in a cell-autonomous manner.

To expand these findings, we determined whether mesenchymal cell contractility regulated mesenchymal condensation at the tissue level. To test the requirement of cell contractility, we inhibited HH3+ chick valve organoids with Blebbistatin, which specifically blocks the binding of non-muscle myosin II to actin, e.g. α SMA in myofibroblasts. Assessment of Blebbistatin inhibited organoid area at 0hr and 24hr (Figure 10K – N) revealed a 20% decrease in tissue compaction compared to the untreated organoids ($P=0.0044$). These results suggest that mesenchymal cell contractility is required for proper valve compaction. Taken together, these data indicate that CXCR4 regulates valve compaction via myofibroblastic activation and contractility of subendocardial cells in a cell-autonomous manner.

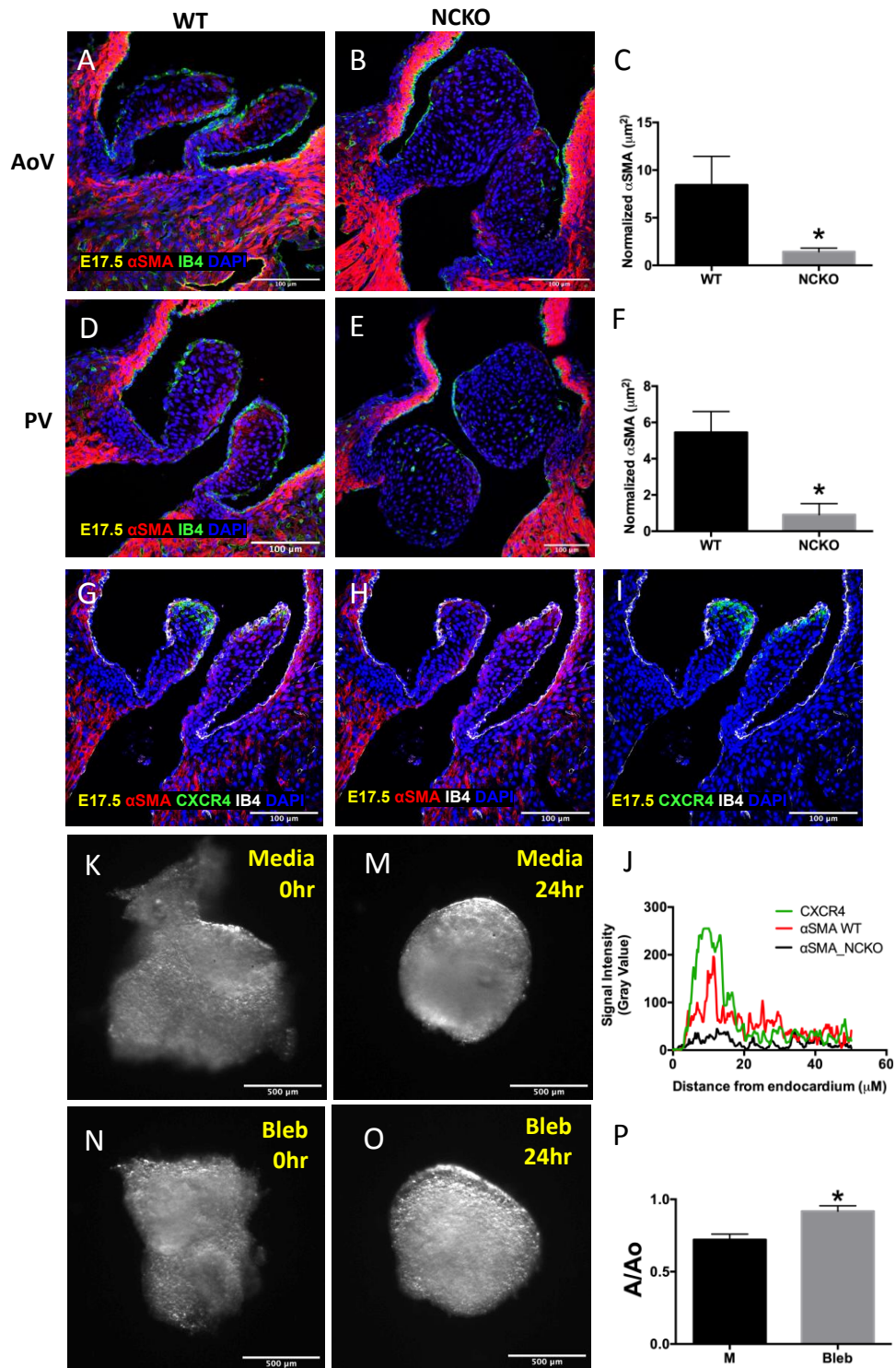


Figure 3.9. Aberrant myofibroblastic activation and contractility in NCKO valves. A – F, Immunostaining of α -smooth muscle actin (α SMA), showing decreased expression of α SMA (red) in both AoV (B) and PV (E) NCKO valves at E17.5. C and F, Quantification

of α SMA expression for (C) and PV valves (F). α SMA expression was normalized by dividing valve area positive for α SMA by total number of mesenchymal cells. Endocardial cells were stained with IB4, while nuclei were stained with DAPI. G – J, Immunostaining of α SMA (H), CXCR4 expression (I), and both (G) at E17.5. J, Plot profile of signal intensity (gray value) of CXCR4 (green), α SMA in WT valve (red), and α SMA in NCKO valve (black) spanning 50um from the endocardium into the mesenchyme. K – N, images of HH33+ chick valve organoids untreated and treated with Blebbistatin at 0hr and 24hr. O, Compaction analysis showing inhibition of cell contractility decreased compaction. Data are means +/- SEM. N=3-6 embryos per group (A – F) and 6 cushions per group (K – O). *p \leq 0.05 via Student *t* test. Scale bars indicate 100um.

3.4.9 CXCR4 regulates valve compaction via modulating BMP activity

To determine whether BMP signaling mediates valve condensation, we inhibited the transcriptional activity of BMP type I receptors (Alk2 and Alk3) using LDN193189 and measured tissue compaction. Valve organoids were cultured in hanging drops for 24 hours as described above. At 24hr, we detected that organoids treated with LDN193189 (Figure 11C and D) compacted on average 14% more than the untreated organoids (Figure 11A and B) (P=0.0008). These results suggest that BMP signaling modulates valve compaction via Alk2 and Alk3, likely via BMP2, 4, or 7 ligands. To determine if BMP modulation of tissue compaction is ligand-dependent, we treated valve organoids with Noggin at 100ng/mL, which scavenges BMP ligands (Figure 11E and F). Similar to the LDN193189-treated condition, valve organoids treated with noggin compacted about 12% more compared to the untreated cushion (P=0.0008), suggesting that BMP regulation of valve compaction is ligand-dependent and in a paracrine fashion.

To ascertain the requirement of BMP signaling for CXCR4-dependent regulation of tissue compaction, we inhibited CXCR4 with AMD3100 and LDN193189 and cultured the organoids for 24 hours (Figure 11G and H). Interestingly, BMP inhibition of LDN193189 rescued the hypocompaction phenotype in CXCR4-inhibited conditions and compacted organoids 12% less than untreated controls ($P=0.0008$), suggesting CXCR4 modulates compaction via BMP signaling.

To expand these findings, we determined whether BMP signaling mediates CXCR4 regulation of compaction by modulating myofibroblastic activation by α SMA immunostaining. Valve organoids treated with AMD3100 expressed about 17% less (Figure 11K) than untreated controls ($P=0.0239$), confirming *in vivo* results (Figure 10A – F). Interestingly, BMP inhibition by LDN193189 increased α SMA expression about 20%, rescuing myofibroblastic phenotype in the absence of CXCR4 signaling. Taken together, these data indicate that CXCR4 attenuates BMP signaling, which modulates myofibroblastic activation, mesenchymal condensation, and tissue compaction.

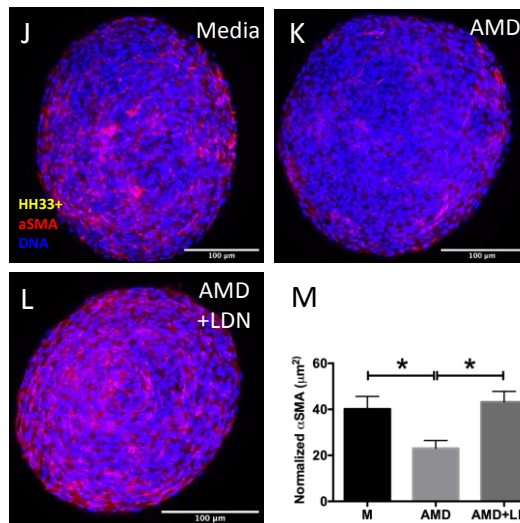
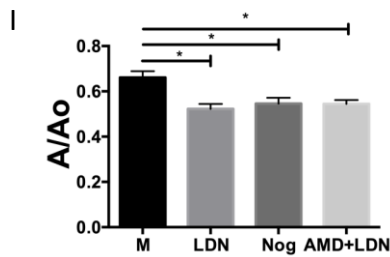
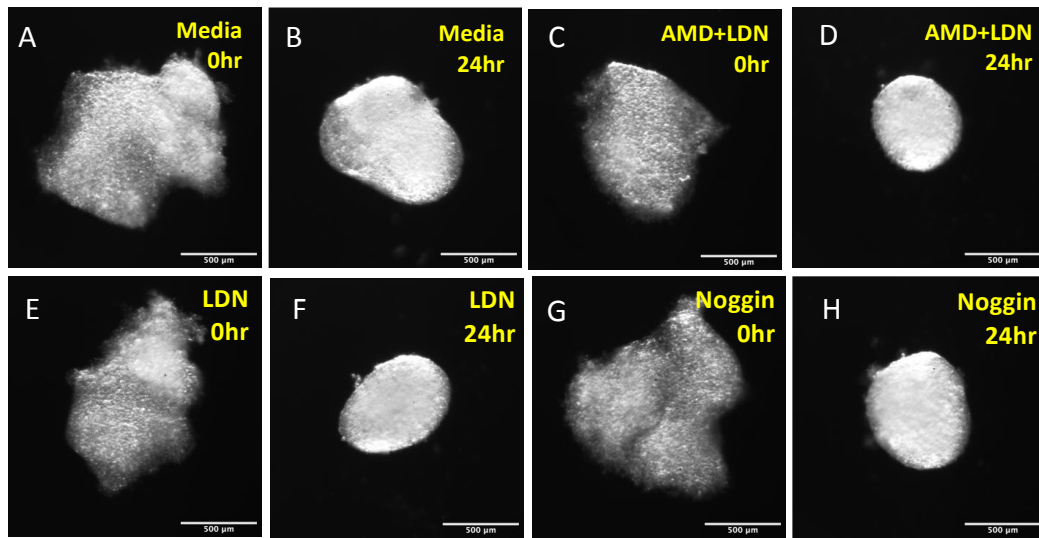


Figure 3.10. CXCR4 facilitated tissue compaction and myofibroblastic activation via modulating BMP signaling. A – I, Images of HH33+ chick valve organoids untreated (A and B) and treated with LDN193189 (C and D) or Noggin (E and F) or with both AMD3100 and LDN193189 (G and H) at 0hr and 24hr. I, Bar graph showing compaction

of valve organoids after 24hr cultured in hanging drops. **J–L**, Immunostaining of α SMA of HH33+ chick valve organoids untreated or treated with AMD3100 and AMD3100/LDN193189. **M**, Quantification of α SMA expression of HH33+ valve organoids based on normalized valve area positive in Z-stacks 60 μ m deep into the organoids. Data are means \pm SEM. N=5-6 organoids per group. * $p \leq 0.05$ via ANOVA with Dunnett multiple corrections test. Scale bars indicate 500 μ m (A – H) and 100 μ m (J – L).

3.4.10 CXCR4 is required for matrix maturation during valve development

Since increased BMP signaling has been associated with immature valve matrix, we assessed markers of extracellular matrix differentiation and patterning. Alcian blue staining at E17.5 revealed that ablation of CXCR4 in the mesenchymal cells resulted in about 2.7 times ($P=0.0007$) proteoglycan content (Figure 12A and B) higher compared WT controls. To confirm these results, we examined the expression of sox9 (red, Figure 12D and E), which has been shown to be downstream of BMP and important for proteoglycan synthesis and deposition in cartilage and valves. At E17.5, we detected about a twofold increase ($P=0.0032$) in the percentage of mesenchymal cells with positive nuclear Sox9 in NCKO valves (Figure 12F), suggesting that the BMP/sox9/proteoglycan axis was upregulated in response to conditional ablation of CXCR4.

Since patterning of valve matrix includes deposition of collagen fibers, we also assessed collagen content by immunostaining for collagen type IA (Col1A). We found that the collagen deposition is mainly restricted to the subendocardial region throughout the valve and more pronounced on the ventricular side (arrow, Figure 12G). Furthermore, there was a 50% decrease in collagen deposition ($P=0.0257$) in the

NCKO valve (Figure 12H and I), compared to WT valve. These findings suggest that CXCR4 signaling is required for collagen deposition in a cell-autonomous manner.

To understand the consequence of the impaired mesenchyme maturation in NCKO valves, we measured the stiffness of CXCR4-inhibited valve organoids using micro-pipette aspirations. HH3+ chick valve organoids were cultured either untreated or treated with AMD3100 to inhibit CXCR4 signaling in hanging drops for 24hr. We then subjected the organoids to various pressures by applying suction on the organoids using a micro-pipettor (Figure 12J – N). Every increment of 1ul volume change was equivalent to 0.1066 Pascals of applied pressure. Given the same applied pressure, AMD3100 treated valve organoids exhibited higher stretch ratios (Figure 12L), i.e. more of the tissue is aspirated into the micropipette (Figure 12N), compared to untreated control (Figure 12M). To quantify stiffness, we calculated the area under the stretch response curves (Figure 12P), which represents the force applied to the organoids (strain energy density, Pascals). The more force, the stiffer the tissue. Interestingly, AMD3100-treated organoids were about 30% less stiff compared to untreated cushions (Figure 12O).

Overall, these data indicate that inactivation of CXCR4 signaling resulted in increased deposition of proteoglycans and decreased collagen content, leading to biomechanically immature valves.

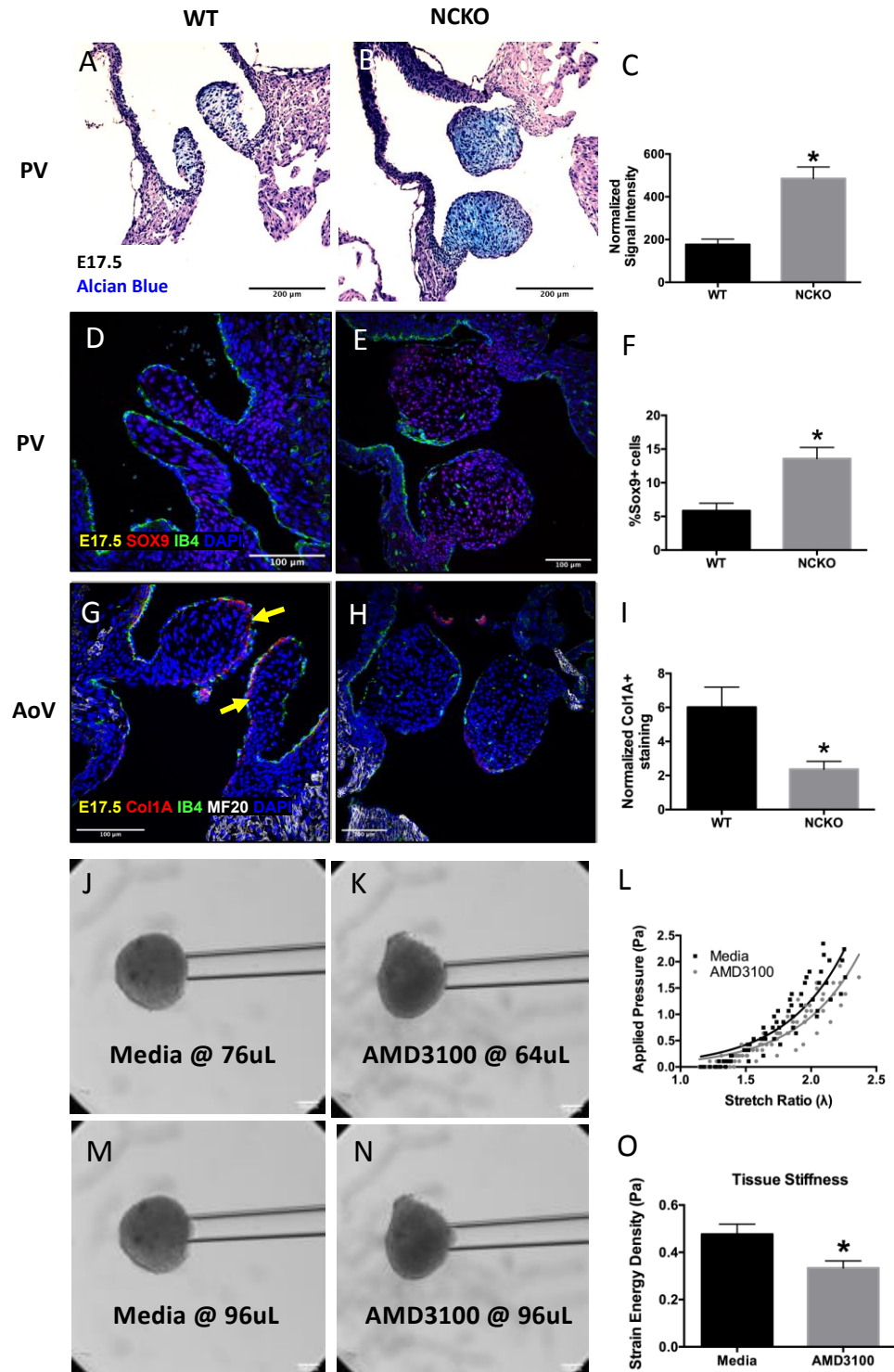


Figure 3.11. Aberrant matrix maturation in CXCR4 mutant valves. **A** and **B**, Alcian blue staining of E17.5 WT and NCKO PV valves to visualize proteoglycan deposition. **C**, Quantification of alcian blue staining signal, normalized by dividing total stained area by total mesenchymal cell number. **D** and **E**, Immunostaining of sox9, showing

increased nuclear translocation of Sox9 in NCKO. **F**, Quantification of sox9 expression based on percentage of cells positive for nuclear sox9 expression. **G** and **H**, Immunostaining for collagen type 1(Col1A), showing decreased collagen deposition in NCKO valves. **I**, Quantification of collagen deposition based on area positive for Col1A, normalized by the total number of mesenchymal cells. Yellow arrows indicate Col1A expression on the ventricular side. MF20 was used to visualize myocardium. Endocardial cells were stained with IB4, while nuclei were stained with DAPI. **J – N**, Images show valve organoids untreated or treated with AMD3100, with baseline applied pressure (J and K) and at 96ul (M and N). **L**, Mechanical response curves, showing applied pressure (Pa) and stretch ratio of organoids. **O**, Quantification of tissue stiffness based on strain energy density of untreated and AMD3100-treated organoids. Data are means +/- SEM. N= 7 embryos per group (A-C), 6 embryos per group (D-F), 6 embryos per group (G-I), and 8 organoids per group (J-O). * $p \leq 0.05$ via Student t test. Scale bars indicate 200um (A – B) and 100um (D – N).

3.4.11 Endocardial Notch1 signaling regulates subendocardial CXCR4 expression

Since CXCR4 expression was restricted to the ventricular side of the OFT valves (Figure 1B and C) and atrial side of the AVC valves (Figure 1H), we suspected that CXCR4 expression might be regulated by unidirectional laminar shear stress (LSS). Moreover, given the restriction of CXCR4 expression to the subendocardial region, we rationalized that the adjacent endocardium could transduce hemodynamic information, i.e. shear stress, into biological programs that regulate CXCR4 expression. Recently, shear-sensitive Notch1 signaling has been associated with CXCR4 transcripts in OFT valves. Interestingly, immunostaining for notch1 intracellular domain (NICD1), revealed that active Notch1 signaling, like CXCR4, was also confined to the ventricular side of the OFT valves (Figure 13A and C) and AVC valves (Figure 13B and D). Furthermore, NICD1 is restricted to the endocardium (yellow arrows, Figure 13C and D), confirming previous reports.

To ascertain whether endocardial Notch1 signaling regulates subendocardial expression of CXCR4, we bred Notch1 floxed mice into the endocardial cell-specific Cre driver line Nfatc1-enCre. Previous fate mapping experiments using Nfatc1-enCre with Rosa26-LacZ reporter mice have shown that Nfatc1 is present on in the valve endocardium. Immunostaining for CXCR4 revealed that Nfatc1-enCre;Notch1^{flox/flox} (N1ecKO) exhibited a 50% decrease in CXCR4 expression (P=0.0434, Figure 13G – I) compared to WT controls, confirming previous RNAseq data. Together, these findings suggest that endocardial Notch1 signaling drives subendocardial CXCR4 expression.

We then determined whether LSS can activate Notch1 signaling in valve endocardial cells. We first tested whether the side-specificity of Notch1 activation was due to the side-specificity of Notch1 expression. Intriguingly, we detected Notch1 on both the arterial side in the OFT (arrow head, Figure 13B) and the ventricular side (arrow head, Figure 13F) in AVC valves. These findings suggest that (1) the absence of Notch1 activation on the arterial side in the OFT (or ventricular side in the AVC) is not due a lack of Notch1 expression, and (2) LSS may activate Notch1 expression by interacting directly with Notch1 receptor, confirming previous reports.

To elucidate the role of shear stress in Notch1 activation, we employed a parallel-plate bioreactor system to expose primary chick embryonic endocardial cells to various shear stress environments. The OFTs of HH33+ chick embryos were isolated, opened, and placed on collagen constructs that left behind a single layer of endocardial cells after 6 hours of incubation. These endocardial cells were then exposed to no flow (static), LSS at 20dynes/cm² (LS220), or oscillatory shear stress at

20dynes/cm² (Figure 14A). After 24 hours in culture, we assessed Notch1 nuclear translocation via immunostaining and detected a 53% increase ($P < 0.0001$) in percentage of endocardial cells positive for nuclear Notch1 (Figure 14D) compared to static control (Figure 14C). These data suggest that LSS20 is sufficient at inducing Notch1 activation in endocardial cells. We then determined whether a magnitude of 20dynes/cm² alone is sufficient to activate Notch1 by exposing endocardial cells to OSS20, which replicates the flow environment on the arterial side of the valve. After 24hr in culture, we detected a 39% decrease in %NICD1+ cells in cells exposed to OSS20 (Figure 14D) compared to those exposed to LSS20 and no difference compared to the static control (Figure 14A). These results suggest that Notch1 activation requires high unidirectional laminar shear.

To expand these findings, we performed qRT-PCR to assess expression of the components of Notch1 pathway in response to varying flow conditions. Surprisingly, we did not detect any significant difference in Notch1 transcripts between LSS20 and static conditions, while LSS20 was significantly higher than OSS20 (Figure 14F). In addition, there was no difference between static, LSS20, and OSS20 with regard with HEY1, a downstream gene target of Notch1 signaling. However, there was a 5-fold increase in HEY2 transcript and a 3-fold increase in JAG1 (both are other downstream targets of Notch1) compared to the static and OSS20 conditions.

Taken together, these findings indicate that high unidirectional shear stress is sufficient to induce endocardial Notch1 activation, which in turn regulates subendocardial CXCR4 expression.

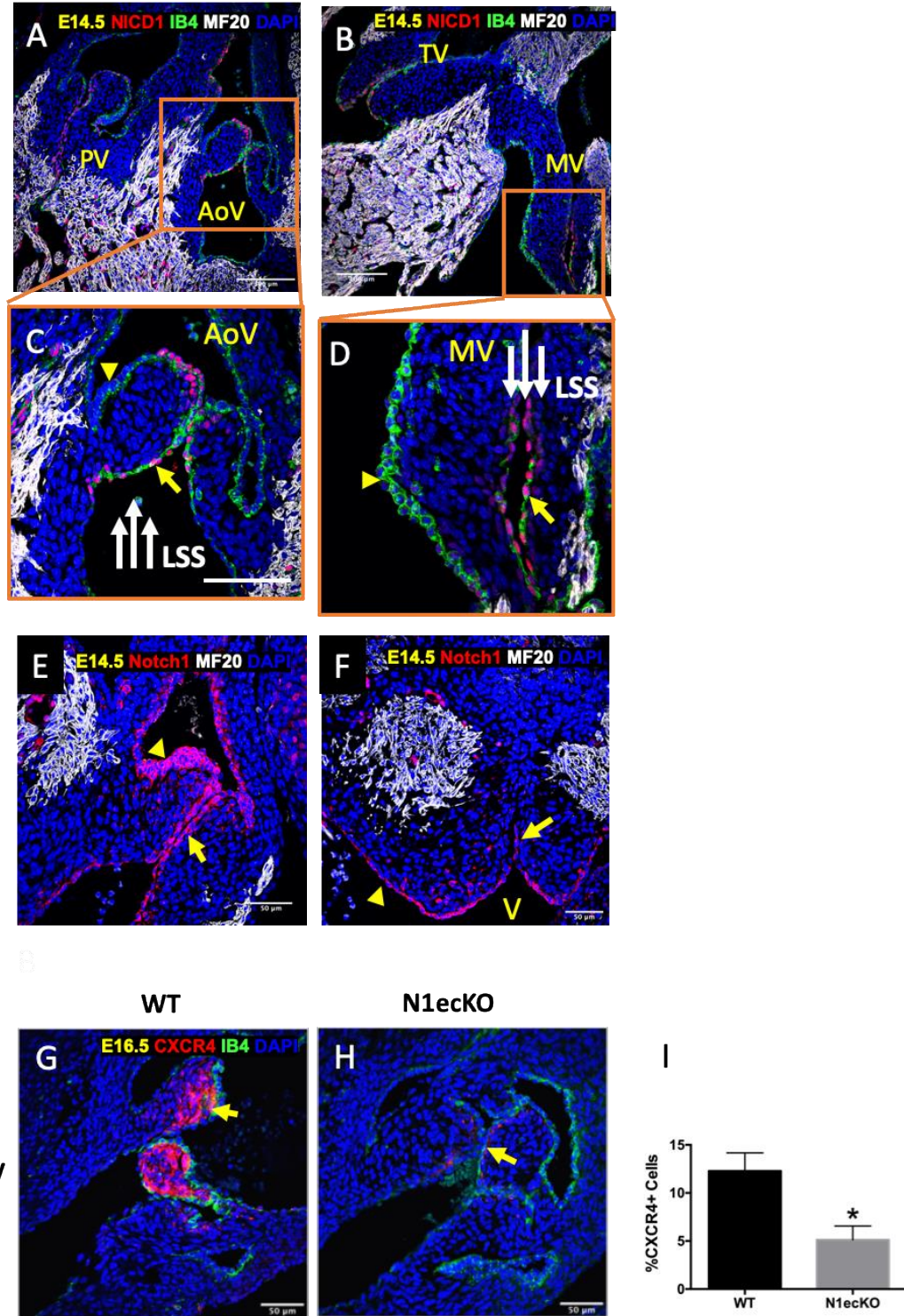


Figure 3.12. Endocardial Notch1 regulates subendocardial CXCR4 expression. **A – D**, Immunostaining for Notch1 intracellular domain (NICD1) in OFT and AVC valves at E14.5, showing that NICD1 expression was restricted to the ventricular side of the OFT valve and atrial side in the AVC. MF20 was used to visualize myocardium. Endocardial

cells were stained with IB4, while nuclei were stained with DAPI. **E**, Immunostaining for Notch1 in OFT valve at E14.5. **F**, Immunostaining for Notch1 in AVC valve at E14.5. Yellow arrows indicate the ventricular side (**C** and **E**) and atrial side (**D** and **F**), while arrow heads indicate arterial side (**C** and **E**) and ventricular side (**D** and **F**). **G** and **H**, Immunostaining for CXCR4 in WT vs. *Nfatc1*-enCre;*Notch1*^{flox/flox} (N1ecKO). Yellow arrows indicate CXCR4 expression (red). **I**, Quantification of CXCR4 expression for **G** and **H**, based on percentage of mesenchymal cells positive for CXCR4. Data are means \pm SEM. N= 3 embryos per group. * $p \leq 0.05$ via Student t test. Scale bars indicate 100 μ m.

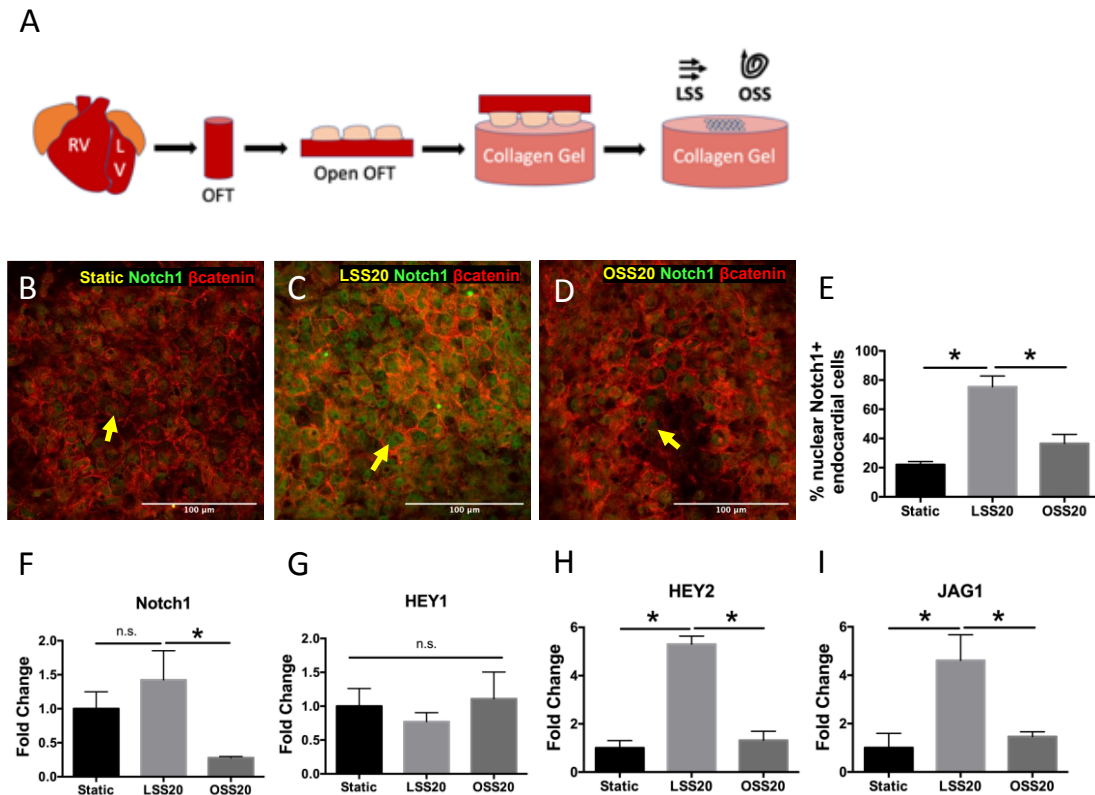


Figure 3.13. Lamina shear stress induces Notch1 activation in primary chick endocardial cells. **A**, Schematic showing how primary valve endocardial cells were harvested from HH33+ chick embryos. **B – D**, Immunostaining for Notch1 in primary endocardial cells exposed to static (**B**), LSS20 (**C**), and OSS20 (**D**). β catenin (red) was used to visualize endocardial cells. Yellow arrows indicate nuclear Notch1 expression. **E**, Quantification of nuclear Notch1 expression based on percentage of endocardial cells positive for nuclear Notch1. **F – I**, qRT-PCR data indicating fold change of the components of Notch1 pathway, normalized to static control. Data are means \pm SEM. N= 10-13 embryos per group (**B-E**) and 4 embryos per group (**F-G**). * $p \leq 0.05$ via ANOVA with Tukey's multiple comparisons test. Scale bars indicate 100 μ m.

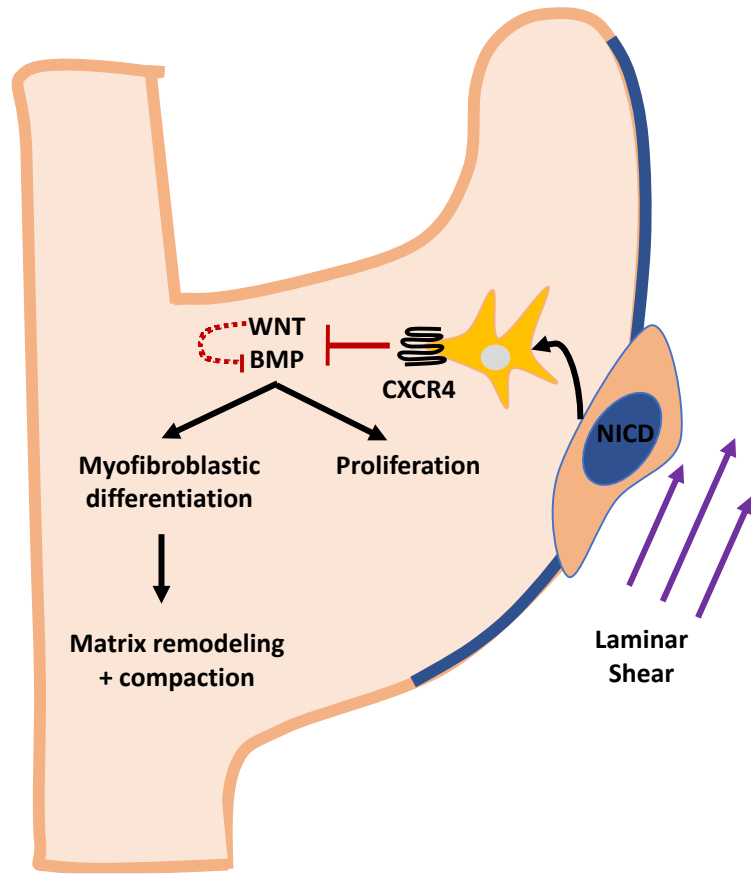


Figure 3.14. CXCR4 regulation of outflow tract valve remodeling. Between E11.5 to P0, endocardial cells sense and transduce high unidirectional shear stress into Notch1 signaling program, which turns on CXCR4 expression in the subendocardial cells. CXCR4 signaling inhibits BMP and canonical WNT signaling programs, which modulate mesenchymal cell proliferation, matrix remodeling, and tissue compaction. As a result, CXCR4 signaling facilitates valve maturation to cope with the increasing hemodynamic stress.

3.5 Discussion

Congenital heart defects can be attributed to any disruption to the valve morphogenetic process. While much of early valve development, e.g. EMT, has been extensively studied, what happens post-EMT is still elusive. Here, we investigated two hallmarks of post-EMT valve remodeling: mesenchymal cell proliferation and matrix

remodeling. Our study has revealed a CXCR4-dependent regulatory program of valve remodeling and yielded several main findings: (1) During valve remodeling, CXCR4 was expressed in the mesenchymal cells in the subendocardial region of both the AVC and OFT valves, while CXCL12 (its ligand) was expressed in the valve mesenchyme and OFT wall; (2) global ablation of CXCR4 resulted in hyperplastic and thickened semilunar valves during late gestation, despite no changes in mesenchymal cell apoptosis; (3) CXCR4 disruption did not lead to hyperplasia and thickened phenotype in LAV and RAV valves; (4) Ablation of CXCR4 in endocardium-derived mesenchymal cells phenocopied our global CXCR4 mutants but did not result in absence of coronary arteries or embryonic lethality; (5) Subendocardial CXCR4 regulates mesenchymal cell proliferation by modulating BMP and canonical Wnt signaling in a non-cell autonomous manner; (6) Subendocardial CXCR4 activity also regulates valve compaction through facilitating mesenchymal cell contractility and mesenchymal condensation. CXCR4 signaling increases cell contractility by inhibiting BMP signaling in a paracrine fashion and increasing α SMA expression in a cell-autonomous manner; (7) CXCR4 signaling matures and stiffens valvular extracellular matrix by inhibiting BMP activity; (8) High unidirectional shear stress confers side-specificity of the activation of endocardial Notch1 and subendocardial CXCR4 expression. Taken together, these data have uncovered a novel mechanism that involves transduction of hemodynamic cues into Notch1 signaling by the endocardial cells, which in turn regulates subendocardial CXCR4 expression and valve remodeling processes. This model also posits that any

aberration in the genetic or mechanical programs regulating valve morphogenesis could result in congenital valve defects.

Our expression analysis provided, for the first time, detailed spatiotemporal distribution of CXCR4 and CXCL12 during valve remodeling. Previous studies reported that CXCR4 was strongly expressed in the endocardium and essential for EMT around E10.5 (Luna-Zurita, 2010, Ivins 2015), while its expression diminished in the mesenchyme during valve remodeling beginning at E12.5 (Sierro, 2007). The findings in these reports were limited by detection of CXCR4 transcripts via *in situ* hybridization, absence of an endocardium-specific marker. In this report, we used ultrasensitive immunostaining techniques and an endocardial marker to detect protein expression of CXCR4 in a distinct population of subendocardial cells between E11.5 and E17.5, both in the OFT and AVC valves. We also detected expression of CXCL12, the only known ligand of CXCR4 (Pawig, 2015), in the subendocardial region and also in the OFT wall, confirming previous findings (Ivins, 2015). Furthermore, while OFT valves developed normally in an early report of global CXCL12 mutant mice (Nagasawa, 1996), a more recent study showed hyperplastic OFT valves in global and conditional CXCL12 mutant mice (Ivins, 2015). In our studies, both global and endocardium-derived mesenchymal cell specific deletion of CXCR4 resulted in hyperplasia and thickened semilunar valves, confirming a role for CXCR4/CXCL12 signaling in regulating mesenchymal cell proliferation during valve remodeling. Our CXCR4 mutant valves phenocopied those in mutant mouse models of CXCR7, which forms heterodimers with CXCR4 and potentiates CXCL12 signaling (Sierro, 2007, Mellado, 2001). Surprisingly,

despite CXCR4 presence in the subendocardial region of AVC valves, we did not detect any hypertrophy in these valves, compared to those in WT controls, suggesting that CXCR4 is not required for regulating remodeling or its lack of expression can be compensated by the “sister receptor” CXCR7 (Levoye, 2009).

Cardiac neural crest cells (cNCCs) populate much of the OFT valve primordia (Jain, 2011) and likely participate in CXCR4 regulation of valve remodeling. Interestingly, inactivation of CXCR4 in endocardium lineage-specific mesenchymal cells resulted in hyperplastic and thickened valve phenotype, suggesting that CXCR4 signaling by endocardium-derived mesenchymal cells (EDMCs) are sufficient to regulate mesenchymal cell proliferation and remodeling. These findings also indicate that endocardial instruction to maintain CXCR4 signaling in the subendocardial cells is indiscriminate towards both cNCCs and EDMCs, which occupy the subendocardial region (Cai, 2013, Peterson, 2018). In this study, we showed that “endocardial signal” can result from Notch1 signaling in the endocardium adjacent to CXCR4-positive cells, as endocardium-specific ablation of Notch1 led to a decrease in CXCR4 expression in the subendocardium. These results confirmed previous RNAseq data showing a decrease in CXCR4 expression in valve primordia of *Nkx2.5-Cre;Jag1^{flox/flox}* mice (McGrogan, 2016). Due to the proximity of Notch1 and CXCR4 expression cells and the graded expression pattern of CXCR4 radiating from the endocardium (Figure 1F), we predict that endocardial Notch1 signaling regulates subendocardial CXCR4 expression via a paracrine factor. However, this interaction remains to be worked out in future studies.

We did not detect any difference in apoptotic activity in the mesenchymal cells of the global CXCR4 mutants at either E14.5 or E17.5, compared to WT controls. Therefore, the hyperplastic phenotype in the absence of CXCR4 cannot be attributed to a decrease in mesenchymal cell apoptosis. Recently, increased mesenchymal cell proliferation and decreased cell apoptosis were observed in endocardium-specific *Nfatc1-enCre;Notch1^{flox/flox}* (Wang, 2015), while only higher mesenchymal cell proliferation was observed in cardiac-specific *Nkx2.5-Cre;Jag1^{flox/flox}* (McGrogan, 2016), compared to WT controls. These data suggest that different Notch ligands dictate whether signaling through endocardial Notch1 regulates mesenchymal cell proliferation or apoptosis. Our Notch1/CXCR4 axis provides a pathway through which endocardial Notch1 regulates mesenchymal cell proliferation.

On a mechanistic level, we found that BMP signaling was elevated in conditional CXCR4 mutant valves. BMP signaling has been linked to mesenchymal cell proliferation during valve development (McCulley, 2008; Choi, 2007; Jackson, 2003). Our data confirm those findings and suggest that CXCR4 signaling suppresses mesenchymal cell proliferation through modulating BMP activity. Intriguingly, we detected augmentation of BMP signaling in mesenchymal cells outside of the subendocardial region in CXCR4 mutant valves, suggesting CXCR4 modulates BMP signaling in a non-cell autonomous manner. Furthermore, conditional ablation of CXCR4 resulted in enhanced β catenin nuclear translocation and LEF1 expression in mesenchymal cells (including those outside of the subendocardial region), suggesting that CXCR4 also modulates canonical Wnt signaling through a non-cell autonomous

fashion. Recently, canonical Wnt signaling has been associated with valve growth by promoting mesenchymal cell proliferation by increasing responsiveness to fibroblast growth factor signaling (Bosada, 2016) or by increasing BMP expression in the myocardium and subsequent BMP activation in mesenchymal cells (Klaus, 2007; Wang, 2018). Taken together, these data indicate a novel mechanism in which the CXCR4/Wnt/BMP axis coordinates endocardial and myocardial signaling to regulate mesenchymal remodeling.

In this study, we also explored the possibility that the thickened valve phenotype in CXCR4 mutants was due to impaired matrix remodeling. Recently, several reports have indicated that mesenchymal condensation and differentiation are also hallmarks of valve remodeling (Combs, 2009; Kruithof, 2007). In particular, maturing valve mesenchymal cells compact the extracellular matrix around them and express α SMA and filamin A (Dupuis 2013; Goddard 2017), which are cytoskeletal proteins associated with valve myofibroblastic contractility and differentiation (Hinz, 2001; Grinnell, 2002). Furthermore, fibroblastic contractility is also associated with tissue-level compaction (Dikosky, 2008) and is therefore thought to facilitate valve compaction. Interestingly, we found that conditional CXCR4 ablation led to decreased mesenchymal cell density and attenuated α SMA expression, suggesting that CXCR4 is required for mesenchymal condensation and myofibroblastic differentiation *in vivo*. Furthermore, we found that CXCR4 signaling facilitates tissue compaction by inhibiting BMP signaling and increasing α SMA expression in valvular organoids. Recent data have suggested that myofibroblastic contractility is associated with tissue compaction

during wound healing (Tomasek, 2002) and valve development (Butcher, 2006; Aikawa, 2006; Gould, 2015). Since α SMA expression is colocalized with CXCR4-positive cells in the subendocardial region, we posit that CXCR4 regulates α SMA expression and therefore contractility in the subendocardial cells in a cell-autonomous manner (Tang, 2019).

These results also corroborate with previous findings showing attenuation of BMP/Sox9 signaling, is required to facilitate mesenchymal cell differentiation and valve maturation (Lincoln, 2007, Akiyama, 2004, MacGrogan, 2016). Overactivation of BMP signaling is also associated with excessive deposition of glycosaminoglycans that precedes calcification in human aortic valves (Ankeny, 2011; Kaden, 2004). In our CXCR4 mutant valves, we detected enhanced Sox9 expression that accompanied higher proteoglycan deposition, indicating that overactive BMP signaling is linked to immature matrix remodeling. In addition, we detected less collagen type I deposition in the subendocardial region, suggesting that CXCR4-positive cells may regulate collagen production in a cell-autonomous manner (Patalano, 2018; Li, 2020). Moreover, increased proteoglycan and decreased collagen deposition also decreased valve organoid tissue stiffness, confirming that CXCR4 signaling is necessary to ensure valvular mechanical sufficiency (Combs, 2009). Our findings corroborate with the downregulation of versican, a proteoglycan, in WNT-inactivated valves (Bosada, 2016). Interestingly, increased BMP/Sox9 signaling and deposition of proteoglycan also precede calcification in diseased valves (Ankeny, 2011; Kaden, 2004).

Due to the proximity of CXCR4-positive subendocardial cells and Notch1-active endocardial cells, we determined whether Notch1 signaling regulated CXCR4 expression. Our results indicated that Notch1 signaling is restricted to the endocardium on the ventricular side and regulates CXCR4 protein expression. Previous RNAseq data showed that ablation of Jag1 in the myocardium led to downregulation of CXCR4 expression in the valve primordia (MacGrogan, 2016). Intriguingly, our data indicate that CXCR4 expression and Notch1 signaling are localized on the ventricular side of the OFT valves and the atrial side of the AVC valves (del Monte, 2007). Furthermore, previous computational modeling of fluid dynamics in the OFT valves by us and others have shown that the ventricular side of the OFT valve experiences high unidirectional shear stress, while the arterial side of the valve is under oscillatory shear stress (Bharadwaj, 2012; Yap, 2012; Yap, 2012). To this end, we tested whether LSS can drive Notch1 signaling in valve endocardial cells. Our bioreactor model provided us a unique advantage to answer this question using primary endocardial chick cells harvested during valve modeling stages. Notch1 signaling has been previously linked to shear stress in endothelial cells (Jahnsen, 2015, Driessen, 2018). Furthermore, reduction of shear stress by modulation of blood flow in the heart was shown to inhibit Notch signaling in endocardial cells in zebrafish (Pestel, 2016; Lee, 2016). Our results demonstrated for the first time that valve endocardial cells upregulated Notch1 activation by LSS but not OSS. Surprisingly, although we detected enhanced nuclear translocation of the intracellular domain of Notch1 and upregulation of its downstream target genes, e.g. HEY2 and JAG1, we did not detect an upregulation of

Notch1 in the LSS20, compared to static controls. Interestingly, a recent study also reported upregulation of Notch1 signaling with no change in Notch1 expression in human endothelial cells exposed to laminar shear stress (Fang, 2017). These findings suggest that Notch1 can undergo receptor cleavage and activation upon direct mechanical interaction with shear stress (Meloty-Kapella, 2012). Moreover, we were not able to amplify and detect DLL4 using qRT-PCR, suggesting that its expression is extremely low in primary endocardial cells during valve remodeling stages. These findings confirm low *in vivo* expression of DLL4 in endocardial cells and the Notch1/Jag1 signaling bias during valve remodeling stages (MacGrogan, 2016).

In conclusion, this study has uncovered a regulatory program involving the transduction of hemodynamic information into endocardial Notch1 signaling that coordinates valve remodeling processes via subendocardial CXCR4 activity. Mechanistically, WNT and BMP signaling mediates CXCR4 regulation of mesenchymal cell proliferation, mesenchymal condensation, and matrix remodeling (Figure 14). Any genetic or mechanical disruption to this program may result in congenital valve defects. Furthermore, reactivation of developmental pathways has been implicated in adult valve pathology (Mahler, 2011). Therefore, it is conceivable that enhanced proliferation of valve interstitial cells and excessive deposition of matrix components that precede valve calcification could be due to aberration to this CXCR4-dependent program. Future studies focusing on determining other components of this developmental program and whether CXCR4 participates in valve disease will be critical to the development of novel therapeutic targets.

3.6 References

1. Aikawa, E., Whittaker, P., Farber, M., Mendelson, K., Padera, R. F., Aikawa, M., & Schoen, F. J. (2006). Human semilunar cardiac valve remodeling by activated cells from fetus to adult: implications for postnatal adaptation, pathology, and tissue engineering. *Circulation*, *113*(10), 1344-1352.
2. Akiyama, H., Chaboissier, M. C., Behringer, R. R., Rowitch, D. H., Schedl, A., Epstein, J. A., & De Crombrughe, B. (2004). Essential role of Sox9 in the pathway that controls formation of cardiac valves and septa. *Proceedings of the National Academy of Sciences*, *101*(17), 6502-6507.
3. Ankeny, R. F., Thourani, V. H., Weiss, D., Vega, J. D., Taylor, W. R., Nerem, R. M., & Jo, H. (2011). Preferential activation of SMAD1/5/8 on the fibrosa endothelium in calcified human aortic valves-association with low BMP antagonists and SMAD6. *PloS one*, *6*(6).
4. Bhakta, S., Hong, P., & Koc, O. (2006). The surface adhesion molecule CXCR4 stimulates mesenchymal stem cell migration to stromal cell-derived factor-1 in vitro but does not decrease apoptosis under serum deprivation. *Cardiovascular Revascularization Medicine*, *7*(1), 19-24.
5. Bharadwaj, K. N., Spitz, C., Shekhar, A., Yalcin, H. C., & Butcher, J. T. (2012). Computational fluid dynamics of developing avian outflow tract heart valves. *Annals of biomedical engineering*, *40*(10), 2212-2227.

6. Bosada, F. M., Devasthali, V., Jones, K. A., & Stankunas, K. (2016). Wnt/ β -catenin signaling enables developmental transitions during valvulogenesis. *Development*, *143*(6), 1041-1054.
7. Buskohl, P. R., Gould, R. A., & Butcher, J. T. (2012). Quantification of embryonic atrioventricular valve biomechanics during morphogenesis. *Journal of biomechanics*, *45*(5), 895-902.
8. Butcher, J. T., & Markwald, R. R. (2007). Valvulogenesis: the moving target. *Philosophical Transactions of the Royal Society B: Biological Sciences*, *362*(1484), 1489-1503.
9. Butcher, J. T., Barrett, B. C., & Nerem, R. M. (2006). Equibiaxial strain stimulates fibroblastic phenotype shift in smooth muscle cells in an engineered tissue model of the aortic wall. *Biomaterials*, *27*(30), 5252-5258.
10. Cai, X., Zhang, W., Hu, J., Zhang, L., Sultana, N., Wu, B., ... & Cai, C. L. (2013). Tbx20 acts upstream of Wnt signaling to regulate endocardial cushion formation and valve remodeling during mouse cardiogenesis. *Development*, *140*(15), 3176-3187.
11. Chiu, Y. N., Norris, R. A., Mahler, G., Recknagel, A., & Butcher, J. T. (2010). Transforming growth factor β , bone morphogenetic protein, and vascular endothelial growth factor mediate phenotype maturation and tissue remodeling by embryonic valve progenitor cells: relevance for heart valve tissue engineering. *Tissue Engineering Part A*, *16*(11), 3375-3383.

12. Choi, M., Stottmann, R. W., Yang, Y. P., Meyers, E. N., & Klingensmith, J. (2007). The bone morphogenetic protein antagonist noggin regulates mammalian cardiac morphogenesis. *Circulation research*, *100*(2), 220-228.
13. Combs, M. D., & Yutzey, K. E. (2009). Heart valve development: regulatory networks in development and disease. *Circulation research*, *105*(5), 408-421.
14. Del Monte, G., Grego-Bessa, J., González-Rajal, A., Bolós, V., & De La Pompa, J. L. (2007). Monitoring Notch1 activity in development: evidence for a feedback regulatory loop. *Developmental dynamics: an official publication of the American Association of Anatomists*, *236*(9), 2594-2614.
15. Dikovsky, D., Bianco-Peled, H., & Seliktar, D. (2008). Defining the role of matrix compliance and proteolysis in three-dimensional cell spreading and remodeling. *Biophysical journal*, *94*(7), 2914-2925.
16. Driessen, R. C. H., Stassen, O. M. J. A., Sjöqvist, M., Suarez Rodriguez, F., Grolleman, J., Bouten, C. V. C., & Sahlgren, C. M. (2018). Shear stress induces expression, intracellular reorganization and enhanced Notch activation potential of Jagged1. *Integrative Biology*, *10*(11), 719-726.
17. Dupuis, L. E., Osinska, H., Weinstein, M. B., Hinton, R. B., & Kern, C. B. (2013). Insufficient versican cleavage and Smad2 phosphorylation results in bicuspid aortic and pulmonary valves. *Journal of molecular and cellular cardiology*, *60*, 50-59.

18. Fang, J. S., Coon, B. G., Gillis, N., Chen, Z., Qiu, J., Chittenden, T. W., ... & Hirschi, K. K. (2017). Shear-induced Notch-Cx37-p27 axis arrests endothelial cell cycle to enable arterial specification. *Nature communications*, *8*(1), 1-14.
19. Goddard, L. M., Duchemin, A. L., Ramalingan, H., Wu, B., Chen, M., Bamezai, S., ... & Scherrer-Crosbie, M. (2017). Hemodynamic forces sculpt developing heart valves through a KLF2-WNT9B paracrine signaling axis. *Developmental cell*, *43*(3), 274-289.
20. Gould, R. A., & Butcher, J. T. (2010). Isolation of valvular endothelial cells. *JoVE (Journal of Visualized Experiments)*, (46), e2158.
21. Gould, R. A., Yalcin, H. C., MacKay, J. L., Sauls, K., Norris, R., Kumar, S., & Butcher, J. T. (2016). Cyclic mechanical loading is essential for Rac1-mediated elongation and remodeling of the embryonic mitral valve. *Current Biology*, *26*(1), 27-37.
22. Grinnell, F., & Ho, C. H. (2002). Transforming growth factor β stimulates fibroblast–collagen matrix contraction by different mechanisms in mechanically loaded and unloaded matrices. *Experimental cell research*, *273*(2), 248-255.
23. Hata, A., Lagna, G., Massagué, J., & Hemmati-Brivanlou, A. (1998). Smad6 inhibits BMP/Smad1 signaling by specifically competing with the Smad4 tumor suppressor. *Genes & development*, *12*(2), 186-197.
24. Hinton, R. B., & Yutzey, K. E. (2011). Heart valve structure and function in development and disease. *Annual review of physiology*, *73*, 29-46.

25. Hinz, B., Celetta, G., Tomasek, J. J., Gabbiani, G., & Chaponnier, C. (2001). Alpha-smooth muscle actin expression upregulates fibroblast contractile activity. *Molecular biology of the cell*, 12(9), 2730-2741.
26. Hoffman, J. I., & Kaplan, S. (2002). The incidence of congenital heart disease. *Journal of the American college of cardiology*, 39(12), 1890-1900.
27. Ivins, S., Chappell, J., Vernay, B., Suntharalingham, J., Martineau, A., Mohun, T. J., & Scambler, P. J. (2015). The CXCL12/CXCR4 axis plays a critical role in coronary artery development. *Developmental cell*, 33(4), 455-468.
28. Ivins, S., Chappell, J., Vernay, B., Suntharalingham, J., Martineau, A., Mohun, T. J., & Scambler, P. J. (2015). The CXCL12/CXCR4 axis plays a critical role in coronary artery development. *Developmental cell*, 33(4), 455-468.
29. Jackson, L. F., Qiu, T. H., Sunnarborg, S. W., Chang, A., Zhang, C., Patterson, C., & Lee, D. C. (2003). Defective valvulogenesis in HB-EGF and TACE-null mice is associated with aberrant BMP signaling. *The EMBO journal*, 22(11), 2704-2716.
30. Jahnsen, E. D., Trindade, A., Zaun, H. C., Lehoux, S., Duarte, A., & Jones, E. A. (2015). Notch1 is pan-endothelial at the onset of flow and regulated by flow. *PloS one*, 10(4).
31. Jain, R., Engleka, K. A., Rentschler, S. L., Manderfield, L. J., Li, L., Yuan, L., & Epstein, J. A. (2011). Cardiac neural crest orchestrates remodeling and functional maturation of mouse semilunar valves. *The Journal of clinical investigation*, 121(1), 422-430.

32. Kaden, J. J., Bickelhaupt, S., Grobholz, R., Vahl, C., Hagl, S., Brueckmann, M., ... & Borggrefe, M. (2004). Expression of bone sialoprotein and bone morphogenetic protein-2 in calcific aortic stenosis. *Journal Of Heart Valve Disease, 13*(4), 560-566.
33. Kawaguchi, N., Zhang, T. T., & Nakanishi, T. (2019). Involvement of CXCR4 in Normal and abnormal development. *Cells, 8*(2), 185.
34. Klaus, A., Saga, Y., Taketo, M. M., Tzahor, E., & Birchmeier, W. (2007). Distinct roles of Wnt/ β -catenin and Bmp signaling during early cardiogenesis. *Proceedings of the National Academy of Sciences, 104*(47), 18531-18536.
35. Kruithof, B. P., Krawitz, S. A., & Gaussin, V. (2007). Atrioventricular valve development during late embryonic and postnatal stages involves condensation and extracellular matrix remodeling. *Developmental biology, 302*(1), 208-217.
36. Lee, J., Fei, P., Packard, R. R. S., Kang, H., Xu, H., Baek, K. I., ... & Chi, N. C. (2016). 4-Dimensional light-sheet microscopy to elucidate shear stress modulation of cardiac trabeculation. *The Journal of clinical investigation, 126*(5), 1679-1690.
37. Levoye, A., Balabanian, K., Baleux, F., Bachelier, F., & Lagane, B. (2009). CXCR7 heterodimerizes with CXCR4 and regulates CXCL12-mediated G protein signaling. *Blood, The Journal of the American Society of Hematology, 113*(24), 6085-6093.

38. Li, F., Xu, X., Geng, J., Wan, X., & Dai, H. (2020). The autocrine CXCR4/CXCL12 axis contributes to lung fibrosis through modulation of lung fibroblast activity. *Experimental and Therapeutic Medicine*, *19*(3), 1844-1854.
39. Lincoln, J., Kist, R., Scherer, G., & Yutzey, K. E. (2007). Sox9 is required for precursor cell expansion and extracellular matrix organization during mouse heart valve development. *Developmental biology*, *305*(1), 120-132.
40. Luna-Zurita, L., Prados, B., Grego-Bessa, J., Luxán, G., Del Monte, G., Benguría, A., ... & De La Pompa, J. L. (2010). Integration of a Notch-dependent mesenchymal gene program and Bmp2-driven cell invasiveness regulates murine cardiac valve formation. *The Journal of clinical investigation*, *120*(10), 3493-3507.
41. Ma, Q., Jones, D., Borghesani, P. R., Segal, R. A., Nagasawa, T., Kishimoto, T., ... & Springer, T. A. (1998). Impaired B-lymphopoiesis, myelopoiesis, and derailed cerebellar neuron migration in CXCR4-and SDF-1-deficient mice. *Proceedings of the National Academy of Sciences*, *95*(16), 9448-9453.
42. MacGrogan, D., D'Amato, G., Travisano, S., Martinez-Poveda, B., Luxán, G., del Monte-Nieto, G., ... & Gómez, M. J. (2016). Sequential ligand-dependent notch signaling activation regulates valve primordium formation and morphogenesis. *Circulation research*, *118*(10), 1480-1497.
43. MacGrogan, D., Luxán, G., Driessen-Mol, A., Bouten, C., Baaijens, F., & De La Pompa, J. L. (2014). How to make a heart valve: from embryonic development

- to bioengineering of living valve substitutes. *Cold Spring Harbor perspectives in medicine*, 4(11), a013912.
44. Mahler, G. J., & Butcher, J. T. (2011). Inflammatory regulation of valvular remodeling: the good (?), the bad, and the ugly. *International journal of inflammation*, 2011.
45. McCulley, D. J., Kang, J. O., Martin, J. F., & Black, B. L. (2008). BMP4 is required in the anterior heart field and its derivatives for endocardial cushion remodeling, outflow tract septation, and semilunar valve development. *Developmental dynamics: an official publication of the American Association of Anatomists*, 237(11), 3200-3209.
46. Mellado, M., Rodríguez-Frade, J. M., Vila-Coro, A. J., Fernández, S., Martín de Ana, A., Jones, D. R., ... & Martínez-A, C. (2001). Chemokine receptor homo- or heterodimerization activates distinct signaling pathways. *The EMBO journal*, 20(10), 2497-2507.
47. Meloty-Kapella, L., Shergill, B., Kuon, J., Botvinick, E., & Weinmaster, G. (2012). Notch ligand endocytosis generates mechanical pulling force dependent on dynamin, epsins, and actin. *Developmental cell*, 22(6), 1299-1312.
48. Nagasawa, T., Hirota, S., Tachibana, K., Takakura, N., Nishikawa, S. I., Kitamura, Y., ... & Kishimoto, T. (1996). Defects of B-cell lymphopoiesis and bone-marrow myelopoiesis in mice lacking the CXC chemokine PBSF/SDF-1. *Nature*, 382(6592), 635-638.

49. Patalano, S., Rodríguez-Nieves, J., Colaneri, C., Cotellessa, J., Almanza, D., Zhilin-Roth, A., ... & Macoska, J. (2018). CXCL12/CXCR4-Mediated procollagen secretion is coupled to cullin-RING ubiquitin ligase activation. *Scientific reports*, *8*(1), 1-11.
50. Pawig, L., Klasen, C., Weber, C., Bernhagen, J., & Noels, H. (2015). Diversity and inter-connections in the CXCR4 chemokine receptor/ligand family: molecular perspectives. *Frontiers in immunology*, *6*, 429.
51. Pestel, J., Ramadass, R., Gauvrit, S., Helker, C., Herzog, W., & Stainier, D. Y. (2016). Real-time 3D visualization of cellular rearrangements during cardiac valve formation. *Development*, *143*(12), 2217-2227.
52. Peterson, J. C., Chughtai, M., Wisse, L. J., Gittenberger-de Groot, A. C., Feng, Q., Goumans, M. J. T., ... & DeRuiter, M. C. (2018). Bicuspid aortic valve formation: Nos3 mutation leads to abnormal lineage patterning of neural crest cells and the second heart field. *Disease models & mechanisms*, *11*(10).
53. Sierro, F., Biben, C., Martínez-Muñoz, L., Mellado, M., Ransohoff, R. M., Li, M., ... & Harvey, R. P. (2007). Disrupted cardiac development but normal hematopoiesis in mice deficient in the second CXCL12/SDF-1 receptor, CXCR7. *Proceedings of the National Academy of Sciences*, *104*(37), 14759-14764.
54. Tang, H., Xu, Y., Zhang, Z., Zeng, S., Dong, W., Jiao, W., & Hu, X. (2019). SDF-1/CXCR4 induces epithelial-mesenchymal transition through activation of

- the Wnt/ β -catenin signaling pathway in rat chronic allograft nephropathy. *Molecular medicine reports*, 19(5), 3696-3706.
55. Tomasek, J. J., Gabbiani, G., Hinz, B., Chaponnier, C., & Brown, R. A. (2002). Myofibroblasts and mechano-regulation of connective tissue remodelling. *Nature reviews Molecular cell biology*, 3(5), 349-363.
56. Wang, Y., Lu, P., Wu, B., Riascos-Bernal, D. F., Sibinga, N. E., Valenta, T., ... & Zhou, B. (2018). Myocardial β -Catenin-BMP2 signaling promotes mesenchymal cell proliferation during endocardial cushion formation. *Journal of molecular and cellular cardiology*, 123, 150-158.
57. Yang, J. X., Zhang, N., Wang, H. W., Gao, P., Yang, Q. P., & Wen, Q. P. (2015). CXCR4 receptor overexpression in mesenchymal stem cells facilitates treatment of acute lung injury in rats. *Journal of Biological Chemistry*, 290(4), 1994-2006.
58. Yap, C. H., Saikrishnan, N., & Yoganathan, A. P. (2012). Experimental measurement of dynamic fluid shear stress on the ventricular surface of the aortic valve leaflet. *Biomechanics and modeling in mechanobiology*, 11(1-2), 231-244.
59. Yap, C. H., Saikrishnan, N., Tamilselvan, G., & Yoganathan, A. P. (2012). Experimental measurement of dynamic fluid shear stress on the aortic surface of the aortic valve leaflet. *Biomechanics and modeling in mechanobiology*, 11(1-2), 171-182.

60. Zou, Y. R., Kottmann, A. H., Kuroda, M., Taniuchi, I., & Littman, D. R. (1998).

Function of the chemokine receptor CXCR4 in haematopoiesis and in cerebellar development. *Nature*, 393(6685), 595-599.

CHAPTER 4. CONCLUSIONS AND FUTURE DIRECTIONS

4.1 Summary of findings and implications

In this dissertation work, we set out to shed light on the embryonic valve remodeling processes of the semilunar valves. Clinically, we were motivated by the prevalence of congenital heart defects, which affect about 3 million people (Roger, 2011) and about 40 thousand births (Reller, 2008) in the United States each year. Congenital valve defects account for 20-30% of those live births and can lead to functional abnormalities that affect cardiac functions after birth (Hoffman, 2002). In fact, we and others in the field believe that many of the developmental programs important for valve development become quiescent during adulthood and reactivated in valve disease (reviewed here Mahler, 2011). Therefore, understanding how valve development works would shed light on mechanisms of valve pathology, and vice versa. Scientifically, much of early valve development, involving EMT, has been studied extensively, but what happens during post-EMT valve development is not well understood. Therefore, this dissertation sought to address three hallmarks of valve remodeling that give rise to the semilunar shape of the arterial valves: cell proliferation, cell differentiation, and matrix maturation. In addressing the regulatory programs of those pillars of valve remodeling, we also elaborated on the interaction between hemodynamics and valve development, as alterations to blood flow resulted in abnormal heart and valve development (Midgett, 2014). We found that endocardial cells transduce hemodynamic information into biological signaling that regulates endocardial and mesenchymal developmental programs.

In chapter 2, we discovered a side-specific endocardial proliferation program that may facilitate valve elongation. Mechanistically, endocardial cells transduce low OSS into BMP signaling that regulates endocardial proliferation and accommodation on the arterial side of the OFT valve and the ventricular side of the AV valves. In contrast, endocardial cells exposed to high shear stress modulate BMP signaling through Notch1 signaling. We predict that this differential proliferation of the endocardium constrains valve growth and allows for the elongation of valves in the direction of flow. Recently, several signaling programs have been linked to endocardial growth, e.g. BMP/Twist1, VEGF, and canonical Wnt (Shelton, 2008; Stankunas, 2010; Wang, 2018). Specifically, Wang et al. showed that canonical WNT signaling via beta-catenin is required for endocardial growth in a cell-autonomous manner.

4.2 Oscillatory shear stress regulates canonical WNT signaling via β catenin

Here, we provide evidence that beta-catenin perinuclear translocation is significantly higher under the influence of OSS5 compared to static controls (Figure 1), suggesting that low OSS is sufficient to induce canonical WNT signaling. Furthermore, OSS5 induced significant more β catenin perinuclear localization, compared to LSS5 and OSS20, suggesting that low magnitude and oscillatory direction are required for shear-induced canonical WNT signaling in endocardial cells.

However, whether canonical WNT signaling regulates BMP activity or vice versa in endocardial cells is unknown. Previous study has suggested that endocardial WNT can activate BMP secretion by the myocardium and BMP signaling in mesenchymal

cells in a non-cell autonomous manner (Wang, 2018). It is also conceivable that shear-induced WNT activation is required for endocardial proliferation but not through BMP activation. In fact, β catenin helps regulate vascular endothelial cell-cell adhesions (e.g. VE-cadherin) by linking them to the cytoskeleton. Recent evidence points to β catenin's sensitivity to OSS and its ability to transduce hemodynamic information into vascular developmental programs (Cha, 2016).

Interestingly, while ablation of β catenin in the endocardial cell lineage leads to stunted valve growth, overexpression of β catenin in the endocardial cells did not result in valvular defects (Wang, 2018), suggesting there are programs in place to modulate WNT signaling in the endocardium. Nonetheless, Wang et al. also found that canonical WNT signaling reporter activity is prevalent in the endocardial and mesenchymal cells on the arterial side of the OFT valves, suggesting that low OSS is associated with canonical WNT signaling *in vivo*. Moreover, these data suggest that mesenchymal growth is region-specific and associated with low OSS. It is possible that differential endocardial growth is accompanied by differential mesenchymal growth that facilitates valve elongation in the direction of flow. It is also possible that endocardial cells secrete factors that increase migration of underlying mesenchymal cells towards those endocardial cells, thereby allowing side-specific valve elongation. Intriguingly, BMP has been associated with increased mesenchymal cell migration (Inai, 2008). Future studies will need to determine the region-specific mesenchymal proliferation using whole-mount spatiotemporal immunostaining and analysis of PHH3 or BrdU incorporation.

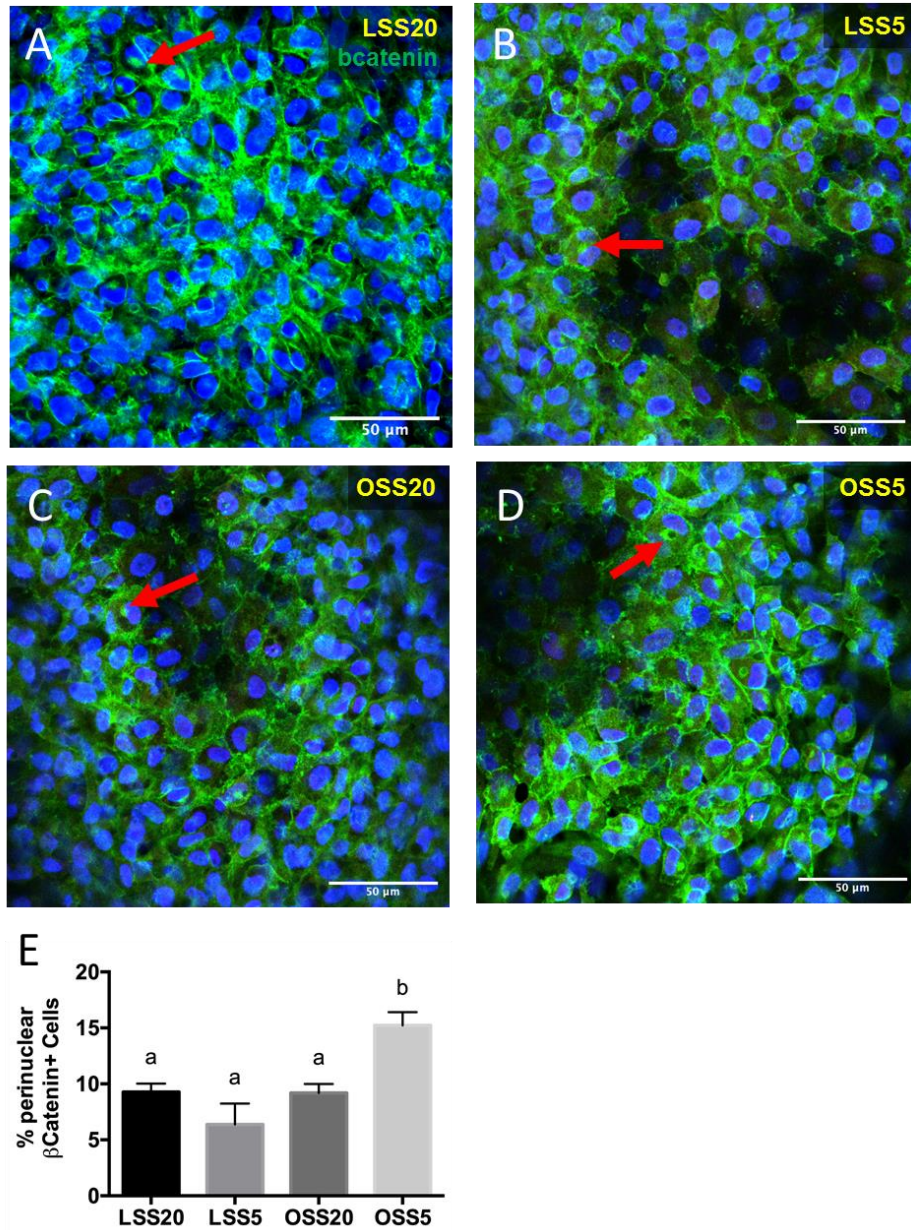


Figure 4.1. Low OSS activates perinuclear localization of β catenin. A-D, immunostaining of β catenin (green) in primary chick valve endocardial cells exposed to various shear conditions. Red arrows indicate perinuclear localization of β catenin, indicating active canonical WNT signaling. E, Quantification of canonical WNT signaling based on the percentage of cells with perinuclear localization of β catenin. * $p < 0.05$ via ANOVA with Tukey's multiple comparisons test. $N = 5$ endocardial patches per group. Bars = 50 μ m.

4.3 Oscillatory shear stress is associated with NFkB signaling

It is conceivable that side-specific apoptotic activity in the mesenchymal cell could also lead to differential growth and valve elongation in the direction of flow. Recall that Notch1 signaling is restricted to the endocardial cells on the ventricular side of the OFT valves and required for modulation of BMP signaling and proliferation. Recent evidence suggests that endocardial signaling regulates endocardial TNFa expression, which is required for apoptosis in the mesenchymal cells (Wang, 2017). Here, we provide evidence that at E14.5, endocardial expression of phosphorylated NFkB, indicative of active inflammatory cytokine signaling (e.g. TNFa), is prevalent in endocardial cells on the ventricular side compared to those on the arterial side (Figure 2). Interestingly, pNFkB nuclear translocation is prevalent in endocardial cells on both sides of the valve from E17.5 onward, indicating that high shear magnitude might be required for activating NFkB programs. More importantly, endocardial expression of pNFkB is associated with Notch1 signaling during mid-gestation valve remodeling. Interestingly, NICD1 has been shown to stabilize NFkB and propagate its downstream targets, suggesting that Notch1 signaling regulates NFkB activity, e.g. expression of TNFa (Espinosa, 2002; Luo, 2013). These data suggest that LSS could regulate Notch1 signaling, which in turn regulates NFkB-dependent propagation of endocardial apoptotic signals to the mesenchymal cells on the ventricular side of the OFT valves.

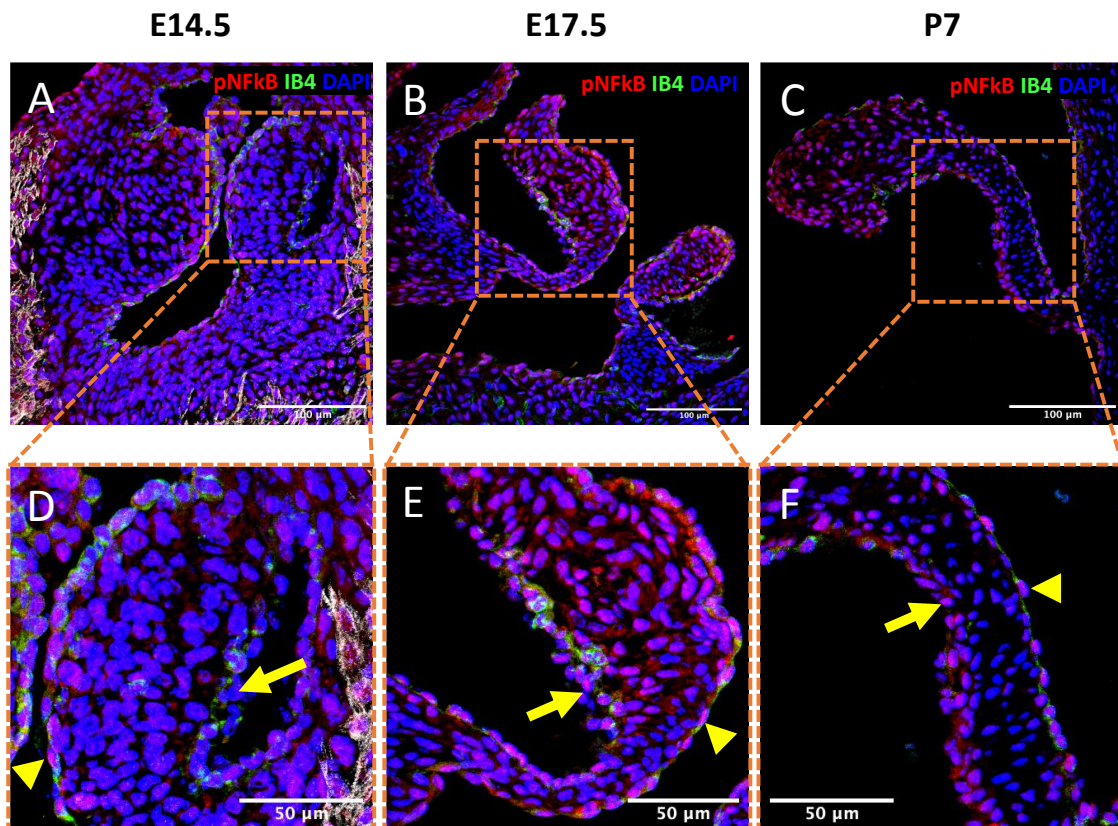


Figure 4.2. Active NFκB signaling is side-specific at E14.5, but not from E17.5 onward. Immunostaining of phosphorylated NFκB, indicating active NFκB signaling, at E14.5 (A, D), E17.5 (B, E), and P7 (C, F). Endocardial cells were stained with IB4 (green). Yellow arrows indicate pNFκB in on the arterial side, while arrow heads indicate pNFκB on the ventricular side. Bars = 100um (A-C) and 50um (D-F).

Future studies will need to analyze the regionality of apoptotic activity in the mesenchymal cells to determine its role in tissue morphogenesis. Future shear experiments will also need to determine whether LSS can activate NFκB signaling, via Notch1 signaling, as well as expression of inflammatory cytokines in primary chick endocardial cells. In addition, computational remodeling taking into account differential growth of the endocardial cells and mesenchymal cells could shed light on how they drive complex 3D tissue morphogenesis during valve remodeling.

4.4 Oscillator shear stress is associated with EMT-inducing Snail1 expression

These data suggest that as mesenchymal cells proliferate, the endocardium also grows to accommodate valve growth. However, we also provided evidence that high shear turns off endocardial proliferation programs. It is conceivable that endocardial accommodation for valve growth also includes endocardial cell stretching. In fact, endocardial cells at E14.5 are more densely distributed compared to those post-natal and adult OFT valves (Anstine, 2016), suggesting that as endocardial cells stop proliferating, they are stretched to accommodate valve growth. In addition, expression of endocardial cell-cell adhesions, such as VE-cadherin and PECAM1, are significantly upregulated in post-natal and 4-month mice, compared to E14.5, suggesting that endocardial cells tightly adhere to each other to maintain barrier integrity. Interestingly, increased permeability and infiltration of leukocytes have been associated with CAVD (Anstine, 2016).

Interestingly, we found that snail1 nuclear expression remains high in the endocardial cells on the arterial side of the OFT valves at E13.5 (Figure 3). Snail1 has been shown to directly repress cell-cell adhesions and is required for EMT-driven early valve formation (Kokudo, 2008). Snail1 expression in mesenchymal cells might indicate that mesenchymal cells are maintaining their mesenchymal phenotype post-EMT. Previous cell lineage tracing experiments using valve endocardium specific Nfatc1-enCre line have shown that no more EMT happens at E13.5 despite snail1 expression (Wu, 2011), suggesting that snail1 expression during valve remodeling is not responsible for EMT. It is conceivable that snail1 expression in the endocardial cells on

the arterial side downregulates cell-cell adhesions to facilitate endocardial proliferation during valve elongation. When the magnitude of OSS is high enough to attenuate BMP signaling and snail1 expression, the endocardial cells upregulate their cell-cell adhesions to allow for endocardial cell stretching to accommodate valve growth while maintaining endocardial barrier integrity.

Interestingly, Notch1 signaling is localized in endocardial cells on the inflow side of the valves and is associated with stabilizing membranous β catenin (chapter 2). The side-specificity of Notch activity is conserved in both OFT and AVC valves as well during mid and late gestation development (Figure 4.3 E-H). Furthermore, during late stage development, endocardial cell density in the endocardium is much lower compared to early valve development (Figure 4I), indicating that endocardial cells are more spaced out and their cytoplasm is more stretched. These results identify another way the endocardium can accommodate for valve growth: endocardial stretching. It is conceivable that since Notch1 has been shown to stabilize intercellular junctions (Wang, 2016), possibly by directly associating with β catenin at the membrane level (Kwon 2011; Kim, 2012), it is conceivable that Notch1 signaling on the inflow side stabilizes intercellular junctions to enforce cell stretching. In contrast, nuclear Snail1 restriction to the endocardium on the arterial side is associated with downregulation of intercellular junctions to facilitate cell proliferation. Both endocardial cell proliferation and stretching may therefore contribute to endocardial accommodation for valve growth. Interestingly, others have reported that presence of snail1 is not sufficient to induce EMT in epicardial cells (Casanova, 2013), suggesting that snail1 can

serve other functions. Furthermore, cell lineage tracking experiments have shown that no EMT is present in OFT valves during post-EMT remodeling stages (Wu, 2011). We suspect that endocardial cells during valve remodeling are sensitive to Snail1 dosage, i.e. there is enough Snail1 to destabilize cell junctions to allow cell proliferation, but not enough to induce EMT

Future studies will need to determine the factors that regulate snail1 expression in endocardial cells. While it is possible that OSS upregulates snail1 expression via BMP signaling (Ma, 2005), what inhibits snail1 expression from transforming endocardial cells and inducing their migration into the mesenchymal remains to be worked out. Interestingly, since endocardium in CAVD exhibits some level of permeability, determining whether shear, BMP, and/or snail1 can induce that permeability will be critical to understanding the endocardial injury that precedes calcification.

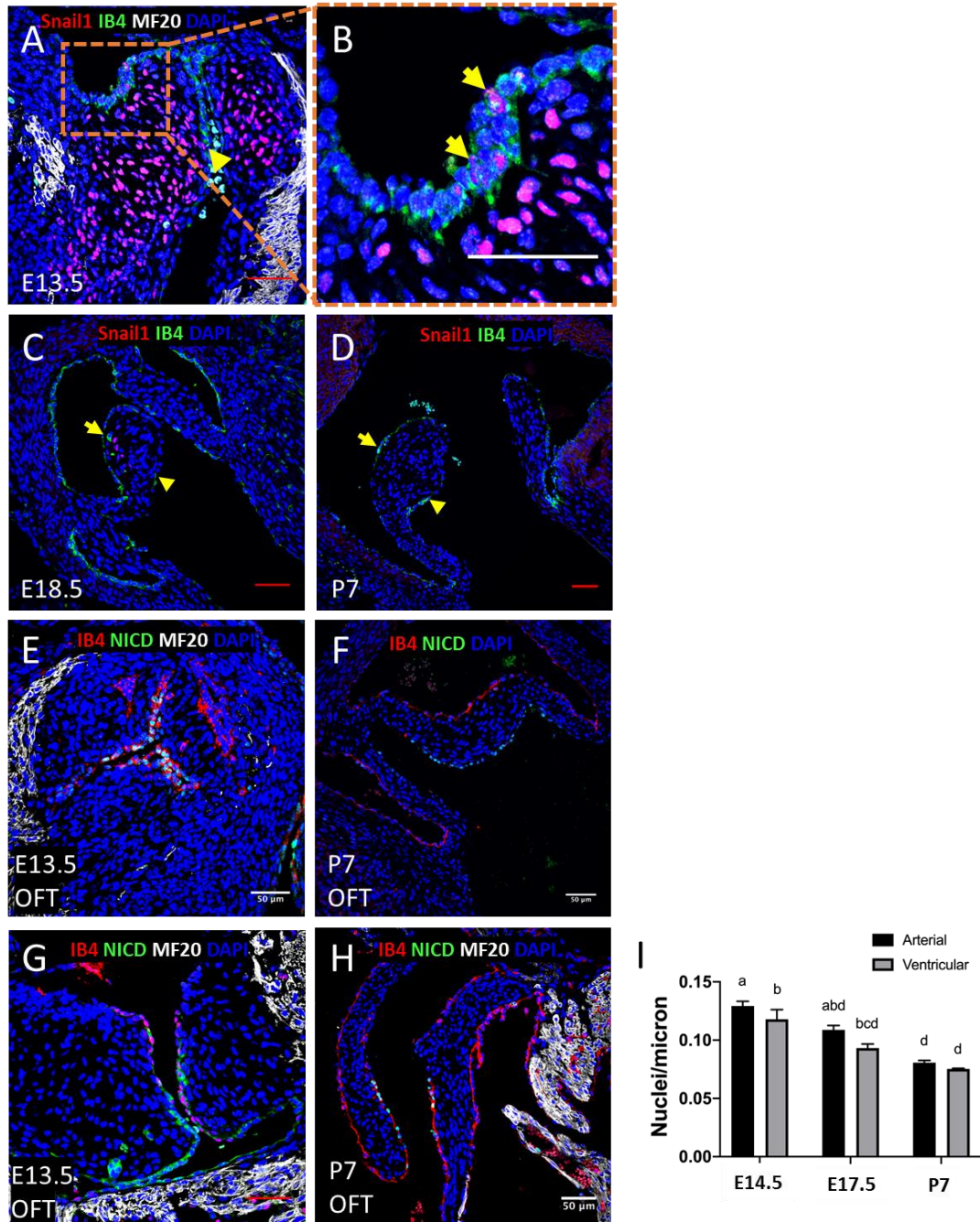


Figure 4.3. Spatiotemporal expression of Snail1 and NICD1 during valve development. Immunostaining of Snail1 in embryos at E13.5 (A and B), E18.5 (C), and P7 (D). Endocardial cells were stained with IB4 (green). Myocardium was stained with MF20 (whit). Yellow arrows indicate positive nuclear Snail1. I, Quantification of endocardial cell density at E14.5, E17.5, and P7. Bars = 50um. Immunostaining of NICD1 (green) in OFT (E, F) and AV valves (G, H) during mid and late gestation. IB4 = red.

4.5. Mechanical regulation of valve compaction in OFT and AV valves via BMP

In chapter 3, we uncovered that laminar shear stress is transduced into endocardial Notch1 signaling that upregulates subendocardial CXCR4 expression, which in turn regulates mesenchymal proliferation, matrix maturation, and valve compaction by modulation of BMP and WNT signaling. We provided evidence for a novel mechanobiological program that relies on CXCR4 signaling and governs tissue morphogenesis during semilunar valve development. Surprisingly, we did not detect any valvular malformations in the mitral or tricuspid valves of CXCR4KO mice, suggesting that CXCR4 signaling is not required for AV valve remodeling processes. Nevertheless, genetics is not the only factor that can influence signaling pathways and valve morphogenesis. In fact, as shown in chapter 2, hemodynamic forces, i.e. shear stress, could induce local BMP signaling that coordinates valve growth and extension.

Interestingly, in the AV valves, we found that compressive stress, induced by hyperosmotic pressure, drives AV cushion growth, while tensile stress, induced by hypoosmotic pressure, induces valve compaction. By increasing the osmolarity of the media, the media causes water efflux and thereby inducing compressive stress on the cell membrane. In contrast, hypoosmotic media causes water influx and turgidity and thereby inducing tensile stress on the cell membrane. Therefore, osmotic stress simulates the tension and compression that the valve experiences during development as a result of ventricular contraction (Thubrikar, 1979). In our culture system, valve organoid compaction was attenuated in response to compressive stress compared to the media (unloaded condition), while tensile stress increased tissue compaction.

Mechanistically, we identified a molecular switch that regulates AV valve growth and maturation. In particular, compressive stress induces BMP-dependent cell proliferation and thereby inducing a growth program. In contrast, tensile stress induces pSer-19-dependent cell contractility as well as matrix compaction and thereby inducing a maturation program. Recall that ablation of CXCR4 also resulted in hypocompaction in the semilunar valves both *in vitro* and *in vivo* and was mediated by BMP signaling. These findings indicate that BMP-induced attenuation of valve compaction is conserved in the OFT and AV valves. As the valves remodel and mature, BMP signaling is modulated by either genetics (e.g. CXCR4) or mechanics (e.g. tensile stretch) to facilitate cell differentiation into myofibroblasts (Goddard, 2017).

Myofibroblastic contractility is thought to facilitate mesenchymal condensation through cellular actomyosin contraction (Dupuis, 2013) that exerts forces on the surrounding matrix (Dikovsky, 2008). In both AV and OFT valves, inhibition of non-muscle myosin II led to hypocompaction of the valve organoids, suggesting that myofibroblastic or mesenchymal cell contractility is required for tissue compaction. On the one hand, compressive stress caused hypocompaction in the AV valves because BMP signaling inhibited phosphorylation of myosin II (Figure 4A-D). On the other hand, in the OFT valves, while BMP signaling modulates α SMA expression, we did not detect any significant elevation in phosphorylation levels of myosin II (Figure 4E and F). These findings suggest that even though BMP modulates tissue compaction in OFT and AV valves, it does so by regulating different parts of the

actomyosin contractile apparatus. It is conceivable that other signaling pathways are required for regulation of mesenchymal cell contractility.

To expand these findings, we determined whether manipulating ventricular contraction *in vivo* would alter BMP signaling. We did this by ligating the left atrioventricular canal (Midgett, 2014). This surgical manipulation essentially decreased ventricular preload, filling, and contractile force according to the Frank-Starling law, which in turn decreased tensile stress on the atrial side of the AV valves or the ventricular side of the OFT valves (Balachandran, 2011). Interestingly, we detected significantly higher %pSMAD15 positive cells in left atrial ligated (LAL) AV valves compared to sham controls (Figure 4H-I). Interestingly, we BMP activated cells are localized on the atrial side of the AV valves, which normally experiences tensile stretch during ventricular filling. These data suggest that tensile stretch is required for valve remodeling. Interestingly, we previously found that chronic cyclic stretch is required for formation of focal adhesion formation, stress fiber alignment, and matrix compaction (Gould, 2016). Future studies need to address the side-specificity of BMP activation in mesenchymal cells *in vivo* and *in vitro* and identify components downstream and upstream of BMP that participate in remodeling.

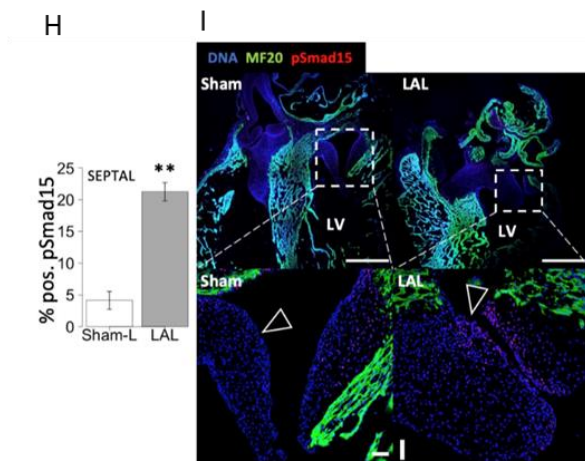
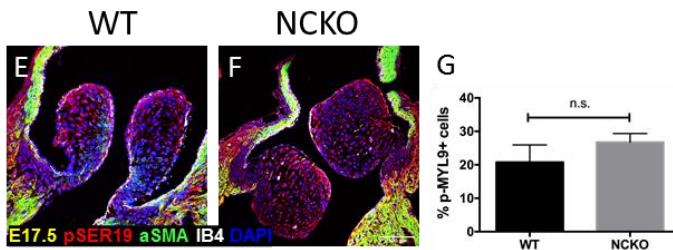
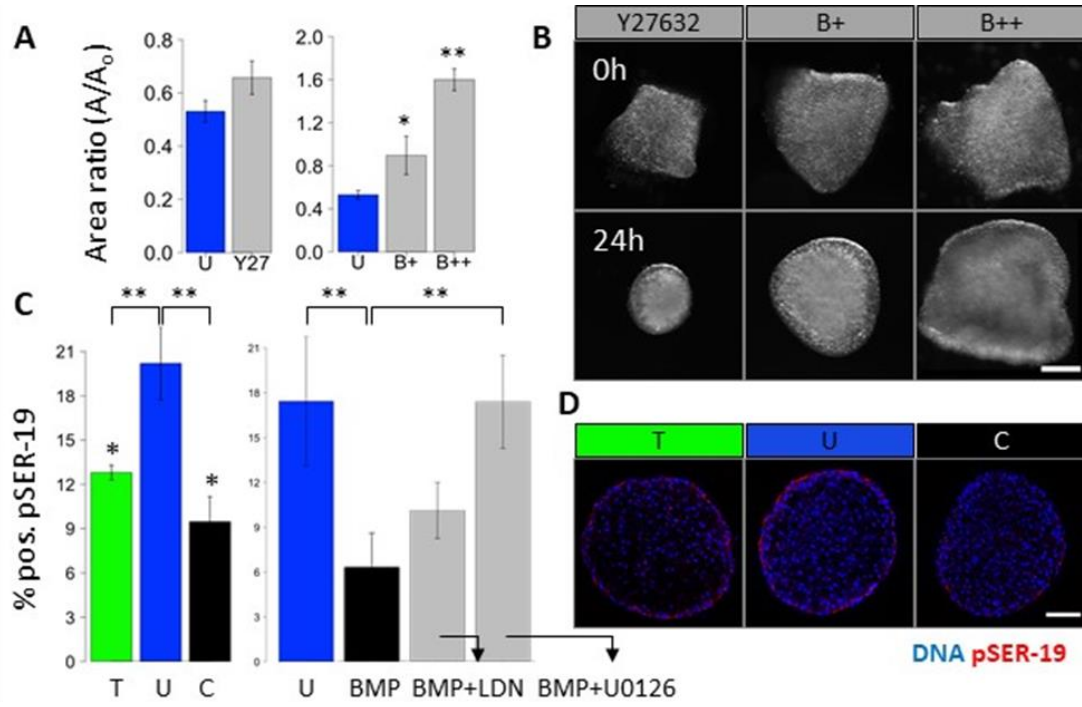


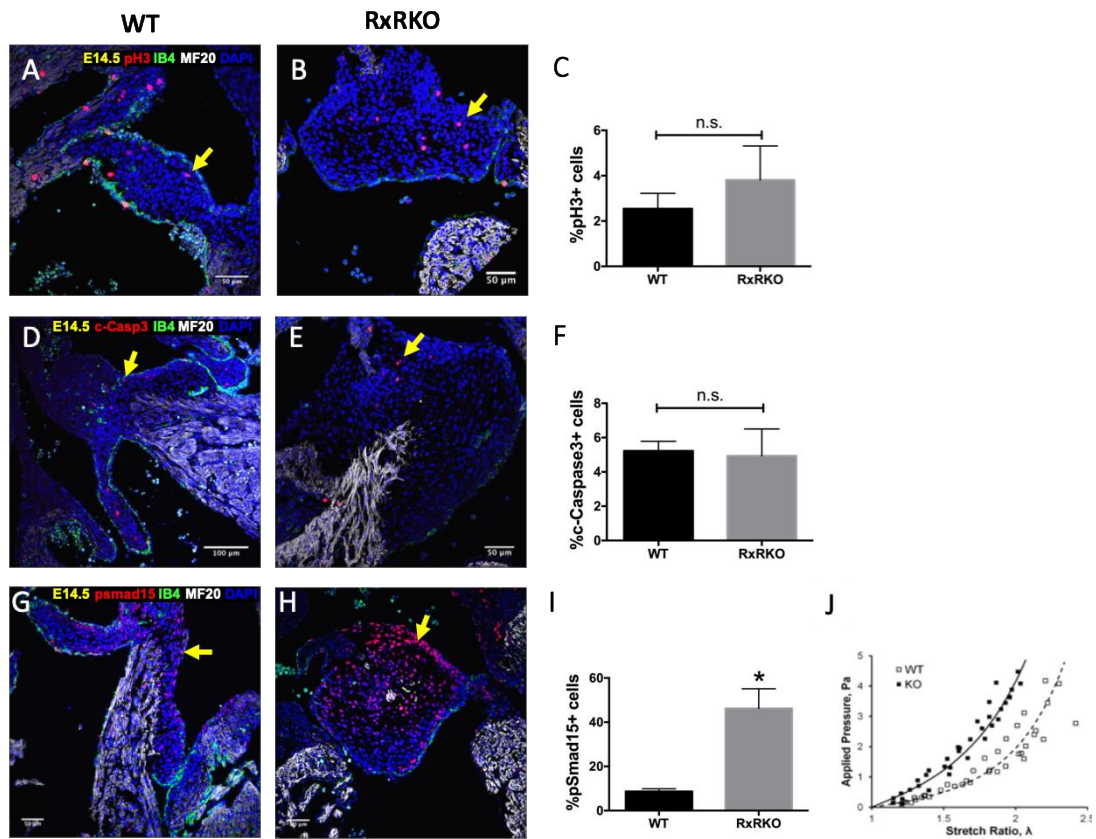
Figure 4.4. Mechanical regulation of BMP signaling during valve development. **A-B**, Quantification and immunostaining of phosphorylated myosin II (pSER19) in unloaded (U) as well as tensile (T) and compressive (C). **C-D**, Quantification of pSER19. BMP indicates BMP treatment at 10ng/mL. LDN indicates BMP inhibition with LDN193189. **E-F**, Immunostaining of pSER19 and α SMA in OFT valves at E17.5 and quantification of pSER19 (**G**). **I**, Immunostaining of pSMAD15, indicative of BMP signaling, in left atrial ligation (LAL) and Sham HH33+ embryos, with quantification (**H**). ** $p < 0.05$ via Student t test. Bars=100um. A-D, H-I were adapted from David Bassen's thesis.

4.6. Retinoic acid signaling regulates AV valve remodeling by modulating BMP

In another investigation focusing on valve remodeling, we found that retinoic acid signaling through retinoic acid receptor alpha (R α Ra), like CXCR4 signaling and tensile stress, modulates BMP activity in AV valves. This is because there was an upregulation of nuclear translocation of pSMAD15 in RxRKO mice compared to WT controls (Figure 5G-I). Ablation of R α Ra led to non-elongated AV valves and increased thickness of the valve primordia, resembling the hypocompaction phenotype seen in CXCR4-ablated or compression-induced valves. Interestingly, we did not detect any difference in proliferation in the RxRKO valves compared to that in WT controls (Figure 5A-C), suggesting that hyperplasia does not explain the hypocompaction. Likewise, there was no significant difference with regard to apoptosis RxRKO and WT AV valves (Figure 5D-F). Taken together, these data suggest that the non-elongated and hypocompacted phenotype seen in RxRKO mice are not due to a change in cell number.

It is likely that BMP signaling in the RxRKO mice like valve organoids under compressive stress affects mesenchymal cell differentiation and myofibroblastic contractility. Interestingly, while BMP is responsible for modulating hyperplasia and matrix remodeling in the OFT valves, BMP signaling is required for matrix remodeling

but not for modulation of proliferation in the AV valves. This suggests that the regulation of cell proliferation in the AV valves might involve other regulatory pathways that compensate and compliment RxR signaling. Future studies will need to examine the expression of α SMA and phosphorylated myosin II and any perturbation to the contractile apparatus. Furthermore, we determined, via pipette aspiration, that RxRKO valve organoids are less stiff compared to WT controls (Figure 5I), suggesting that matrix remodeling might be altered. As for CXCR4KO valves, we detected an upregulation of proteoglycan deposition and downregulation of collagen expression, while inhibition of CXCR4 with AMD3100 decreased tissue stiffness in valve organoids. It is conceivable that higher proteoglycan content could increase hydration of the tissue, thereby decreasing its stiffness. Future studies need to determine the matrix content of th RxRKO valves, e.g. collagen and elastic fibers, and transcription factors downstream of BMP, e.g. Sox9. We also need to determine how BMP signaling can differentially regulate matrix remodeling and compaction in the AV vs. OFT valves.



4.7 Reactivation of CXCR4 signaling during valve stenosis and calcification

In chapter 2, we also found that CXCR4 signaling downregulates deposition of proteoglycans by inhibiting BMP/Sox9 signaling. In addition, CXCR4 also regulates the expression of collagen type I in the subendocardial region. This maturation of the extracellular matrix allows for the valves to cope with the mechanical stress induced

by ventricular contraction and blood flow. Interestingly, we found an upregulation of CXCR4 in the valves of mice homozygous for the low-density lipoprotein receptor (LDLR) mutation and fed a high-fat diet (Sider, 2011) (Figure 6), suggesting that CXCR4 signaling is associated with aortic valve calcification. We and others in the field now believe that developmental pathways become quiescent during homeostasis and reactivated in valve disease. For example, during development EMT gives rise to the valve primordia and ceases around E10.5-E11.5 as mesenchymal cell proliferation drives valve growth.

However, recent cell lineage tracking experiments have shown that EMT precedes valvular osteogenesis (Hjortnaes, 2015). Furthermore, while inflammation is a well-known player in aortic valve calcification, there is now evidence that inflammatory mediators are also important for valve development (reviewed in Mahler, 2011). Our findings suggest that the reactivation of the CXCR4 program may lead to inappropriate collagen deposition (sclerosis) that precedes valvular calcification (Hutson, 2016). Interestingly, microarray data showed that patients with calcific aortic valves upregulate CXCL12 and CXCR4, while downregulating CXCR7 (Prof. Jordan Miller, Mayo Clinic). Recall that while CXCR4 and CXCR7 bind to CXCL12, they can agonize or antagonize each other (Duda, 2011).

Future studies will need to address the contributions of CXCR4 and CXCR7 to valvular sclerosis and calcification. Coculture experiments of CXCR4+ and CXCR7+ valve interstitial cells can reveal the interplay between those chemokine receptors in regulating collagen deposition and inflammatory response during valve disease

pathology. In addition, determining the upstream and downstream components of their pathways will be critical to identifying therapeutic agents for calcific aortic valve disease (CAVD).

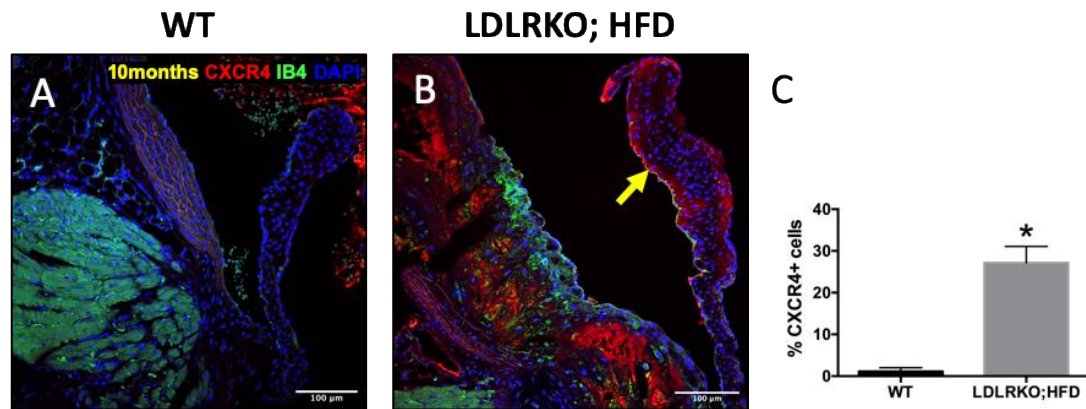


Figure 4.6. Upregulation of CXCR4 in mice prone to developing calcific aortic valve disease. **A-B**, Immunostaining of CXCR4 (red) in WT and LDLR ablated mice on a high-fat diet. Endocardium was stained with IB4 (green). **C**, Quantification of CXCR4 expression based on percentage of CXCR4 positive valve interstitial cells. Data are means +/- SEM. N=3 mice per group. * $p < 0.05$ via Student t test. Bars = 100um.

4.8 Shear stress regulation of the endocardium in development and disease

One of these upstream regulators could be shear stress, whose contributions to the CXCR4-driven developmental program were elaborated in chapter 2. In short, endocardial cells on the ventricular side sense and transduce LSS into Notch1 signaling that in turn turns on the CXCR4 expression in subendocardial cells. In contrast, *in vitro* shear experiments using primary endocardial cells harvested from the ventricular side of the valve indicate that OSS is not sufficient to induce Notch1 signaling. These data suggest that *in vivo*, OSS modulates signaling on the arterial side, possibly to allow for

differential endocardial proliferation and side-specific valve extension (as evident in Chapter 3). Interestingly, while OSS at 20 dyne/cm² inhibits Notch1 signaling, we detected a significant increase in the percentage of endocardial cells positive for nuclear Notch1 under the influence of OSS at 5 dyne/cm² compared to static controls (Figure 7A), suggesting that low magnitude shear stress is sufficient to induce Notch1 signaling. In addition, we detected upregulation downstream target genes of Notch1 signaling, such as HEY2 and JAG1 (Figure 7B and D).

Surprisingly, neither Notch1 or Notch2 transcripts were not upregulated in OSS5, suggesting that OSS5 directly interacts with the pre-existing Notch1 receptors. As development progresses, shear stress increases in magnitude. However, it is difficult to determine the exact magnitude of shear at any given point during development because of the constantly changing hemodynamics of ventricular contraction. Recent computational simulations have shown that shear stress on the arterial side of the OFT valves in adult mice peaks around 21.3dyne/cm² (Yap, 2012). It is conceivable that OSS magnitude was closer to 5dyne/cm² as the ejection volume and velocity are much lower. Since Notch1 signaling is required for EMT (Timmerman, 2004), it is possible that low OSS facilitates EMT through Notch1 signaling early on during valve formation. In fact, we have shown that both low LSS and OSS upregulated EMT genes, such as α SMA, snail, and TGF β , in porcine aortic valve endothelial cells. Furthermore, cell invasion assays showed that low LSS and OSS increased cell migration into the collagen gel, solidifying the association between low magnitude shear stress and EMT initiation (Gretchen, 2014).

A critical question is how does increasing shear magnitude favors homeostasis of endocardial cells on the ventricular side when they exhibit active notch1 signaling both *in vivo* and *in vitro*? Interestingly, recent evidence suggests that while Notch1/Dll4 signaling is active during and required for valvular EMT, it is dispensable during valve remodeling stages. Instead, Notch1 signaling through Jag1 directs post-EMT valve remodeling (MacGrogan, 2016). This study also suggests that Manic-Fringe (a glycosyltransferase) can glycosylate Notch1, thereby favoring Notch1/Dll4 during early valve formation. It would be interesting to determine how low shear stress affects this Notch1 signaling biasing mechanism. In our shear experimental system, we were not able to sufficiently amplify the cDNA samples to examine DLL4 expression in response to different shear conditions. This was likely due to the low concentration of cDNA as we use a one-step protocol to isolate RNA from endocardial patches. It would be beneficial to try adding higher cDNA volume to the reaction mix to increase the concentration of DLL4 transcripts. Another approach is to increase the input of RNA volume to increase the cDNA amount.

Oscillatory shear stress has also been associated with the onset of CAVD as it upregulates BMP-driven inflammation (Ankeny, 2011) and downregulates nitric oxide-dependent protection against calcification (Richards, 2013). It is likely that disturbed hemodynamics could downregulate homeostatic programs and reactivate developmental programs that drive aortic valve pathogenesis. In fact, we recently found that Jag1 expression decreased substantially in diseased background mice (Figure 7E-F), supporting the notion that EMT is linked to CAVD (Hjortnaes, 2015).

During development, LSS drives subendocardial CXCR4 expression via endocardial Notch1 signaling. Defective notch1 signaling has been associated with CAVD (Garg, 2016), while CXCR4 is upregulated. It is possible that Notch1 signaling switches from “protective” Jag1 to EMT-prone DLL4-dependent Notch signaling, which could inappropriately drive expression of CXCR4 and sclerosis. Interestingly, Notch1 signaling via DLL4 has been associated with NFkB activation and recruitment of monocytes in atherosclerosis (Fukuda, 2012). Future studies will need to determine the ligand requirement and interaction with shear stress in driving CAV pathogenesis.

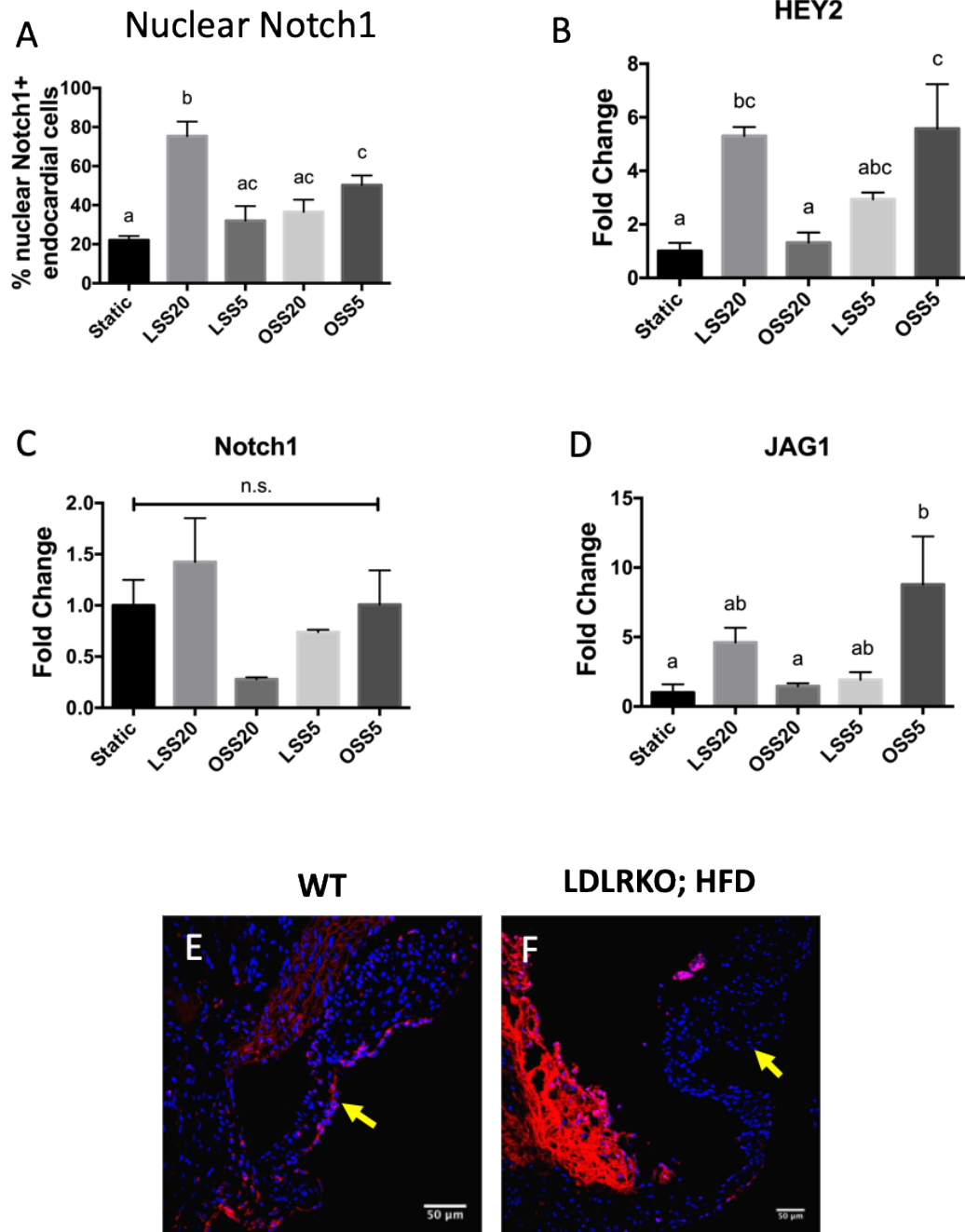


Figure 4.7. Low OSS activates Notch1 signaling in chick endocardial cells.

A, Quantification of Notch1 signaling based on the percentage of nuclear Notch1 positive cells. **B-D**, Expression of HEY2, Notch1, and JAG1, via qRT-PCR. **E-F**, immunostaining of Jag1 in WT vs LDLRKO;HFD mice. Data are means +/- SEM. N=4 endocardial patches per group (A-D). N=3 mice per group (E-F). Bars that do not share any letters are significantly different ($p < 0.05$ via ANOVA with Tukey multiple comparisons correction). Bars = 50um

4.9 References

1. Ankeny, R. F., Thourani, V. H., Weiss, D., Vega, J. D., Taylor, W. R., Nerem, R. M., & Jo, H. (2011). Preferential activation of SMAD1/5/8 on the fibrosa endothelium in calcified human aortic valves-association with low BMP antagonists and SMAD6. *PloS one*, *6*(6).
2. Balachandran, K., Sucusky, P., & Yoganathan, A. P. (2011). Hemodynamics and mechanobiology of aortic valve inflammation and calcification. *International journal of inflammation*, *2011*.
3. Cha, B., Geng, X., Mahamud, M. R., Fu, J., Mukherjee, A., Kim, Y., ... & Dixon, J. B. (2016). Mechanotransduction activates canonical Wnt/ β -catenin signaling to promote lymphatic vascular patterning and the development of lymphatic and lymphovenous valves. *Genes & development*, *30*(12), 1454-1469.
4. Dikovsky, D., Bianco-Peled, H., & Seliktar, D. (2008). Defining the role of matrix compliance and proteolysis in three-dimensional cell spreading and remodeling. *Biophysical journal*, *94*(7), 2914-2925.
5. Duda, D. G., Kozin, S. V., Kirkpatrick, N. D., Xu, L., Fukumura, D., & Jain, R. K. (2011). CXCL12 (SDF1 α)-CXCR4/CXCR7 pathway inhibition: an emerging sensitizer for anticancer therapies?. *Clinical cancer research*, *17*(8), 2074-2080.
6. Dupuis, L. E., Osinska, H., Weinstein, M. B., Hinton, R. B., & Kern, C. B. (2013). Insufficient versican cleavage and Smad2 phosphorylation results in bicuspid

- aortic and pulmonary valves. *Journal of molecular and cellular cardiology*, 60, 50-59.
7. Espinosa, L., Santos, S., Inglés-Esteve, J., Muñoz-Canoves, P., & Bigas, A. (2002). p65-NFκB synergizes with Notch to activate transcription by triggering cytoplasmic translocation of the nuclear receptor corepressor N-CoR. *Journal of Cell Science*, 115(6), 1295-1303.
 8. Fukuda, D., Aikawa, E., Swirski, F. K., Novobrantseva, T. I., Kotlianski, V., Gorgun, C. Z., ... & Aster, J. C. (2012). Notch ligand delta-like 4 blockade attenuates atherosclerosis and metabolic disorders. *Proceedings of the national Academy of Sciences*, 109(27), E1868-E1877.
 9. Garg, V. (2016). Notch signaling in aortic valve development and disease. In *Etiology and Morphogenesis of Congenital Heart Disease* (pp. 371-376). Springer, Tokyo.
 10. Goddard, L. M., Duchemin, A. L., Ramalingan, H., Wu, B., Chen, M., Bamezai, S., ... & Scherrer-Crosbie, M. (2017). Hemodynamic forces sculpt developing heart valves through a KLF2-WNT9B paracrine signaling axis. *Developmental cell*, 43(3), 274-289.
 11. Hjortnaes, J., Shapero, K., Goettsch, C., Hutcheson, J. D., Keegan, J., Kluin, J., ... & Aikawa, E. (2015). Valvular interstitial cells suppress calcification of valvular endothelial cells. *Atherosclerosis*, 242(1), 251-260.
 12. Hoffman, J. I., & Kaplan, S. (2002). The incidence of congenital heart disease. *Journal of the American college of cardiology*, 39(12), 1890-1900.

- Mahler, G. J., & Butcher, J. T. (2011). Inflammatory regulation of valvular remodeling: the good (?), the bad, and the ugly. *International journal of inflammation*, 2011.
13. Hutson, H. N., Marohl, T., Anderson, M., Eliceiri, K., Campagnola, P., & Masters, K. S. (2016). Calcific aortic valve disease is associated with layer-specific alterations in collagen architecture. *PloS one*, 11(9).
14. Inai, K., Norris, R. A., Hoffman, S., Markwald, R. R., & Sugi, Y. (2008). BMP-2 induces cell migration and periostin expression during atrioventricular valvulogenesis. *Developmental biology*, 315(2), 383-396.
15. Jackson, L. F., Qiu, T. H., Sunnarborg, S. W., Chang, A., Zhang, C., Patterson, C., & Lee, D. C. (2003). Defective valvulogenesis in HB-EGF and TACE-null mice is associated with aberrant BMP signaling. *The EMBO journal*, 22(11), 2704-2716.
16. Kokudo, T., Suzuki, Y., Yoshimatsu, Y., Yamazaki, T., Watabe, T., & Miyazono, K. (2008). Snail is required for TGF β -induced endothelial-mesenchymal transition of embryonic stem cell-derived endothelial cells. *Journal of cell science*, 121(20), 3317-3324.
17. Loomes, K. M., Underkoffler, L. A., Morabito, J., Gottlieb, S., Piccoli, D. A., Spinner, N. B., ... & Oakey, R. J. (1999). The expression of Jagged1 in the developing mammalian heart correlates with cardiovascular disease in Alagille syndrome. *Human molecular genetics*, 8(13), 2443-2449.

18. Luo, J., Zhou, H., Wang, F., Xia, X., Sun, Q., Wang, R., & Cheng, B. (2013). The hepatitis B virus X protein downregulates NF- κ B signaling pathways through decreasing the Notch signaling pathway in HBx-transformed L02 cells. *International journal of oncology*, 42(5), 1636-1643.
19. Ma, L., Lu, M. F., Schwartz, R. J., & Martin, J. F. (2005). Bmp2 is essential for cardiac cushion epithelial-mesenchymal transition and myocardial patterning. *Development*, 132(24), 5601-5611.
20. MacGrogan, D., D'Amato, G., Travisano, S., Martinez-Poveda, B., Luxán, G., del Monte-Nieto, G., ... & Gómez, M. J. (2016). Sequential ligand-dependent notch signaling activation regulates valve primordium formation and morphogenesis. *Circulation research*, 118(10), 1480-1497.
21. Mahler, G. J., & Butcher, J. T. (2011). Inflammatory regulation of valvular remodeling: the good (?), the bad, and the ugly. *International journal of inflammation*, 2011.
22. Midgett, M., & Rugonyi, S. (2014). Congenital heart malformations induced by hemodynamic altering surgical interventions. *Frontiers in physiology*, 5, 287.
23. Reller, M. D., Strickland, M. J., Riehle-Colarusso, T., Mahle, W. T., & Correa, A. (2008). Prevalence of congenital heart defects in metropolitan Atlanta, 1998-2005. *The Journal of pediatrics*, 153(6), 807-813.
24. Roger, V. L., Go, A. S., Lloyd-Jones, D. M., Adams, R. J., Berry, J. D., Brown, T. M., ... & Fox, C. S. (2011). Heart disease and stroke statistics—2011 update: a report from the American Heart Association. *Circulation*, 123(4), e18-e209.

25. Shelton, E. L., & Yutzey, K. E. (2008). Twist1 function in endocardial cushion cell proliferation, migration, and differentiation during heart valve development. *Developmental biology*, 317(1), 282-295.
26. Sider, K. L., Blaser, M. C., & Simmons, C. A. (2011). Animal models of calcific aortic valve disease. *International journal of inflammation*, 2011.
27. Sierro, F., Biben, C., Martínez-Muñoz, L., Mellado, M., Ransohoff, R. M., Li, M., ... & Harvey, R. P. (2007). Disrupted cardiac development but normal hematopoiesis in mice deficient in the second CXCL12/SDF-1 receptor, CXCR7. *Proceedings of the National Academy of Sciences*, 104(37), 14759-14764.
28. Stankunas, K., Ma, G. K., Kuhnert, F. J., Kuo, C. J., & Chang, C. P. (2010). VEGF signaling has distinct spatiotemporal roles during heart valve development. *Developmental biology*, 347(2), 325-336.
29. Thubrikar, M., Bosher, L. P., & Nolan, S. P. (1979). The mechanism of opening of the aortic valve. *The Journal of thoracic and cardiovascular surgery*, 77(6), 863-870.
30. Timmerman, L. A., Grego-Bessa, J., Raya, A., Bertrán, E., Pérez-Pomares, J. M., Díez, J., ... & de la Pompa, J. L. (2004). Notch promotes epithelial-mesenchymal transition during cardiac development and oncogenic transformation. *Genes & development*, 18(1), 99-115.
31. Wang, Y., Lu, P., Wu, B., Riascos-Bernal, D. F., Sibinga, N. E., Valenta, T., ... & Zhou, B. (2018). Myocardial β -Catenin-BMP2 signaling promotes

mesenchymal cell proliferation during endocardial cushion formation. *Journal of molecular and cellular cardiology*, 123, 150-158.

32. Wang, Y., Wu, B., Farrar, E., Lui, W., Lu, P., Zhang, D., ... & Xu, D. (2017).

Notch-Tnf signalling is required for development and homeostasis of arterial valves. *European heart journal*, 38(9), 675-686.

33. Yap, C. H., Saikrishnan, N., Tamilselvan, G., & Yoganathan, A. P. (2012).

Experimental measurement of dynamic fluid shear stress on the aortic surface of the aortic valve leaflet. *Biomechanics and modeling in mechanobiology*, 11(1-2), 171-182.

APPENDIX A. TRIPLE-AMPLIFICATION IMMUNOSTAINING FOR FFPE

SECTIONS

DAY 1 (5 HOURS)

Sample collection and processing:

- Fix embryos in freshly made 4%PFA:
 - To make 100ml 4% PFA: in a 200mL beaker, add 4g of PFA to 50mL DI H₂O. Add 1mL of 1M NaOH and stir gently on heating block at 60C until dissolved. Add 10ml of 10X PBS and allow mixture to cool to room temp. Adjust to pH 7.4 with ~1mL 1M HCl, then add more DI H₂O until V = 100mL. Filter through a 0.45um membrane. Use 50mL to fix about 10 embryos and freeze the rest at -20C.
 - For IHC, 1mm/hr at 4C, E9.5 to E11.5 (day4 or younger in chick) embryos = 2 hrs at 4C, E12.5 to E14.5 (day5 to day7) embryos = 4 hrs at 4C, E15.5 to E18.5 to adult hearts (day 8 or older) = overnight at 4C.
 - For cushions: fix for 30 min at 4C.
 - For collagen or matrigel constructs in glass bottom dish: fix for 1hr at RT.
 - For in situ hybridization, fix at 4C overnight.
- For tissue: Rinse in PBS with rocking 3x5min. Wash in PBS 3x20min.
- For explants and constructs: wash in PBS without rocking 3x20min.
- Transfer to 70% ethanol then run them to the vet school ASAP.

De-paraffinization and Rehydration (1 HR)

- Sections can be 5-8um
- Place slides in 50C oven ON on 45angle slide rack.
- **Make sure alcohol solutions are not gross.**
- Xylene, 3 changes for **5 minutes each**
- 100% ethanol, 1 changes, **5 minutes**
- 95% ethanol, 1 change, **3 minutes**
- 70% ethanol, 1 change, **3 minutes**
- Rinse in de-ionized water for **2x5minutes**.

Antigen retrieval (1 HR)

- Microwave in glass box for 10 minutes: 2-3 minutes at Power 10 to boil, then 2x5min at Power 3. Cover with plastic wrap with poked holes. **Make sure the holes are not too close to the edges.**
- **Rapidly cool samples** by pipetting water into the chamber (use 10mL serological).
- Incubate in tap water 3x4min **on rocker**.
- Draw a hydrophobic circle around samples using hydrophobic pen. Make sure the slides are as dry as possible without drying the samples (dabbing motion with aspirator). If hydrophobic pen comes in contact with water, it will dissolve and smear, creating a membrane on top of your samples. If this happens, use really fine forceps to get rid of the membrane.

- Wash in TBS 1x5min
- Make H₂O₂ solution in a separate container.

Blocking endogenous peroxidase (optional)

- Incubate in 1.2% H₂O₂ in 100% methanol for 40 minutes @RT to inhibit endogenous peroxidase
 - o Dilute 2ml of 30% H₂O₂ in 43ml of 100% methanol.
- **While waiting, make block buffer** as Tween and BSA are a bitch to dissolve.
 - o Make for 40ul per section.
 - o 3% BSA, 20mM MgCl₂, 0.3% Tween20, 5% donkey serum, 0.3M glycine, 0.001% Avidin (-20C, add separately, and only if avidin/biotin blocking is necessary) in TBS for 1hr at RT.
 - o to make 8ml: 0.24g of BSA, 160ul of 1M MgCl₂, 24ul of Tween20, 400ul of donkey serum, 0.18g glycine, 1:1000 from 1% w/v avidin stock (add separately) in 7.4ml TBS.
 - o 1M MgCl₂: 0.38g in 4mL of TBS.
- When 40' is up. Rinse once with DI water, then transfer to a new container containing TBS.
- Wash in TBS 2x5min

Permeabilization

- Wash in 0.3% Triton in TBS 1x20min
 - o For 0.3% Triton, dilute 1.5ml of TritonX-100 to 500ml of TBS.
 - o Keep bottle in the dark. Keep cap clean and bottle capped.

- Rinse 2x in DI water. Remember to fill water up to the mouth to get rid of as much triton as possible.
- Wash in TBS 1x3min

Block (1 HR)

- Apply 39ul/section
- Do not block more than 2hr at RT. Over-blocking decreases staining intensity.
- **If avidin is in block buffer**, wash 1x5min.

Primary antibody application (ON)

1. Prepare dilutions in block buffer.
 - Make for 40ul/section
 - If avidin is in block buffer, Primary Ab Block buffer **MUST** include 0.001% Biotin.
 - Dilute 1:100 from 0.1% stock (-20C)
2. Aspirate block buffer.
3. Apply 39ul/section primary antibody
4. Incubate overnight (at least 16-20hr) at 4oC

DAY 2 (5 HOURS)

Secondary antibody application (5 HOURS)

1. Make 5% BSA: 0.2g of BSA to 4mL TBS.
2. Wash in TBS 2x5min
3. Wash in 0.3% Triton in TBS 2x5min

4. Rinse in 1x in DI water. Then put TBS back into containers.
5. Prepare 2o ab solution:
 - a. Biotinylated anti-X, 15ug/ml (4C box, 1:100) in 5% BSA in TBS
 - i. or HRP-conjugated anti-X, 15ug/m (4C box, 1:100) | in 5% BSA
in TBS
 - b. Other 2o Ab at 1:100 dilution (15-20ug/ml, 1:100, 4C box) in 5% BSA in
TBS
6. Incubate at RT for 1hr.
 - a. **Prepare Avidin/biotin HRP** during this incubation
 - i. 1 drop of reagent A and B to 5ml TBS.
 - ii. Blitz for 2x1second
 - iii. Allow to this mixture to sit for 30 minutes at RT on rocker.
7. Wash in TBS 3x5min
8. Wash in 0.3% Triton in TBS 1x10min
9. Rinse in DI water. Put TBS back in.
10. Incubate sections in
 - a. **Avidin/biotin-HRP** at RT for 1hr.
 - b. OR **fluorescent Streptavidin** (if secondary is Biotinylated) at 10ug/ml
or 1:200 in TBS, at RT, 1hr.
 - i. Need to include DAPI (1:2000)
 - c. OR proceed to TSA step if secondary is HRP-conjugated.
11. Wash in TBS 2x5min

12. Wash in 0.3% Triton in TBS 1x10min

- a. Prepare TSA solution now. Make for **25ul/section**.
- b. Dilute TSA Stock solution 1:50 in Amplification Diluent
 - i. Use brightest Fluorophore for least abundant protein.
(cy5>cy3>FITC)
 - ii. Use 1:100 dilution for 3.5 min for less amplification.
- c. Incubate sections at RT for **3 mins**.

13. Rinse in DI water. Put TBS back in.

14. Apply TSA solution. 24ul/section. Start timer after applying on first section. Do about 15 sections at a time.

15. Wash in TBS 3x5min.

- a. Prepare IB4+DAPI in TBS. Make for 40ul/section.
- b. Dilute DAPI (-20C box) FIRST at 1:2000.
- c. IB4 (4C box) at 1:100

16. Incubate at RT for 1 hr.

17. Wash in TBS 3x5min

Mounting

1. Melt wax
2. Apply mounting medium. Doesn't need much. Just slightly dab droplet on section.
3. Apply coverslips. Prevent bubble formation by applying coverslip gently.
4. MUST let slides cure for at least 24 hours. Signal is good for about 2 weeks.

*To stain for another protein whose Ab was raised in the same species as those Abs used in the first round, strip the first antibody complex using 25mM Glycine-HCl 10%SDS pH2, and proceed to **washing + permeabilization**. No need to block endogenous peroxidase.*

Stripping procedure:

1. To make 25mM Glycine-HCl 10%SDS pH2 solution:
 - a. Mix 0.94g glycine in 25ml 20%SDS
 - b. Add distilled water to 500ml
 - c. Adjust pH to 2 with HCl
2. Heat buffer to 50C
3. Incubate slides on shaker in 50C buffer for 30 minutes.
4. Rinse quickly with water.
5. Wash in PBS 3x10min.

Oil immersion 1.51 RI

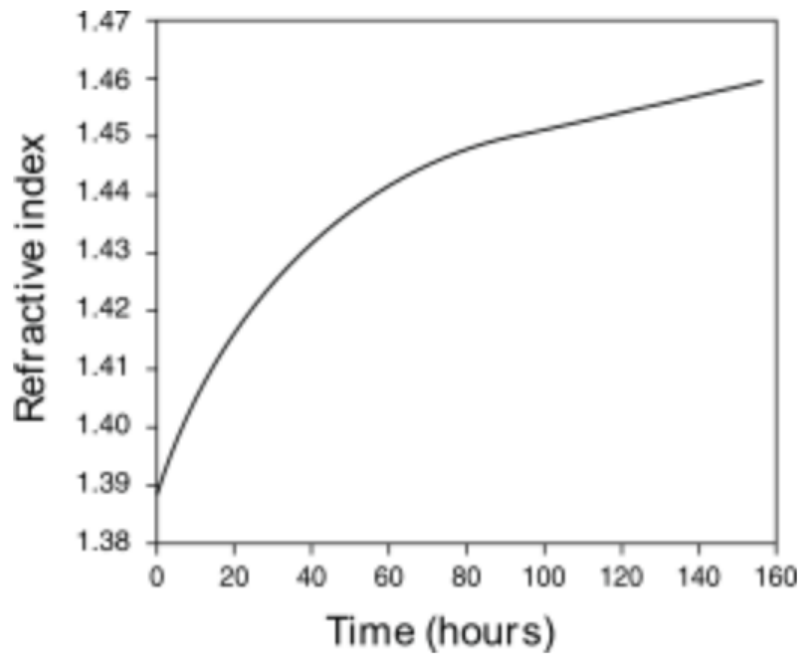
Glass 1.52 RI

Prolong gold 24hr 1.42 RI

Prolong gold 3D 1.44 RI

Prolong gold 7D 1.47 RI

Figure 2 Increase in the refractive index of ProLong[®] Gold process.



APPENDIX B. IMMUNOSTAINING FOR WHOLEMOUNT TISSUES

Wholemount Staining (E18.5 hearts)

1. Transfer samples to 4-well plate
2. Permeabilize with methanol/DMSO 4:1 for 30 minutes at 4C.
 - a. Make 1% triton in TBST
3. Bleach samples with methanol/DMSO/30% H₂O₂ 4:1:1 for 1hour at RT.
 - a. Make block buffer (10% donkey serum, 2% BSA in 1%triton TBS)
4. Wash with 1% triton in TBS 4x5min
5. Block for 1hr at RT.
 - a. Prepare primary solutions in block buffer
6. Incubate in primary Ab overnight at 4C on rocker.
 - a. Can draw a hydrophobic circle in well and place samples there to conserve Ab
7. Wash with 1%triton in TBS 4x15min
 - a. Prepare secondary solutions (1:500 in TBST)
8. Incubate in secondary Ab overnight at 4C on rocker.
9. Wash with 1%triton in TBS 4x15min
10. Incubate samples in methanol 2x10min
11. Transfer to a glass-bottom plate.
12. Withdraw as much methanol as possible. Don't let samples dried out.

13. Apply clearing solution (VISIKOL) under the hood. And make sure to orient appropriately.
14. Let cure overnight.
15. Image
16. Store at 4C after 24hr.

Wholemout staining (E14.5 hearts or younger embryos)

1. Wash 1x10min with 1% triton in 4 or 6 well plates on rocker
2. If needed, block endogenous peroxidase with 3% H₂O₂ in TBS for 40 minutes.
3. Wash 3x10min with 1% triton on orbitor
4. Block with Ducbloc for 1hr at RT on shaker
5. Incubate with primary Ab for 18-24 hrs at 4C.
6. Wash 4x10min with 1% triton on orbitor
7. Incubate with secondary Ab for 1hr at RT on shaker
8. Wash 4x10 min with 1% triton on orbitor
9. Amplify with TSA at 1:100 for 7 min in 0.015% H₂O₂ diluted in TSA diluent on shaker
10. Wash 3x10min with TBS
11. 10 minutes in Methanol
12. Clear with Solution 1 and/or 2 (VISIKOL)

APPENDIX C. PROGENITOR CELL AND TISSUE CULTURE

The day before:

1. Prepare sterile EBSS
 - a. Add 8.7g of EBSS (TS1009-20L, HiMEDIA) to 800mL of 18MO water
 - b. Add 2.2g sodium bicarbonate
 - c. Bring pH to 7
 - d. Bring solution to 900mL
 - e. Cover and leave 4C overnight
 - f. pH again to make sure it's at pH at 4C
 - g. Bring solution to 1000mL
 - h. Sterilize the solution through 0.2um filter
2. Prepare sterile M199 culture medium
 - a. Add 1 package of M199 to 700mL 18MO water
 - b. Add 2.2g of Sodium Bicarbonate
 - c. Add 10mL (1%) of Pen-Strep
 - d. Adjust the pH to 7
 - e. Bring solution to 990mL
 - f. Sterilize the solution through 0.2um filter
 - g. Right before culturing:
 - i. Add Insulin-Transferrin-Selenium-G supplement at 1:100
 - ii. Add sterile chicken serum at 1:100
3. Prepare sterile M199 4X culture medium

- a. Add 1 package of M199 to 200mL 18MO water
 - b. Add 0.55g of Sodium Bicarbonate
 - c. Adjust the pH to 7.2
 - d. Add 2.5mL of Pen-Strep
 - e. Bring solution to 250mL
 - f. Sterilize the solution through 0.2um filter
 - g. Right before culturing:
 - i. Add 250ul sterile 100X Insulin-Transferrin-Selenium-G supplement
 - ii. Add 2.5mL (1%) sterile chicken serum
4. Autoclave tools

The day of isolation:

- 1. Prep the hood:
 - a. Pipet EBSS into two 50ml conical tubes. Place one on ice, the other one in fridge
 - b. 1 petri dish for collecting eggs.
 - c. P200 pipetor + wide bore tips
 - d. 1 4-well plate for collecting cushions. Label accordingly. Fill with EBSS.
 - e. 1 petri dish for OFT isolation. Shallow = isolation; deep = wash + heart
- 2. Isolate OFT cushions in EBSS, transfer to a small petri dish, and place on ice.
- 3. Place the cushions into one well of 4-well plate with media (4C). Agitate.

4. Prepare medium conditions in the other wells of the 4-well plate.
5. Place the cushions into the conditioned media.
6. Create droplets.
7. Stop culturing at 24hr

Isolation of mesenchymal cells:

8. Place in the incubator for
9. Centrifuge at 15xg for 3 minutes
10. Remove EBSS
11. Add 1ml of 0.25% Trypsin-EDTA
12. Incubate in warm water bath at 37C
13. Add 100ul of chicken serum to quench trypsin.
14. Centrifuge at 160 xg for 5 minutes
15. Remove supernatant
16. Resuspend in 2mL of M199 medium and mix by pipetting.
 - a. Keep tube in 37C
 - b. Count cells via 10ul
17. Plate cells at 250K cells/mL.

Resuspension in gel solution:

18. Spin cells at 160 xg for 5 minutes.
19. Remove supernatant

20. Resuspend in gel solution in this order: 3X M199, water, chicken serum, collagen, and 0.1M NaOH.

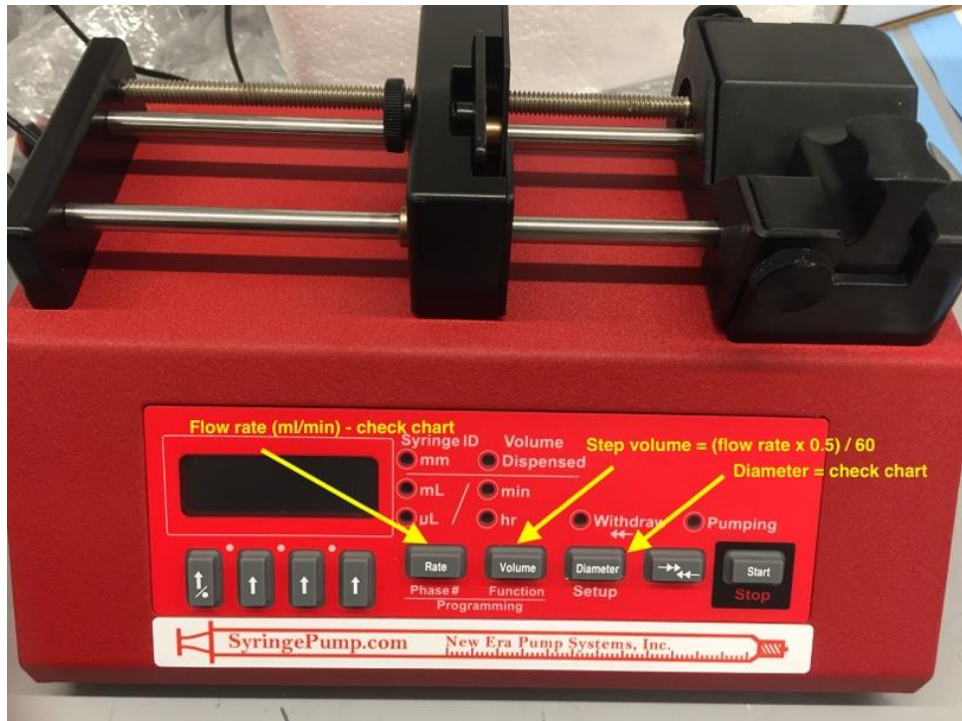
a. 400k cells/mL

21. Mix by gentle pipetting.

APPENDIX D. SHEAR STRESS EXPERIMENT WORKFLOW

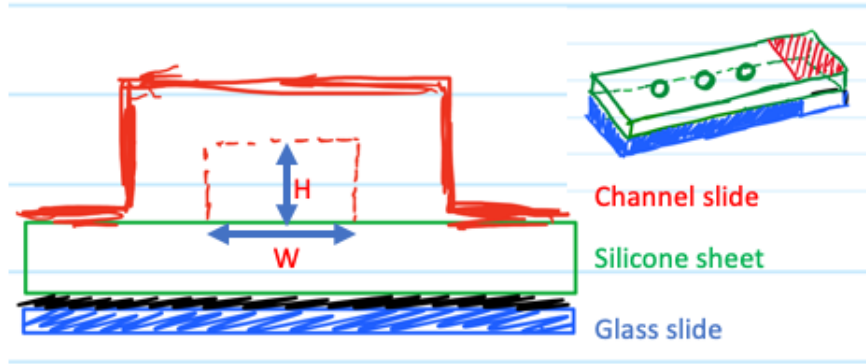
Day 1:

1. Assemble (glass slide + tape + silicone sheet) = bottom
2. Assemble (tubing + micro slide) = top
3. Autoclave top and bottom components + forceps + 1 sterile container.
 - a. If running steady shear, also autoclave: tubing+luerlocks, media bottle, pulse dampener.
4. For the adaptors, rinse in 70% ethanol for 1hr in sterile container
 - a. Rinse in sterile 18MO water for 3x10min
 - b. Air dry under UV in petri dish in BSL2 overnight.
5. Equilibrate top and bottom pieces at 37C
6. Set up the pump: diameter of syringe, Flow rate (ml/min) and step volume (ml).
 - a. Set flow rate and step volume for both Ph:02 and Ph:03.
 - b. Change phases by pressing and holding Rate.
7. Check if there's enough EBSS and that the pH still 7 every week
 - a. To do this, aliquot 35ml under sterile conditions into a conical tube
 - b. PH this, if its not 7 that we need to repH and filter the stock solution.



12.7 Syringe Diameters and Rate Limits

Syringe Manufacturer (all names TM)	Syringe (mL)	Inside Diameter (mm)	Maximum Rate (mL/hr)	Minimum Rate (µL/hr)	Maximum Rate (mL/min)
B-D	1	4.699	53.07	0.73	0.884
	3	8.585	177.1	2.434	2.952
	5	11.99	345.5	4.748	5.758
	10	14.43	500.4	6.876	8.341
	20	19.05	872.2	11.99	14.53
	30	21.59	1120	15.4	18.67
	60	26.59	1699	23.35	28.32



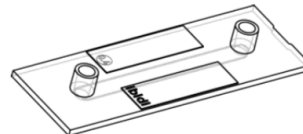
Shear Stress table for μ -Slide I^{0.8} Luer for viscosity $\eta=0.0072$ dyn·s/cm²:

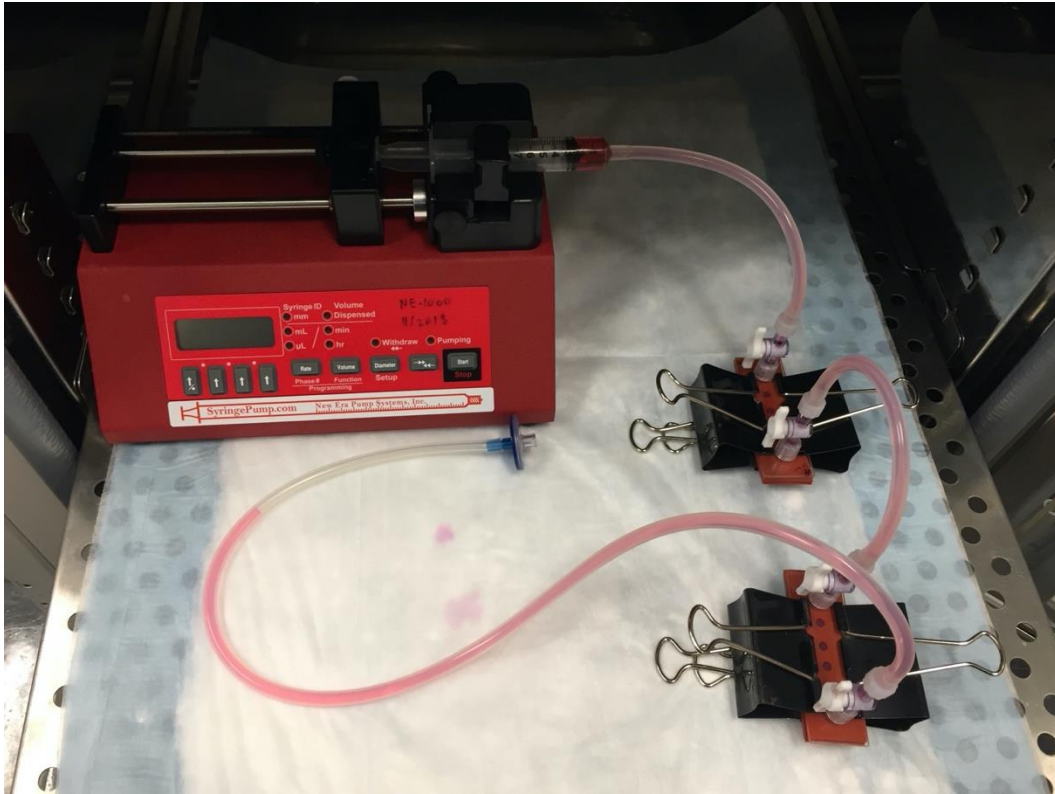
τ [dyn/cm ²]	Φ [ml/min]	τ [dyn/cm ²]	Φ [ml/min]	τ [dyn/cm ²]	Φ [ml/min]
0.1	0.40	3.5	14.01	25	100.06
0.2	0.80	4	16.01	30	120.08
0.3	1.20	4.5	18.01	35	140.09
0.4	1.60	5	20.01	40	160.10
0.5	2.00	5.5	22.01	45	180.12
0.6	2.40	6	24.02	50	200.13
0.7	2.80	7	28.02	55	220.14
0.8	3.20	8	32.02	60	240.15
0.9	3.60	9	36.02	65	260.17
1	4.00	10	40.03	70	280.18
1.2	4.80	11	44.03	75	300.19
1.4	5.60	12	48.03	80	320.20
1.6	6.40	13	52.03	85	340.22
1.8	7.20	14	56.04	90	360.23
2	8.01	15	60.04	95	380.24
2.2	8.81	16	64.04	100	400.26
2.4	9.61	18	72.05	105	420.27
2.6	10.41	20	80.05	110	440.28
2.8	11.21	22	88.06	115	460.29
3	12.01	24	96.06	120	480.31

Shear Stress table for μ -Slide I^{0.4} Luer for viscosity $\eta=0.0072$ dyn·s/cm²:

τ [dyn/cm ²]	Φ [ml/min]	τ [dyn/cm ²]	Φ [ml/min]	τ [dyn/cm ²]	Φ [ml/min]
0.1	0.11	3.5	3.69	25	26.38
0.2	0.21	4	4.22	30	31.66
0.3	0.32	4.5	4.75	35	36.94
0.4	0.42	5	5.28	40	42.22
0.5	0.53	5.5	5.80	45	47.49
0.6	0.63	6	6.33	50	52.77
0.7	0.74	7	7.39	55	58.05
0.8	0.84	8	8.44	60	63.32
0.9	0.95	9	9.50	65	68.60
1	1.06	10	10.55	70	73.88
1.2	1.27	11	11.61	75	79.15
1.4	1.48	12	12.66	80	84.43
1.6	1.69	13	13.72	85	89.71
1.8	1.90	14	14.78	90	94.98
2	2.11	15	15.83	95	100.26
2.2	2.32	16	16.89	100	105.54
2.4	2.53	18	19.00	105	110.82
2.6	2.74	20	21.11	110	116.09
2.8	2.96	22	23.22	115	121.37
3	3.17	24	25.33	120	126.65

$$\tau \left[\frac{\text{dyn}}{\text{cm}^2} \right] = \eta \left[\frac{\text{dyn} \cdot \text{s}}{\text{cm}^2} \right] \cdot 131.6 \cdot \Phi \left[\frac{\text{ml}}{\text{min}} \right]$$





Day 2:

1. Set up hood for dissection
2. Make collagen gel (2mg/ml)
 - a. Let solidfy for 1hr at 37C
3. Isolation (4 embryos/8 OFTs max per hour) in EBSS
4. Transfer OFT onto silicone sheet in a droplet.
5. Transfer OFT into media bubble on gel
 - a. Orient OFT

- b. Withdraw as much EBSS as possible
6. Incubate at 37C for 6 hours.
 - a. Make media: 10-15ml for OSS; 70ml for LSS; 5ml extra.
 - b. Equilibrate media at 37C in conical tube with filter cap.
7. Assemble flow circuit and equilibrate in incubator.
8. After 4hrs, peel off the cushions by going in from the side with forceps.
9. Place the TOP piece on top; connect the adaptors.
10. Secure clamps on the reactor.
11. Grab a filter cap.
12. Grab pump and place on metal tray.
13. Attach filter cap to tubing and tubing to syringe
14. Secure syringe on the pump.
15. Slowly pump media through channel via the pump
16. Move the tray to incubator.
17. Plug the pump in.

NOTE: For steady flow experiments, the tubing in contact with the rotor needs to be

[Masterflex® L/S Pharmed BPT Tubing, Cole Parmer - Size 16; L/S® Pump Flow Range:](#)

[0.08 to 480 mL/min. \(600 rpm\), 0.016 to 80 mL/min. \(100 rpm\) 06508-16](#) Catalog

Number 76049-354

APPENDIX E. QRT-PCR FOR ENDOCARDIAL PATCHES

Cells-to-CT RNA Isolation

1. Use BSL2 hood
2. Thaw lysis buffer at 37C and stop solution and DNase at room temp.
3. Acquire ice bucket: flick+place stop solution, DNase, and EBSS on ice + lysis buffer at RT
4. Get 2 petri dishes
5. Get 1.5ml tubes + label them.
6. Mix lysis buffer at 1:100
 - a. Lysis solution: $49.5\text{ul} \times 8 = 396 \text{ ul}$
 - b. DNase I: $0.5\text{ul} \times 8 = 4 \text{ ul}$
 - c. Mix with pipette
7. Prepare pipettors: 5ul, 35ul, 50ul, and 100ul (use p1000).
8. Disassemble bioreactors and place in petri dishes.
9. Aspirate media
10. Place a bubble of 100ul EBSS on samples
11. Incubate for 30s
12. Aspirate EBSS
13. Pipet 48ul of lysis buffer+Dnase to each gel.
14. Mix up and down 6x
 - a. Start the timer for 6 min after the first sample.
15. Incubate at RT
16. Collect 40ul into eppendorf tubes.

17. Store at -80C for 5 months max or 2 hours on ice.

cDNA synthesis

1. Program the thermal cycler as below:

Table 3. Thermal Cycler Settings for RT

	Stage	Reps	Temp	Time
Reverse transcription (hold)	1	1	37°C	60 min
RT inactivation (hold)	2	1	95°C	5 min
Hold	3	1	4°C	indefinite

2. Thaw primers and master mix components: +1rxn extra

Component	Each rxn	96 rxns	384 rxns
2X RT Buffer	25 µL	2.64 mL	10.56 mL
20X RT Enzyme Mix*	2.5 µL	264 µL	1.056 mL
Nuclease-free Water	12.5 µL	1.32 mL	5.28 mL
final volume RT master mix	40 µL	4.22 mL	16.9 mL

* For the minus-RT control, use Nuclease-free Water in place of 20X RT Enzyme Mix.

3. Mix thoroughly, centrifuge, and place master mix on ice
4. Distribute master mix to PCR tubes
5. Add 10ul of cDNA and mix up and down 10 times
6. Run the RT thermal cycler program
7. Products can be stored at -20C

Real time qPCR

1. Primer prep:

a. Stock = check information sheet to make 100uM

b. Working = dilute 1:10 from stock (to make 10um)

2. Prepare reaction mix: sample # = samples + 1 extra

	HK*sample#*	Volum	Gene	Volum	Gene	Volum	Gene	Volum
	2	e	1	e	2	e	3	e
H2	4ul		4ul		4ul		4ul	
O								
M	10ul		10ul		10ul		10ul	
M								
Pf	1ul		1ul		1ul		1ul	
Pr	1ul		1ul		1ul		1ul	

3. Distribute 16ul of reaction mix to PCR wells

	Sample	2	3	4	5	6	7	8	9	10	11	12
Gene A												
A												
Gene B												
B												
Gene C												
C												

Housekeeping													
Housekeeping													

4. Add 4ul of cDNA to wells
5. Open Protocol for Tm 58
6. Run

APPENDIX F. FIJI IMAGE ANALYSIS CODE DEVELOPMENT

Written by Charles Dai

Motivation

The motivation for creating scripts to analyze images of the endocardial patches came from the large number of cells that had to be counted. There are thousands of cells in some images, so counting by hand would have been time-consuming and prone to error. In addition, due to the variation in the appearance of stained cells under the microscope, it was difficult to determine qualitative criteria for what constituted a positive signal. The scripts were written with the desire to minimize human error and subjectivity. They were written using Fiji's custom Jython language.

Methods

The first script written calculated the percentage of positive cells by counting the total number of cells and the number of cells with a positive protein signal. From an image, it extracted the channels of the protein of interest and the nuclear channel. Because the nuclear signal was consistent over all images, the nuclear channel was

processed by simply auto-thresholding the image (Fiji's Make Binary method), then applying a watershed transformation to accentuate the boundaries of the cells. Total cells were counted using the Analyze Particles function in Fiji. A certain minimum cell size was required in order to filter out small artifacts from this analysis.

The protein channel was processed by thresholding the image using a pre-determined brightness threshold. For each cell counted in the nuclear channel, the same region in the protein channel was analyzed. If the total signal in the region of the cell was above a percentage threshold, it was counted as a positive cell. The final percentage of positive cells was calculated by dividing the number of positive cells by the total number of cells.

One of the challenges when working with the script was determining the appropriate brightness threshold for the protein channel. We were able to deal with this challenge in several ways. Noting that most of the proteins of interests were nuclear proteins, the primary brightness threshold was determined by minimizing false positive signal, protein signal outside of cell nuclear regions. The same primary threshold was used for each image in a single experiment. The analysis was also repeated with several thresholds around the primary threshold. For each image, the value closest to the median values of all calculated values were recorded. In this way, the analysis was more resistant to noise and small photometric shifts.

Because endocardial cells can transition to mesenchymal cells in the bioreactor system, we desired a method to be able to differentiate the two cell types when counting them. Therefore, a second script was written that only counted endocardial

cells. Because there is not a well-known nuclear, chick endocardial marker, we used bright b-catenin signaling as a marker for endocardial cells. Noting that endocardial cells tend to have a bright ring of b-catenin around them, we designed the script to count cells that were enclosed in a bright ring of b-catenin.

The b-catenin channel was processed by determining an appropriate threshold and thresholding the image. The holes were filled (using the Fill Holes function). Then, only nuclear particles that were completely within the filled b-catenin area were counted as endocardial cells. From the counted endocardial cells, cells positive for protein signal were counted. The threshold for b-catenin signaling was determined by minimizing non-endocardial signaling and was held constant for all images in the same experiment.

Source Code

The source code for the second script, which counts endocardial cells, is reproduced below.

```
from __future__ import print_function

#-----UI To Grab Parameters-----
#@ File (label = "Input directory", style =
"directory") src_file
#@ String (label = "File extension", value=".czi") ext
#@ String (label = "File name contains", value = "")
contain_string
#@ String (label = "Protein Channel", choices={"1", "2",
"3", "4", "None"}, style="radioButtonHorizontal", value =
"1") pch
#@ String (label = "Nuclear Channel", choices={"1", "2",
"3", "4"}, style="radioButtonHorizontal", value = "2")
nch
#@ String (label = "B-catenin Channel", choices={"1",
"2", "3", "4"}, style="radioButtonHorizontal", value =
"3") bch
```

```

#@ Integer (label = "Protein of Interest Threshold",
value = 70) P_THRESHOLD
#@ Integer (label = "Protein Area Threshold", value = 50)
P_PERCENT
#@ Integer (label = "Minimum Cell Size (um^2)", value =
30) MIN_CELL_SIZE
#@ Integer (label = "B-Catenin Threshold", value = 50)
B_THRESHOLD
#@ Boolean (label = "Show Image", value = False)
show_image

import os, sys
from ij import IJ, ImagePlus, Prefs, ImageStack
from ij.plugin import ChannelSplitter as CS, ZProjector
as ZP, RGBStackMerge as SM
from ij.plugin.filter import ParticleAnalyzer as PA
from ij.plugin.filter import Analyzer
from ij.plugin.frame import RoiManager as RM
from ij.measure import ResultsTable as RT, Measurements
as MS
from loci.plugins import BF

#-----Run Through Directory-----
def run():
    src_dir = src_file.getAbsolutePath()
    for root, directories, file_names in
os.walk(src_dir):
        file_names.sort()
        for file_name in file_names:
            # Check for file extension
            if not file_name.endswith(ext):
                continue
            # Check for file name pattern
            if contain_string not in file_name:
                continue
            process(src_dir, root, file_name,
show_image)

#-----Process Single File
def process(src_dir, current_dir, file_name, show_image):
    # Opening the image
    print(file_name, end = '\t')

    imp = BF.openImagePlus(os.path.join(current_dir,
file_name))[0]
    #if imp is None:

```

```

#    imp = IJ.openImage(os.path.join(currentDir,
fileName))

#-----Find Channel Nubmers-----
plchannel = int(pch) - 1
nchannel = int(nch) - 1
bchannel = int(bch) - 1

#-----Split Channels-----
channels = CS.split(imp)
protein_imp = channels[plchannel].duplicate()
nuclear_imp = channels[nchannel].duplicate()
bcat_imp = channels[bchannel].duplicate()

#-----Pre-process Nuclear Channel-----
Prefs.blackBackground = True;
IJ.run(nuclear_imp, "Make Binary", "method=Default
background=Default calculate black")
IJ.run(nuclear_imp, "Fill Holes", "stack")
IJ.run(nuclear_imp, "Watershed", "stack")
#nuclear_imp.show()

#-----Pre-process B-catenin Channel-----
IJ.setRawThreshold(bcat_imp, B_THRESHOLD, 255, None)
IJ.run(bcat_imp, "Convert to Mask", "method=Default
background=Dark black")
IJ.run(bcat_imp, "Fill Holes", "stack")
#bcat_imp.show()

#-----Pre-process Protein Channel-----
IJ.setRawThreshold(protein_imp, P_THRESHOLD, 255,
None)
IJ.run(protein_imp, "Convert to Mask",
"method=Default background=Dark black")
IJ.run(protein_imp, "Fill Holes", "stack")

# Create Output Stacks
inside_neg_stack = ImageStack()
inside_pos_stack = ImageStack()

#-----Convert to Stacks-----
nuclear_stack = nuclear_imp.getStack()
bcat_stack = bcat_imp.getStack()
protein_stack = protein_imp.getStack()
size = nuclear_stack.size()

```

```

#-----Find positive/total inside cells over all
slices-----
    positive_cells = 0
    total_cells = 0

    for i in xrange(1, size + 1):
        #-----Set up Images-----
        nuclear_stack_slice =
ImagePlus(nuclear_imp.getTitle() + ' ' + str(i),
nuclear_stack.getProcessor(i))
        bcat_stack_slice =
ImagePlus(bcat_imp.getTitle() + ' ' + str(i),
bcat_stack.getProcessor(i))
        protein_stack_slice =
ImagePlus(protein_imp.getTitle() + ' ' + str(i),
protein_stack.getProcessor(i))

        # If there's no b-cat, skip this slice
        if bcat_stack_slice.getStatistics().max == 0:
            continue

        #-----Process Nuclear Channel-----
        #-----Set up particle analyzer-----
        options = PA.SHOW_MASKS
        pa = PA(options, 0, RT(), MIN_CELL_SIZE,
sys.maxint)
        pa.setHideOutputImage(True)
        rm = RM(False)
        pa.setRoiManager(rm)

        #-----Run particle analyzer-----
        pa.analyze(nuclear_stack_slice)
        rm.runCommand(imp, "Show None") # for some
reason, this works.

        #-----Process B-catenin Channel-----
        #-----Create ROI from b-catenin mask-----
        IJ.run(bcat_stack_slice, "Create Selection",
""")
        IJ.run(bcat_stack_slice, "Make Inverse", "")
        rm2 = RM(False)
        rm2.runCommand(bcat_stack_slice, "Add")

        #-----Find all cells completely inside b-cat---
--
        inside_pos_indices = []

```

```

        inside_neg_indices = []

        nuclei = rm.getRoisAsArray()
        bcat_points =
set(rm2.getRoi(0).getContainedPoints())

        for i in xrange(len(nuclei)):
            nucleus = nuclei[i]
            nucleus_points =
nucleus.getContainedPoints()

            # If nucleus is completely inside b-
catenin, add to inside
            if
set(nucleus_points).issubset(bcat_points):
                total_cells += 1

                #-----Set up analyzer to measure
amount of protein signal-----
                an = Analyzer(protein_stack_slice)
                rm.select(protein_stack_slice, i)
                an.setMeasurements(Analyzer.MEAN)
                an.measure()

                # If protein signal above certain
threshold, add to positive
                if
an.getResultsTable().getValueAsDouble(1, 0) > P_PERCENT *
255.0 / 100:
                    positive_cells += 1
                    inside_pos_indices.append(i)
                else:
                    inside_neg_indices.append(i)

        if show_image:
            #-----Create Inside Image-----
            #-----Inside negative nuclei-----
            #nuclear_mask = pa.getOutputImage()
            inside_neg_slice = IJ.createImage('', '8-
bit black', imp.getWidth(), imp.getHeight(), 1)
            IJ.setForegroundColor(255, 255, 255)
            for nuclei in inside_neg_indices:
                rm.select(inside_neg_slice, nuclei)
                IJ.run(inside_neg_slice, 'Fill', '')

```

```

        inside_neg_stack.addSlice(inside_neg_slice.getProcess
sor())

        #-----Inside positive nuclei-----
        inside_pos_slice = IJ.createImage('', '8-
bit black', imp.getWidth(), imp.getHeight(), 1)
        IJ.setForegroundColor(255, 255, 255)
        for nuclei in inside_pos_indices:
            rm.select(inside_pos_slice, nuclei)
            IJ.run(inside_pos_slice, 'Fill', '')

        inside_pos_stack.addSlice(inside_pos_slice.getProcess
sor())

        #-----Create final image-----
        if show_image:
            inside_neg_imp = ImagePlus('',
inside_neg_stack)
            inside_pos_imp = ImagePlus('',
inside_pos_stack)
            #inside_pos_imp.show()
            final_imp = SM.mergeChannels([inside_pos_imp,
None, \
            nuclear_imp, channels[bchannel],
inside_neg_imp], False)
            final_imp.show()

        #-----Output totals-----
        print('Positive Cells: ' + str(positive_cells), end
= '\t')
        print('Total Cells: ' + str(total_cells))

run()

```